

PARSONS ISLAND, MARYLAND: SYNTHESIS OF GEOARCHAEOLOGICAL INVESTIGATIONS, 2013–2020



By

Darrin L. Lowery, Ph.D.

Chesapeake Watershed Archaeological Research Foundation

Monograph prepared for the
Maryland Historical Trust

July 5, 2021

Parsons Island, Maryland: Synthesis of Geoarchaeological Investigations, 2013- 2020

Authored by:

Darrin L. Lowery

With contributions by:

Dennis Stanford, Dan Wagner, John Wah, Kathryn Puseman, Chad Yost, Andrea Nurse, Jonathan Burns, Pegi Jodry, Bruce Bradley, Norman K. Brady, David R. Thompson, Joseph Clemens, Michael O'Neal, Neeshell Bradley-Lewis, Jack Lowery, Joshua Lowery, Jacob Lowery, John Fagan, Cam Walker, Mike Waters, James Feathers, Linda Scott Cummings, and Christopher Moore.

Final Report

7-5-2021

© Darrin L. Lowery 2021



I dedicate this volume to Dr. Dennis Stanford. He was a mentor, a colleague, and a friend.

ACKNOWLEDGEMENTS

The research at Parsons Island, Maryland involved the cooperation of numerous individuals. First and foremost, the ability to conduct this research would not have occurred had it not been for the landowners. The unfettered assistance, cooperation, and access to the property offered by the Corckran family deserves the utmost recognition. Their kindness and support remind me of a by-gone Eastern Shore era when landowners openly welcomed visitors and strangers. Dennis Stanford, Pegi Jodry, Stephen Loring, and Torben Rick represent some of the faculty at the Smithsonian Institution who were either directly or indirectly involved with this project. The initial fieldwork was supported by Dr. John Wah and Dr. Dan Wagner. These two soil scientists have served as colleagues during our collective endeavors to unravel the late Pleistocene upland stratigraphy of the Delmarva Peninsula. The list of fieldwork contributors is immense. First and foremost, I offer my humble appreciation to Mr. Norman K. Brady and Mr. David R. Thompson, who traveled many miles with me over the years and made countless discoveries; some controversial and some not. Kathryn Puseman, Chad Yost, Andrea Nurse, Ugo Zoppi, Linda Scott Cummings, Marvin Kay, Russell Graham, Christopher Moore, and James Feathers all contributed to this research and offered specialized insights into the island's geoarchaeological record. Bruce Bradley was involved in the Smithsonian's excavation and also contributed insights into the lithic technology noted at 18QU1047. It is rare to have the ability to debate a scholar on regular basis. Over the past decade or more, Stuart Fiedel and myself have "locked horns" time and time again over issues that 99.9% of the population could not care less about! As a scholar who is a "die-hard Clovis-first" advocate, Stuart has provided the "temper", which has hardened the evidence we have uncovered. In sum, we have agreed on some ideas; but disagreed on others. Other scholars that have offered valuable insights include Joseph McAvoy, who originally unearthed the "pre-Clovis" material at Cactus Hill, Virginia. I have told him time and time again that at least now he is not the only "screw-ball" who has found early archaeological remains in the Middle Atlantic. Over the years, I have embraced visits to Parsons Island by numerous scholars and skeptics. These visitors include Stuart Fiedel, Michael Waters, Arthur Spiess, Jonathan Lothrop, James Dixon, David Thulman, Joseph Gingerich, Michael Faught, and Zac Singer. Offers to visit the island were extended to many other scholars, however, only the ones mentioned above actually embraced the invitation. I believe it is important to foster face-to-face open discussions; not behind the scene "passive-aggressive" academic publication attacks. Other individuals who supported this project include Dennis Fenwick, Jack Broderick of the Kent Island Heritage Society, Doug Harris of the Narragansett Tribe, Senator Stephen Hershey, Delegate Steven Arentz, Delegate Jay Jacobs, and Nicholas Redding of Preservation Maryland. The funding provided by the Maryland Historical Trust, the Smithsonian Institution, and the Chesapeake Watershed Archaeological Research Foundation made this research possible and permitted the creation of this monograph. Finally, I must thank my family; Brooke, Jack, Coby, and Finch. When the rest of the world had shut down, the Lowery boys helped me excavate the test units at Parsons Island.

TABLE OF CONTENTS

1. INTRODUCTION.....	8
1.1. Methodology.....	9
2. BACKGROUND.....	22
2.1. Parsons Island History and Coastal Erosion.....	22
2.2. Parsons Island Area Geology.....	23
2.3. Synopsis of Chesapeake Regional Paleoindian Archaeology.....	41
2.4. Synopsis of Chesapeake Regional Pre-Clovis or Paleo-American Archaeology.....	57
2.5. Synopsis of Chesapeake Localities with Radiometrically-Dated Tilghman Paleosol Surfaces.....	71
3. PARSONS ISLAND RESEARCH 2013 to 2019.....	72
3.1. Synopsis of Macrofloral, Phytolith, and Pollen Data for Parsons Island and Elliott’s Island.....	81
3.1.1. Macrofloral Sampling and Identification Methodology.....	82
3.1.2. Phytolith Sampling and Identification Methodology.....	83
3.1.3. Pollen Sampling and Identification Methodology.....	84
3.1.4. Parsons Island 6Ab horizon (41,451 ± 451 cal. yrs. BP D-AMS 003536).....	84
3.1.5. Parsons Island 5Ab horizon (35,096 ± 426 cal. yrs. BP D-AMS 003535).....	88
3.1.6. Parsons Island 4Ab2 horizon (29,563 ± 372, 31,846 ± 460, or 32,756 ± 97 cal. yrs. BP D-AMS 003532).....	89
3.1.7. Parsons Island 4Ab1 horizon (20,761 ± 198 cal. yrs. BP D-AMS 003533).....	94
3.1.8. Elliott’s Island 5Ab horizon (23,946 ± 318 cal. yrs. BP Beta-286851).....	95
3.1.9. Paleoenvironmental Summary and Conclusions.....	97
3.2. Synopsis of Archaeological Remains Found at Parsons Island.....	103
3.2.1. Northeast Parsons Island (18QU1065).....	103
3.2.2. South Parsons Island (18QU1066).....	106
3.2.3. Parsons Island Well (18QU1067).....	107
3.2.4. Parsons Island (18QU1047).....	111

Bipoint Bifaces.....	116
Other Bifaces and/or Biface Fragments.....	122
Lanceolate Bifaces.....	126
Blade Cores and Blades.....	130
Shouldered Points/Knives on Blades or Blade-Like Flakes.....	144
Flake Tools and Utilized Flakes.....	149
Hammerstones, Anvils, Battered Cobbles, Wind Polished Pebbles, and Rock Features.....	154
Debitage and Waste Flakes.....	154
4. EXCAVATIONS AND ARCHAEOLOGICAL TESTING AT 18QU1047.....	167
4.1. Smithsonian 2017 Archaeological Test Investigation Summary.....	167
4.2. CWAR 2020 Archaeological Test Investigation Summary.....	170
4.4. CWAR 2020 Geoarchaeological Summary at 18QU1047.....	181
5. PARSONS ISLAND ARCHAEOLOGICAL SURVEY AND EXCAVATIONS SUMMARY AND CONCLUSIONS.....	191
REFERENCES CITED.....	209
APPENDIX I: Blood Residue Analysis Report for Two In-Situ Artifacts found along the Eroded Bank Profile at Parsons Island, Maryland.....	222
APPENDIX II: Luminescence Dating of Sediments from Parsons Island, Chesapeake Bay.....	233
APPENDIX III: Soil Profile Descriptions for Parsons Island, Maryland.....	243
APPENDIX IV: GPR Data for Parsons Island, Maryland.....	255
APPENDIX V: Identified and Dated Charcoal from the 4Ab1 and 4Ab2 Strata at Parsons Island.....	262

1. INTRODUCTION

On May 20th, 2013, Dr. John Wah and myself visited Parsons Island, Maryland (see Figures 1.1 and 1.2). The expedition on that day represented my second excursion to Parsons in twenty-one years. My first visit to Parsons occurred in 1992 as part of a collective multi-year archaeological survey of the Kent Island area (see Lowery 1993), which was conducted for the Kent Island Heritage Society, the University of Delaware, and the Maryland Historical Trust. In 1992, Parsons Island encompassed 99-acres (see Figure 1.2) and when we re-visited the island in 2013, the island had eroded to ~78-acres. In 2019, the island had been reduced to ~71-acres and presently Parsons consists of ~69-acres. The perimeter of exposed shoreline also changed markedly during this period of time. In 1992, the island had 2.11 linear miles (3.4 km or 11,159 feet) of coastline and by 2019 the amount of coastline had been reduced to 1.65 linear miles (2.66 km or 8,716 feet). Over the twenty-seven-year period, the island has collectively lost about one-acre of land per year to coastal erosion. With the gradual reduction in linear miles of shoreline over this period, it is clear that the rate of annual land loss has actually increased in recent years. Notably, most of the land loss is focused along the island's southwest margin.

Our re-visit to Parsons Island on May 20th, 2013 (see Figure 1.3), originated as a result of our late Pleistocene stratigraphic and geoarchaeological investigations conducted at nearby Miles Point, Talisman Farm, and Barnstable Hill (see Figure 1.4). The collective research conducted at Parsons Island over the succeeding seven years culminated into a better understanding of the Middle Atlantic's Paleo-American archaeological record (see Figure 1.4), a higher-resolution evaluation of the region's late Pleistocene upland stratigraphy, and a means to quantify some of the site formation processes along eroding coastal margins. This monograph synthesizes the results of these investigations. Regardless of the possible age of the Paleo-American record noted at Parsons Island, the primary objective has always been salvage. Some "academicians" and a few "cultural resource managers" view investigations at eroding coastal archaeological sites in the Chesapeake Bay region as being "biased" and "anecdotal" (see Custer 2018: 202). It should be obvious, the erosive effects by the estuarine water of the Chesapeake Bay are unbiased and these waters will indiscriminately destroy both historic sites, as well as prehistoric sites. The results of our collective investigation at Parsons Island also proves that if follow-up investigations are made at "untrustworthy" (Ibid) sites, "anecdotal" discoveries can make major contributions to the regional, as well as North America's geoarchaeological record.

In 2019, the Chesapeake Watershed Archaeological Research foundation applied for a non-capital grant from the Maryland Historical Trust. The goal of the proposal was to synthesize all of the prior work at Parsons Island, document the island's archaeological record, and conduct limited excavations inland of the shoreline at 18QU1047 to determine if any in-situ cultural deposits remained. Earlier work conducted by the Smithsonian Institution in 2017 had uncovered a small in-situ quartz flake and charcoal located two-meters beneath the ground surface and within a buried paleosol. Like several other radiometric ages on charcoal associated with lithic artifacts found in-situ and exposed along the eroding bank, the Smithsonian date was greater than 20,000 years old. Paleo-botanical remains from this surface are consistent with the presumed age and the OSL-ages on the overlying sediments indicate comparable estimates for the underlying buried surface.

This monograph, which was funded by the Maryland Historical Trust's Historic Preservation Non-Capital Grant program, attempts to synthesize the collective analytical results conducted by various researchers. The monograph also shows that the discoveries at Parsons Island are not "anecdotal"

(Ibid). The follow-up testing at 18QU1047 funded by the non-capital grant indicate additional in-situ archaeological remains occur immediately inland from the shoreline. Even with the current data, we do not know the inland extent of the two surviving archaeological sites currently located on Parsons Island. Because of the ongoing effects of coastal erosion, we may be seeing the beginning, the middle, or the tail-end of these two sites. Most importantly, additional investigations of Parsons Island could be conducted. With our objective to assist the landowners of Parsons Island, the research outlined in this monograph should augment the urgency and the immediacy for shoreline stabilization. Archaeological resources; regardless of their significance, have typically been viewed as an obstacle (see Lowery 2007) by landowners. In short, the generous support and access afforded by the landowners of Parsons Island should illustrate to others that collaborations between scholars and landowners can result in mutual objectives; i.e., site preservation via shoreline stabilization.

In sum, the data presented in this monograph should illustrate to landowners, academicians, cultural resource managers, members of the interested public, and outside scholars about the unique and somewhat discouraging coastal erosion scenarios noted along a small portion (see Figure 1.5) of the Chesapeake Bay's 11,684 linear miles (18,804 km) of shoreline. The land and archaeological site loss noted at Parsons Island (see Figure 1.5) is common along raw exposed shorelines throughout the region. With respect to both site loss and coastal erosion in the Middle Atlantic region, I once stated in a professional lecture that you are "*not in Kansas anymore*".

Hopefully, the work synthesized in this monograph will help the public to better understand the daunting issues surrounding coastal erosion and archaeological site loss in the Chesapeake Bay area. Between 1992 and 2018 along solely a ~360-meter (~1180 feet) section of Parsons Island's southwestern margin, over 55,000 cubic meters (~72,162 cubic yards) of sediment eroded into the Chesapeake Bay. During this twenty-six-year period, the amount of sediment eroded and sieved by the actions of both water and waves would fill over 5,000 commercial-sized dump trucks. In 2015, the State Archaeologist of Virginia asked me, "*Why is it you find so many interesting archaeological remains along shorelines?*" Note that Virginia has 7,213 linear miles (11,608 km) of shoreline. The answer to this question is simple. I doubt that there has ever been a single professional archaeological excavation in North America where so much sediment has been extracted and sieved for archaeological remains (i.e., artifacts) over such a short period of time. Remarkably, the rate of erosion and land loss noted at Parsons Island is not uncommon along vast sections of the Chesapeake Bay and its tributaries. It is fascinating that some professional archaeologists in the region (see Custer 2018) do not recognize coastal erosion as the principal variable resulting in increased probability for artifact discovery. Hopefully, this monograph will provide some guidance and rectify many of the crucial misunderstandings about the region.

1.1. Methodology:

In conducting similar surveys, Lowery (2019 and 2020a) has identified some of the unique aspects of archaeological site survey in coastal settings and the numerous variables that require consideration. Prior experience was important in shaping and defining the methodology employed in this project. The first research objective was to conduct a pedestrian shoreline survey of Parsons Island. Unlike many prior shoreline surveys, Parsons Island was re-visited over a period of seven years and shoreline surveys were conducted ninety-three (93) times. During each visit all artifacts in the intertidal

zone were documented. Another goal was to conduct a systematic pedestrian surface survey of the 25-acres of tilled fields (see Figure 1.6) located on the island and record any artifacts on the surface. Interestingly, the tilled field areas had been surveyed in 1993 (Lowery 1993) and at the time the tilled area encompassed 44.6 acres; a loss of 19.6 acres of arable land over 27 years. In 1993, no archaeological sites were discovered in the tilled fields. Any previously unrecorded sites along the shorelines or within the eroding fields were to be documented using the official Maryland Inventory of Historic Properties, Archaeological Site Form. Another objective was to evaluate the presence or absence of in-situ archaeological remains immediately inland of the eroded bank margin of 18QU1047. The orientation and placement of the four (4) one-by-one meter excavation units were determined by the patterning of in-situ artifacts found along the eroding bank margin.

With respect to the ninety-three (93) pedestrian shoreline surveys, the approach chosen was to concentrate on examining all bank profiles and intertidal zones around Parsons Island (see Figure 1.7), assess the bank exposures for archaeological features or artifacts (see Figure 1.8), document the location of any in-situ or displaced artifacts using GPS, and photographically record the condition of each site. The drawback to the shoreline survey approach is that it is difficult, and largely impossible, to accurately gauge the inland or landward extent of each site and the variety of possible features at each site without extensive subsurface testing inland of the shoreface. As such, most of the sites found during this survey have only two dimensions (i.e., length or width and thickness) accurately recorded. The discovery dates of each archaeological specimen were noted over the seven-year period. As a result, we were able to assess whether new archaeological features were exposed and sieved by wave actions as the shoreline retreated. The marked appearance of artifacts along a shoreline over various time intervals may imply that unseen features and archaeological strata extend inland from the actively eroding shoreline. The bank edge retreat and erosion over the seven-year period were also monitored. With these data, we could evaluate how the various natural events (i.e., tropical storms, hurricanes, and ice) impact erosion and the appearance of displaced archaeological remains.

Notwithstanding the drawbacks, a shoreline survey has several distinct advantages. First, exposed and eroded shorelines allow for the detection of geologic strata and archaeological sites without extensive subsurface testing. Sub-surface testing is time-consuming and consequently covers less ground during any given period. This is particularly true in many settings around the Chesapeake Bay, where layers of tidal marsh peat and waterlogged soils make excavation more time-consuming; if not impossible. Coring with an auger is also often impossible; as suction associated with these waterlogged settings usually makes it difficult to examine the soils associated with drowned archaeological sites.

Another objective was to investigate the island's geology and its relationship to the various site formation processes. Several soil profile descriptions and particle-size data were prepared by Dr. John Wah and Dr. Dan Wagner (see Figure 1.9 and Appendix III), which helped define the spatial extent of the buried surfaces along the island's eroded margins. A series of AMS radiocarbon dates and OSL dates on various organic mineral horizons and aeolian strata along the western side of Parsons Island provided chronostratigraphic benchmarks, which expanded upon earlier research (see Lowery et al. 2010 and Markewich et al. 2009). The various dated samples were submitted to two independent labs. The first series of radiocarbon dates, which consisted of seven samples, were submitted to Direct AMS. To evaluate the initial results, four additional carbon samples were submitted to PaleoResearch Institute. Six OSL samples from various aeolian strata were collected by Dr. Chris Moore (see Figure 1.10) and

analyzed by Dr. James Feathers at the University of Washington (see Appendix II). Over the seven-year period, samples of the organic carbon from the various dated and buried paleosols were also subjected to archaeobotanical analyses (see Puseman et al. 2014). The archaeobotanical research results prepared by Puseman et al. (2014) have been synthesized in this monograph. Finally, the sediment within the intertidal and sub-tidal zones adjacent to 18QU1047 were sieved as a result of the Smithsonian research in 2017 using a Keene Engineering sluice dredge in an attempt to retrieve any unseen and dislodged artifacts that had eroded from the site. Ground penetrating radar (GPR) and LiDAR investigations of the island were also conducted by Dr. Michael O'Neal and Ms. Neeshell Bradley-Lewis (see Appendix IV). However, the results of these investigations are not included in this monograph and are included as a separate thesis document (see Bradley-Lewis 2021).

Parsons Island was accessed by boat. During periods of potentially hazardous wave-weather conditions, a 15' Boston Whaler was used during the fieldwork. To carry equipment and field crew to the island, a 17' Carolina Skiff was used. All shorelines around the island were examined at maximum low tide. The tidal cycles for the study area were accessed online to coordinate the fieldwork during periods when the tide was low at or near mid-day. As such, the mid-day timing of low tide would provide the maximum daylight hours for fieldwork. Low tide conditions expose larger sections of the eroding strata and offer greater opportunities to uncover displaced artifacts.

Obviously, weather impacted the timing of fieldwork within the study area over the seven-year period. Even during weekly episodes with ideal tidal conditions, wind direction and velocity greatly influenced if fieldwork could be performed. Each stretch of shoreline around the island has its own unique fetch variables. The same wind and wave action processes that are destroying the archaeological sites also effect whether Parsons Island could be safely accessed.

All of the sites and dislodged artifacts discovered during the seven-year investigation were photographed with a digital camera. A Pentax WG-III camera was used throughout the project. The camera has GPS and north-axis orientation capabilities. As such, the longitude, the latitude, and the orientation relative to true north were automatically recorded within the metadata of each digital photograph. The precision of the GPS data and the orientation documented for each photo were tested against georeferenced satellite images. The GPS coordinates for stationary navigational beacons were recorded as photographs and these positions were compared with georeferenced satellite imagery, which accurately portrayed the beacons. With the tests, all photographs of bank profiles and artifacts at Parsons Island were then accurately relocated and plotted on the GIS satellite imagery layer.

During the fieldwork, the artifacts from each site location were tallied, documented and photographed. Non-diagnostic artifacts, such as debitage, were also collected and recorded. Data relevant to each site (i.e., site name and the GPS coordinates) were noted on separate artifact bags. The boundaries of each site and the positions of artifacts along the shoreline were recorded on georeferenced satellite images. As required by the Maryland Historical Trust, the site locations were also noted on the associated QUEENSTOWN, MD U.S.G.S. 7.5' minute quadrangle. However, continued erosion and subsequent land-loss at Parsons Island clearly exposed the inaccuracies of the quadrangle as a recordation mapping tool. Historic coastal survey field maps, which are housed at the National Archives cartographic division, were used evaluate the changes to the island over the past 170 years. Historical published maps, which relied heavily on these coastal survey field maps, were not used because cartographic transcription errors were noted. Finally, historic land records housed with the

Kent Island Heritage Society were evaluated to better understand the deed history of the island. Interesting historical and anecdotal events about Parsons Island were also gathered from online newspaper databases.

Archaeological site data were recorded and uploaded to the Maryland Historical Trust. New MIHP archaeological site numbers were issued for previously undocumented site locations. Rough chronological time constraints for the artifact assemblages found during this seven-year investigation were gauged based on recognized diagnostic artifact types for the region. The quantity of artifacts and a description of the assemblages were noted within each site data form. Photographs were also taken and graphics were prepared illustrating details about each site assemblage. Finally, this monograph was completed in an attempt to synthesize the results of this seven-year investigation.

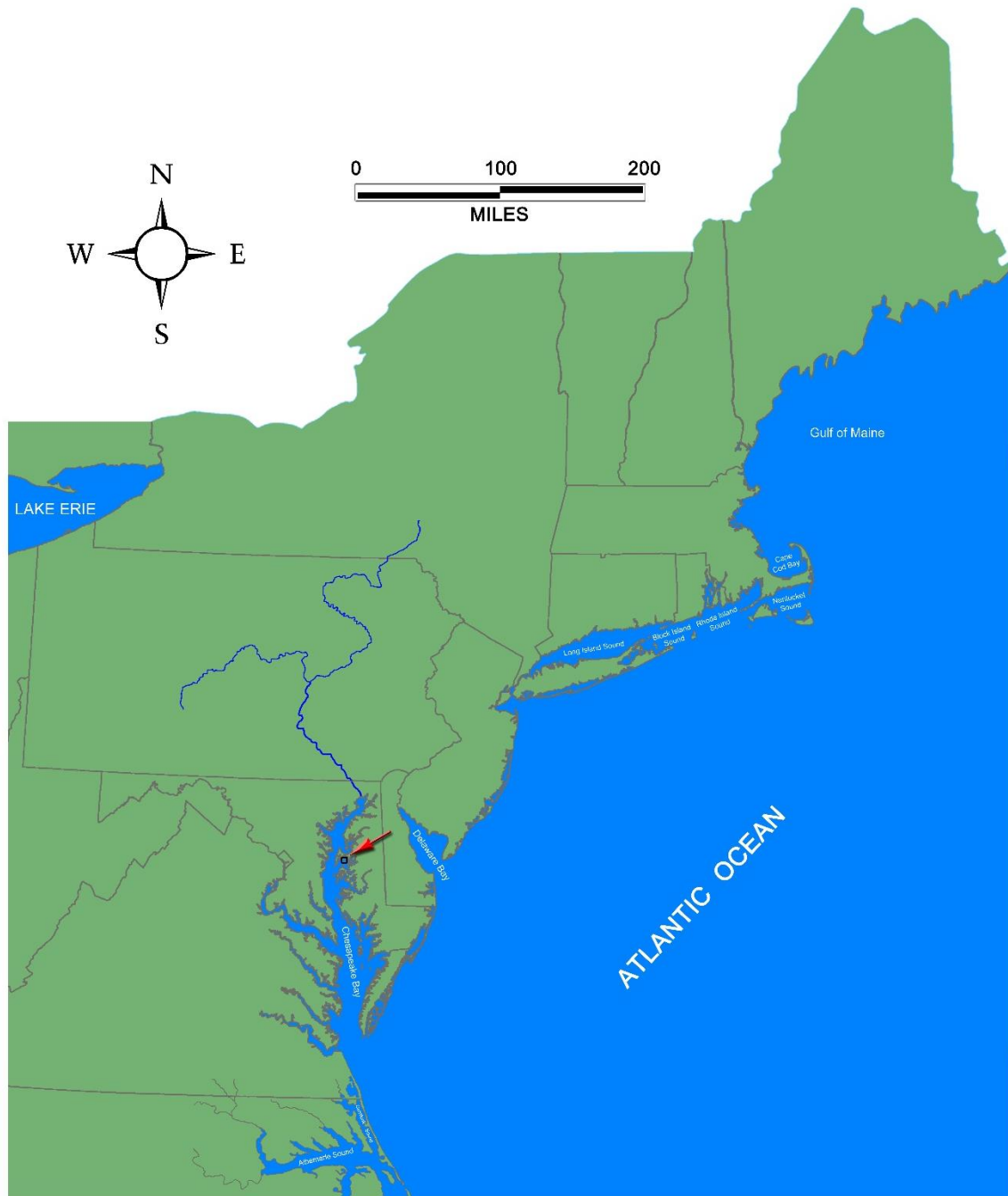


Figure 1.1. The northeast regional map shows the location of Parsons Island within the upper central portion of the Chesapeake Bay.

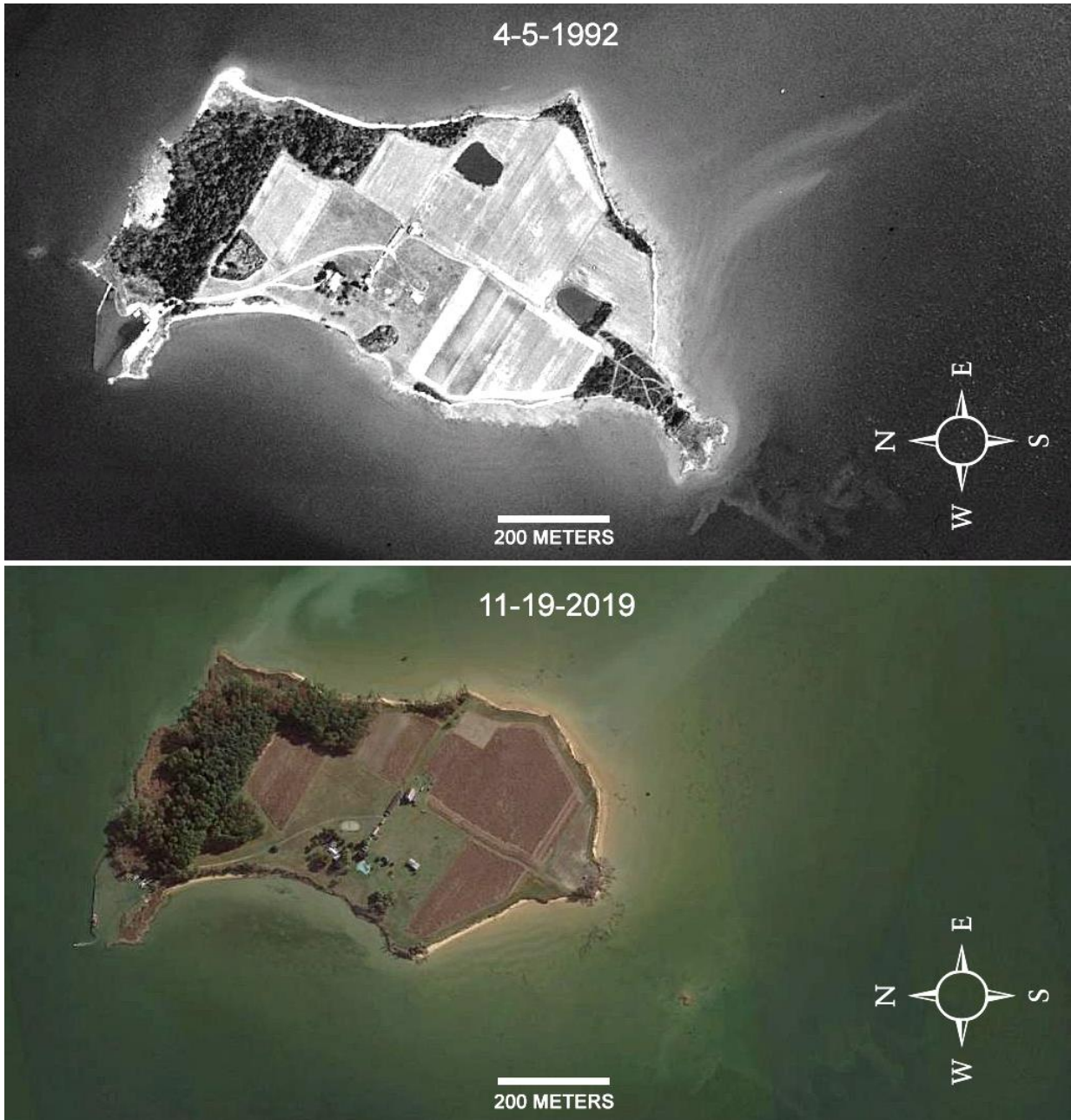


Figure 1.2. In 4-5-1992, Parsons Island encompassed 99 acres (top). In 11-19-2019, Parsons Island encompassed about 71 acres; a loss of ~28 acres over a 27-year period. The island, as of 2021 currently encompasses ~69 acres. Based on these data, the island loses ~1 acre of land per year to coastal erosion.



Figure 1.3. The photograph shows the eroded bank profile containing a deeply buried paleosol along the southwest side of Parsons Island as seen on May 20th, 2013 at 2:10pm.

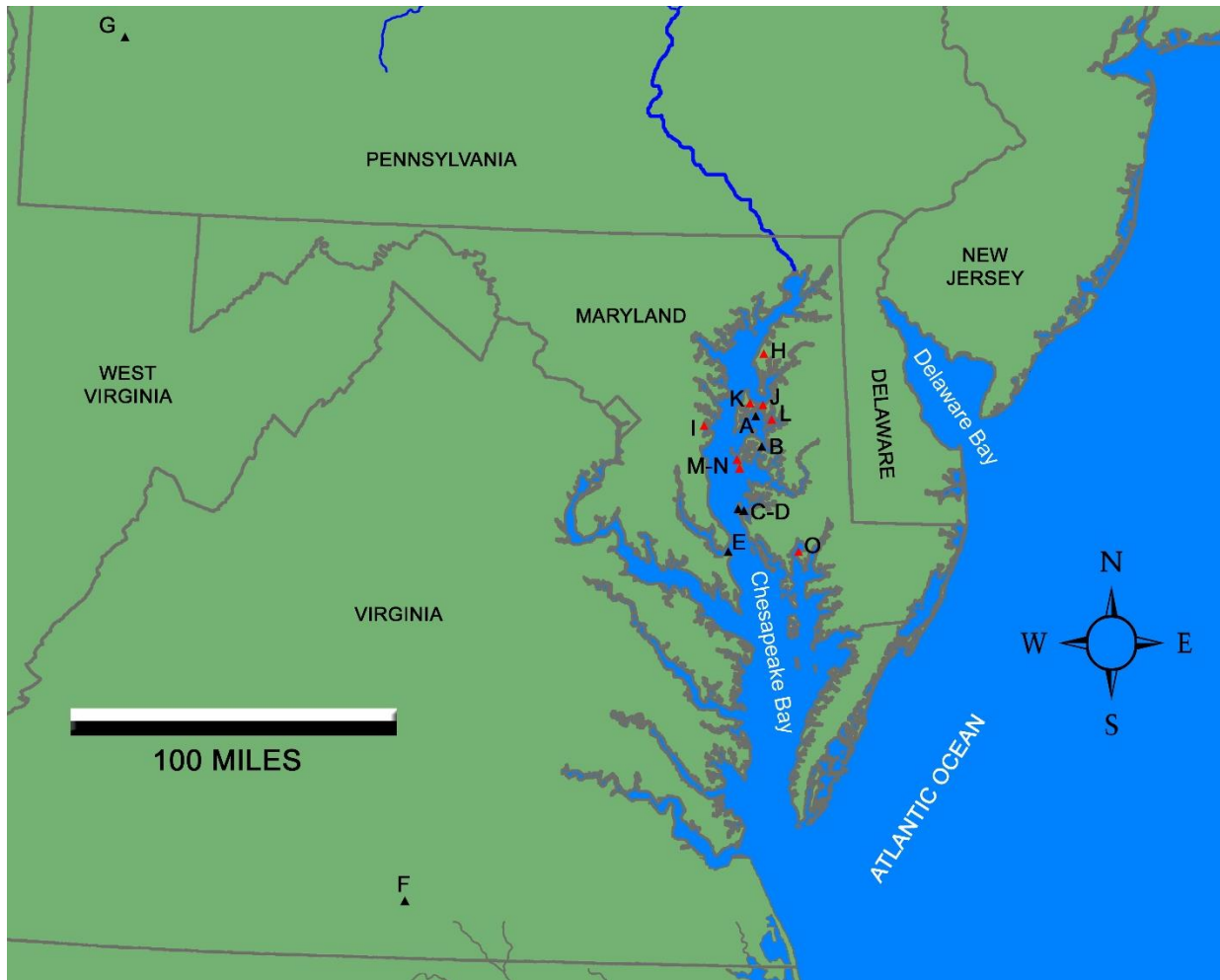
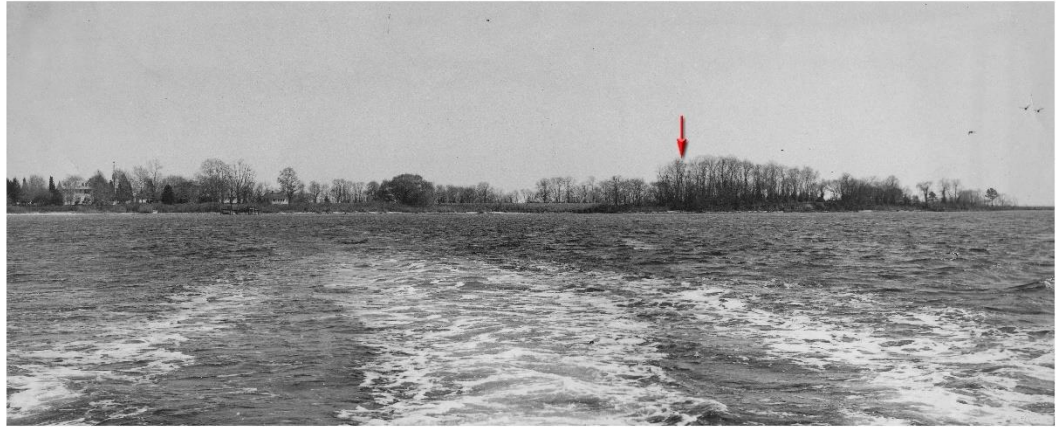


Figure 1.4. The map shows the locations of all Paleo-American sites mentioned in the text, as well as, the late Quaternary sites containing a radiometrically-dated buried paleosol surface. The possible Paleo-American sites mentioned in the text include Parsons Island (A), Miles Point (B), Oyster Cove (C), Cator’s Cove (D), Patuxent River (E), Cactus Hill (F), and Meadowcroft Rockshelter (G). The late Quaternary sites include Chesapeake Farms (H), SERC (I), Talisman Farm (J), Barnstable Hill (K), Wye Island (L), Paw Paw Cove (M), Blackwalnut Point (N), and Elliott’s Island (O).

May 26, 1969



February 1, 2016



Figure 1.5. The two photographs show a partial WNW view of Parsons Island over a forty-seven (47) year period. The top photo was taken on May 26th, 1969 and the bottom photo was taken on February 1st, 2016. The arrow in both photographs denotes the location of 18QU1047.



Figure 1.6. The photograph shows the plowed field conditions at Parsons Island on May 13th, 2020 at 12:24pm.



Figure 1.7. The photograph shows a pedestrian shoreline survey of Parsons Island being conducted on January 4th, 2017 at 12:51pm.



Figure 1.8. The photograph shows an in-situ bipoint biface found within the exposed and eroding paleosol on July 23th, 2017. The location of this find was recorded as longitude 76° 14' 55.668" W and latitude 38° 54' 29.0879" N.



Figure 1.9. The photograph shows Dr. Dan Wagner preparing a soil profile description along the eroding bank margin at Parsons Island, Maryland. Wagner is examining the vertical disturbance feature associated with the historic well (18QU1067) when it was initially exposed as a result of coastal erosion in 2013.



Figure 1.10. The image shows the OSL sampling being conducted on April 5th, 2018.

2. BACKGROUND

2.1. Parsons Island History and Coastal Erosion:

In 1650, William Portor of Kent Island took ownership of 340-acres of land associated with a peninsula called Parsons Neck. A portion of this neck would later be called Parson's Island. In 1665, Pasco Dunn purchased a 200-acre portion of Portor's farm at Parsons Neck. Presently, it is unclear how both Portor's and Dunn's parcel correlates to the extant island. The origin of the property's name is also unknown. Cronin (2005: 53) speculated that John Parsons, a Kent Island landowner in 1700, may have contributed to its name. John Parsons in 1700 acquired two tracts of land on Kent Island. The first tract was named "Parsons his Chance" and encompassed 115-acres. The second tract was named "Parsons Recovery" and encompassed only 22-acres. It is unclear where these tracts were located on Kent Island. However, if you combine John Parson's circa 1700 land acreage total with Pasco Dunn's 1665 parcel size, the collective total closely approximates William Portor's original 340-acre Parsons Neck property. The difference of about ~3-acres could simply be the result of survey error or coastal erosion land loss. Most importantly, the name Parsons affiliated with this tract precedes John Parsons property interests by about 50 years. There is some documentation (see Skirven, 1923), which suggests Parsons Island may have derived its name as a result of the initial Virginia settlement of Kent Island. In August 1631, Claiborne brought to the "Isle of Kent" from Hampton, Virginia, the Reverend Richard James, a minister of the Church of England, who conducted the first Christian Services held in the territory and now within the bounds of Maryland. These services were performed in a virgin forest along the shores of Eastern Bay, hence referred to as Parsons Point. The reference would explain why the name "Parsons" had been applied to this portion of Kent Island, which predated William Portor's 1650 land grant and well before John Parsons appeared in the region. As noted, the name Parsons Neck appears in the 1650 deed and references to "Parson's Point" are noted on Augustine Herrman's 1673 map of the Chesapeake Bay (see Figure 2.1) and all predate John Parsons by three to five decades.

During the early history, Parson's Point (see Figure 2.2) and/or Parsons Neck may have had a protective veneer of tidal marsh circumnavigating the forested upland. If this were the case, erosion may have been delayed and the annual land loss during the colonial era may have been negligible during these early years.

Erosion seems to have separated the peninsula from Kent Island just a few years before the preparation of the first coastal survey map. The T-223 survey, which was drafted during the months of June, July, August, and September of 1847, represents one of the actual field maps used to record features and document the margins of the coastline in the area. These field maps are extremely accurate and show many land use details that were either edited or excluded from the published charts. Notably, a small narrow ~500-foot gap through a long slender marshy peninsula can be seen on this survey. Given the geometry of the shoreline and the patterned tidal flow, the initial breach through the marsh separating the terminal end of the peninsula from the mainland would have expanded very rapidly. It is estimated that sometime between about 1840 and 1845, the terminal end of Parsons Point was detached from the mainland as a result of erosion; thus, forming Parsons Island. Using geo-referenced benchmarks, Parson's Island in 1847 (see Figure 2.3) encompassed about 200 acres of tilled-fields and forests. By 1899 (see Figure 2.4), Parsons Island had been reduced to approximately 173 acres of land. Less than forty-years later (see Figure 2.5), erosion had reduced the island to about 160 acres. In 1944, the island was described in a real estate advertisement (see Figure 2.6) as containing

about 155 acres of cultivated fields, woods, and marsh. By 1992, the island had eroded to ~98.4 acres in size. The island was further reduced to ~76.1 acres of land in 2013. Finally, the island's area as of October 18th, 2018 consists of ~70.1 acres. Most of the early erosion and land loss was focused along the southwest side of the island. However, as the protective veneer of tidal marsh was stripped from the south and eastern margins of the island, land loss increased in this area during the 20th century. The north and northeastern sides of the island have remained relatively stable. The northwest and west sides of the island were stabilized during the mid-20th century with the installation of bulkhead and rip-rap.

2.2. Parsons Island Area Geology:

Because Parsons Island was connected to Kent Island, the underlying geology would be defined as belonging to the Kent Island Formation. Owens and Denny (1979) named the Kent Island Formation for deposits bordering the Chesapeake Bay near Kent Island, Maryland. These deposits are assumed to be upper Pleistocene in age and correlating with Marine Isotopic Stage 3 (~60 and 29 ka BP). More recent age estimates (see Scott et al. 2010) have suggested that the antiquity of the Kent Island Formation can be confined to a tighter time frame between >30 ka to ~43 ka BP. The more restricted time frame for the Kent Island Formation was based solely on a single optically stimulated luminescence date of 37,000 ± 6,100 on sand grains (see Pavich et al. 2006). Some researchers (DeJong et al. 2015) have interpreted the Kent Island Formation as a relative high sea stand deposit and suggested that estuarine environments prevailed throughout the Chesapeake region during MIS 3. Interestingly, global proxies show that eustatic sea level was ~40–80 meters below present during MIS 3 (see Lambeck et al., 2014). If DeJong et al. (2015) are correct, the Delmarva region would have to be isostatically-depressed >40 meters during MIS 3 to permit the creation and formation of these estuarine deposits.

Based on the original Kent Island formation description, Owens and Denny (1979: 24) noted that *“exceptional exposures, which are as much as 4.5 m high, are found in bluffs on the north side of Kent Island along the Chester River. This area has been designated as the type locality of the Kent Island Formation. Here the formation consists of thick beds of loose, light-colored cross-stratified sand that overlies dark-colored massive to thinly laminated clay-silt. Gravel as much as 10 cm (4 in.) in diameter occurs in thin beds with the sand or as scattered clasts in both the sand and clay-silt. Locally large tree stumps in growth position are encased within the clay-silt.”* The Kent Island formation (*Ibid*: 25) *“overlies and has entrenched into the clay-silt and sand of the lower part of the Chesapeake Group (Calvert(?) and Choptank Formations). The Kent Island beds appear to have been deposited largely in an estuary—an expanded Chesapeake Bay. Freshwater conditions prevailed during the deposition of the Kent Island beds well down the bay. Spatially, the Kent Island seems to be correlated with the Sinepuxent Formation. This lowland surface probably was cut during the middle Wisconsin or Sinepuxent time; certainly, the surface up to 3 to 4.5 m (10 to 15 ft) above sea level was formed during this interval. The Kent Island Formation is probably the old Chesapeake Bay bottom that preceded the formation of the modern Chesapeake Bay (a late Wisconsin regression, which was then followed by the now ongoing Holocene transgression).”* Based on a single radiocarbon date on peat, Owens and Denny (*Ibid*: 26) concluded that *“In middle-Wisconsin time (ca. 30,000 years), sea level rose again to about 1.5 m (5 ft) above present sea level; the Sinepuxent and Kent Island Formations were deposited at this time. This rise was followed by lowering of sea level during Wisconsin ice maximums.”* The circa 30,000-year-old peat (*Ibid*) associated with the Kent Island Formation was said to contain the micro-floral remains of pine, birch, alder; and spruce or hemlock; suggesting that cool-temperate climate prevailed during the time of

deposition (Ibid). Mixon (1985) noted that along the Virginia part of the Delmarva, no data have been obtained supporting the concept of a high sea level stand during the middle Wisconsin time.

The type location associated with the Kent Island Formation was re-discovered by Lowery (1993) during an archaeological survey of the Chester River in Queen Anne's County, Maryland (see Figure 2.7). The eroded shoreline in 1993 consisted of an exposure of bald cypress stumps and knees at the base of an eroded 4+ meter high bank (see Figure 2.8). The cypress remains were firmly embedded within a dense gray estuarine silt/clay encapsulated beneath a layer of rounded rocks, cobbles, and boulders. The cobble/boulder bed signified a high-energy fluvial deposit that had been reworked and currently it is characterized as a lag formation. A 3-meter mixture of surficial aeolian material and various fluvial sand strata have enveloped the cobble/boulder layer.

When judging the "Kent Island" type section (see Figure 2.8) within a circa 43,000-year time frame, it is obvious that the natural processes involved would have to be tremendously dynamic to result in the formation of these geologic deposits under the narrow time constraints. There are some recent data suggesting that the "*large tree stumps in growth position*" observed by Owens and Denny (1979: 24) within the lower portion of the Kent Island formation are much older than MIS 3. A sample of wood associated from a small in-situ cypress knee was submitted to a lab for AMS dating. If the antiquity of the cypress knee were indeed between 30 ka and ~43 ka BP, the lab analysis would produce a worthwhile AMS age estimate. If the cypress wood were beyond radiometric dating, the lab analysis would preclude any results. The sample was submitted to Beta Analytic Inc. on November 21, 2018 and the report date was received on November 30, 2018. A raw date of >43,500 BP (Lab #: Beta – 510628; $\Delta 14C < -995.6$ o/oo) suggests the age of the cypress stump is beyond the limits of radiocarbon dating and clearly not within the circa 30,000 to ~43,000-year time frame associated with the Kent Island Formation.

Additional data indicate that the Kent Island Formation may not exist as defined by Owens and Denny (1979: 24). Note that Parsons Island is precariously wedged between a series of Pleistocene-age paleochannel features of varying ages and the Kent Island Formation type section (see Figure 2.9) is located east of an early Pleistocene paleochannel (see Schubel and Zabawa 1972). Various locations along the eastern margin of this early Pleistocene paleochannel (see Figure 2.9) show similar erosional, environmental, and depositional geologic sequences. Along the Wye River (see Figure 2.10) an indurated or silicified Miocene stratum is enveloped beneath a younger Miocene marine/estuarine gray silty-clay stratum. Historically, Miocene-age land mammals (see Figure 2.11) have been discovered within this "stiff clay". Additional Miocene-age gomphothere teeth (see Figure 2.12) have been found within this same dense gray-blue clay along the same section of the Wye River. These extinct Miocene mammal species may have once lived in a swampy low salinity setting analogous to the bald-cypress (*Taxodium distichum*) forest noted within the Kent Island type section along the Chester River (see Figures 2.7 and 2.8). Further south, the bank exposures along La Trappe Creek (see Figures 2.13 and 2.14) contain a light gray silty-clay stratum indicative of a marine type Miocene environment. Importantly, all of the of the gray, blue, light gray silty-clay strata in the region are situated beneath a layer of reworked coarse sand, gravel, pebbles, cobbles, and boulders associated with a former paleochannel. Along La Trappe Creek, these rounded clasts have been incorporated within a paleosol (see Figures 2.13 and 2.14) containing vitrified carbon associated with a cool-adapted upland forest/grassland that has been regionally-dated to MIS2 to MIS3 (see Lowery et al. 2010). The AMS ages

generated for this gravelly-paleosol do not reflect the period when these pebbles, cobbles, and boulders were initially deposited. The pebbles, cobbles, and boulders seem to indicate reworked and deflated paleochannel deposits. In sum, the only portion of the “Kent Island Formation” type section (see Figure 2.8) possibly associated with MIS2 or MIS3 is represented by a narrow cross-bedded medium-fine sand stratum situated 85 and 115 centimeters below the modern ground surface. The strata immediately underlying the cross-bedded medium-fine sand layer could be associated with MIS5e (~125 ka BP), MIS7e (~240 ka BP), MIS9e (~320 to 340 ka BP), or MIS11c (~400 to 425 ka BP); which represent recognized Pleistocene high sea stand events. More importantly, the thin cross-bedded sand stratum associated with the Kent Island type section is expressive of an upland aeolian environment; not a fluvial/estuarine environment.

Aeolian deposits have been documented throughout the Delmarva Peninsula. Based on an extensive series of AMS dates, OSL dates, as well as localities with buried archaeological remains, it is evident that aeolian activity occurred during the late Pleistocene and during portions of the Holocene (see Lowery 2002a and 2016, Lowery et al. 2010, Lowery et al. 2012, Markewich et al. 2015, Wagner et al. 2019, Wah 2003, Wah et al. 2014, and Wah et al. 2018). The earliest reported aeolian deposit (see Markewich et al. 2015: Figure 20) in the Middle Atlantic coastal plain is associated with MIS4 and dates between ~55,000 to 70,000 years BP. A loess deposit (i.e., Miles Point loess) chronologically-associated with MIS3 and the initial phase of MIS2 has been OSL-dated between 25,000 to 41,000-years BP (see Lowery et al. 2010). A post-last glacial maximum aeolian dune formation, which is younger than 24,000 BP and >13,000 years old, has been recognized at Elliott’s Island in Dorchester County, Maryland (Lowery et al. 2012).

The most apparent aeolian deposit in the region is indicated by a terminal Pleistocene loess (i.e., Paw Paw loess), which is chronologically associated with the Younger Dryas cold event dated to between circa 12,700- and 11,600-years BP (see Lowery 2002a and Lowery et al. 2010). The first age estimate and recognition of upland loess on the eastern shore of Maryland was reported by Foss et al. (1978). The work at Parsons Island (see Figure 4.19A) has refined the earlier age estimate initially reported by Foss et al. (Ibid). Dated charcoal found at the base of the Paw Paw loess suggests upland loess deposition began circa $12,781 \pm 28$ cal. yrs. BP (D-AMS 043965: $10,753 \pm 37$ rcybp). The Paw Paw loess has the greatest regional areal extent and consists of a thin 40 to 110-centimeter layer of surface silt (Wah 2003, Wah et al. 2014, and Wah et al. 2018). The pre-European thickness of the Paw Paw loess may have been much greater, however. Agricultural tilling over the past 300 years has denuded the topographic elevation of much of the region’s land surface. It is important to note that the surface contact between the Paw Paw loess and any underlying strata is indicated by an unconformity. The erosional event that produced this unconformity may have had a duration of less than half-a-century (see Figure 4.19A). As such, the initial onset of the Younger Dryas circa 12,800 years ago seems to have markedly destabilized the region’s upland landscape. It is unclear what caused this significant upland erosion across such a vast area. It is assumed that the destabilization and upland erosion are the result of marked climatic changes coupled with upland vegetation stress, as well as biota overgrazing.

The most recent regional aeolian deposits are confined to coastlines along isolated areas throughout the Middle Atlantic (see Lowery 2016 and Wagner et al. 2019). These aeolian deposits are late Holocene-age coastal dune formations that are generally stable at the present time. The overlying

dunes have enveloped a pre-contact landscape, which consists of a previously exposed upland surface containing late Prehistoric (<1000 cal AD) archaeological remains. These late Holocene sand dunes typically parallel the coastline and can extend inland several hundred meters. It is assumed that these young dunes developed during a period of marked climatic change and along coastlines with greater tidal amplitudes than at present. Prehistoric anthropogenic burning (see Davis 2020) within these coastal areas may have also contributed to the inland migration of these dunes.

Over the past 24,000 years, sea level and sea level rise have played a major role in the altering and sculpting the geology of the region. As outlined above, Parsons Island has lost 130 acres of its original landmass over the past 171 years; which is about three-quarters of an acre land loss per year. The recent coastal erosion has been exacerbated by a period of relatively slow sea level rise. The research presented by Lambeck et al. (2018) have shown that global eustatic sea level dropped to -134 meters (-439 feet) lower than present ~21,000 years ago. Aside from freshwater rivers, creeks, and springs/or spring seeps that traversed the region, all of the area shown in Figure 2.15 would have been dry land during the last glacial maximum. The research outlined by Markewich et al. (2009) has shown that the winds, which dominated the central Chesapeake Bay area during the last glacial maximum, originated out of the northwesterly direction. When sea level was at its lowest circa 21,000 years ago, Parsons Island represented the downwind southeastern terminus of the Kent Island peninsula. Presumably, aeolian transported material (i.e., loess and sand) accumulated along the elevated southeastern margins of Kent Island as a result of the topographic low areas, which encircled the Parsons Island peninsula.

Another low sea stand topographic variable may have contributed to the accumulation of aeolian material along the Parsons Island peninsula. Parsons Island and the peninsula associated with the island's platform represent a noticeable topographic rise or promontory near the headlands of a deeply-incised low sea stand valley, which was oriented in a southwesterly direction (see Figure 2.15). As implied by Markewich et al. (Ibid), the initial winds accompanying a high-pressure system moving across the region originate from a northwesterly direction. As a high-pressure system moves across the region and off the coast, southwesterly winds follow. As such, additional aeolian transported material (i.e., loess and sand) may have been deposited over the island's landmass by southwesterly winds, which were focused by the geometry of the nearby low sea stand river valley.

By simply applying a local eustatic sea level curve to the current bathymetric depth contours noted in the region (see Figure 2.15), the consequences may offer a false sense of initial salt-water intrusion into the topographic low areas currently situated beneath the current Chesapeake Bay and its affiliated tributaries. For example, the deepest location in the modern Chesapeake Bay is encompassed within the area shown in Figure 2.15. A deep bathymetric "hole", which is 174 feet below the current surface of the bay, is located immediately west of Kent Point. Using a eustatic sea level curve, we would assume that this hole was invaded by rising sea water about 13,500 year ago. However, the bathymetric low expressed by this "hole" may have been augmented by late Holocene tidal scouring processes and its current exaggerated depth may not represent the physical expression of the former low sea stand river valley.

Around 20,000 years ago, global sea level rose markedly in response to the melting and retreating global ice sheets (see Lambeck et al. 2014: Figure 4). Lothrop et al. (2016: Figure 17) have provided a local eustatic sea level curve for the Middle Atlantic region. Combined with the data shown in Figure 2.15, we can conclude that the topographic low river channels and valleys, which are presently drowned, were initially invaded by saline water during the early Holocene. Given the rate of sea level rise noted throughout the late Pleistocene and continuing into the early Holocene, inundation of former upland landscapes outpaced coastal shoreline erosion and retreat. However, during the late Holocene when sea level rise slowed to a level within ~5 meters of its current position, coastal shoreline erosion dominated the region. Over the past 3,000 years, the broad open-bodies of water that appeared in the area encouraged fetch or wave-related shoreline erosion. As a result of coastal erosion, the shoreline dimensions present today (see Figure 2.15) differ greatly from the upland area available just three-centuries ago.

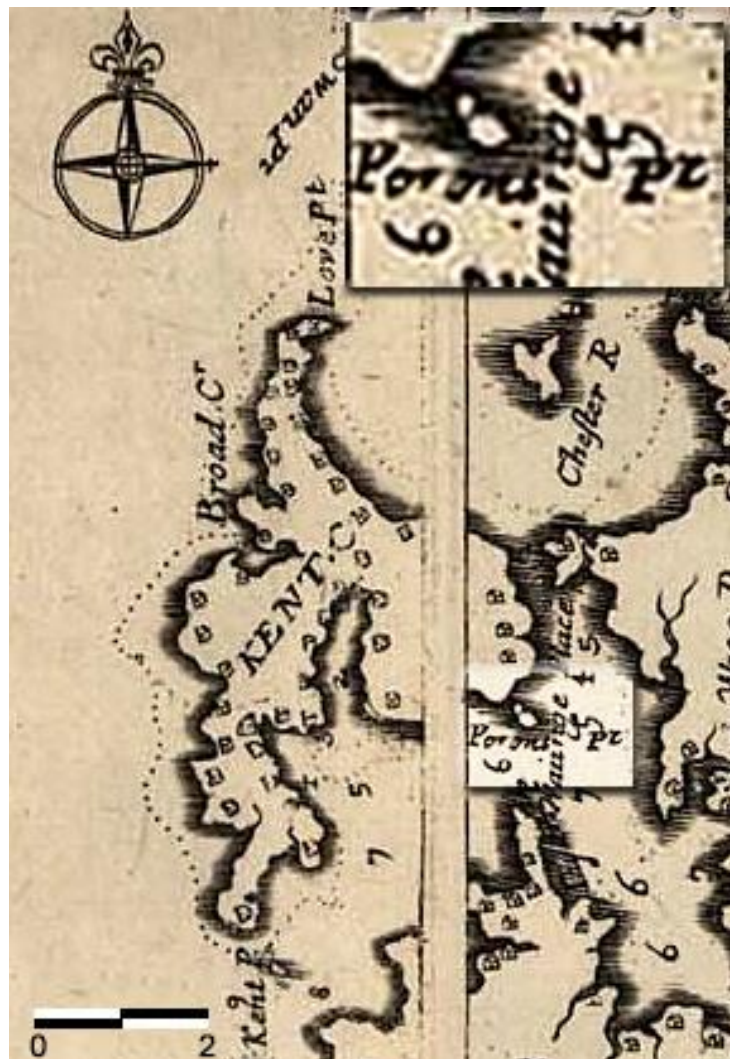


Figure 2.1. The image shows a portion of Augustine Herrman's 1673 map of the Chesapeake Bay, which shows the area associated with Parsons Point (Porons Pt) along the southeast side of Kent Island, Maryland.

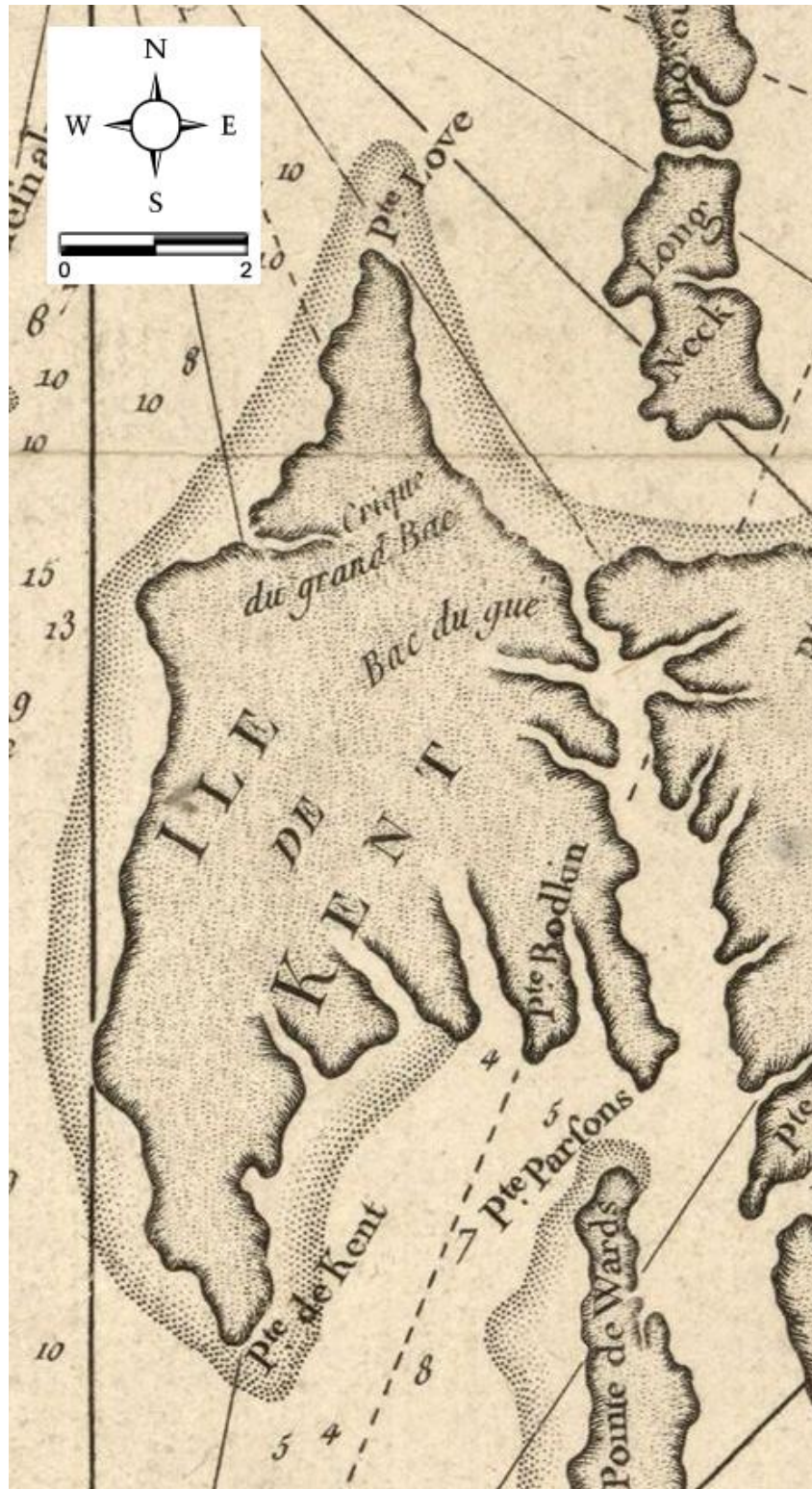


Figure 2.2. The image shows a portion of M. De Sartine's 1778 *Carte de la Baie de Chesapeake* map, which shows the area associated with Parsons Point (Pte. Parsons) along the southeast side of Kent Island, Maryland.

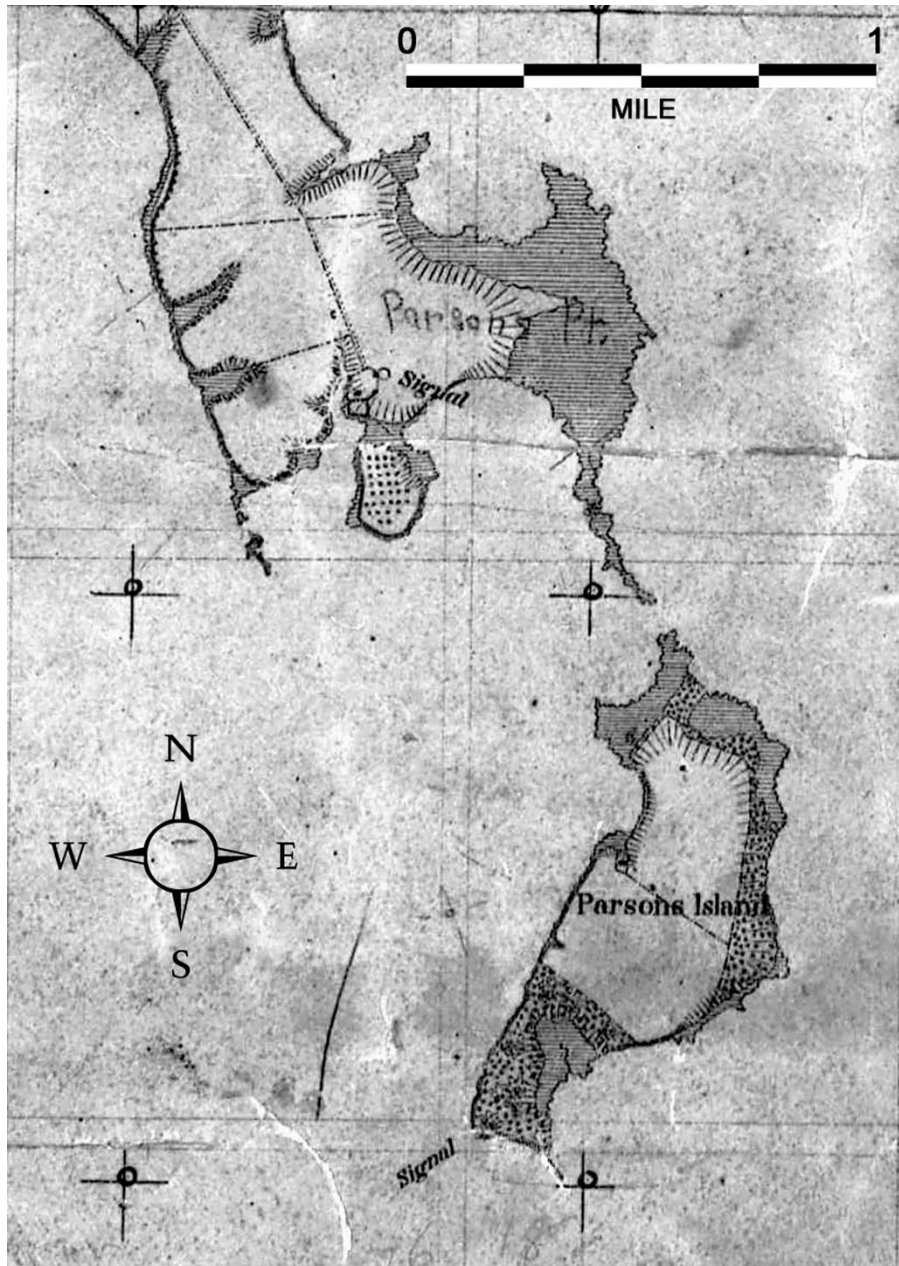


Figure 2.3. The image shows Parsons Island in 1847, based on field data, recorded on a portion of the T-223 U.S. Coastal Survey Map of the Eastern Shore of Maryland from Love Point to Choptank River.

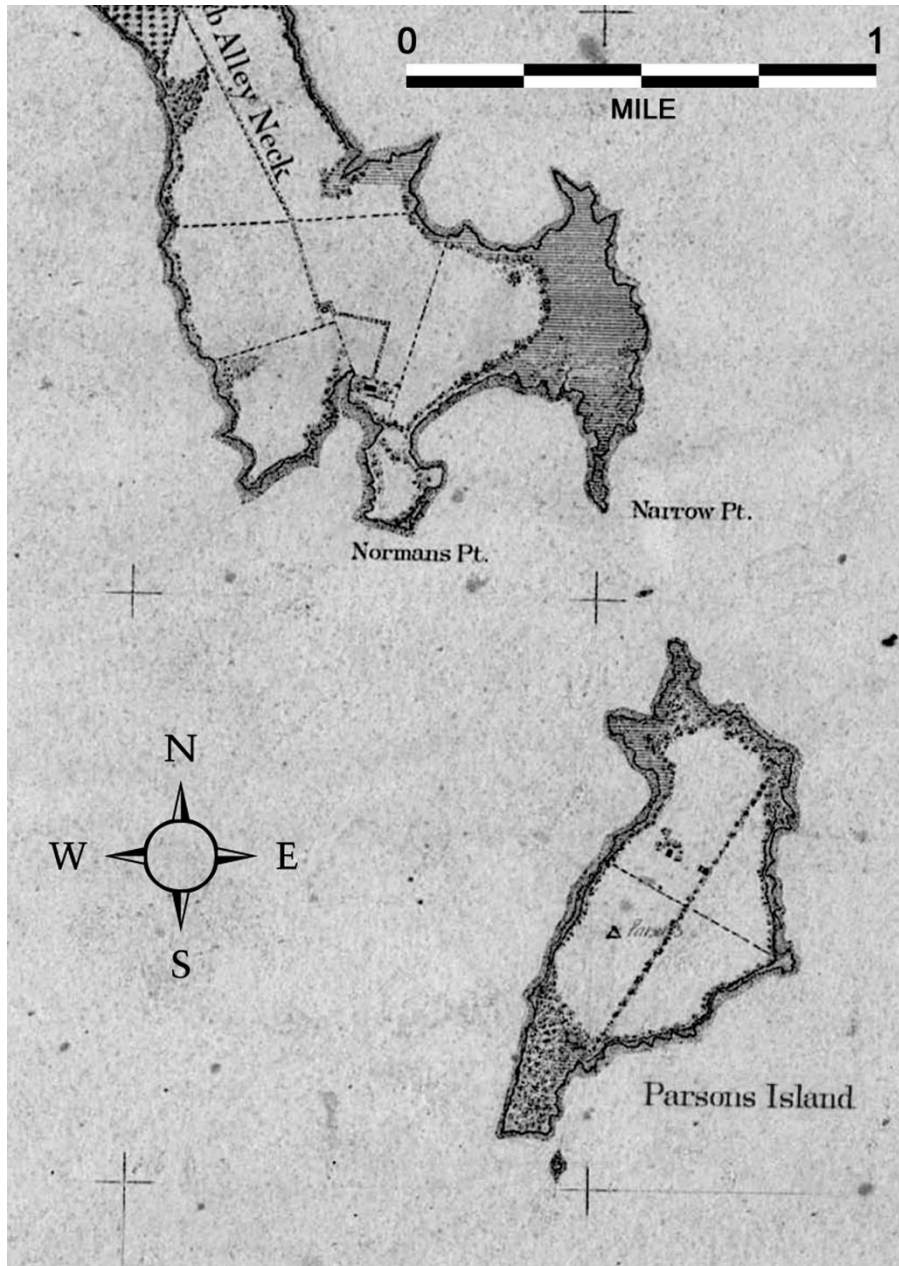


Figure 2.4. The image shows Parsons Island in 1899, based on field data, recorded on a portion of the T-2294 U.S. Coastal Survey Map of *Kent Island, Maryland*.

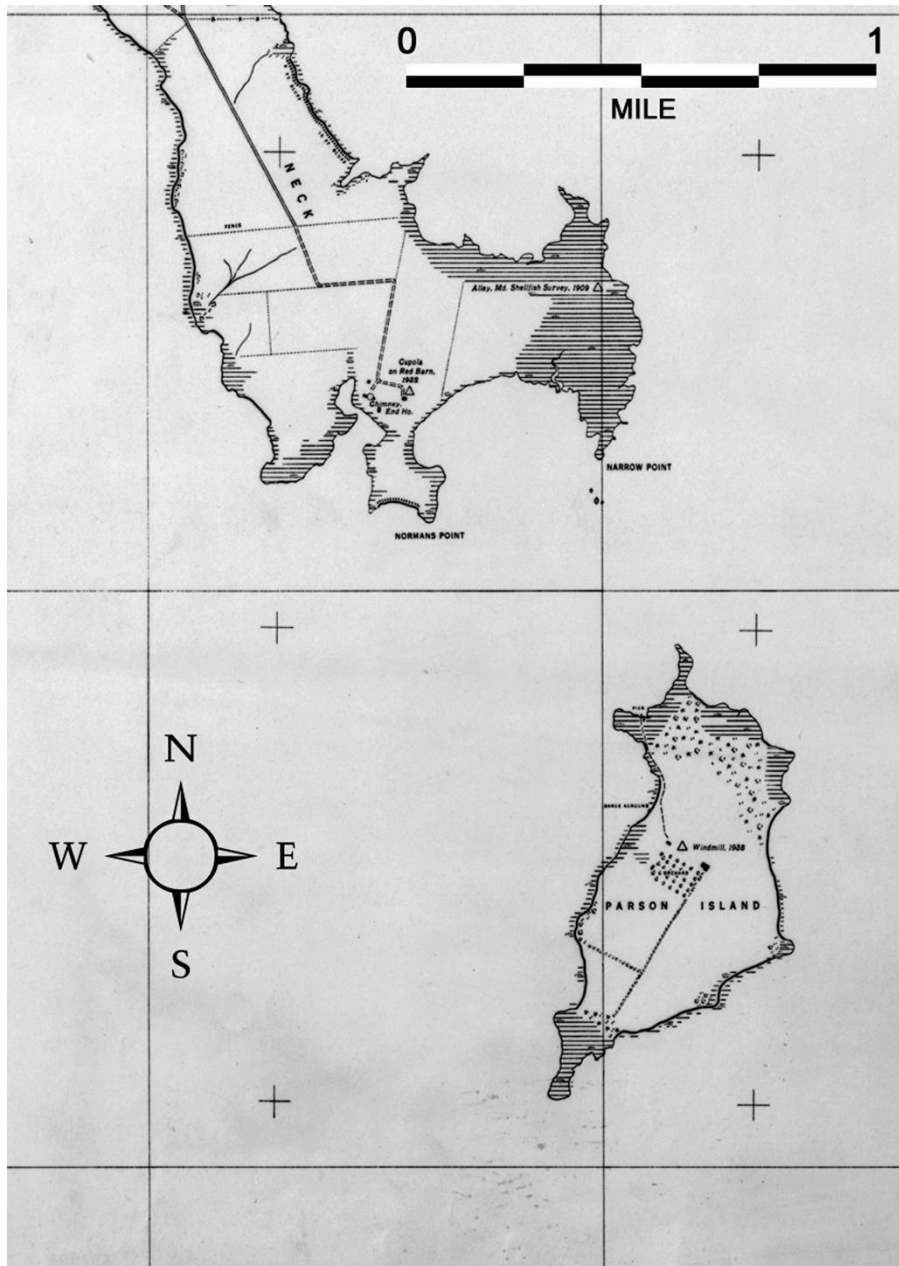


Figure 2.5. The image shows Parsons Island in 1937, based on field and aerial photography data, recorded on a portion of the T-5705 U.S. Coastal Survey Map of *Eastern Bay, Crab Alley Bay, and Vicinity*.

Miscellaneous

MARYLAND

PARSONS ISLAND SPORTSMAN'S DOMAIN FOR SALE 3 MILES OF SHORE LINE

A complete island located in Eastern Bay, $\frac{3}{4}$ mile from mainland, near Centerville, Maryland, only 8 miles to the Annapolis and Baltimore Ferry. Property consists of a main residence built in 1938—completely decorated and furnished. Electricity, running water, 2 baths and telephone.

Superintendent's house of 10 rooms and bath. 2 guest houses. Stock barn, 40 ft.x 50 ft., built in 1937.

4 farm out-buildings; miscellaneous chicken, turkey and hog houses. Approximately 125 acres under cultivation. Nearly 30 acres of Woodland. Extensive marshes. Fresh Water Pond; $\frac{1}{3}$ mile of concrete walks. Boathouse; 70 ft. wharf; 400 ft. bulkhead. Power & rowboats. Complete line of necessary farm implements, including Parmall tractor, 4 shore duck blinds and 1 off-shore blind. Goosefield. Over 500 pheasants stocked on the property. Garage, dock and telephone on the mainland. Taxes under \$200.00 annually. Priced at \$40,000. Write: Kenneth S. Clark, 1600 Locust st., Philadelphia 3, Pa.

Figure 2.6. The image shows a real estate advertisement announcing the sale of Parson's Island as it appeared in the January 23, 1944 edition of the *Philadelphia Inquirer*.



Figure 2.7. The images show in-situ bald cypress (*Taxodium distichum*) tree stumps along the Chester River near Kent Island, Maryland. The bottom photo was taken in 1993 and the top photo was taken in 2018. The area represents the type section associated with the Kent Island Formation. One of the small cypress knees associated with this stump was submitted for a radiometric-age estimate. The resultant age on the cypress knee was radiocarbon dead and produced an age of >43,500 years BP (Beta-510628).

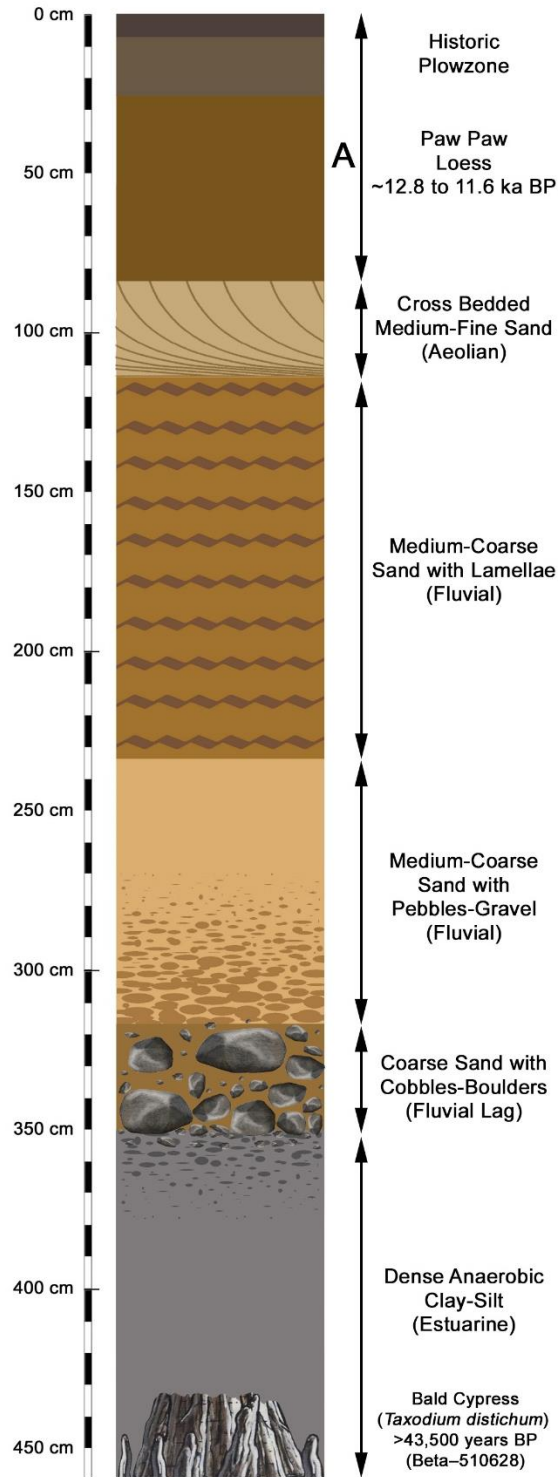


Figure 2.8. The graphic illustrates the profile associated with the “Kent Island Formation” (38.983271°N & -76.187249°W) type section. The time constraints defined by this profile are the covering of circa 12.8 to 11.6 ka BP loess. The in-situ tree stumps near the base of the profile have been dated. The stumps are beyond radiocarbon dating and are essentially radiocarbon “dead”.

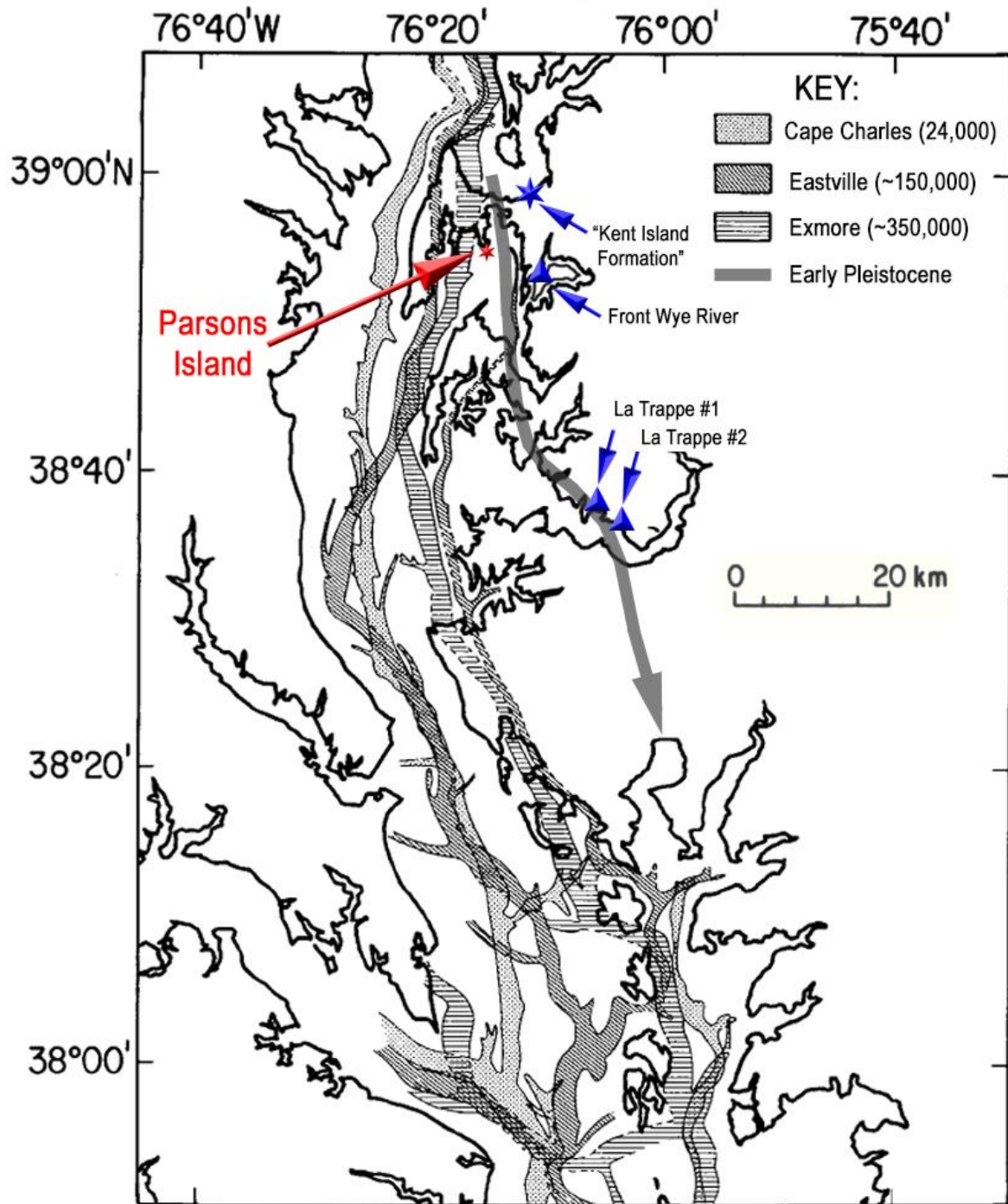


Figure 2.9. The map (see Colman et al. 1990: Figure 8) delineates the various Pleistocene paleochannels associated with the central Chesapeake Bay region. The location of Parsons Island and the type section associated with the Kent Island Formation have been plotted on this map.



Figure 2.10. The photo shows the geology along the western portion of the Wye River (Front Wye River). The exposure is located immediately south of the “Kent Island Formation” type section. Note the presence of a light gray silt-clay stratum situated immediately over a Miocene-age silicified sandstone deposit. The silicified deposit contains *Chesapeake* scallop impressions. A layer of rounded cobbles, pebbles, and coarse sand occurs immediately above the gray silt-clay stratum. At the surface, a covering of aeolian material envelops this modern landscape.

On the eastern shore of Maryland, in Queen Ann's county, an enormous grinder of the Asiatick elephant was likewise dug up, on the plantation of Mr. *Carmichael*, enveloped in a stiff blue clay. This I have in my possession.

Figure 2.11. The image shows an excerpt from Horace Hayden (see Hayden 1820: 17), which provides a brief description of the Gomphothere tooth found at Carmichael plantation along the front Wye River embedded within a "stiff blue clay" in Queen Anne's County, Maryland.



Figure 2.12. The image illustrates one of two Miocene-age gomphothere teeth found within the dense gray-blue clay along the Wye River.



Figure 2.13. The photo shows the geology along the western margins of La Trappe Creek (La Trappe #1) in Talbot County, Maryland. The surface stratum consists of late Pleistocene age loess that envelops an MIS2 to MIS3 paleosol. Reworked early Pleistocene gravels, cobbles, and boulders associated with a former paleochannel are incorporated within the MIS2 to MIS3 paleosol. A Miocene-age gray silty clay stratum containing fragmented *Chesapecten* scallop remains occurs beneath the paleosol.



Figure 2.14. The image shows the eroded bank profile along the eastern margins of La Trappe Creek (La Trappe Creek #2) in Talbot County, Maryland. The surficial seventy-five-centimeter layer encompasses a late Pleistocene loess deposit, which encapsulates an MIS2 to MIS3 buried organic layer. The buried organic surface at this location consists of a gravelly paleosol. The paleosol incorporates rounded pebbles associated with deflated and reworked early Pleistocene fluvial deposits. The basal stratum underlying the paleosol represents a Miocene marine formation.

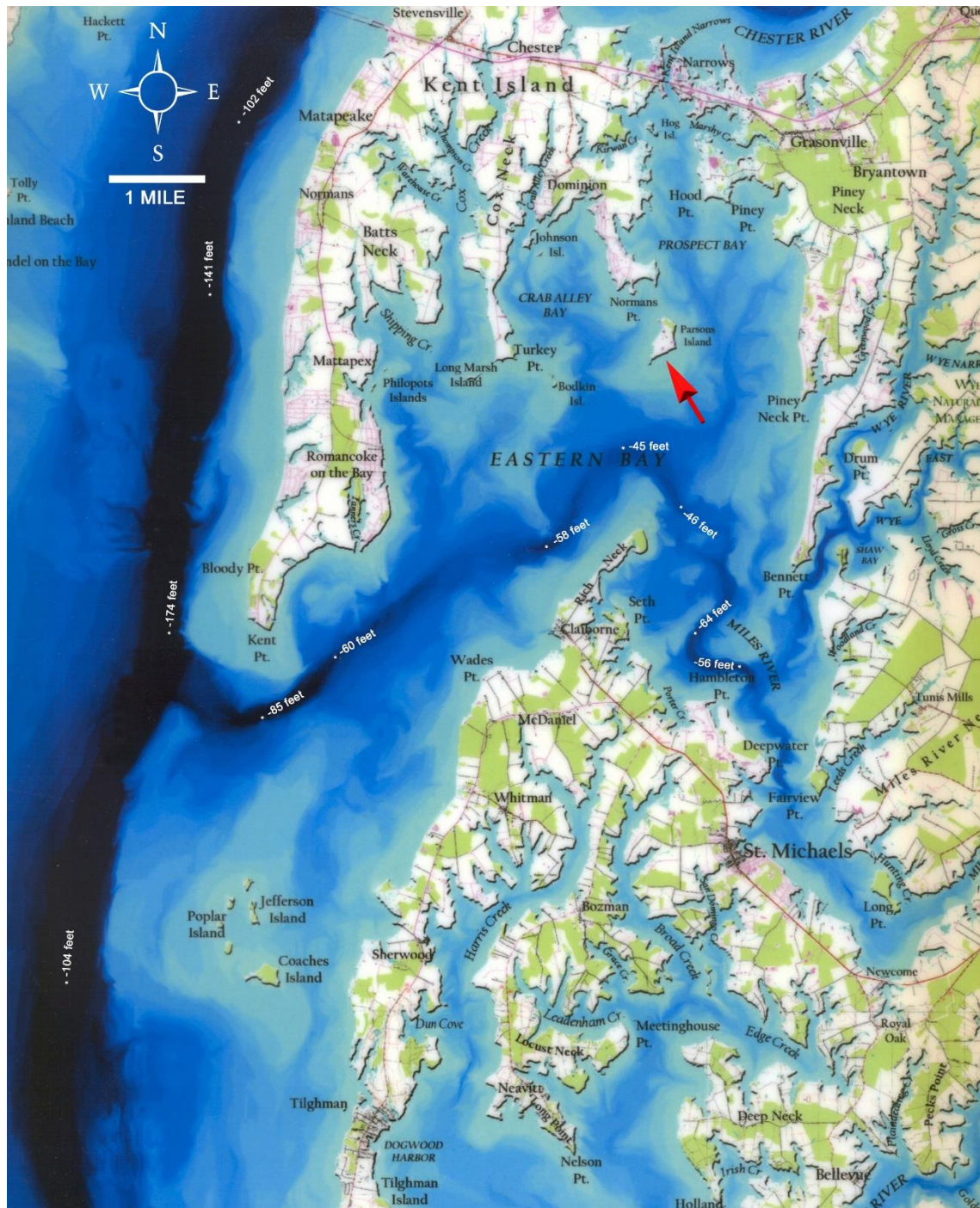


Figure 2.15. The map denotes the location of Parsons Island and accentuates the current bathymetry in the region. The approximate locations of low sea stand drainages and channels can be seen. The current depths noted in these channel or drainage areas may have been accentuated by sub-bottom tidal scouring or hidden by sediment accumulation. For example, the deepest portion of the Chesapeake Bay can be found immediately west of Kent Point. In 1970, the bathymetry map recorded its depth as being -174 feet. The current 2018 bathymetry map records the depth in the same area as being -163 feet; a net accumulation of ~11 feet of sediment in this localized area over 48 years.

2.3. Synopsis of Chesapeake Regional Paleoindian Archaeology:

Because Parson's Island was an interior upland setting when it was initially occupied, it is important to understand the regional archaeological expressions and adaptations typically associated with these early settlements; especially considering that most of the land area available to these prehistoric cultures are now beneath the bay (see Figure 2.15) or inundated on the Middle Atlantic continental shelf. The regional archaeological record associated with the Paleoindian period is rather extensive. Like much of the local prehistory, most of the tangible remains have been found along eroding shorelines, within the surface of plowed fields, or exhumed from the bay's bottom as a result of fisheries activity. However, even without good context, the Paleoindian archaeological data do provide an understanding of how the extant upland area was being utilized or exploited circa 13,000 years ago. The data associated with several sites (see Figure 2.16) will be highlighted as a method to better understand local interior upland Paleoindian adaptations in the coastal plain.

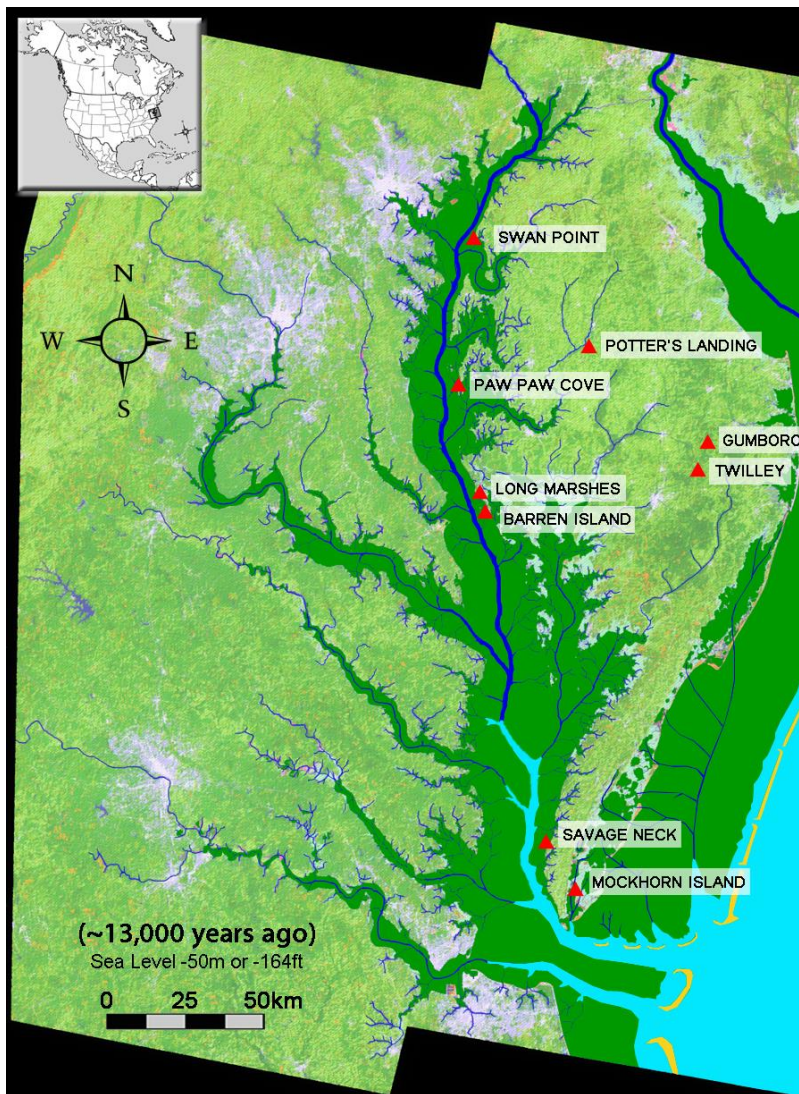


Figure 2.16. The map shows the approximate shoreline margins and drainage patterns circa 13,000 years ago. Nine Paleoindian site locations have been plotted.

Paw Paw Cove, Talbot County, Maryland:

The Paw Paw Cove site complex consists of three distinct site locations situated along the west side of Tilghman Island (Lowery 2002a). The sites are adjacent to the modern Chesapeake Bay, slightly above modern sea level, and eroded via fetch-related swash and berm zone processes. The sites are situated near a series of first-order spring-fed streams, which drained westward toward the Susquehanna River paleo-channel during the last low sea stand. The assemblages from each locality include a similar suite of stone tools. The northern locality (i.e., 18TA211a) revealed seven fluted points, three bifaces, one drill, ten scrapers, four utilized flakes, one graver, one wedge, and twenty waste flakes. The central locality (i.e., 18TA212a) revealed fifteen fluted points, fifteen bifaces, one drill, forty-nine scrapers, one hundred and nineteen utilized flakes, ten graters, ten wedges, five cores, and one waste flake. The southern locality (i.e., 18TA212b) revealed nine fluted points, five bifaces, two drills, twenty-eight scrapers, forty-seven utilized flakes, three graters, two wedges, and seven waste flakes. A few of the projectile points found at these locations were clearly made small. Whereas other points associated with these sites are highly re-sharpened, show distal-end trauma, and many include only the basal sections of a hafted fluted projectile point (see Figure 2.17 A-F). The average length of eleven complete fluted points from 18TA211a, 18TA212a, and 18TA212b is 36.01 millimeters, the width is 21.1 millimeters, and the thickness is 5.82 millimeters. Limited debitage and waste debris found at these locations suggest some retooling occurred at these locations. However, projectile point manufacturing did not occur in these upland settings. Formal flake tools, such as side-scrapers and end-scrapers are common (see Figure 2.17 H-K). Utilized flakes with rounded cobble cortex are also relatively common; suggesting some use of local secondary paleochannel lithic materials. A few of the utilized flakes were made from *outré passé* or over-shot flakes (see Figure 2.17 G) that were detached from large bifaces. In summation, most of the stone tools from the Paw Paw Cove complex seem to have been made from secondary cobbles. However, the site complex is within seven-kilometers (4.36 miles) of a major outcropping of Miocene silicified sandstone; a primary coastal plain non-cryptocrystalline lithic resource (see Lowery 2002b). Along with silica, the Miocene lithic material is rich in calcium carbonate, which degrades rapidly in acidic soils. As such, the occupants at the Paw Paw Cove site could have been utilizing the local Miocene lithic resources to make larger tools and bifaces. Any artifacts made of this material would have long ago disintegrated and reverted back to nothing more than sand particles. The extant Paw Paw Cove assemblage would imply that secondary cobble sources were an important to Paleoindians living on the Delmarva Peninsula.

A series of excavations (see Lowery 2002a) at one of the sites included within the complex have revealed buried Paleoindian artifacts lying on an eroded or truncated surface. The 13,000-year-old Clovis artifacts were excavated on a paleosol, which has been radiometrically-dated to the last glacial maximum or slightly younger. The site formation processes would imply that a period of severe upland erosion occurred during the onset of the “Younger Dryas” circa 12,800 to 12,700 years ago. The episode of erosion was followed by upland aeolian loess deposition during latter phase of the Younger Dryas circa 12,700 to 11,600 years ago. The stratigraphic sequence unearthed at Paw Paw Cove can be found throughout the western portion of the Delmarva Peninsula. The work at Paw Paw Cove and several other sites in the region imply that the upland Paleoindian artifacts and cultural deposits represent a regional lag deposit (see Lowery and Stanford 2013). Much of the Paleoindian-age archeological lag material has been buried by terminal Pleistocene-age loess (ibid). However, over the past 300 years, agriculturally-induced surface erosion and subsequent deflation has removed much of these surficial

loess deposits; especially in areas >20 kilometers (>12.5 miles) east of the current Chesapeake Bay coastline.

The Paw Paw Cove complex is significant in many respects. However, the assemblages from these three sites provide a glimpse into the Paleoindian use of upland landscapes. Each locality is situated near a drainage divide. With sea level 50 meters (i.e., 164 feet) lower 13,000 years ago, the sites were situated at the boundary between the Susquehanna River drainage to the west and the Choptank River drainage to the east. The upland drainage divides and the associated freshwater springs seem to have been a focus of hunting-related activity throughout the Paleoindian period (see Lowery 2002). Even though the types of tools discarded at each site within the complex show some consistent patterns, the artifacts found at each locality show variation in lithic material preference, display varying degrees of modification, and exhibit variable functional size-ranges. These observations seem to imply that some spring-fed drainage divide areas were episodically revisited, reused, and reoccupied as upland hunting areas over a protracted period of time. As such, the assemblages discarded or lost at each location could have slowly accumulated over decades or even centuries.

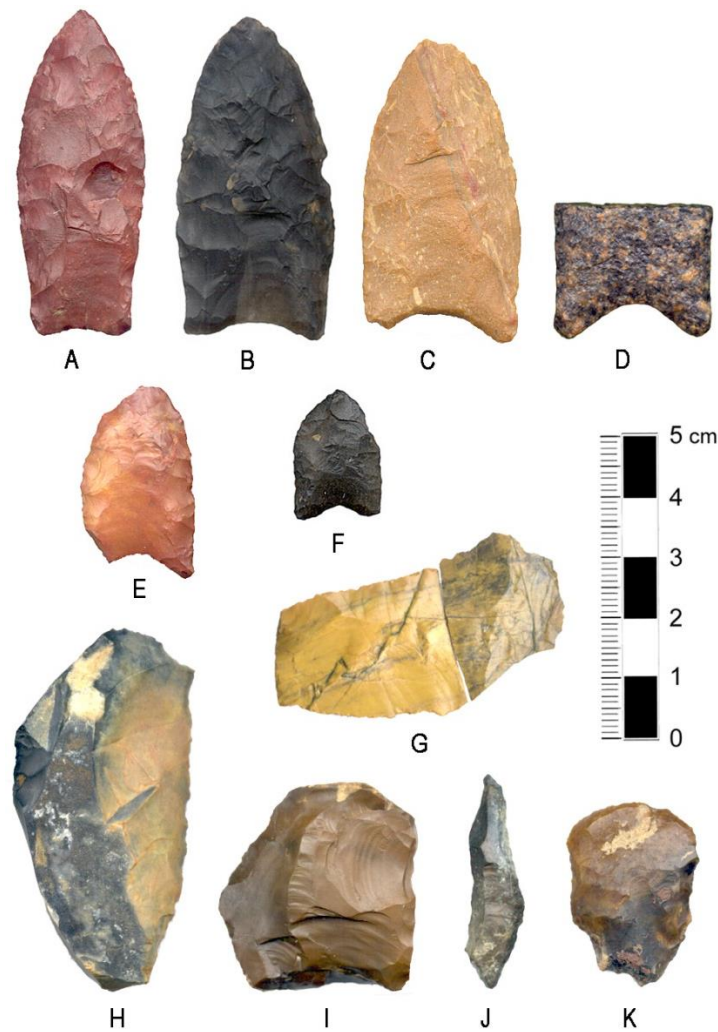


Figure 2.17. The image illustrates a small sample of the Paleoindian artifacts associated with the Paw Paw Cove site complex in Talbot County, Maryland.

Long Marshes, Dorchester County, Maryland:

The Long Marshes site (i.e., 18DO327) represents one locality within the Meekin's Neck Paleoindian site complex (Lowery and Phillips 1995) located in western Dorchester County, Maryland. The complex is situated along the modern margins of the Chesapeake Bay. The Long Marshes site is inundated and deposits are situated below modern sea level. Fetch-related wave activities have eroded the shoreline and swash and berm processes have transported the offshore archaeological remains onto the modern beaches and tidal marshes. The shoreline at the Long Marshes site has retreated between 661 meters (2171 feet) and 66 meters (261 feet) over the past 26 years. Given the fact that the site is drowned, it is hard to assess its actual geologic and geographic setting. It is presumed that the Long Marshes site was situated at the upland drainage divide of the Susquehanna, the Honga, and the Choptank watersheds, which was positioned immediately east of the main Susquehanna paleo-channel. The site may have also been associated with a series of first-order spring-fed streams. The assemblage from this locality includes an array of stone tools similar to those observed at Paw Paw Cove. Like Paw Paw Cove, projectile points represent a large proportion of the site's lithic assemblage. At present, seven Clovis points and fragmentary sections of points or fluted bifaces have been discovered (see Figure 2.18 A-G). However, the complete Clovis points from the Long Marshes site seem to be larger (see Figure 2.18 A-C), on average, than those found at the Paw Paw Cove site complex. In the sample of four complete specimens from 18DO327, the points are on average about 54.22 millimeters in length, 26.57 millimeters in width, and 6.92 millimeters in thickness. All of the Long Marshes points are re-sharpened and show some evidence of distal-end impact trauma damage (see Figure 2.18 D-E). Two basal fragments or sections have also been found at the site. Preforms and projectile point manufacturing failures are non-existent. Formal flake tools, such as side-scrapers (Figure 2.18 O), end-scrapers (Figure 2.18 L), spokeshaves (Figure 2.18 M), and graters (Figure 2.18 N) are common at the Long Marshes site. Utilized flakes are also relatively common. Most important, tools made from blades or blade-like flakes dominate the Long Marshes site assemblage (see Figure 2.18 H-K). However, no blade cores have been found. Many of the blade tools retain rounded cobble cortex on one or more edges suggesting that secondary cobbles were also important to the Paleoindian occupants at the Long Marshes site.

Most of the artifacts found at the Long Marshes site have a distinctive black or dark discoloration. One artifact from the site has iron-oxide staining on one surface and a chalky matrix (Figure 2.18 A). In contrast, the opposite face still has a marked black coloration. Another specimen found at the site has been completely corroded exposing a degraded chalky surface (Figure 2.18 E). The black exterior coloration on the artifacts is largely associated with sulfidization (Lowery and Wagner 2012); a biogeochemical process noted on artifacts exposed to anaerobic tidal marsh environments. A basal section of a fluted-drill (Figure 2.18 G) found at the site disintegrated as a by-product of rozenite crystal formation along the fissures and fractures within the rock matrix. The iron-oxide staining, rozenite crystal formation, and silica degradation noted on some specimens are byproducts of sulfuricization (*ibid*), which occurs after being dislodged from primary anaerobic contexts and exposed to aerobic conditions. Exposure to an aerobic environment can happen either in the swash and berm zone or as a curated artifact.

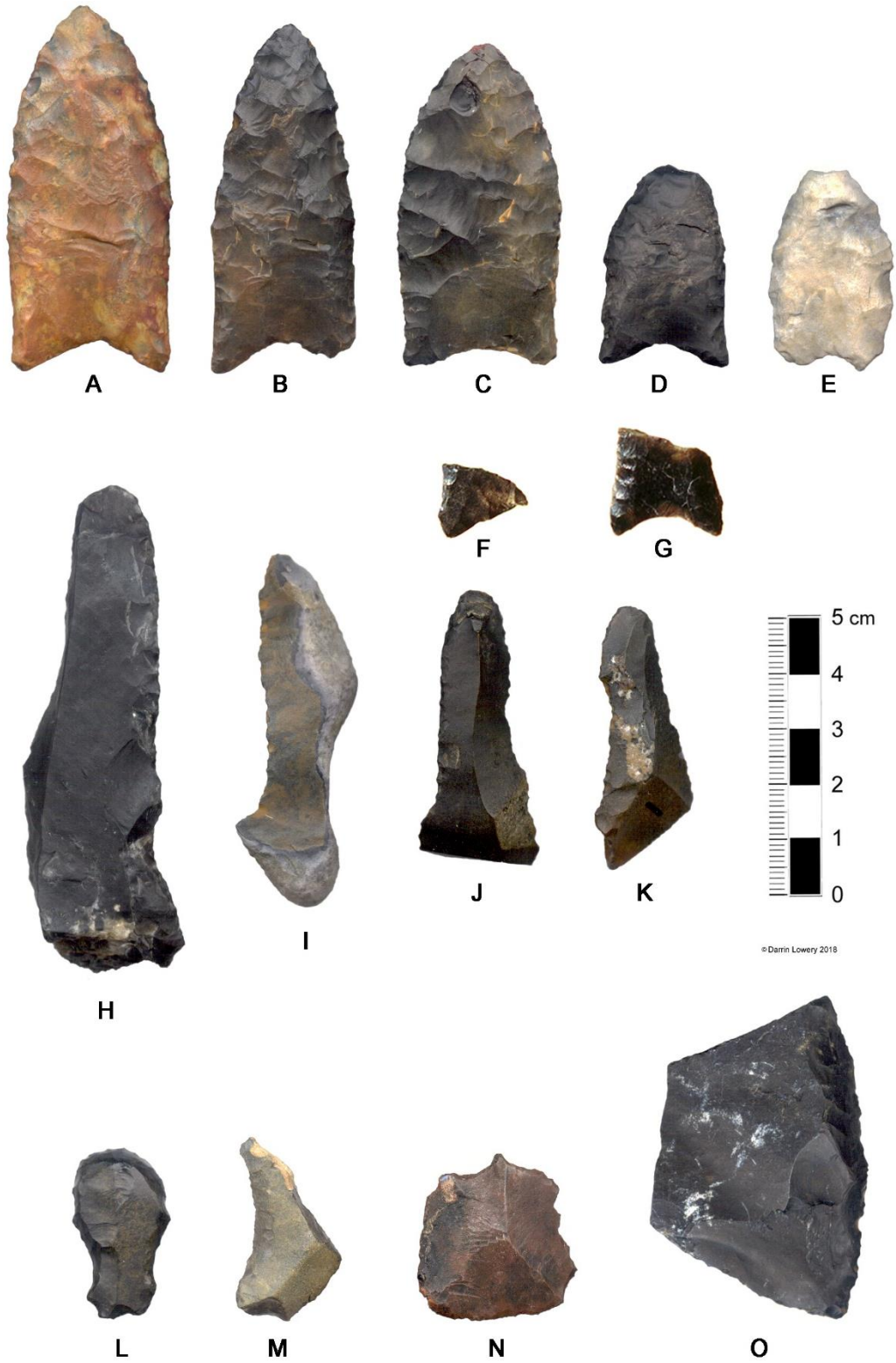


Figure 2.18. The image illustrates a small sample of the Paleoindian artifacts associated with the Long Marshes site (18DO327), which is part of the Meekin's Neck site complex in Dorchester County, Maryland.

Savage Neck, Northampton County, Virginia:

The Chesapeake Bay shoreline adjacent to Savage Neck along the southern end of Northampton County, Virginia has revealed thirteen (13) complete and broken fluted projectile points, as well as some formal unifacial tools (see Lowery 2016). Like the settings noted for both Paw Paw Cove and Meekins Neck further up the Chesapeake, 44NH435 on Savage Neck is situated near a drainage divide at a spring-fed first order stream. However, 44NH435 is located next to the mid-peninsula drainage divide; a physiographic region noted (see Custer 1989) for dense concentrations of both Paleoindian and Early Archaic-age sites. The Paleoindian archaeological remains (see Figure 2.19) found at Savage Neck were also buried by a Younger Dryas-age aeolian material (see Figure 2.20 B and C); as well as thick deposit of recent late Holocene coastal dune sediments (see Figure 2.20 A). Based on the presence of two in-situ lithic artifacts (see Figure 2.19 C and F), the Paleoindian stratum is located beneath ~80-centimeters of aeolian silt (see Figure 2.20 B), which is analogous to the Paw Paw loess noted further north along the eastern flanks of the Chesapeake Bay.

The assemblage from 44NH435 contains a diverse mixture of lithic materials, which includes jasper, chalcedony, chert, orthoquartzite, white quartz, quartzite, and mylonite. In the sample of nine complete fluted point specimens from 44NH435, the points are on average about 63.05 millimeters in length, 26.03 millimeters in width, and 8.58 millimeters in thickness. In an area which has pebble-sized secondary lithic materials and no primary lithic material, the artifacts are markedly larger than those noted at comparable-age sites further north. However, the range and quantity of tool types in the assemblage from 44NH435 is analogous to those found at northerly Paleoindian sites paralleling the Chesapeake Bay. Like the northerly sites, the assemblage from 44NH435 includes predominantly projectile points and knives (see Figure 2.19 F-I), endscrapers (see Figure 2.19 A-C), graters (see Figure 2.19 D), sidescrapers (see Figure 2.19 E and J), and little or no lithic debris indicating that stone tool manufacturing did not occur at this location.

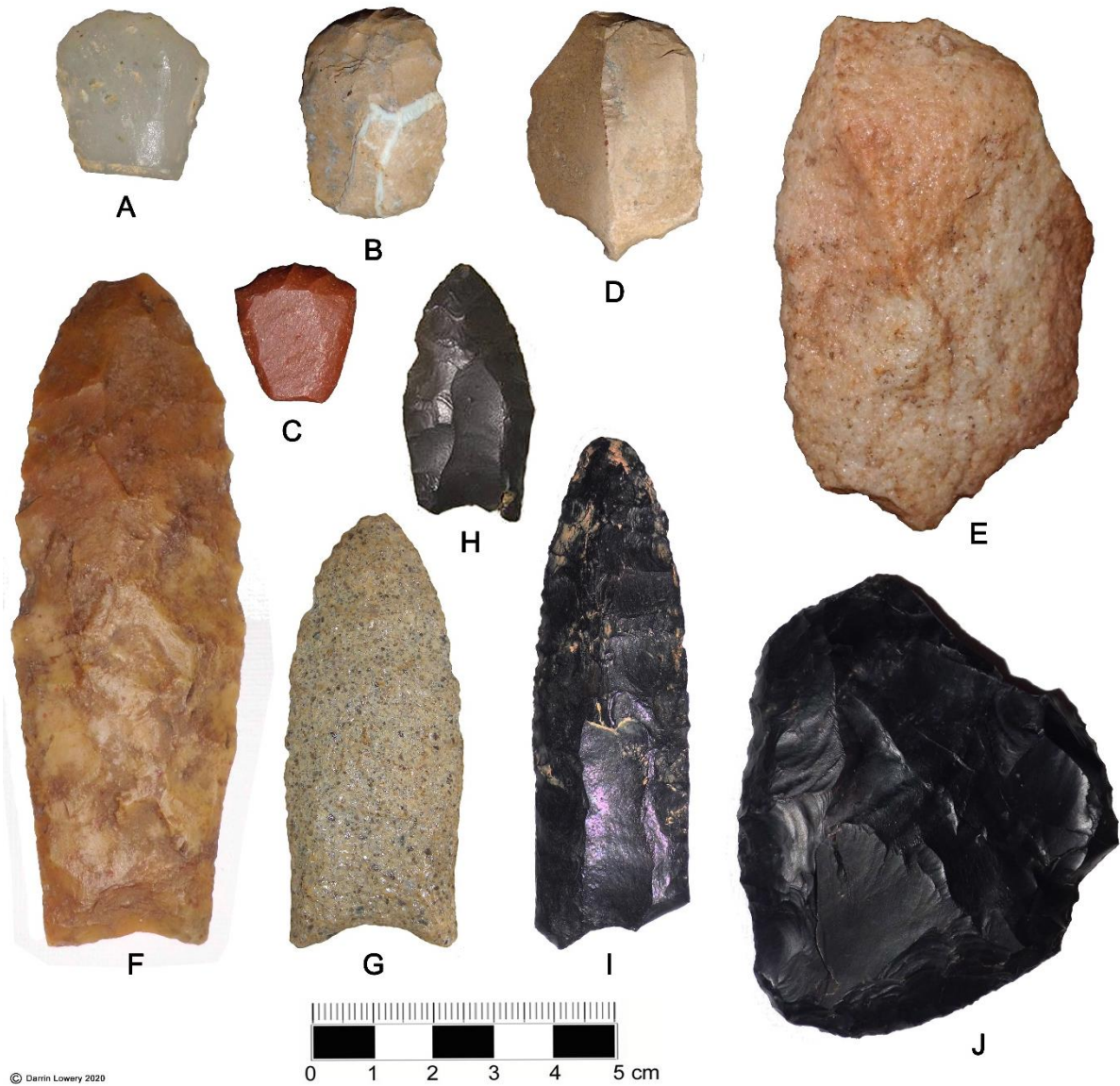


Figure 2.19. The image illustrates ten of the artifacts found at the Savage Neck site (44NH435) in Northampton County, Virginia. The assemblage in this image includes unifacial endscrapers (A-C), a unifacial graver (D), two large unifacial sidescrapers (E and J), and four fluted points or knives (F-I).

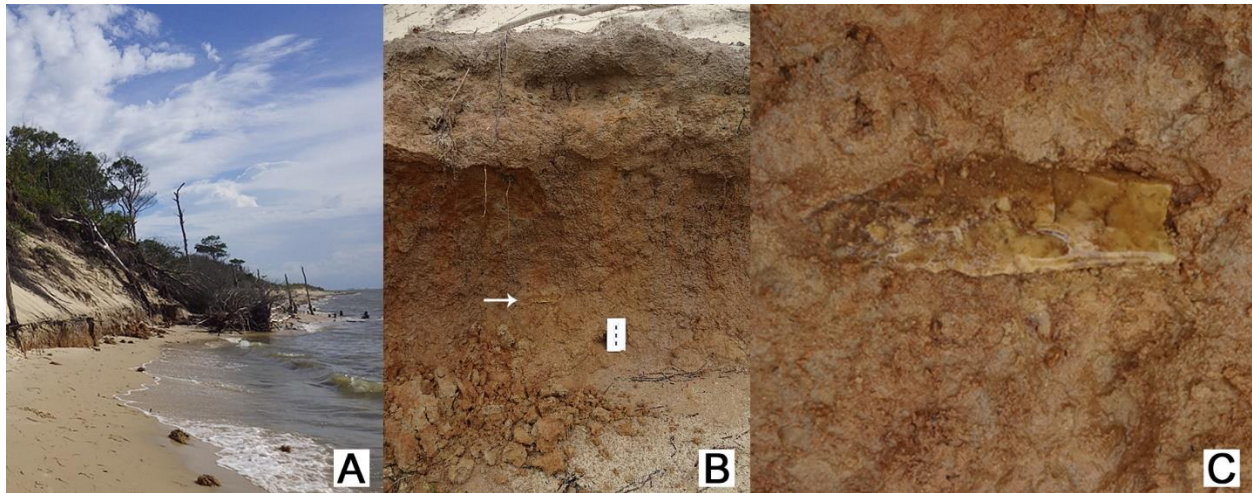


Figure 2.20. The photographs show the eroding shoreline at 44NH435 (A), the in-situ Clovis point in the bank profile (B), and a close-up image of the projectile point buried beneath loess (C).

Mockhorn Island, Northampton County, Virginia:

Mockhorn Island is situated along the Atlantic coastline of the lower Delmarva Peninsula and located immediately north of the former shoreline of the primordial Chesapeake Bay (see Figure 2.16). A series of Paleoindian sites have been found on Mockhorn Island (see Lowery 2010). Only one site (i.e., 44NH233) has been adequately tested or evaluated. The Paleoindian occupation surface at 44NH233 is inundated at high tide. Like the previously described sites, the setting associated with 44NH233 at the time of occupation was an upland located away from any active stream or waterway. There may have been some active spring or freshwater source nearby when the site was occupied.

A diagnostic Paleoindian point from the site (i.e., Virginia fluted point number 731) was first reported by McCary (1985: 4, 6, and 10). The large point (see Figure 2.21 D), which was found on September 9, 1984 by Mr. John Cowan, is made of flow-banded rhyolite stained by iron-oxides from the surrounding coastal soil. The site was initially visited and assessed by Lowery (2003a) and he noted a dense accumulation of wedges or pieces esquilles along the active shoreface. During the period between 2003 and 2010, the site location was re-visited multiple times while conducting archaeological investigations at various sites on Mockhorn Island (see Lowery 2010). The various controlled shoreline evaluations ultimately revealed the intertidal stratum, which was the primary source of the displaced and dislodged artifacts found within the swash and berm zone. Considering the logistics (see Lowery and Stanford 2013), testing was intermittently conducted at the site between 2011 and 2012. The excavations revealed an intact buried and partially drowned Clovis occupation surface. The research showed how the actions of storm surge and wave activity can rapidly transport and move artifacts.

The assemblage from 44NH233 includes knives (see Figure 2.21 A), complete and damaged projectile points (see Figure 2.21 B-J), utilized blade-like flakes (see Figure 2.21 K), a few endscrapers (see Figure 2.21 L-N), hundreds of wedges or pieces esquilles (see Figure 2.21 O-Q), spokeshaves (see Figure 2.21 R), gravers (see Figure 2.21 S-T), simple drill tips, bow drill-related paraphernalia, chipped stone adzes, and heated rounded rocks with organic residue. The organic residue on the rounded rocks

was identified as carbonized birch sap or tar. As indicated by oxidation, the rounded rocks also showed evidence of repeated heating or burning. Based on ethnographic data, Stanford et al. (2018) suggested that birch pitch may have functioned as a water-proofing agent as well as a preservative seam caulking. The heated rocks could have been used to melt the birch caulk and seal joints or seams against leakage. The use of birch tar as a mastic or adhesive has recently been documented at inundated sites dating to ~50,000 years old and associated with the Middle Paleolithic of Europe (see Niekus et al. 2019). Use-wear studies conducted on the wedges and adzes found at 44NH233 suggest extensive wood and/bark working activities also occurred (see Stanford et al. 2018). Given the region's circa 13,000-year sea level data, a shallow low salinity primordial Chesapeake estuary would have existed along the lower end of the Delmarva peninsula (see Figure 2.22). Strategically, 44NH233 was only 6.7 miles from this estuary. The site is also <1000 feet east of the low-sea stand Magothy Valley drainage, which would have afforded easy access to the primordial Chesapeake estuary. Collectively, Stanford et al. (2018) have interpreted the residues and wood-working focused assemblage found at 44NH233 as evidence that Paleoindians ~13,000 years ago may have been manufacturing birch-bark canoes to navigate the nearby estuary.

Being situated within the Atlantic coastal watershed, 44NH233 represents one of the eastern-most Clovis sites in North America. Even though 44NH233 was affiliated with a former upland, its location makes it one of the few Paleoindian-period sites that can be directly connected to a developing estuary (see Figure 2.22). The dense accumulation of wedges or pieces esquilles at this location, as compared to other sites in the region, implies that some sort of unique task was being performed at the time of occupation.

The fluted points from the terminal end of the Delmarva Peninsula reflect some interesting patterns. Considering the lack of both local primary and secondary lithic outcrops, the fluted point morphometric data for southern Northampton County, Virginia (see Figure 2.22) differ markedly than the metric data for points discovered further north. The sample of fifty-five (55) fluted-points discovered along the lower Delmarva Peninsula are markedly larger than those found at sites further north. Thirteen (13) complete specimens from lower Northampton County, Virginia (see Figure 2.22) had an average length of 69.4 mm, and average width of 27.9 mm, and an average thickness of 8.7 mm. A similar sample of thirteen (13) complete fluted points found 140 kilometers further north in far western Dorchester County, Maryland had an average length of 46.6 mm, and average width of 24.8 mm, and an average thickness of 6 mm. Finally, thirteen (13) complete fluted points found 180 kilometers north in western Talbot County, Maryland had an average length of 35.7 mm, and average width of 21.1 mm, and an average thickness of 5.7 mm. Notably, there are numerous secondary and a few silicified primary coastal plain lithic resources immediately near both the Talbot and Dorchester county fluted point clusters.

The terminal end of the Delmarva Peninsula is geologically-young and accreted ~125,000 to 100,000 years ago (i.e., MIS5) during the last high sea stand. The underlying parent geology along the lower end of the peninsula consists of bedded sand with layers of rounded pebbles, which are too small to manufacture stone tools. Therefore, all stone material used to manufacture the various tools found at Paleoindian sites along the southern Delmarva had to originate from primary or secondary sources outside of the region. The closest above sea level cobble outcrops are located ~78 kilometers (~48 miles) north of the region. With sea level ~50 meters (~164 feet) lower than today, exposures containing secondary cobbles could have been situated much closer along the margins of the low sea-

stand Cape Charles paleochannel and within the nearby Susquehanna River valley. The largest fluted points in the former uplands paralleling the eastern flanks of the former Susquehanna are situated furthest from any primary or secondary lithic outcropping and located in an area that is deprived of lithic material. The assemblages of both complete and broken fluted points found at 44NH233, 44NH435, and other small sites along the southern terminus of the Delmarva Peninsula (see Figure 2.22) indicate that some sort of local resource in this area was important to Paleoindians. Maybe the resources were associated with the developing low salinity estuary accompanying the primordial Chesapeake Bay.

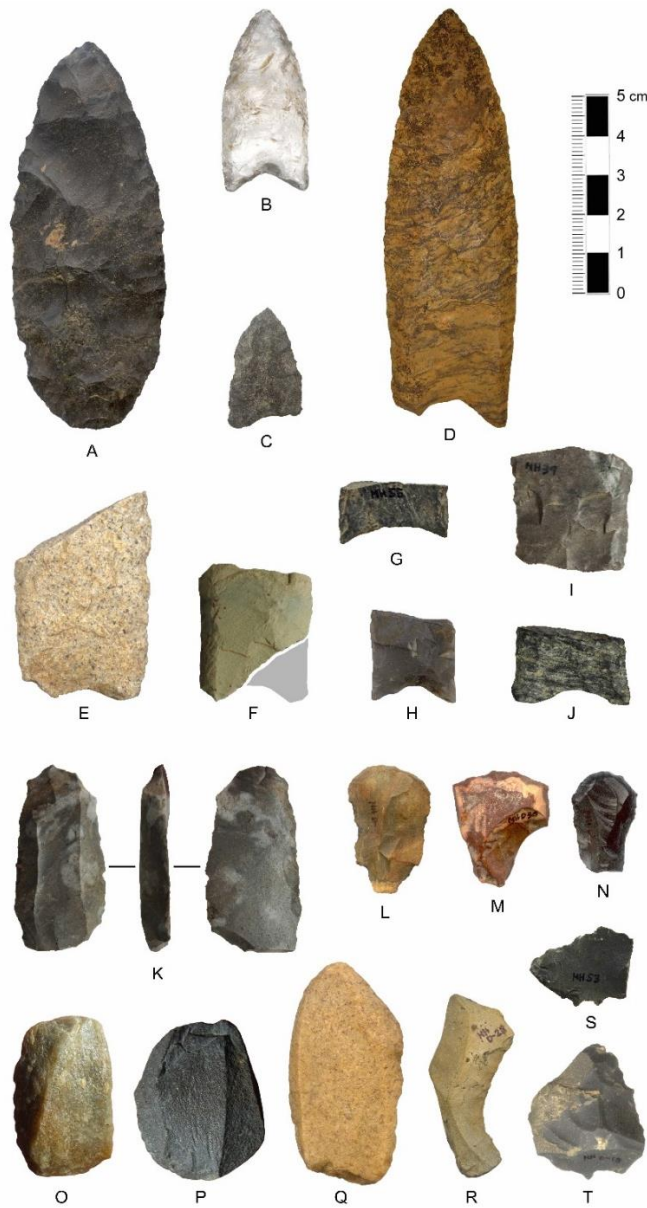


Figure 2.21. The image illustrates a representative sample of the artifacts found at 44NH233 on Mockhorn Island in coastal Northampton County, Virginia. Included is a late stage preform (A), three relatively complete points (B-D), six basal point sections (E-J), a unifacial sidescraper (K), three unifacial endscrapers (L-N), three wedges or pieces esquilles (O-Q), a unifacial spokeshave (R), and two graters (S-T).

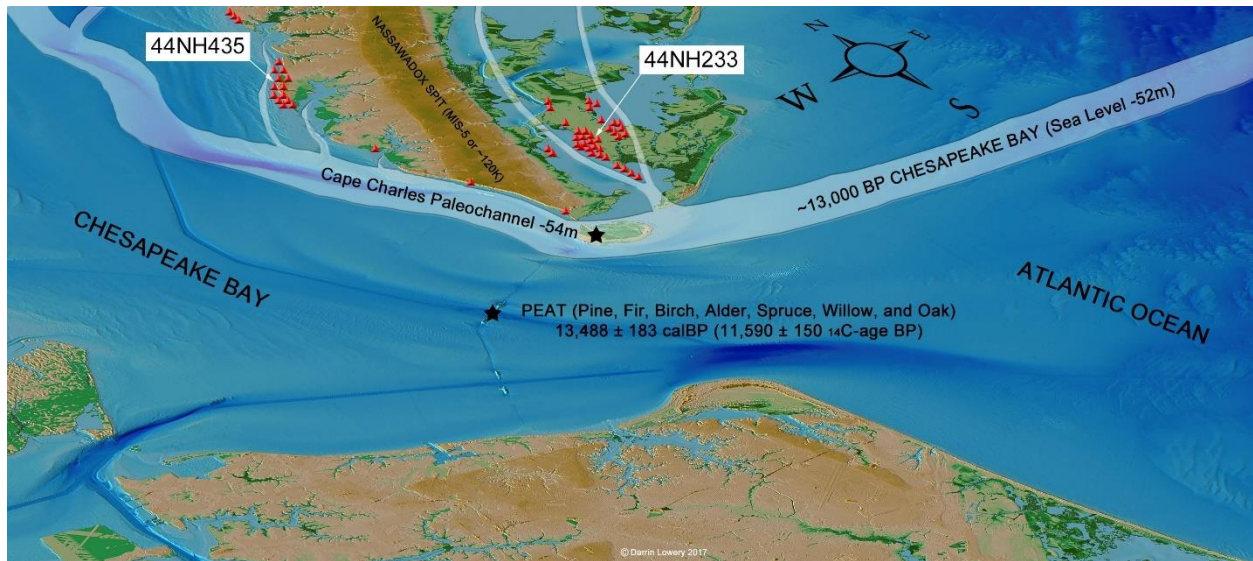


Figure 2.22. The map shows the lower end of the Delmarva Peninsula, which encompasses the southern portion of Northampton County, Virginia. All fifty-five (55) fluted point discovery locations have been plotted along with the specific site locations of both 44NH233 and 44NH435. The approximate location of the Cape Charles paleochannel, which represents the most recent drainway of the Susquehanna River, has been demarcated. The depth to the river base beneath Fisherman’s Island is noted as -54 meters (-177 feet). The regional sea level curve indicates that sea level circa 13,000 years ago was ~52 meters (-170 feet) below present. Collectively, the data would imply that a ~2.1 meters (~7 feet) deep low salinity estuary existed ~9.65 kilometers (~6 miles) south of 44NH233. From beneath the modern bay, plant remains within a ~13,500-year-old peat stratum were identified as pine, fir, birch, alder, spruce, willow, and oak.

Twilley, Wicomico County, Maryland:

The Twilley site (18WC209) represents a small interior upland Paleoindian encampment located near the drainage divide of the Pocomoke, Nanticoke, and Wicomico river watersheds in Wicomico County, Maryland. The setting encompasses a five-acre sand dune associated with Lakeland-type soils. At some time over the past fifty-years, these deposits were agriculturally-tilled. A combination of circumstances reactivated the underlying sand dune sediments causing it to migrate southward. As the dune migrated south, the site area was used by local motorcyclists and all-terrain vehicle riders as a recreational track. The artifacts associated with the Paleoindian occupation, which were originally buried, were exposed as a result of all of these combined modern disturbances.

The assemblage found at the Twilley site is interesting when the size of the eroded dune landscape is taken into consideration. Over the past two decades, the deflated five-acre sand dune has revealed eleven fluted projectile points and fragments. Seven of the fluted points consist of only the basal portions. Of the four complete points, one is 4-inches (~100 mm) in length and the other three are highly re-sharpened and less than 1.6-inches (40 mm) in length. Figure 2.23 illustrates three of the fluted points found at the site. The five-acre site has also revealed one bifacial knife made of orthoquartzite, thirty-two scrapers, and twelve utilized flakes made of chert, jasper, and chalcedony.

Interestingly, the debitage or waste flakes found at this location consist of only fifty-eight small pressure and/or billet flakes, which are probably the result of the sharpening and retooling damaged projectile points and dulled scrapers. In sum, only 114 artifacts have been found over a five-acre area.

Before the site was eroded, the buried occupation levels may have been “archaeologically invisible” using traditional shovel-testing methodologies. Even if a few pressure flakes were uncovered via traditional shovel-testing, the site may have been disregarded as “archaeologically insignificant”. Meanwhile, the five-acre dune associated with the Twilley site actually contains one of the largest Paleoindian assemblages within the central Delmarva Peninsula.

Some of the fragmentary fluted points found at the Twilley locality clearly postdate Clovis and would easily be classified as Bull Brook, Gainey, Cumberland, and/or Barnes types (see Lothrop et al. 2016). Based solely on the diverse styles of fluted points, it would seem that the Twilley site was revisited and reused as a Paleoindian hunting-camp over several centuries. The early human interest in this location seems to be directly associated with a confluence of watershed boundaries adjoining the mid-peninsula drainage divide. The character of the site’s assemblage mimics the assemblages reported from both Paw Paw Cove and Meekin’s Neck. Given the Paleoindian dataset, we can conclude that the archaeological deposits within the extant terrestrial uplands of the Delmarva Peninsula are biased towards hunting-related activities. Archaeological remains associated with the Delmarva Peninsula that characterize other facets of Paleoindian lifestyles (i.e., quarry-related sites, lithic reduction sites, riverine-oriented encampments, and coastal oriented settlements) are missing as a result of marine transgression.



Figure 2.23. The image illustrates a heavily resharpened fluted point and two projectile point basal sections found at the Twilley site in Wicomico County, Maryland.

Gumboro, Sussex County, Delaware:

Paleoindian hunting activities are emphasized at other sites found on the Delmarva Peninsula. A small poorly-drained tilled field near Gumboro, Delaware has revealed three fluted projectile points (see Figure 2.24) made of jasper. The site assemblage is suggestive of a Paleoindian kill site. Each of these projectile points shows marked impact trauma along the distal end and all three were all found within a tight cluster situated within a larger tilled-field area.

Unlike the dry sand dune setting associated with the Twilley site in Maryland, the Gumboro locality is situated in a low basin that, until recently, retained water throughout the year. The area, which once included a bald cypress swamp, was channelized and drained in the early-20th century for agriculture. As such, the plowed area associated with the site currently has a dark Ap soil horizon and gleyed sub-soil deposits. The three projectile points all have an oxidized surface staining. The staining may represent a geochemical byproduct resulting from the site's current seasonal wet and dry conditions in tandem with the tannic acid rich-environment once associated with the bald cypress swamp.

Repeated examinations of the poorly-drained tilled field associated with the Gumboro site have produced no associated stone tools or debitage. The lack of tools and waste debris signify that the site was not an encampment. The damage to each point and the tight clustering would be characteristic of projectiles that were used and lost during a single hunting event. Given the acidity of Delmarva's soils, bone preservation in these settings is uncommon. Several decades ago, a weathered and oxidized fragment of a Columbian mammoth (*Mammuthus columbi*) tooth was found in the same area of the field. On November 1st, 2013, the Gumboro mammoth tooth fragment was submitted to Dr. Jonathan Lothrop, Curator of Archaeology, and Dr. Robert Feranec, Curator of Pleistocene Vertebrate Paleontology at the New York State Museum. The goal was to determine its age relative to the circa 13,000-year-old diagnostic artifacts found nearby. However, repeated attempts failed to extract enough collagen to provide an age estimate and assess if the mammoth remains were contemporaneous with the Clovis points.

The Gumboro assemblage implies that the site represents a hunting/kill locality. The assemblages from several bona fide Clovis hunting/kill sites support this assumption. At the Naco site in Arizona for example, the remains of a Columbian mammoth were uncovered and it was associated with eight Clovis points (see Haury 1953). Most of these points had distal impact trauma. The lack of associated butchering tools and the articulation of the skeleton suggested that the Naco mammoth had escaped after being hunted. At the Domebo site in Oklahoma (see Leonhardy 1966), three Clovis projectile points, a point mid-section, and two flake scrapers were unearthed in association with a disarticulated mammoth skeleton. Two of the Domebo points and the mid-section fragment also showed definitive impact damage. In the east, five fluted bifaces and a fragment of an endscraper were found with the bones of a mastodon at the Hiscock site in New York (see Laub 2002). Interestingly, the complete points had a distinctive edge notching analogous to the largest point found at the Gumboro locality. Minus the bone preservation, the Gumboro site assemblage is similar in many respects to assemblages from both the Naco and Domebo sites. However, unlike Domebo, no flake tools or scrapers have been uncovered at the Gumboro site. As such, the Gumboro assemblage may represent an escaped kill.



Figure 2.24. The image illustrates the entire lithic assemblage associated with the Gumboro site in Sussex County, Delaware.



Figure 2.25. The image shows a section of a Columbian mammoth (*Mammuthus columbi*) tooth unearthed via plowing at the same location as the Gumboro site fluted point assemblage (see Figure 2.24).

Potter's Landing, Caroline County, Maryland:

In the mid-20th century, Mrs. Henry Wright of Williston, Maryland uncovered three Clovis points (see Figure 2.26) in a tilled field near Potter's Landing (Brown 1979). The field is located on a dry river terrace adjacent to the Choptank River in Caroline County, Maryland. The Clovis points are made of diverse lithic materials, which included jasper, chert, and patinated chalcedony.

The assemblage from Potter's Landing suggests a hunting/kill site. Like the specimens found at the Gumboro site in southern Delaware, the Clovis points from Potter's Landing all have damage associated with impact trauma. According to Mrs. Wright, the fluted points were found within a small

concentrated area of the tilled field. No bone and no additional lithic artifacts were uncovered. The lack of bone is a result of the dry setting and the low pH associated with the region's soils. In comparison to the highly curated and resharpened points typical of hunting encampment sites on the Delmarva Peninsula, the Clovis points found at both the Gumboro site and the Potter's Landing site are comparatively large. The size would suggest that the points at both localities were probably lost before the end of their effective use-life.

Isolated Finds:

The bulk of the fluted points found on the Delmarva Peninsula consist of isolated finds (see Figure 2.27). As a general category, these finds may indicate additional hunting-related base camp localities or the locations of other hunting/kill sites. The isolated finds could also represent nothing more than the "end point" of a projectile trajectory. Regardless, very few of the isolated find locations (see Brown 1979) have been subjected to follow-up investigations. The meaning of these locations, with respect to Paleoindian settlement patterns, is therefore largely unknown.

In summation, we can confidently state that virtually all of the extant terrestrial Paleoindian sites on the Delmarva Peninsula can be linked to upland-related hunting activities. The biases towards upland hunting activity are probably the result of post-Pleistocene sea level rise and its impact on the Paleoindian archaeological record associated with the drowned valleys within the Chesapeake Bay and on the continental shelf.



Figure 2.26. The image shows three fluted points with impact damage found in the plowzone at the Potter's Landing site along the eastern terrace of the Choptank River in Caroline County, Maryland.

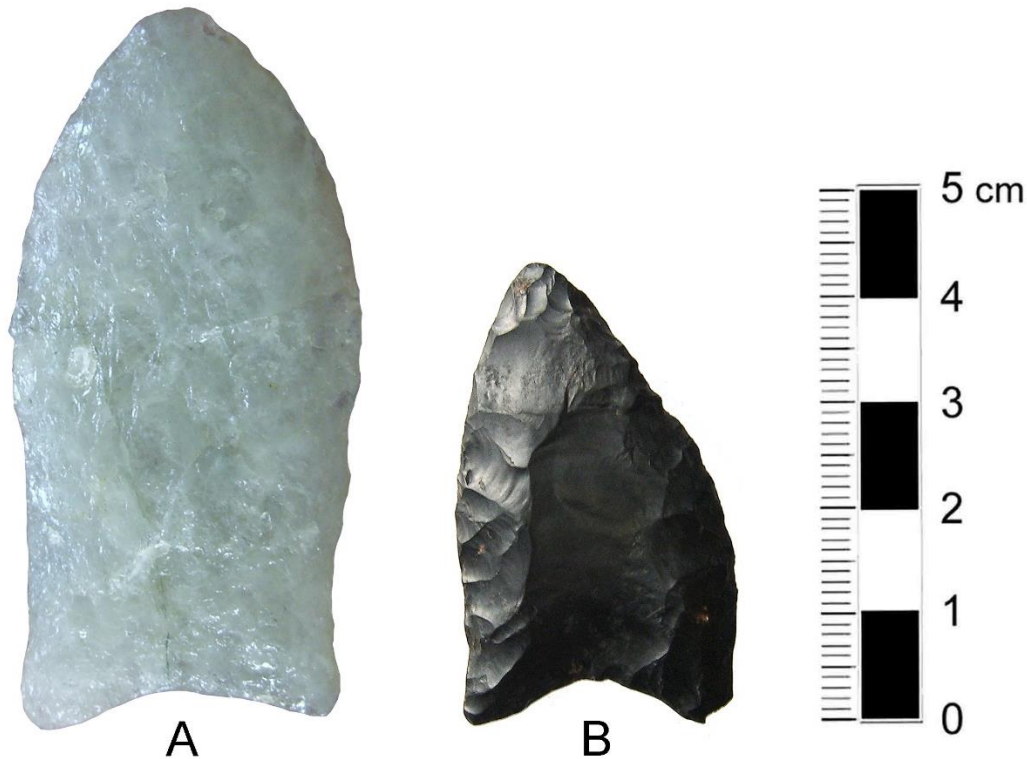


Figure 2.27. The image shows a quartz Clovis point (A) found along the shoreline at Barren Island in Dorchester County, Maryland. The dark chert or sulfidized jasper fluted point (B) was exhumed from the bottom of the Chesapeake Bay off of Swan Point in western Kent County, Maryland. The asymmetrical re-sharpening evident on the Swan Point specimen (B) suggests that it was re-tooled while hafted.

2.4. Synopsis of Chesapeake Regional Pre-Clovis or Paleo-American Archaeology:

Because Parson's Island has what seems to be a Paleo-American human occupation pre-dating the time frame of when people are suspected to have arrived in the America's (see Lothrop et al. 2016), it is important to provide a synopsis of the archaeological sites in the region that have revealed suggestive evidence for a pre-14,000-year human presence in the Middle Atlantic. The sites outlined below have been subjected to varying levels of research, survey, excavation, and investigation.

Cactus Hill, Virginia:

The Cactus Hill site was initially investigated and reported by Joe and Lynn McAvoy (see McAvoy and McAvoy 1997 and 2015). The site is a multi-component site, which has revealed continuous human occupations spanning the Paleoindian through Woodland periods. The setting encompasses an aeolian dune ridge situated near the Nottoway River in southern Virginia. Most importantly, the site has revealed a dated Clovis occupation surface. Five AMS dates on this Clovis occupation zone suggest an age between 12,717 to 13,102 calibrated calendar years before present for the early Paleoindian occupation at the Cactus Hill site. Beneath the Clovis surface, the McAvoy's (Ibid) unearthed a Pre-Clovis occupation zone containing small lanceolate triangular points, blade cores, and blades. The

associated age estimates for the Pre-Clovis occupation stratum at Cactus Hill suggest the site was initially occupied sometime between 18,037 to 22,277 calibrated calendar years ago.

The technological attributes expressed by the Pre-Clovis assemblage at Cactus Hill is reminiscent of being an antecedent to the Clovis stone tool technology in the region. However, the Clovis and the Pre-Clovis assemblages have an age difference spanning approximately 5,000 years. More importantly, only a few prehistoric assemblages spanning the four to five millennia time gap have been reported in North America (see Waters 2019) and most of these sites are less than 15,000 years old. At Cactus Hill, the vertical separation between the Clovis and Pre-Clovis assemblages varies between 7 to ~20 centimeters. Cactus Hill does offer supporting data, which implies that human colonizers had reached the Middle Atlantic region a millennium or two following the last glacial maximum. Interestingly, the current interpretation of the genetic data would imply that sometime between ~22,000 and ~18,100 ago ancient Beringians branched from the ancestral indigenous Americans (ibid). However, most researchers believe that these initial colonizers were confined to Alaska for several millennia until (see Tamm et al. 2007) ~16,000 or more years ago and then passed through the ice-free corridor or along the west coast thus spreading throughout both North and South America.

Meadowcroft Rockshelter, Pennsylvania:

The excavations and discoveries made at Meadowcroft Rockshelter have taken on an aura of “myth” and “legend” in both the professional and academic community. The site was meticulously excavated by Dr. James Adovasio and his students in the 1970’s and 1980’s (see Adovasio et al. 1977, 1980, 1990, and 1991). Like Cactus Hill, the site had multiple occupations spanning the region’s entire prehistory. Meadowcroft Rockshelter also produced a small lanceolate point, small prismatic blades, a knife-like flake tool, and other lithics excavated near a dated hearth feature.

The small lanceolate (i.e., Miller) point (see Figure 2.29) was excavated at 46 centimeters within the middle of stratum A1 and associated with a roof spall event. The point was found with thirty other lithic artifacts on an occupation floor. McConaughy (1999) noted *"There is at least one very well-defined basin-shaped hearth that was reused over a period of time. It was composed of alternating layers of charcoal and burned earth. The lanceolate projectile point, named the Miller Lanceolate, was found near this hearth"*. The radiometric date on this hearth was reported in the 1970’s as 11300 ±700 radiocarbon years before present. At the time the site information was being published, researchers did not fully understand the marked discrepancy between radiocarbon years and real calendar years. Even at the time, the resultant radiocarbon date had a large error or standard deviation of plus or minus 700 years. Given our current understanding of radiocarbon calibration, we can better understand and critically evaluate the radiocarbon ages for Meadowcroft Rockshelter. When calibrated, the radiocarbon age for the hearth and presumably the associated lithic assemblage from middle stratum A1 could be as young as 12,316 years old (post-Clovis or Middle Paleoindian) or as old as 14,242 years old (Pre-Clovis or Paleo-American). Technologically, the Meadowcroft assemblage could be reflective of a Pre-Clovis or Paleo-American tool kit; but it could also be analogous to later Paleoindian tool kits, as well. All dated late Pleistocene-age strata from Meadowcroft Rockshelter have very large standard deviations. The errors can vary from as low as ±165 radiocarbon years to as high as ±2400 radiocarbon years. By today’s standards, these radiocarbon age results would be unacceptable. In sum, the site should be re-dated using current radiocarbon and/or AMS laboratory procedures (see Lothrop et al. 2016).

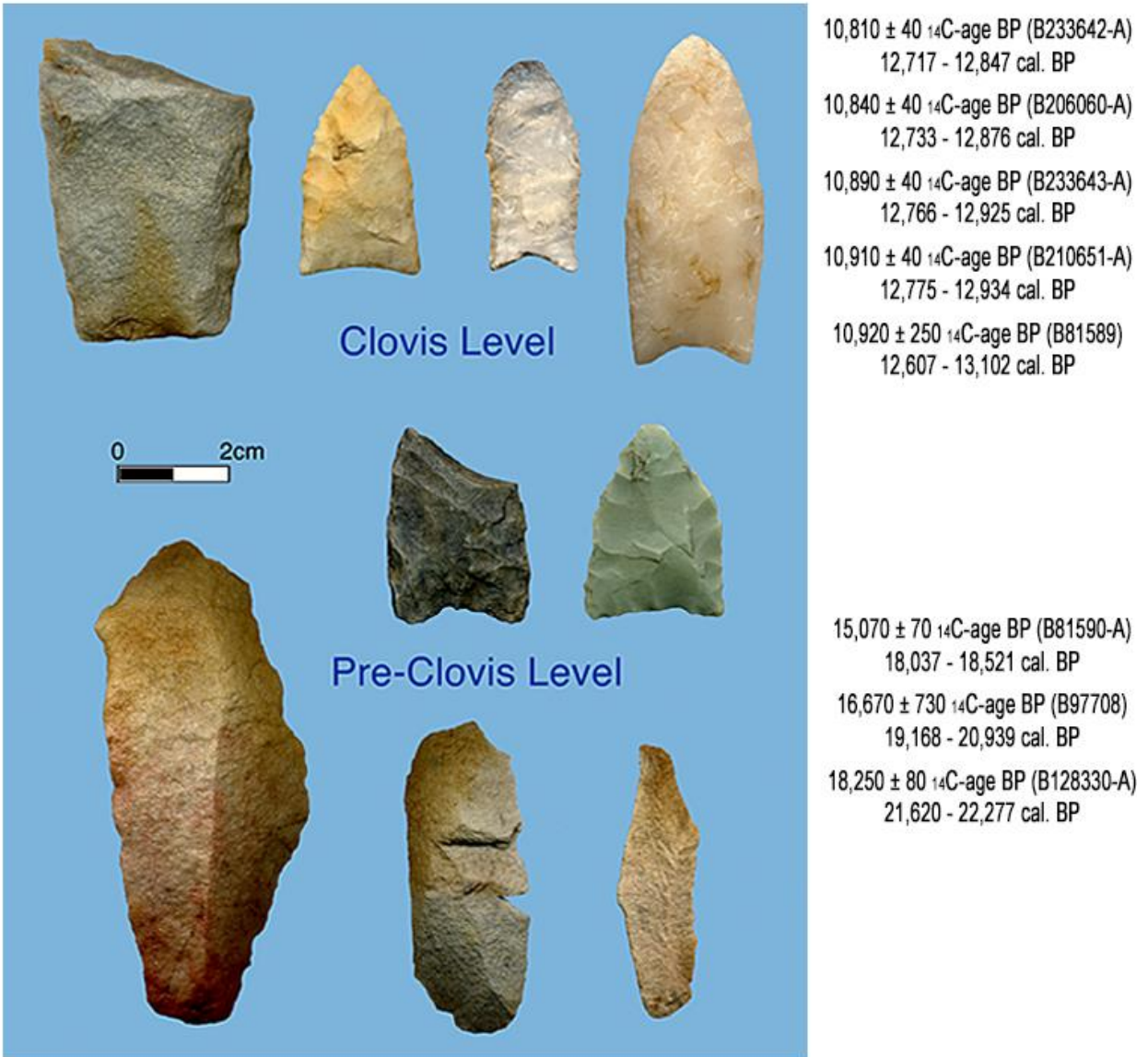


Figure 2.28. The image shows a representative sample of the Clovis and Pre-Clovis artifacts (left) found at the Cactus Hill site in Virginia. The associated AMS age-estimates for these two discrete cultural occupations are also portrayed (right).



Figure 2.29. The image shows the Miller point unearthed at Meadowcroft Rockshelter in western Pennsylvania. Based on associated radiometric estimates, the point could be 14,242 years old or as young as 12,316 years old; an age range spanning almost 2000 years.

Miles Point, Maryland:

The Pre-Clovis or Paleo-American discoveries made at Miles Point were found along an eroding shoreline margin. The Miles Point property was investigated between November 2006 and January 2007 as part of a mandated cultural resource management study (see Lowery 2007), which was required by the Maryland Historical Trust. While conducting this research, an artifact concentration was exposed along the shoreline near the base of a buried paleosol surface. This cluster consisted of an in-situ quartzite anvil, a wedge, two blade-like flake tools, and a hammerstone (see Figure 2.30). As the shoreline continued to erode, additional artifacts were found in-situ within the same buried stratum. Other stone artifacts were found nearby, but eroded out of context, along the active shoreface. A similar buried surface had been radiometrically-dated only at a few locations in the region. The collective data at the time implied the in-situ artifacts at Miles Point were greater than 13,000 years old. Earlier research conducted at nearby Paw Paw Cove (see Lowery 2002a) also suggested that the cultural material exposed along the shoreline at Miles Point was stratigraphically and chronologically older than Clovis.

The buried stratum containing the stone artifacts was initially dated to $21,490 \pm 140$ ^{14}C -yrs BP or $25,613 \pm 385$ calBP (Beta -236977). However, three additional AMS dates (see Figure 2.31) generated on charcoal for the same zone produced much older age estimates ranging from $25,670 \pm 160$ ^{14}C -age BP or $30,742 \pm 365$ calBP (Beta -248315), $26,920 \pm 230$ ^{14}C -age BP or $31,687 \pm 198$ calBP (Beta -239559),

and $27,240 \pm 230$ ^{14}C -age BP or $31,911 \pm 181$ calBP (Beta -239558). Collectively, the AMS-dates generated on carbon within the thin ~19-centimeter buried surface at Miles Point span approximately seven thousand years. No modern analog for this situation is known. Scanning electron microscopic (SEM) analyses of the organic carbon within this zone revealed carbonized wood identified as spruce, pine, fir, and "krumholtz" yellow birch. The helical cellular structure of the yellow birch wood suggests a very windy and cool environment. Phytoliths within the Tilghman soil at Miles Point are also indicative of an upland setting containing cool and dry-adapted C3 grass species. Surprisingly, the SEM analyses of the Tilghman soil at Miles Point revealed mammalian hair fragments (see Figure 2.33). Two strands were identifiable as belonging to the family Canidae (see Figure 2.33A). Another strand belonged to the family Felidae (see Figure 2.33B). As evident by the coatings of clay films, the hair fragments are indeed ancient and not modern contaminants.

At Miles Point, the Tilghman Soil formed within and on the surface of a loess. To evaluate the timing of this earlier loess deposition, optically-stimulated luminescence (OSL) ages were generated for the underlying silt stratum within and beneath the buried paleosol. OSL age estimates suggest that aeolian loess deposition had ceased prior to $27,940 \pm 1635$ yrs. BP (UIC2020BL) and/or circa $29,485 \pm 1720$ yrs. BP (UIC2019BL). The initial onset of loess deposition in this earlier aeolian stratum began approximately 40,000 years ago. The onset age is based largely on three consistent OSL ages of circa $40,895 \pm 2370$ yrs. BP (UIC2013BL), $41,090 \pm 2360$ yrs. BP (UIC2012BL), and $40,570 \pm 2670$ yrs. BP (UIC2011BL) at or near the base of the loess stratum. Lowery et al. (2010) have termed the MIS 3 aeolian stratum in the region the Miles Point loess. The Miles Point loess pre-dates the terminal Pleistocene Paw Paw loess by approximately 28,000 years.

The combined geoarchaeological and stratigraphic investigations at both Paw Paw Cove and Miles Point provide insights into the region's upland late Pleistocene stratigraphy. However, the range of radiocarbon dates for the 19-centimeter-thick Tilghman soil at Miles Point causes some concern. The Miles Point dates would seem to imply that, unlike today, organic terrestrial carbon circa 20,000 to 30,000 years ago was not decaying, breaking down, or being naturally recycled. With respect to organic carbon in cold environmental settings, recent research (see Pastor et al. 2020) has shown that soil temperature, moisture and active layer depth, have strong effects on soil microbial processes and the breakdown of carbon. Individual flecks of terrestrial carbon (see Figure 2.32) within the Tilghman soil were too small to provide individual AMS dates. Therefore, it was necessary to pool carbon flecks to provide an adequate sample size for AMS dates. In doing so, old residual carbon and young carbon from the same horizon could have easily been mixed, resulting in an inadvertently averaged age. Therefore, the true age of the artifacts lying just below this horizon remains equivocal. Broad typological similarity to the artifact assemblage exposed on Parson's Island suggests that these are related components of about the same age, but at face value, the Miles Point artifacts would be 3,000 to 12,000 years older. This disparity is improbable. With regard to speculation concerning a relationship to the Cantabrian Solutrean (see Stanford and Bradley 2012), an age of 32,000 years would place the Miles Point assemblage 6,000 years before the oldest known Lower Solutrean sites in Europe. The younger date of 25,000 years old would, nevertheless, make the assemblage contemporaneous with Cantabrian Solutrean (Ibid).

The work at Miles Point does, however, offer the potential for a future avenue of research in an area with generally poor preservation of late Pleistocene faunal remains. The presence of preserved hair (see Figure 2.33) in tandem with the recent advances in DNA research may afford the ability to

determine the genus and species associated with the ancient hair fragments encapsulated within buried paleosols; like the Tilghman soil.

The 2007 cultural resource management report suggested testing be conducted immediately behind the shoreline near the actively eroding and in-situ artifact concentration. A State and Federal permit application, which mandated the initial archaeological survey, proposed that the shoreline area at Miles Point be graded, the offshore area was to be filled, and the shoreline would be stabilized with granite rip-rap. It was hoped that testing could be conducted near the artifact concentration before these alterations and disturbances to the site area would occur. However, the state compliance reviewer mandated that no additional archaeological investigations were required under the premise that the stabilization would “preserve the site in place” (see Lowery 2007, Appendix I: 89-92). As a result, no additional archaeological investigations were conducted inland or immediately adjacent to the in-situ artifact cluster at Miles Point. Four years would pass before the shoreline area was ultimately stabilized and during the forty-eight-month period coastal erosion continued to dislodge artifacts from the Tilghman soil. An attempt was made by faculty at the Smithsonian to sieve the sediment immediately in front of the eroding bank profile to salvage any dislodged artifacts. The Maryland State terrestrial archaeologist mandated that a Maryland Department of the Environment permit, as well as an Underwater Archaeology permit would be required. Before these permit applications were reviewed, the state and federally-permitted stabilization, filling, and grading activities had begun along the shoreline at Miles Point. As a result, no additional artifacts were salvaged from this site. Grading, fill, and granite rip-rap have permanently altered the natural landscape, rendering future investigation problematic at best.

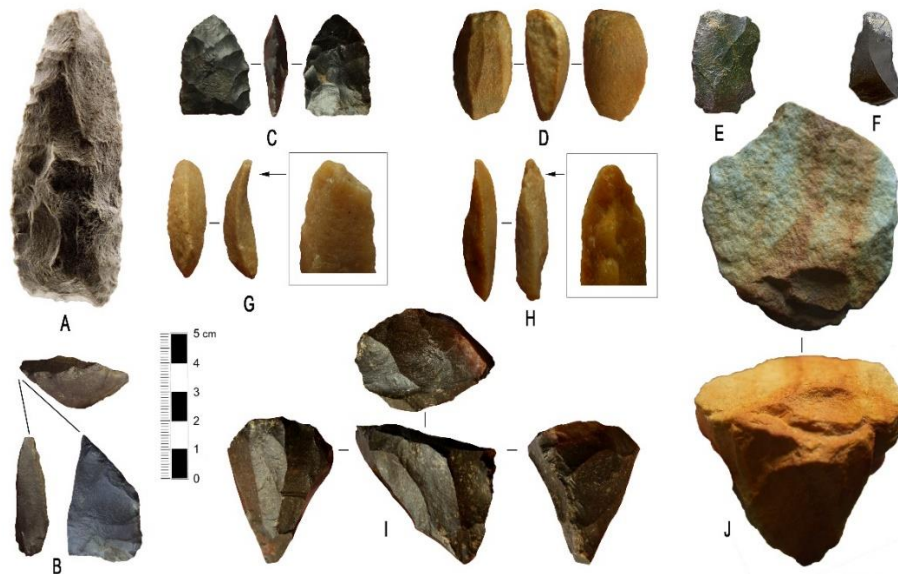


Figure 2.30. The image shows most of the artifacts found at Miles Point located near St. Michaels, Maryland. The assemblage includes a silicified Miocene sandstone knife (A), a fractured chert biface fragment converted to a burin (B), a small chert lanceolate point (C), a quartzite wedge (D), two chert utilized flakes (E and F), two small utilized quartzite blades (G and H), a small chert polyhedral blade core (I), and a quartzite polyhedral blade core (J). Some of the artifacts (C-D, and G-I) were found in-situ within the buried surface along the eroded shoreface. Other artifacts (A-B, E-F, and J) were found eroded out of context near the in-situ artifact bearing stratum.

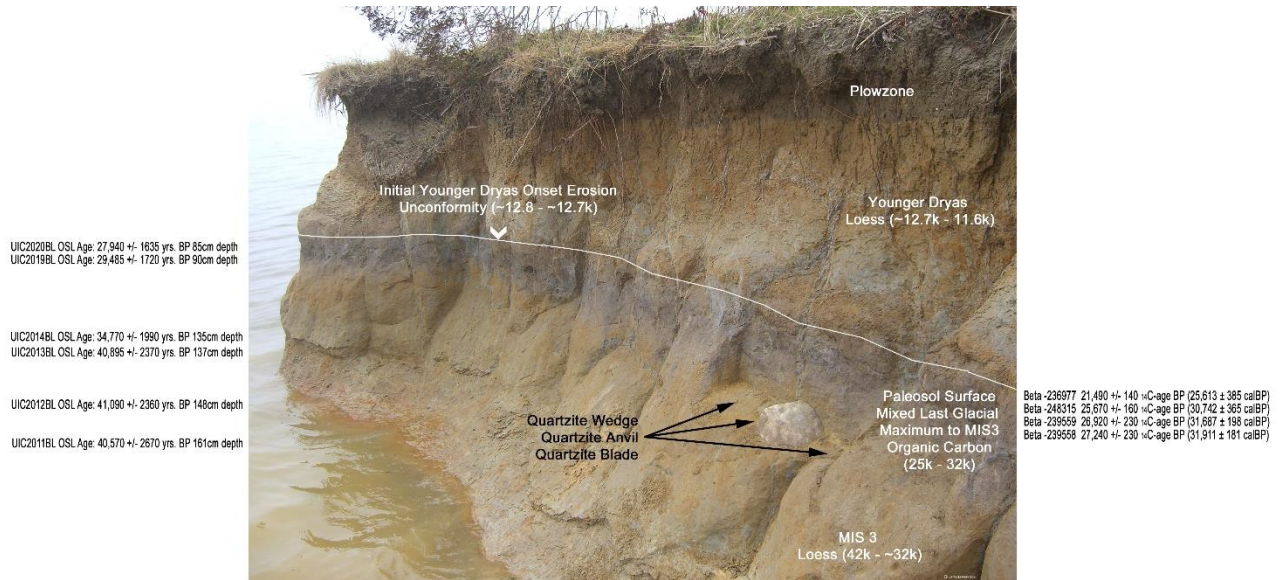


Figure 2.31. The photograph shows the eroding shoreline at Miles Point with the in-situ anvil still in place. The locations of the in-situ wedge and quartzite blade are also delineated. The various radiometric and OSL ages generated for each stratum are also indicated. Regionally a middle to late Younger Dryas age loess (Paw Paw loess) envelopes an eroded and truncated surface. The erosion of this surface is indicated by a lag of Clovis-age (circa 13,000-year-old) artifacts lying unconformably on a much older (circa $17,820 \pm 170$ radiocarbon years BP or $21,358 \pm 415$ calibrated years BP) paleosol at nearby Paw Paw Cove. At Miles Point, however, the paleosol surface (i.e., Tilghman soil) has revealed environmental carbon, which has produced a series of AMS-dates spanning 25,000 to circa 32,000 years old; roughly 7,000 years. The in-situ artifacts at Miles Point have been found within this 19-centimeter thick Tilghman soil surface. Phytoliths and wood charcoal associated with the Tilghman soil indicate an environment containing cold-adapted grasses, spruce, pine, fir, and "krumholtz" yellow birch; indicative of an intense winds. The Tilghman soil formed in an earlier loess (Miles Point Loess) deposited sometime between $\sim 42,000$ and $\sim 32,000$ years ago.

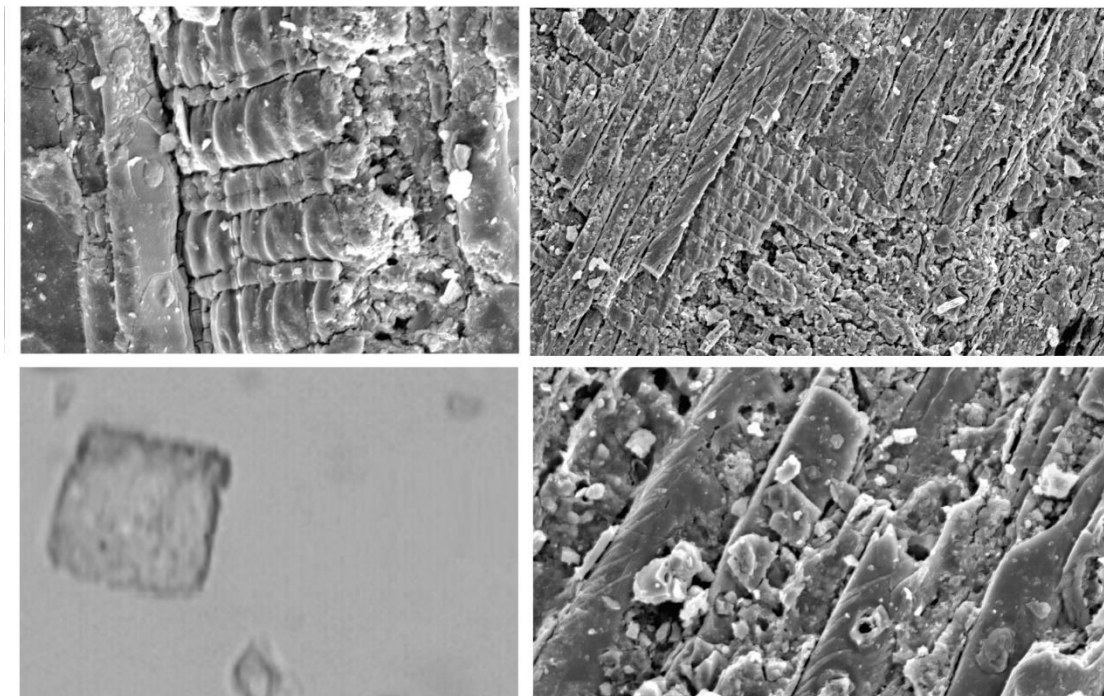
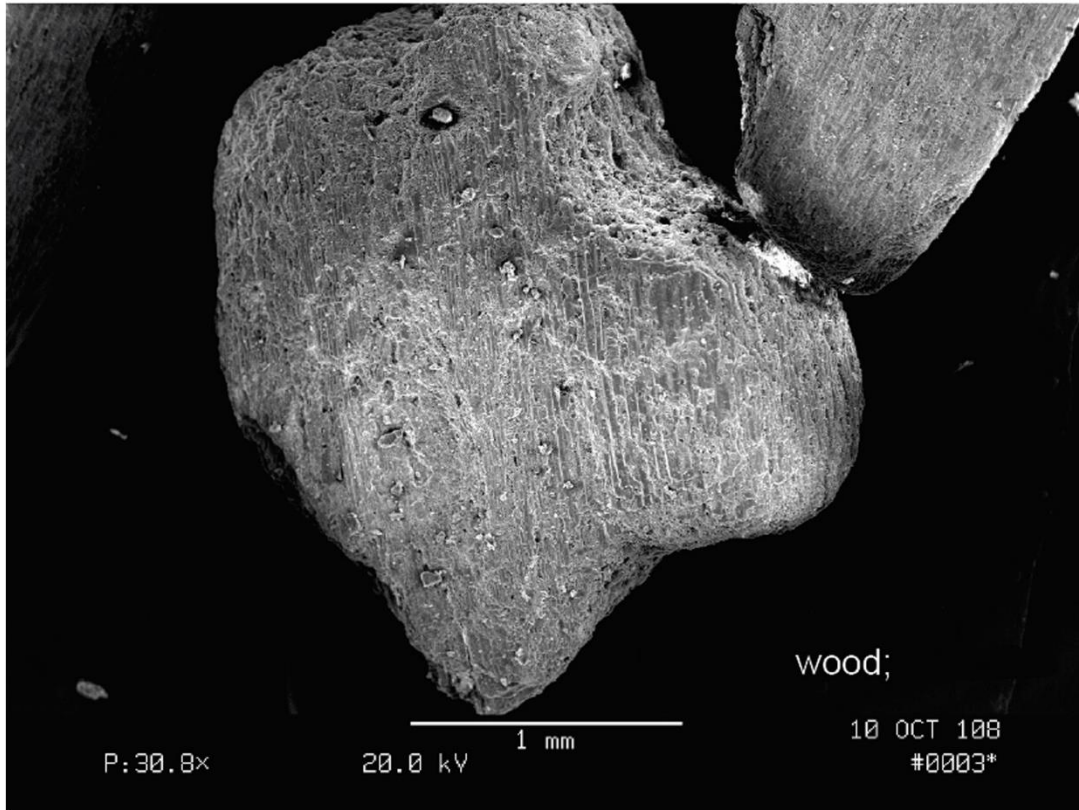


Figure 2.32. The scanning electron microscopic images show the arboreal carbonized wood and phytoliths found within the Tilghman soil at Miles Point, Maryland. The carbonized remains of spruce, pine, fir, and "krumholtz" yellow birch have been identified. Phytoliths associated with C3 or cold-adapted grasses have also recognized at this locality.

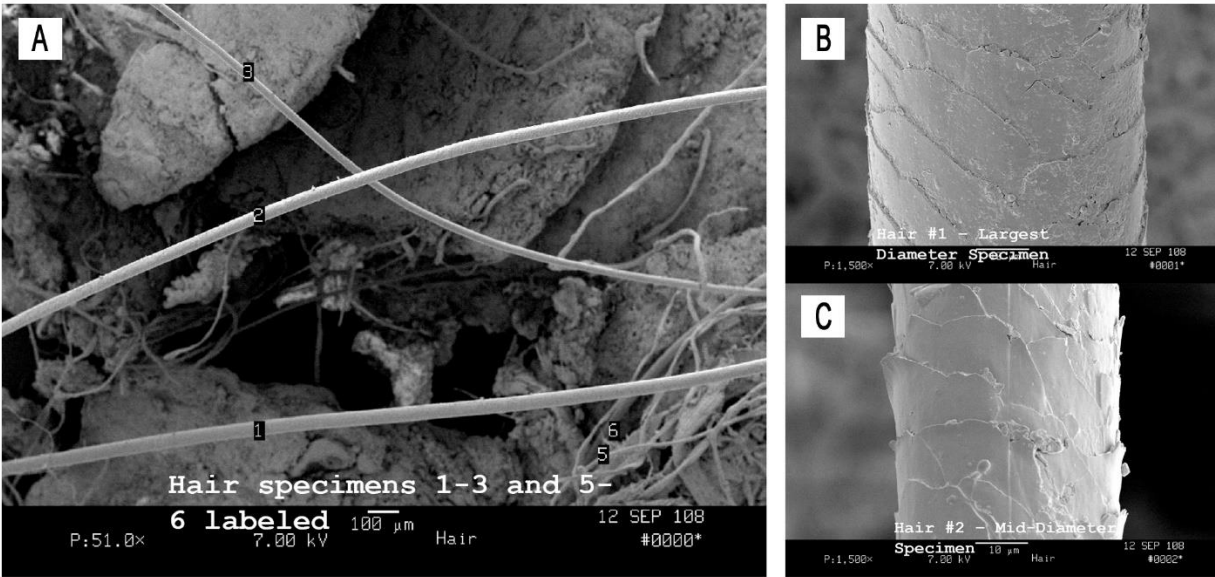


Figure 2.33. The scanning electron microscopic images show strands of fragmented hair found within the Tilghman soil at Miles Point, Maryland. At least two of the strands could be identified to the family level. One strand was identified as belonging to the family Canidae (A). Another strand belonged to the family Felidae (B). Other unknown mammalian hair fragments were also present in the sample.

Interestingly, clay films can be seen on the surface of each hair stand, which would imply these are indeed very old hair samples.

Oyster Cove, Maryland:

Oyster Cove represents another possible Pre-Clovis or Paleo-American site situated along the eroding shorelines of the Chesapeake Bay (see Figure 2.34). Like Miles Point, a small assemblage of flaked stone artifacts has been found embedded within a buried A-horizon associated with the Tilghman soil. The Oyster Cove locality is recorded as an archaeological site (i.e., 18DO359). The site has revealed both prehistoric through historic-era artifacts. Diagnostic prehistoric artifacts, spanning the region’s entire prehistory, have been found dislodged and re-deposited along the shoreline at this archaeological site. The assemblage found embedded in the bank profile in 2004 consisted of a stubby lanceolate point, a small blade-like flake, and a battered quartzite cobble. Again, like Miles Point, pooled charcoal flecks from the buried A-horizon and in the area of the in-situ artifacts produced a radiometric date of $25,800 \pm 120$ ¹⁴C-age BP or $30,843 \pm 349$ calBP (Beta -281696). The dynamic wave and tidal activity at Oyster Cove resulted in the marked retreat of the shoreline. Almost immediately after artifacts were observed embedded within the bank profile, the items were rapidly dislodged from their primary context and removed before any systematic excavation or testing could be undertaken.

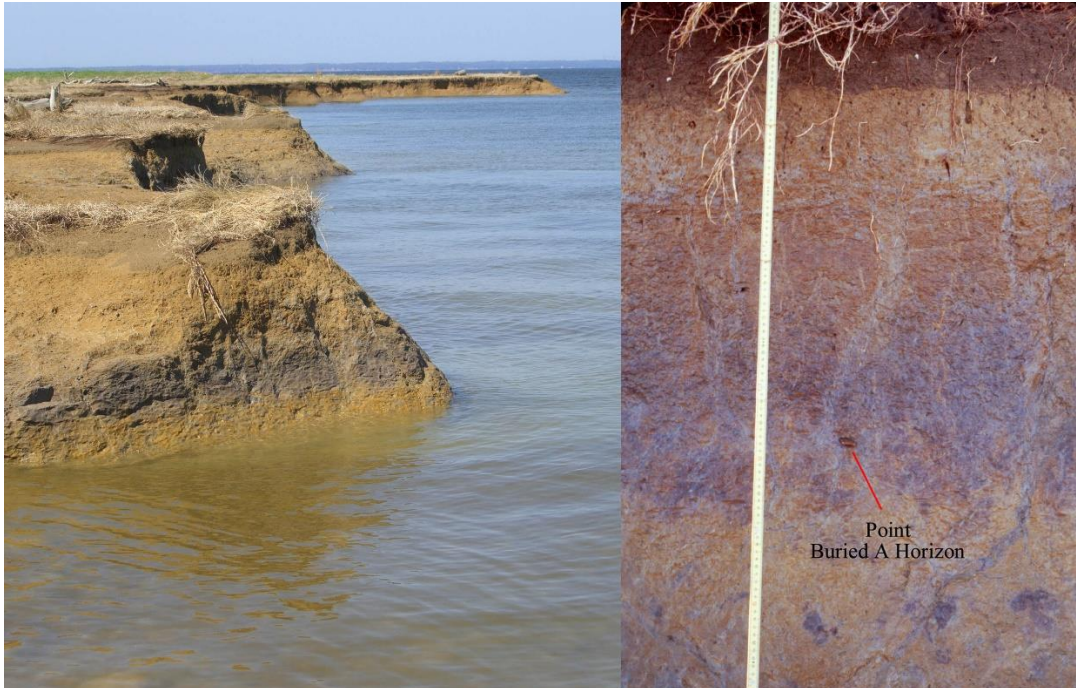


Figure 2.34. The photograph shows the eroding shoreline at the Oyster Cove locality (left) in northwestern Dorchester County, Maryland. The basal end of a lanceolate point can be seen embedded within the Tilghman soil (right) near a ped face.

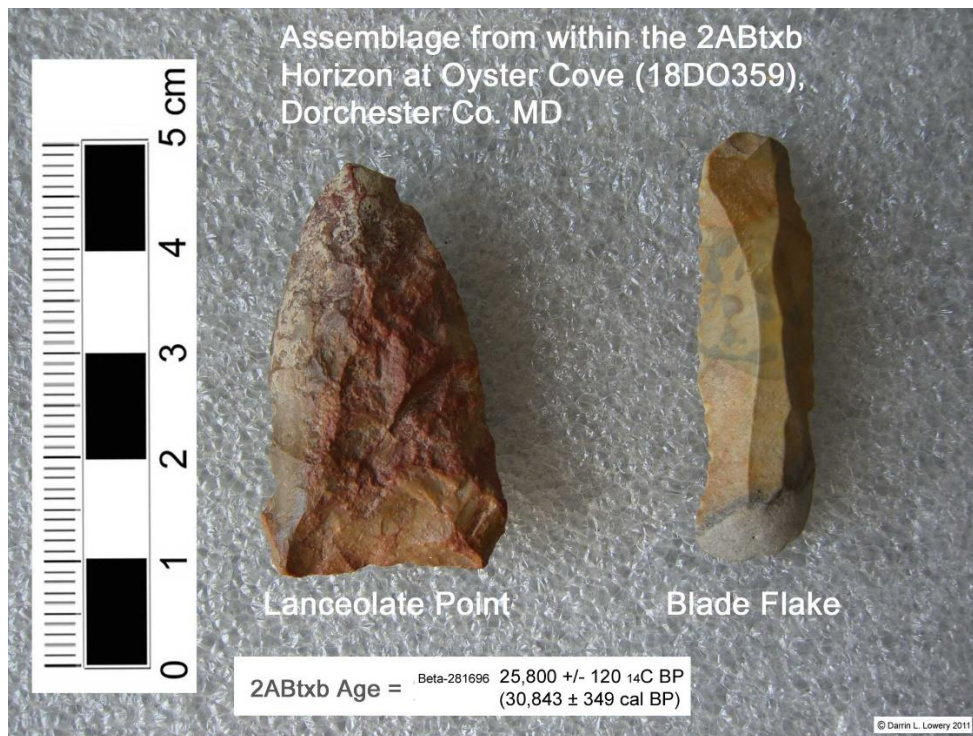


Figure 2.35. The photograph shows the two flaked stone artifacts found embedded within the Tilghman soil at Oyster Cove. The dated charcoal provided an age-estimate of 25,800 ± 120 ¹⁴C-age BP or 30,843 ± 349 calBP (Beta -281696) for the Tilghman soil at this locality.



Figure 2.36. The photograph shows an in-situ battered quartzite cobble exposed along the shoreline and embedded in the Tilghman Paleosol at Oyster Cove.

Cators Cove, Maryland:

Cators Cove is located about one-mile east of Oyster Cove along the eroding northern margin of Taylors Island, Maryland. In 2010, the research for an optical cable crossing at Taylors Island was being prepared. As a result of this project, eroded bank profiles along the margins of Taylors Island were examined for archaeological remains. In doing so, a jasper flake with rounded cobble cortex was observed embedded within the Tilghman soil at Cators Cove (see Figure 2.37). Limited testing in the same area revealed two conjoining small prismatic blade flakes made of Aquia orthoquartzite (see Figure 2.38). The small prismatic blade flakes both retained the platform areas and indicate sequential removal from the parent blade core. About 12 to 14 millimeters from the platform, both of the small blades were intentionally snapped and the distal portions are missing. The remaining distal blade sections are both flat and lack a marked curvature. The assumption being that the distal flattened portions of both prismatic blades may be retained and inserted into some sort of composite tool. Pooled carbon flecks from the Tilghman soil at Cators Cove in the same location as the in-situ artifacts produced a radiometric date of $22,050 \pm 100$ ^{14}C -age BP or $26,466 \pm 345$ calBP (Beta -309098). The site was re-visited multiple times of the subsequent years and no additional artifacts were discovered along

the shoreline or in-situ within the retreating bank profile. In 2016, a trianguloid-lanceolate point and a small blade core were found at this location eroded; however, both were eroded out of context.

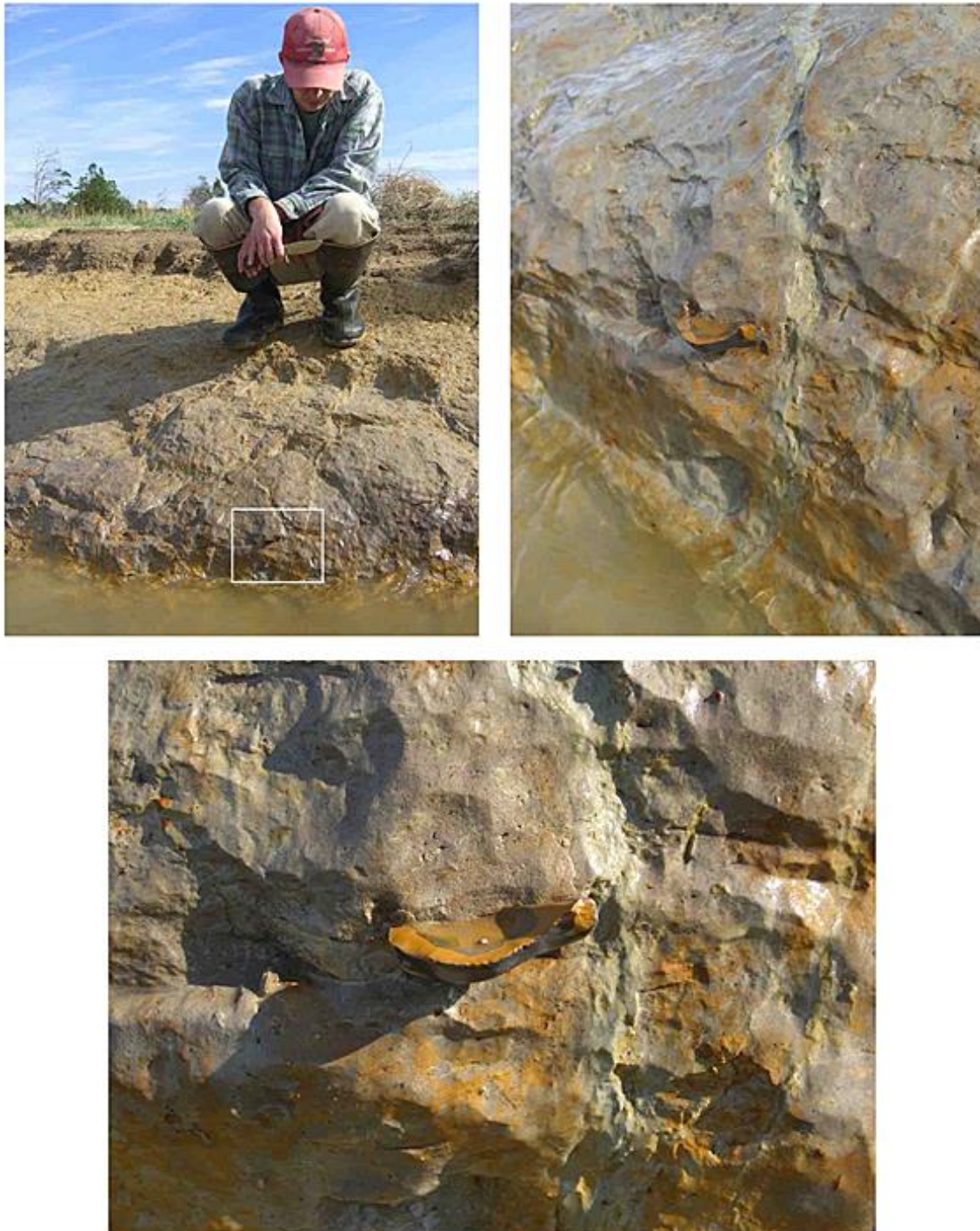


Figure 2.37. The photograph shows multiple views of the jasper flake found embedded within the eroded bank profile at the Catons Cove site along the north shore of Taylors Island in Dorchester County, Maryland.

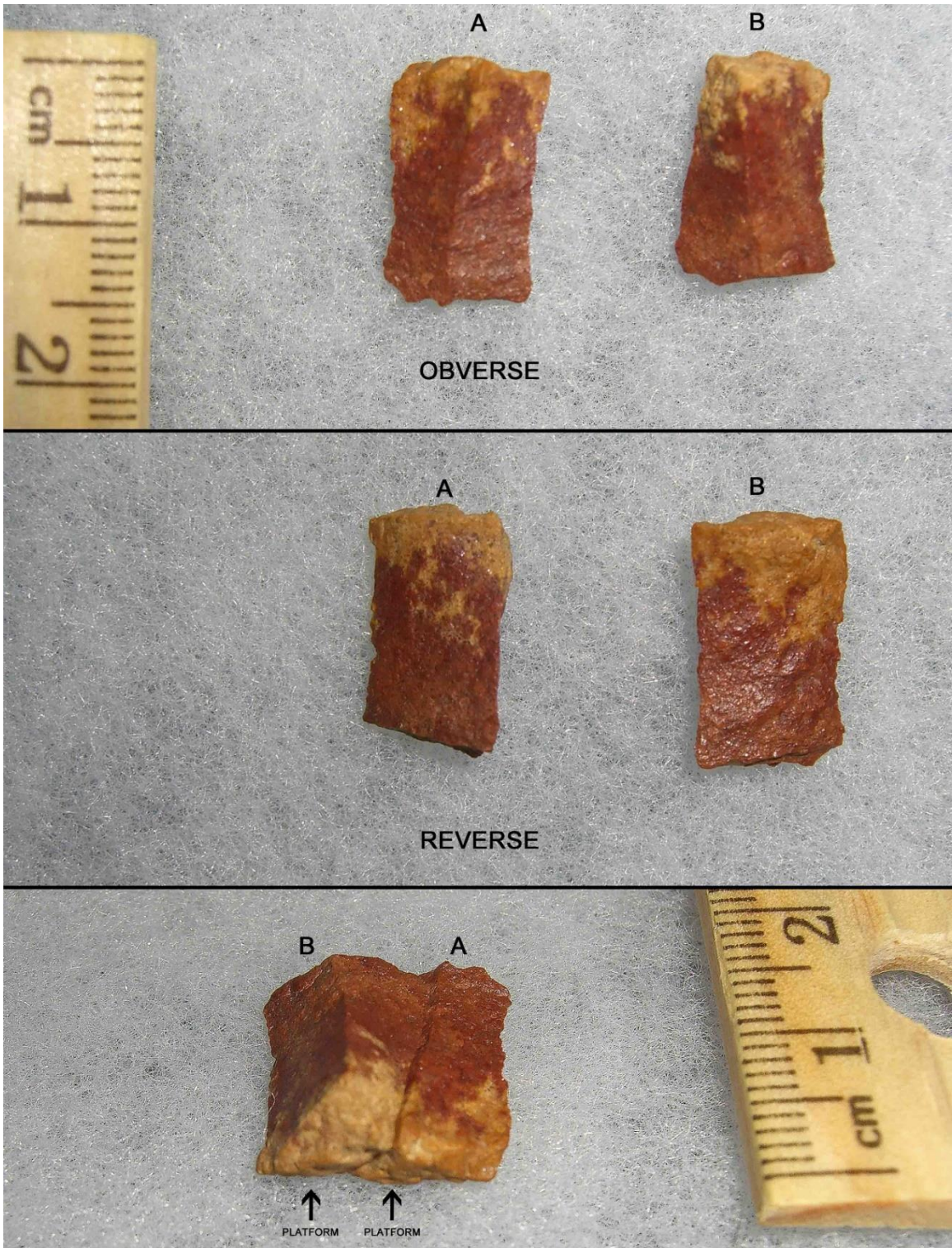


Figure 2.38. The photograph shows multiple views of the conjoined prismatic blade flake segments found during the test excavations conducted at the Catons Cove locality.

Patuxent Naval Base, Maryland:

The Patuxent Naval Base is located along the western side of the Chesapeake Bay near the mouth of the Patuxent River. In 2013, the cultural resource management firm of Louis Berger and Associates conducted an assessment of the archaeological resources on the property (see Wagner 2013). Numerous sites were examined. One site, which consisted of a steep eroded bank profile, revealed a buried surface about two-meters beneath the modern ground surface. A battered and thermally-altered hammerstone was found 202-centimeters below the surface and embedded within the 3Ab buried soil horizon (see Figure 2.39). Carbon within the same stratum and associated with the hammerstone was dated. An AMS-date of $14,976 \pm 98$ ^{14}C -age BP or $18,239 \pm 243$ calBP (D-AMS 003913) was garnered for this stratum and the associated artifact. The consulting firm made recommendations to conduct follow-up testing along the eroding bank profile to determine the inland extent of any additional archaeological material. At present, the U.S. Navy has not conducted any additional testing or excavations at this locality.



Figure 2.39. The photographs show the Patuxent Naval Airforce Base Locality 11 bank profile (left). A closeup of the embedded and in-situ battered hammerstone is shown (right, bottom). Multiple views of the hammerstone are also shown (right, top).

2.5. Synopsis of Chesapeake Localities with Radiometrically-Dated Tilghman Paleosol Surfaces:

Eleven AMS-age estimates have been generated on organic remains (i.e., organic sediment, charcoal, humates, and plant macro-remains) within buried surfaces affiliated with the Tilghman Paleosol. Collectively, the dates span ~13,000 years. The earliest date of circa 29,000 years old was generated on pooled-carbon within organic sediment at Chesapeake Farms in Kent County, Maryland. The youngest date of circa 16,000 years old is associated with an individual charcoal fleck exhumed from a paleosol at Talisman Farm in Queen Annes County, Maryland; which is situated east of Parsons Island. Most interesting are the dates from Blackwalnut Point, which is located on the southern end of Tilghman Island, Maryland. A date from Blackwalnut Point was on a singular fleck of charcoal and the resultant age estimate was ~18,800 years old. Organic sediment, which would have included pooled or mixed flecks of charcoal, resulted in an age estimate of ~24,800 years old, which is ~6,000 years older than the singular charcoal fleck from the same stratum. Both dated samples at Blackwalnut Point (i.e., the charcoal and the organic sediment) were collected at the same exact location within the bank profile. Like the information gleaned from Miles Point, the disparity would imply that late Pleistocene organic terrestrial carbon in the Middle Atlantic was not decaying, breaking down, or being naturally recycled as it is today. Presumably, the colder and drier conditions played a major role in the long-term preservation of carbon during this era.

TABLE 2.1. SUMMARY OF AGE ESTIMATES FROM LOCALITIES THAT HAVE REVEALED NO ASSOCIATED ARCHAEOLOGICAL REMAINS

LOCALITY:	COUNTY:	BURIED SOIL c_{14} AGE	CALIBRATED AGE:	LAB NUMBER:	SAMPLE:	Depth:
Chesapeake Farms	Kent County	24270 ± 150 ^{14}C -age BP	29028 ± 422 calBP	Beta-247960	Organic Sediment	120 cm
SERC (Smithsonian)	Anne Arundel	18140 ± 160 ^{14}C -age BP	21864 ± 370 calBP	Beta - 468060	Organic Sediment	110 cm
Talisman Farm	Queen Annes	13350 ± 30 ^{14}C -age BP	16291 ± 412 calBP	UGAMS-13696	Singular Charcoal Fleck	160 cm
Barnstable Hill #1	Queen Annes	19776 ± 118 ^{14}C -age BP	23682 ± 290 calBP	DAMS-2194	Organic Sediment	110 cm
Barnstable Hill #1	Queen Annes	19433 ± 90 ^{14}C -age BP	23206 ± 295 calBP	DAMS-2194	Humates	110 cm
Wye Island	Queen Annes	17070 ± 180 ^{14}C -age BP	20418 ± 420 calBP	Beta-165424	Organic Sediment	90 cm
Paw Paw Cove	Talbot	17820 ± 170 ^{14}C -age BP	21358 ± 415 calBP	AA-3870	Organic Sediment	125 cm
Blackwalnut Point	Talbot	20850 ± 90 ^{14}C -age BP	24837 ± 224 calBP	Beta-168267	Organic Sediment	100 cm
Blackwalnut Point	Talbot	15590 ± 60 ^{14}C -age BP	18858 ± 205 calBP	Beta-168268	Singular Charcoal Fleck	100 cm
Elliott's Island (N)	Dorchester	20020 ± 80 ^{14}C -age BP	23946 ± 318 calBP	Beta-286815	Twig (Peat)	500 cm
Elliott's Island (S)	Dorchester	20400 ± 90 ^{14}C -age BP	24342 ± 305 calBP	OS-81222	Twig (Peat)	140 cm

3. PARSONS ISLAND RESEARCH 2013 to 2019

Parsons Island was first surveyed for archaeological sites in 1992 (see Lowery 1993). The shorelines were examined and the plowed fields were subjected to a systematic surface collection. At that time, no archaeological remains were discovered and/or documented. In March and April 2013, the coastline at Talisman Farm, which is located east of Parsons Island, and Barnstable Hill, which is located north of the island, were subjected to soil profile analyses. Samples were collected from paleosol exposures at both Talisman and Barnstable and submitted to independent labs for AMS dating (see Table 2.1). A shoreline reconnaissance survey along the eroding west side of Parsons Island conducted on May 20th 2013 (see Figure 3.1) indicated the presence of a thick deposit of aeolian sediments over an organic-rich buried surface. The initial survey of Parsons Island was conducted by Dr. John Wah (see Figure 3.2) and Dr. Darrin Lowery. A block of sediment along the island's southern terminus was collected during this initial visit. The sediment block was associated with a buried surface (see Figure 3.3) and carbon from within this surface was submitted to DirectAMS for dating. The resultant age associated with the 4Ab2 soil horizon was $27,897 \pm 171$ ¹⁴C-years BP or $32,411 \pm 298$ calBP (D-AMS 003044). The circa 32,411 calBP age was the first date generated for the buried surface at Parsons Island.

Several visits were made to Parsons Island over the period spanning May and August 2013. Dr. Dennis Stanford, Dr. Dan Wagner, Dr. John Wah, Mr. Norman Brady, and Mr. David Thompson participated in these visits, as well as the shoreline re-examinations. The objective was to thoroughly evaluate the stratigraphic profile with hopes of clarifying the regional late Pleistocene-age upland stratigraphy and providing a higher resolution sequence of aeolian deposition. During a visit to Parsons Island on August 4th, 2013, a bi-pointed artifact was found in-situ (see Figure 3.4) within the buried 4Ab1 soil horizon ~200 meters (656 feet) north of the area previously sampled and dated 4Ab2 horizon. The setting of the in-situ artifact consisted of a buried surface 70-centimeters higher in the bank profile and slightly better drained. The artifact was embedded within the basal portion of the 4Ab1 soil horizon, which is stratigraphically above the circa 32,411-year-old 4Ab2 horizon previously dated further to the south. Charcoal flecks (see Figure 3.5) associated with this artifact were collected and the resultant AMS age estimate was $17,133 \pm 88$ ¹⁴C-years BP or $20,761 \pm 198$ cal. yrs. BP (D-AMS 003533).

Additional carbon rich-sediment samples were collected with the assistance of Dr. Dan Wagner from the southern eroding bank profile at Parsons Island on August 8th, 2013. The southern end of Parsons Island contained four buried, superimposed, and stratigraphically-stacked A-horizons (see Figure 3.6 and Appendix III). The samples were collected in a vertical stratigraphic column, which encompassed the lower 85-centimeter section of the exposed bank profile. The resultant age estimates for these surfaces span $27,640 \pm 217$ (4Ab1), $29,563 \pm 372$, $31,846 \pm 460$, or $32,756 \pm 97$ (4Ab2), $35,096 \pm 426$ (5Ab), and $41,451 \pm 451$ (6Ab) calendar years before present. With the possible exception of the 4Ab1 and 4Ab2 soil horizons, the dated strata suggest little or no carbon mixing between these stratigraphically-confined former-upland surface units.

On September 1st 2013, a second bifacial quartzite bi-pointed knife-form was found at the same general location as the first in-situ bi-pointed artifact. However, the second bi-pointed knife had eroded out of context. Other less diagnostic artifacts found on that day included two quartz flakes and a battered hammerstone made from a rounded cobble. These had also eroded out of context and were immediately in front of the bank profile. Several additional re-visits to the shoreline area in early

September 2013 were conducted and only non-diagnostic quartz flakes were found. However, on September 25th 2013, a second in-situ bi-pointed bifacial knife was found exposed within the bank profile (see Figure 3.7). No large single carbon fragments were found directly associated with the second in-situ artifact found at 18QU1047.

In early 2014, the two bi-pointed bifaces found in-situ, which had been kept with sediment coatings, were submitted to Archaeological Investigations Northwest, Inc. for blood-residue analysis. Repeated analyses (see Appendix 1) indicate that the in-situ gray chalcedony bi-pointed knife found on August 4th, 2013 tested positive to bovine antiserum. Repeat analyses (see Appendix 1) indicate that the larger in-situ black chert bi-pointed knife found on September 25th 2013 tested positive to camel antiserum, which suggests the presence of camelid blood residue on this artifact. These artifacts are the only in-situ stone tools from the site that were subjected to blood-residue analysis. Interestingly, late Pleistocene vertebrate teeth found along the shoreline (see Figure 3.8) suggest that both bovinds and camelids were present at this locality. The identification of the species associated with the fossil teeth found along the shoreline at Parson's Island were made by Dr. Russell Graham of Penn State University. On March 2nd, 2014, two fossilized bison (*Bison* sp.) molars were found along the eroded shoreline and out of context. The large size of one molar would be indicative of the giant long-horned bison (*Bison latifrons*). On July 26th, 2014, two molars from a Woodland Musk Ox (*Bootherium bombifrons*) and a molar from a large headed llama (*Hemiauchenia macrocephala*) were also discovered along the eroded shoreline and out of context. A few months later on September 26th, 2014, another fossilized molar associated with a large headed llama (*Hemiauchenia macrocephala*) was also discovered. Finally, a fossilized carnassial tooth belonging to a coyote (*Canis latrans*) was found along the shoreline on February 8th, 2015. The identified vertebrate remains mentioned above represent the only late Pleistocene faunal found at this locality. It is unclear whether these fossil remains are associated with the stratum containing cultural artifacts or predate the cultural material by ten to twenty thousand years. Interestingly, the residues purportedly found on the two bi-pointed knives do indeed match some of the genre of late Pleistocene animals found at this locality. More importantly, the fossil teeth indicate that the buried interdunal pond or wetland did attract animals. Apparently, the wetland also seems to be the reason humans visited this locality.



Figure 3.1. The image shows the continuous exposure of a buried organic-rich paleosol surface at Parsons Island, Maryland. The photograph was taken on May 20th, 2013 at 2:26pm.



Figure 3.2. The photograph shows Dr. John Wah documenting the eroding bank profile exposure at Parsons Island on May 20th, 2013 at 2:35pm.



Figure 3.3. The photograph shows the area described and analyzed during the initial visit to Parsons Island on May 20th, 2013. The



Figure 3.4. The image shows the first in-situ artifact found at 18QU1047, which was discovered on 8-4-2013 at 10:17am. Given the dynamic erosive nature of the shoreline, the artifact was excavated from the bank margin and its position was recorded with a hand-held GPS device. A bi-pointed gray chalcedony biface is shown in-situ.



Figure 3.5. The photograph shows the carbon-rich soil situated above the in-situ bi-pointed biface found on 8-4-2013, which was exposed along the eroding bank profile at Parsons Island. The carbon (see inset) was submitted to Direct AMS laboratory for dating. The resultant age estimate of $20,761 \pm 198$ calibrated calendar years before present (D-AMS 003533: $17,133 \pm 88$ ^{14}C -age BP) was received on September 9th, 2013.

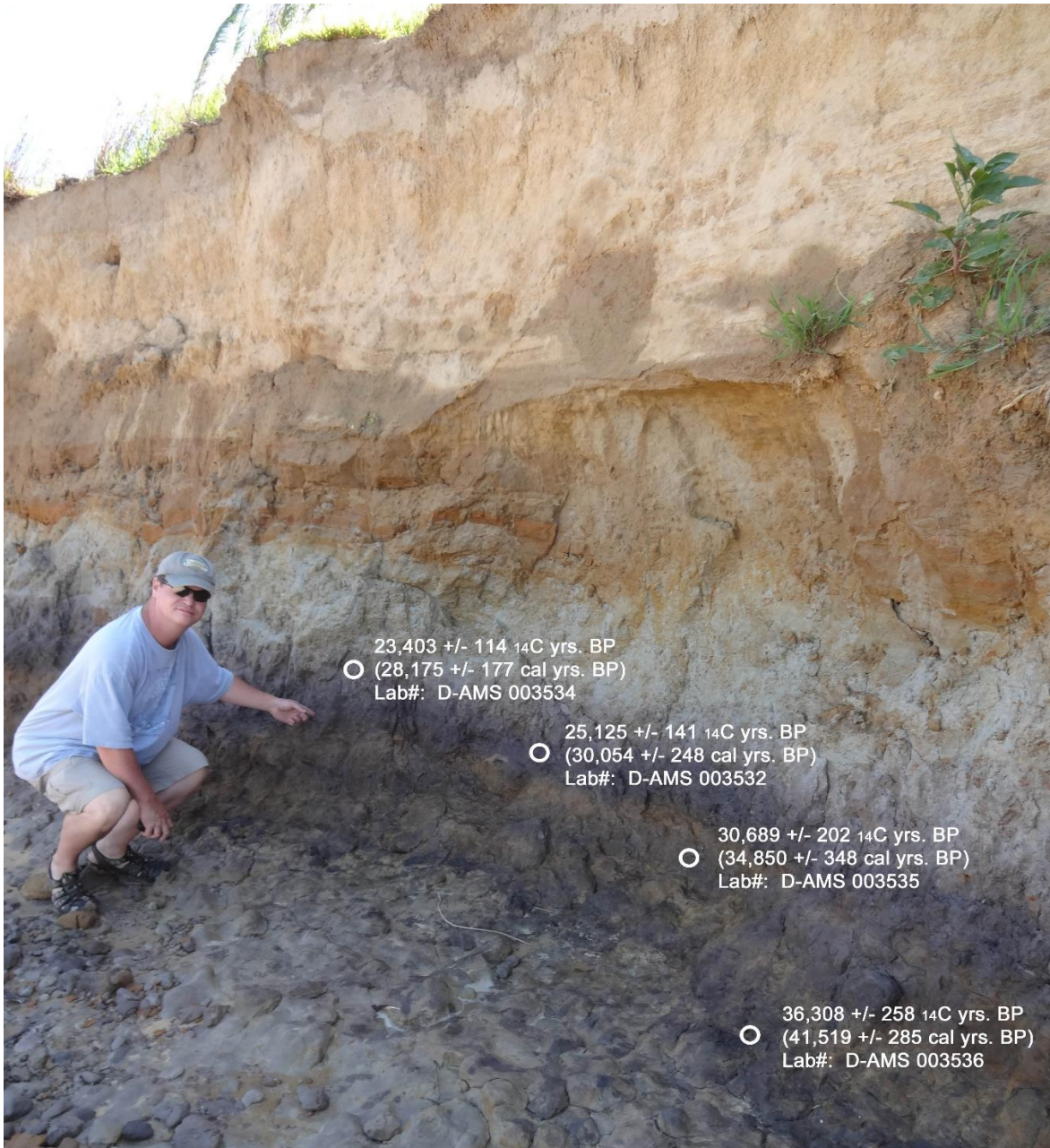


Figure 3.6. The photograph shows the southern end of Parsons Island (see Appendix III: 251-252), which contains stratigraphically-stacked and buried carbon-rich A-horizons. Carbon within the 4Ab1 soil located 290 to 304-centimeters beneath the ground surface was dated to $23,403 \pm 114$ ^{14}C -years BP or $27,640 \pm 217$ cal. yrs. BP (D-AMS 003534). At 304 to 318-centimeters beneath the ground surface, carbon within the 4Ab2 soil was dated to $25,125 \pm 141$ ^{14}C -years BP or $29,563 \pm 372$, $31,846 \pm 460$, or $32,756 \pm 97$ cal. yrs. BP (D-AMS 003532). A cambic soil horizon (4Bwb) separates the 4Ab2 soil from the underlying carbon-rich 5Ab soil horizon. At 333 to 343-centimeters beneath the ground surface, carbon within the 5Ab soil was dated to $30,689 \pm 202$ ^{14}C -years BP or $35,096 \pm 426$ cal. yrs. BP (D-AMS 003535). Another cambic soil horizon (5Bwb) separates the 5Ab soil from the underlying carbon-rich 6Ab soil horizon. At 364 to 375-centimeters beneath the ground surface, carbon within the 6Ab soil was dated to $36,308 \pm 258$ ^{14}C -years BP or $41,451 \pm 451$ cal. yrs. BP (D-AMS 003536).

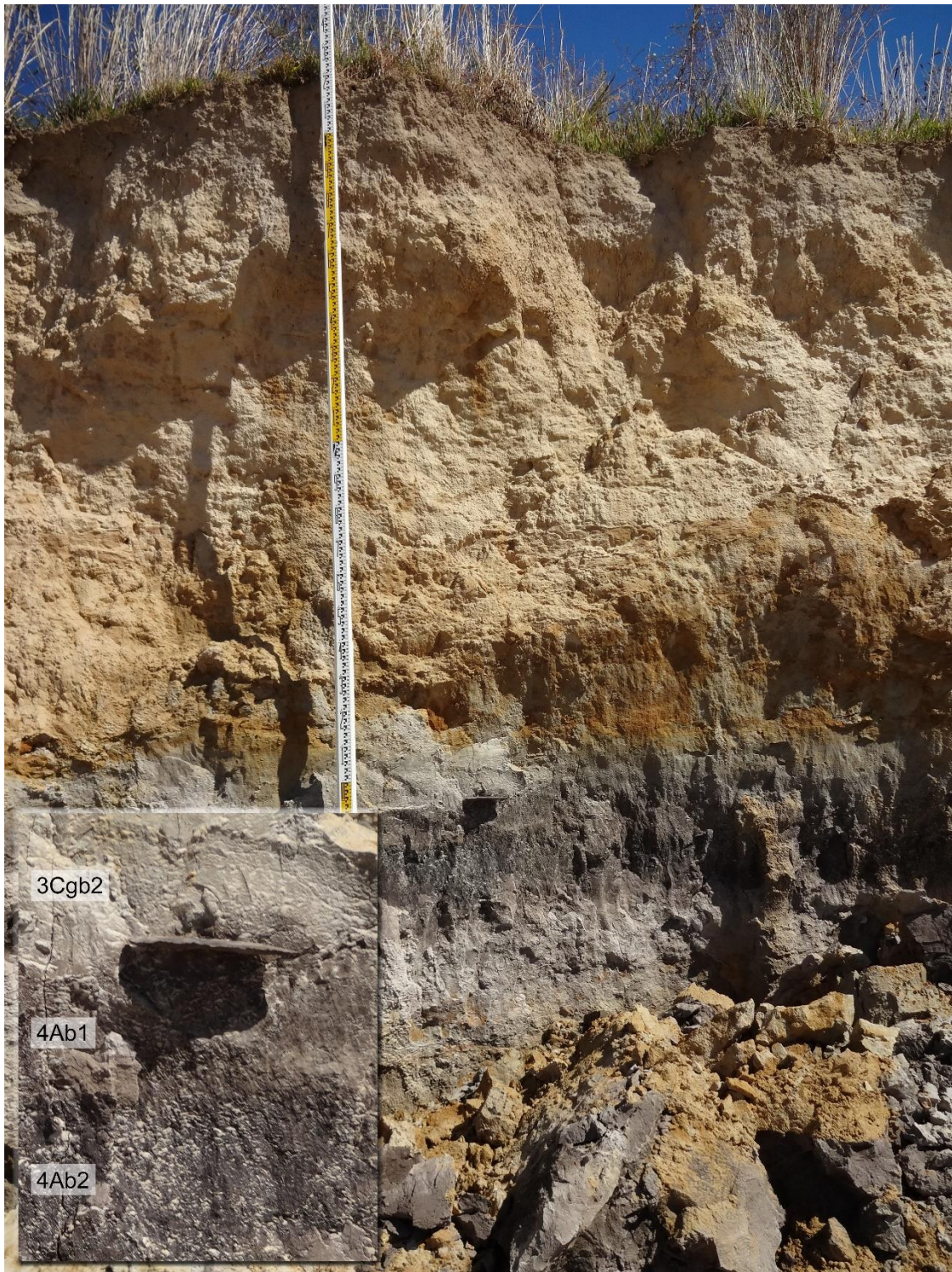


Figure 3.7. The photograph shows the eroding bank profile at 18QU1047 an in-situ chert bi-pointed knife can be seen lying flat and situated stratigraphically at or near the contact between the 3Cgb2 and the upper portion of the 4Ab1 soil horizons.

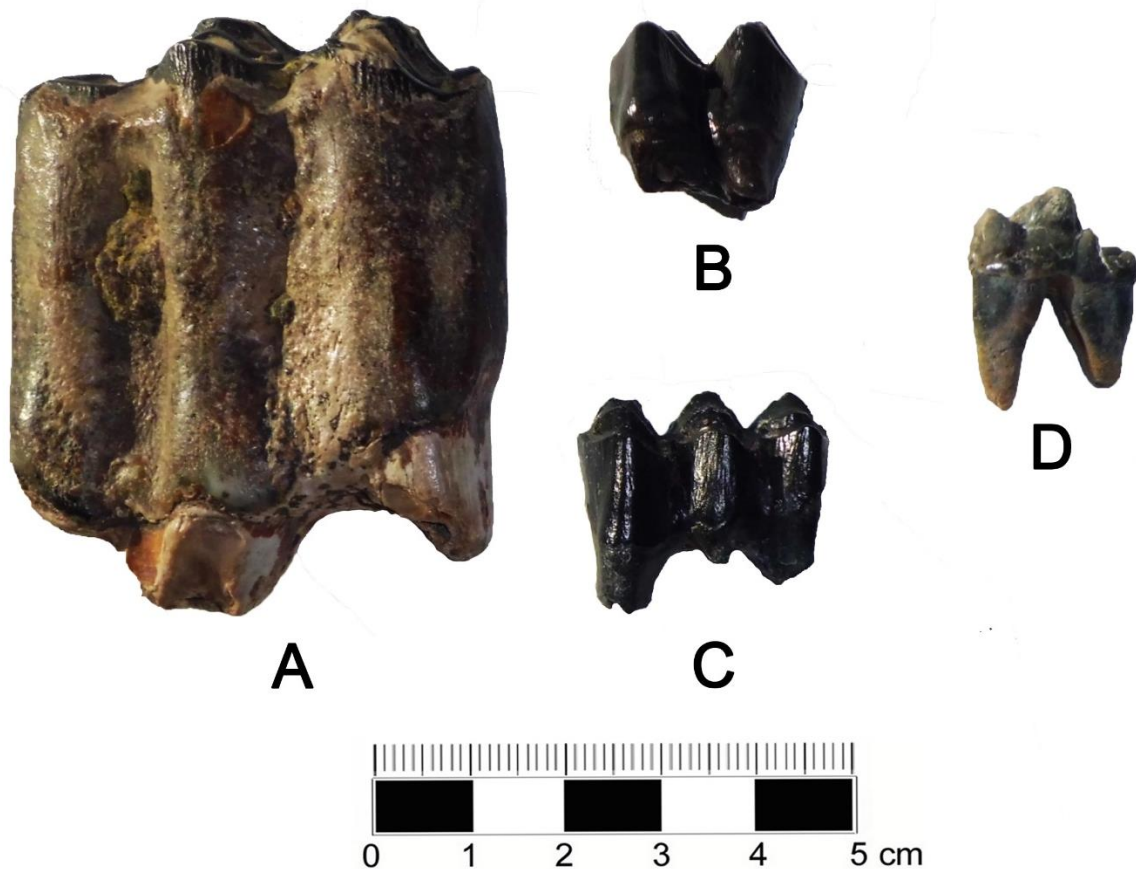


Figure 3.8. The image shows some of the late Pleistocene vertebrate remains found along the shoreline near 18QU1047. The teeth include giant long-horned bison (A) or *Bison latifrons*; woodland musk ox (B) or *Bootherium bombifrons*; large headed llama (C) or *Hemiauchenia macrocephala*; and coyote (D) or *Canis latrans*.

3.1. Synopsis of Macrofloral, Phytolith, and Pollen Data for Parson's Island and Elliott's Island:

After the discovery of the first in-situ artifact on August 4th, 2013, soil samples from the buried surfaces along both the southern and northern ends of Parsons Island (see Figure 3.6) were collected. The soil samples collected on August 8th, 2013 were gathered for the purpose of conducting several specific types of investigation. Charcoal within the buried organic soil horizons would provide a means to determine the ages of each horizon. If collected in a vertical sequence, the resultant radiocarbon ages for each horizon would help assess potential mixing and/or bioturbation impacts of these buried strata. Finally, plant macrofloral and micro-floral remains from each buried horizon would provide important paleo-environmental data and potentially rectify our understanding of regional late Pleistocene environmental change over time.

Samples from each buried surface (i.e., 4Ab1, 4Ab2, 5Ab, and 6Ab) along the southern end of Parsons Island were collected in a vertical sequence (see Figure 3.9, left and right) and submitted to DirectAMS for analyses. Carbon within the 4Ab1 soil located 290 to 304-centimeters beneath the ground surface was dated to $23,403 \pm 114$ ¹⁴C-years BP or $27,640 \pm 217$ cal. yrs. BP (D-AMS 003534). At 304 to 318-centimeters beneath the ground surface, carbon within the 4Ab2 soil was dated to $25,125 \pm 141$ ¹⁴C-years BP or $29,563 \pm 372$, $31,846 \pm 460$, or $32,756 \pm 97$ cal. yrs. BP (D-AMS 003532). A cambic soil horizon (4Bwb) separates the 4Ab2 soil from the underlying carbon-rich 5Ab soil horizon. At 333 to 343-centimeters beneath the ground surface, carbon within the 5Ab soil was dated to $30,689 \pm 202$ ¹⁴C-years BP or $35,096 \pm 426$ cal. yrs. BP (D-AMS 003535). Another cambic soil horizon (5Bwb) separates the 5Ab soil from the underlying carbon-rich 6Ab soil horizon. At 364 to 375-centimeters beneath the ground surface, carbon within the 6Ab soil was dated to $36,308 \pm 258$ ¹⁴C-years BP or $41,451 \pm 451$ cal. yrs. BP (D-AMS 003536). With an AMS age of $27,640 \pm 217$ cal. yrs. BP (D-AMS 003534), the 4Ab1 soil horizon along the southern end of Parsons Island (see Figure 3.6) seems to be ~7,000 years older than age on the comparable 4Ab1 horizon (D-AMS 003533: $20,761 \pm 198$ Cal. Yrs. BP or $17,133 \pm 88$ ¹⁴C-age BP) situated along the northern end of the island (see Figures 3.4 and 3.5). However, carbon mixing between the 4Ab1 and the 4Ab2 along the southern section of Parsons Island may explain the perceived age discrepancy. Interestingly, a similar ~7,000-year age disparity was also noted for the 2ABtxb horizon or Tilghman soil at Miles Point (see Figure 2.31). The resultant radiometric-age estimates generated on the ~85-centimeter 4Ab through 6Ab soil vertical column along the southern end of Parsons Island imply very little stratigraphic mixing and/or bioturbation occurred within these surfaces before being buried by aeolian-deposited sediments. The generally consistent stratigraphic age estimates noted for the buried soil horizons observed along the island's northern and southern shoreline would imply that organic-carbon during this period of cooler and drier environmental conditions was not breaking down. Under certain circumstances, like the situation noted at Miles Point, mixtures of old and young carbon were persisting upon the landscape.

Given the observed stratigraphic age parameters, samples from the buried 4Ab1 surface along the northern bank profile and samples from the 4Ab2, 5Ab, and 6Ab surfaces along the southern bank profile at Parsons Island were also collected and submitted to the Paleosciences Archaeobotanical Services Team (i.e., PAST) at Bailey, Colorado for macrofloral, phytolith, and pollen analyses. Ms. Kathryn Puseman performed the macrofloral taxonomic groupings. Mr. Chad Yost conducted the phytolith identifications and Ms. Andrea Nurse conducted the pollen classifications for each buried surface. The primary goal was to determine if regional climatic and local environmental changes were evident within the various buried soil horizons reflecting different ages. The following outline presents their methods, results, and interpretations, as originally summarized in a report prepared by Puseman et al. (2014).

3.1.1. Macrofloral Sampling and Identification Methodology:

Sediment samples were floated to recover macrofloral remains using a bucket system. Samples were measured and added one liter at a time to a bucket filled with water. The sample was swirled, then the floating material (light fraction) was poured through a 150-micron-mesh sieve. This process was repeated with additional water until all floating material was recovered. After the heavy fraction remaining in the bottom of the bucket was poured through a 0.5-mm-mesh screen, the floated light and heavy fractions were dried.

After the light fractions were weighed, they were screened using a series of graduated screens (US Standard Sieves with 4-mm, 2-mm, 1-mm, 0.5-mm, and 0.25-mm openings). The contents of each screen then were examined. Charcoal fragments were examined under a Bausch and Lomb Stereozoom microscope at a magnification of 70x and a Nikon Optiphot 66 microscope at magnifications of 100-600x. Whenever possible, both counts and weights were recorded. Weights were taken using a top-loading Tree® high resolution electronic balance with an accuracy level to 0.001 g.

Organic material remaining in the 4-mm, 2-mm, 1-mm, 0.5-mm, and 0.25-mm screens was examined under a Bausch and Lomb Stereozoom microscope at magnifications of 10-70x. The light fraction material smaller than 0.25 mm in size was not examined. Macrofloral remains were recorded as charred and/or uncharred, whole and/or fragments using counts, weights, and/or frequencies. An asterisk (*) in the macrofloral table notes an estimated frequency calculated from sorting a portion of the total volume, typically 1/4 or 1/8. Macrofloral remains and charcoal fragments were identified using standard identification manuals (Carlquist 1988; Core et al. 1976; Davis 1993; Delorit 1970; Hoadley 1990; Martin and Barkley 2000; Panshin and deZeeuw 1980), internet web sites (InsideWood 2004) and a modern comparative collection.

3.1.2. Phytolith Sampling and Identification Methodology:

Aliquots of 2 cm³ of sediment from each sample (5 cm³ for sample 2) were placed in a 400 mL beaker with 20 mL 37% hydrochloric acid (HCl) and 100 mL 70% nitric acid (HNO₃), and then boiled for 1 hour to remove the acid soluble fraction. Samples were then rinsed five times with reverse osmosis deionized water (RODI) water. Next, 5 mL of a 10% solution of potassium hydroxide (KOH) was added to each sample for 10 minutes to remove the base soluble fraction, followed by five rinses with RODI water. A 10% solution of sodium hexametaphosphate was then mixed into each sample, the samples were allowed to settle by gravity for 1.5 hours, and the samples were then decanted to remove any clay-sized particles still in suspension. This step was repeated until the supernatant was clear after two hours of settling time. The samples were then transferred to 50 mL centrifuge tubes and dried under vacuum in a desiccator. The dried samples were then mixed with 10 mL of lithium metatungstate (LMT, density 2.3 g/mL) and centrifuged for 10 min at 1,500 rpm to separate the phytolith fraction, which will float, from the heavier inorganic mineral and silica fraction. Each sample was then rinsed five times with RODI water to remove the LMT solution. The samples were spiked with a 1 mL aliquot containing 25,000 ± 8% microspheres (10-20 µm diameter) for phytolith concentration calculations. The samples were then rinsed twice in 99% isopropyl alcohol and stored in 1.5 mL vials. For microscopy, the samples were mounted in optical immersion oil and the cover glass was sealed with fingernail polish. Phytolith counting was conducted with a transmitted light microscope using a magnification of 500x. A total count of 300 taxonomically significant phytoliths was first conducted, after which, each slide was scanned for any rare phytolith types of ecological significance. A percentage diagram of relative abundance was produced using Tilia, with diatoms, sponges, and microscopic charcoal percent abundance calculated outside of the phytolith sum. Using the microsphere counts, phytolith concentrations (#/cm³) were calculated, and the total phytolith concentration for each sample was included on the percentage diagram. Because of the interpretive value, normalized percent relative abundance based only on phytoliths diagnostic of C₃, C₄ Panicoideae and C₄ Chloridoideae grasses was calculated and included on the diagram.

3.1.3. Pollen Sampling and Identification Methodology:

PAST submitted 2-cc sediment aliquots from each site to the Paleoecology Research Laboratory at the Climate Change Institute, University of Maine, for pollen analysis. Pollen concentration techniques followed chemical methods presented by Faegri et al. (1989) and heavy liquid floatation methods adapted from Vandergoes (2000). After defloculation of the original 2-cc samples, sieving removed particulate matter larger than 125 μm . The pollen was separated from the fine sand and clay by floatation in liquid sodium polytungstate (sp.gr. 2.27), treated chemically to dehydrate the pollen and remove humic acids and polysaccharides, and suspended in silicone oil. The silicone-pollen suspension was mounted on microscope slides and examined under 40x magnification. A minimum of 300 terrestrial pollen cells were counted and identified. Pollen types were plotted as a percent of the total pollen count using Tilia and Tilia Graph programs version 1.7.16 (Grimm 2011). The graphs report concentration of charcoal particles larger than 50 μm^2 as a guide to relative fire activity.

3.1.4. Parsons Island 6Ab horizon (41,451 \pm 451 cal. yrs. BP D-AMS 003536):

Macrofloral remains in sample 5, which correlates with the 6Ab horizon (see Appendix III: 251-252), include five charred seed endosperm fragments and two charred monocot/herbaceous dicot stem fragments, as well as an uncharred *Panicum virgatum* (a C4 grass) floret, a few uncharred stem/leaf fragments, a few uncharred root bark fragments, and a small amount of unidentified organic material. The sample yielded several pieces of hardwood charcoal too small for further identification. Many pieces were slightly vitrified. Vitrified charcoal has a shiny, glassy appearance that can range from still recognizable in structure “to a dense mass, completely ‘molten’ and non-determinable” (Marguerie and Hunot 2007; McParland et al. 2010:2679). Recent experiments by McParland et al. (2010) demonstrated that it is currently not clear exactly what conditions produce vitrified charcoal. It likely is a combination of factors such as burning at high temperature and/or burning green wood. The largest piece of unidentified hardwood charcoal exhibited scleriform intervessel pitting (Figure 3.10 A). This type of intervessel pitting is the least common type. Table 3.1 lists woody plants found in the Eastern United States that exhibit scleriform intervessel pitting. No other identifying characteristics were visible on these charcoal fragments. A few small flecks of conifer charcoal also were present. One piece of identifiable *Picea* charcoal was present. The woods of red spruce (*Picea rubens*), white spruce (*Picea glauca*), and black spruce (*Picea mariana*) cannot be separated from one another on the basis of wood anatomy (Hoadley 1990: 153). One piece of conifer charcoal exhibited a fusiform ray (Figure 3.10 B), indicating the presence of conifers with resin canals such as spruce, Douglas-fir, pine, or larch. The absence of helical thickenings on the conifer charcoal fragments suggests that it might also reflect *Picea* charcoal or possibly *Pinus* (pine).

The phytolith record for the 6Ab soil horizon is characterized by the highest normalized relative abundance of C4 Chloridoideae grass phytoliths (Figure 3.15 C) for the entire Parson’s Island record (17%). Chloridoideae grasses are warm climate grasses that require full sun, thrive under hot and dry conditions, and often grow on coarse-grained substrates such as desert, beach, dune, and shoreline soils. A few Panicoideae grass phytoliths were also recovered (3%), indicating some summer precipitation and soil moisture. This sample also marks the start of a continued decline in C4 grasses for the remainder of the record, suggesting progressively cooler summers as a gradual return to full glacial

conditions progresses. It is interesting to note the high microscopic charcoal concentrations in the pollen record, further indicating periods of dry and warm conditions. The high conifer pollen percentages suggest that a forest habitat predominated; however, the presence of open habitat grasses indicates that there were enough openings for light penetration to the forest floor or that the forest boundary was nearby. This sample also exhibited the highest abundance of Cyperaceae stem phytoliths. Although they are not diagnostic, these phytoliths are typical of those produced by *Scirpus* and *Schoenoplectus*. With a phytolith concentration of 750,000 phytoliths per cm³ of sediment, either grasses and sedges were dense, or alternatively, sedimentation rates were low.

Diatom frustules and sponge spicules, biogenic silica microfossil indicators of water, had their highest levels of abundance in the 6Ab soil horizon. Both centric and pennate diatoms were observed. Centric diatoms tend to be indicators of fresh water bodies such as ponds and lakes. Pennate diatoms can occur in a wide variety of moist and wet habitats, including standing and flowing water, wet soil and stems of aquatic plants. While diatoms and sponge spicules can be transported in wind-blown dust from drying lakes and rivers to more upland settings, sponge gemmoscleres have delicate ornamentation that may not survive wind and water transport. One gemmosclere was observed in this sample (Figure 3.11), indicating that water was located nearby circa 41,500 years ago. The 6Ab surface, however, shows no indication of being below sea level during or after its time of deposition. The underlying 6Bwgb also implies a protracted period of terrestrial pedogenic weathering pre-dating the age of the 6Ab surface.

Pinus dominated the pollen record (57%) in the 6Ab soil horizon. Sample 5 also yielded the highest percentage of *Picea* pollen (17%) pollen and the lowest percentage of Cupressaceae pollen of all the Parson's Island samples, noting a coniferous forest with more spruce and pine and less cedar and cypress. The only *Alnus viridis* (Green Alder) pollen was noted in sample 5. This shrub can occur as an understory dominant in open conifer forests with black spruce, white spruce, lodgepole pine, and jackpine overstories, as well as singly or in thickets along streams, lakeshores, coasts, and bogs. Alders are associated with moist soils, but *Alnus viridis* is adapted to somewhat drier conditions than other alders. Upland herbs are represented only by a small amount of Liliaceae pollen. A decrease in pollen from upland herbs suggests a more closed-canopy forest regionally. Juncaceae was the only wetland pollen type present, and Lemnaceae was the only aquatic pollen type noted in the sample.

In summary, the combined macrofloral, phytolith, and pollen records for the 41,500-year-old 6Ab soil horizon suggest that regionally, a coniferous forest comprised mostly of pines dominated the upland settings. Grasses, sedges, and rushes occurred in an open riparian habitat that may have been a low energy system. Although global mean air temperatures were much cooler than today (see Figure 3.17), insolation was much higher, and summers were warm enough to support some C₄ vegetation, in particular Chloridoideae grasses and panic grass, and dry enough to cause periodic wildland fires.

The Parsons Island 6Ab soil macrofloral and microfloral data stand in stark contrast with many perceptions about local sea levels during Marine Oxygen Isotope stage 3 (67–32 ka) within the Chesapeake Bay region. In 2006, Pavich et al. (2006: 226) reported optically stimulated luminescence (OSL) ages on estuarine sands ranging between 43,100 and 30,900 years old (37+/- 6.1 ka) associated with high sea stand deposits located along the Potomac River. The estuarine deposits documented by

Pavich et al. (Ibid) have been linked to the Kent Island Formation (see Owens and Denny 1979); a mixture of reportedly late Pleistocene-age fluvial/estuarine deposits. Recently, DeJong et al. (2015) have suggested that relative sea level in the central Chesapeake Bay during MIS 3 was <8 m (<26 feet) above present and estuarine conditions prevailed, at least intermittently, during most of MIS 3. In stark contrast, Ramsey (2010) has indicated the Delmarva Peninsula did not experience high-stand deposition any time after MIS 5 or during the past 100,000 years. Importantly, data from nearby New Jersey (see Wright et al. 2009: Table 1) indicate that local Middle Atlantic sea levels about 45,000 years ago were - 60 ± 10 meters lower than present. The purported ages associated with MIS 3 high sea stand formations noted by Pavich et al. (2006) and DeJong et al. (2015) are largely based on optically-stimulated luminescence (OSL) dates. OSL age estimates are fraught with potential timing errors based on assessing the average moisture content of the formation over time and the possibility that the strata may have been partially exposed to sunlight at some interval during the formation's history. Considering that the circa 41,500-year-old 6Ab soil horizon is currently below relative sea level at high tide, the presence of an upland coniferous forest with grasslands and wildfires would be environmentally, ecologically, and geologically impossible if this surface was below sea level as implied by both Pavich et al. (2006) and DeJong et al. (2015).



Figure 3.9. The photos show the stratified buried surfaces (4Ab1, 4Ab2, 5Ab, and 6Ab) along the southern end of Parsons Island (left) that were sampled (right) in a vertical column sequence. Each stratified surface was dated and sampled for macro-floral remains, phytoliths, and pollen.

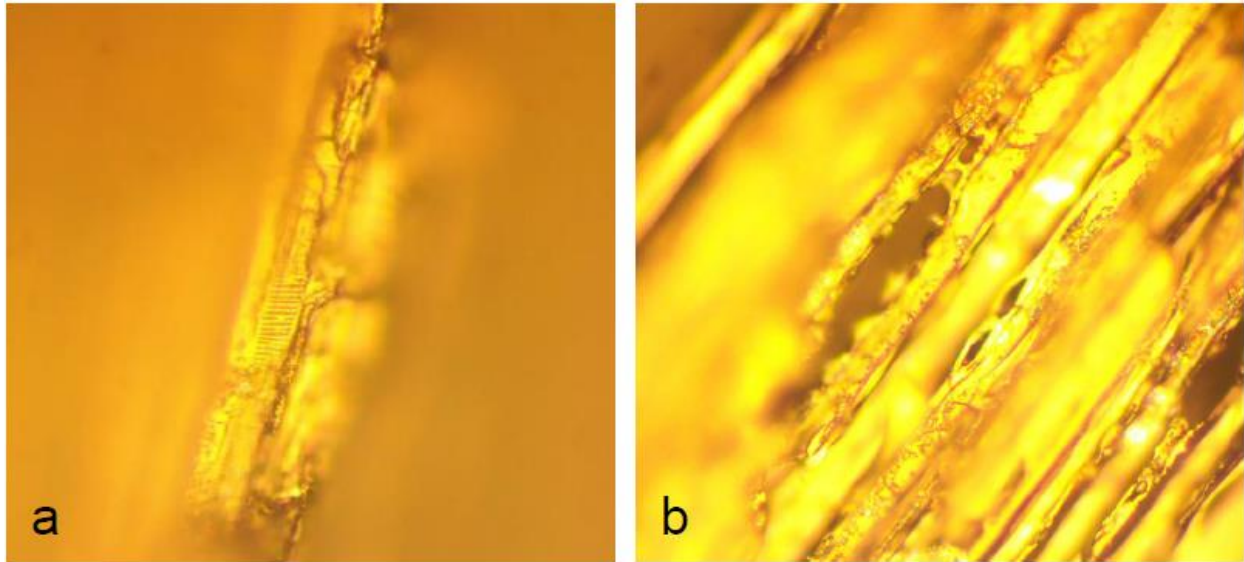


Figure 3.10. The micrographs show selected charcoal images from Parsons Island sample 5 (6Ab soil horizon). All micrographs taken at 600X magnification. One image (A) shows scleriform intervessel pitting on a vessel wall; tangential view. Another image (B) shows a fusiform ray; tangential view. Image from Puseman et al. (2014: 25).

TABLE 3.1. LIST OF PLANTS IN THE EASTERN UNITED STATES THAT EXHIBIT SCLARIFORM INTERVESSEL PITTING (Image from Puseman et al. 2014: 26)

Scientific Name	Common Name
<i>Ampelopsis</i> spp.	Peppervine
<i>Cornus</i> spp.	Dogwood
<i>Hamamelis virginiana</i>	American witchhazel
<i>Ilex decidua</i>	Possumhaw
<i>Liquidambar styraciflua</i>	Sweetgum
<i>Magnolia</i> spp.	Magnolia, Sweetbay, Cucumber tree
<i>Nyssa</i> spp.	Blackgum, Tupelo
<i>Parthenocissus</i> spp.	Woodbine, Virginia creeper
<i>Ribes</i> spp.	Currant
<i>Vaccinium</i> spp.	Blueberry, Cranberry
<i>Vitis</i> spp.	Grape



Figure 3.11. The micrograph photo, which was taken at 500X magnification, shows a sponge (Spongillidae) gemmosclere found within the 6Ab soil horizon. The gemmosclere is part of the reproductive structure.

3.1.5. Parsons Island 5Ab horizon (35,096 ± 426 cal. yrs. BP D-AMS 003535):

Macrofloral plant remains found in sample 4, which correlates with the 5Ab soil horizon (see Appendix III: 251-252), include a few fragments each of uncharred root bark, rootlets, stem/leaf, and unidentified organics. Several small fragments of conifer charcoal were also identified. Two of the charcoal fragments exhibited *Picea* Type 1 ray tracheid pitting (Figure 3.12 A and 3.12 B), indicating these fragments of charcoal are *Picea*. The presence of piceoid cross field pitting, bordered pits in single rows, and helical thickenings, as well as the absence of *Larix*-type ray tracheid pitting, on another piece of charcoal reflect *Pseudotsuga menziesii* (Douglas-fir). Helical thickenings were noted on four other pieces of charcoal (Figure 7c and 7d), but no other identifying characteristics were present. Helical thickenings are found in *Pseudotsuga* (Douglas-fir), *Taxus* (yew), and occasionally in *Larix* (larch, tamarack). Three fragments of hardwood charcoal were too small for further identification.

The phytolith record for the 5Ab soil at Parsons Island exhibited a strong affinity with that discussed for the 6Ab soil horizon, with a few exceptions. No C₄ Panicoideae phytoliths were recovered; however, C₄ Chloridoideae grass phytolith percentages were still relatively high at 15%. Summer insolation was much higher than present-day values, as the northern hemisphere was approaching an insolation maximum (see Figure 3.17). Phytoliths diagnostic of C₃ Stipeae grasses appear for the first time, as do keeled rondels typical of some Pooideae grasses (see Figure 3.15 A), indicating increased grass diversity. Increases in plant diversity are also reflected in the pollen record.

Siliceous freshwater sponge spicules rise dramatically in the 5Ab soil at Parsons Island, most likely due to once submerged shallow water margins and their inhabitant sponge community drying up,

releasing the spicules to depositional processes and erosional transport. This scenario is supported by the absence of aquatic pollen types and a dramatic rise in pioneering and disturbance species in the pollen record.

The pollen record for the 5Ab soil is best characterized by a reduction in pine and spruce pollen and a dramatic rise in alder (*Alnus* sp.). Pollen from deciduous trees such as poplar (*Populus*), birch (*Betula*), and hophornbeam (*Ostrya* sp.) also rises dramatically in the 5Ab soil, and hazelnut (*Corylus* sp.) pollen appears for the first time. Thus, it appears that a once regionally dense conifer-dominated forest is opening up and becoming increasingly diverse and multilayered with overstory and understory taxa. The riparian zone also appears to be diversifying, as willow, river birch, and low-spine Asteraceae become established.

In summary, the combined macrofloral, phytolith, and pollen records for the circa 34,850-year-old 5Ab soil, suggest that regionally, a once dominant coniferous forest was shifting towards a mixed conifer-hardwood forest. Over the 6,000 years since the formation of the underlying 6Ab soil, the northern hemisphere is on a trajectory of increasing summer insolation that is approaching a maximum (see Figure 3.17). This increasing insolation appears to have had an effect on the local vegetation and hydrology. With local isostatic sea levels approximately 30 meters lower than present at this time (see Wright et al. 2009: Table 1), an expanded riparian zone with a diverse mixture of grasses, sedges, herbs, and deciduous trees and shrubs appears to have existed, and summers were still warm enough to support a C₄ grass community with some wildland fire activity.

3.1.6. Parsons Island 4Ab2 horizon (29,563 ± 372, 31,846 ± 460, or 32,756 ± 97 cal. yrs. BP D-AMS 003532):

Macrofloral plant remains within the 4Ab2 (see Appendix III: 251-252) soil horizon (sample 3) yielded several very small fragments of identifiable charcoal. One piece of charcoal exhibiting *Picea* Type 1 ray tracheid pitting and one piece of charcoal exhibiting a fusiform ray and no helical thickenings reflects *Picea* charcoal (Figure 3.13 A and 3.13 B). Other fragments of conifer charcoal also did not exhibit helical thickenings, but no other identifiable characteristics were present. Two pieces of hardwood charcoal exhibited sclariform intervessel pitting (Figure 3.13 C), reflecting one of the taxa listed in Table 3.1. Recovery of Ericaceae pollen in the 4Ab2 horizon (sample 3) indicates that members of the heath family were growing in the area. *Vaccinium* (blueberry/cranberry) is a member of the Ericaceae family. It is possible that the charcoal with sclariform intervessel pitting might reflect *Vaccinium*. Other fragments of hardwood charcoal were too small and vitrified for identification. The sample also contained a few uncharred fragments of unidentified organic material.

The phytolith record for the 4Ab2 soil horizon (sample 3) is best characterized by a sharp reduction in C₄ Chloridoideae grass phytoliths and a peak in abundance of C₄ Panicoideae phytoliths (Figure 3.14) for the Parson's Island record. The observed abundance of Panicoideae phytoliths suggests that soil conditions may have been too wet for Chloridoideae grasses to thrive but optimal for Panicoideae grasses. This also suggests that although summers were still warm, there was at least a moderate amount of summer precipitation. Cool climate C₃ grass phytoliths continue their gradual rise in abundance, which seems to be mirroring long-term global cooling as the LGM approaches. There is also a sharp rise in trapeziform sinuate phytoliths (Figure 3.15 B) that are typical of pond, lake,

and/or river margin grasses such as *Calamagrostis* (reedgrass), *Glyceria* (mannagrass), *Phalaris* (canarygrass), and others. Grass and sedge phytolith concentrations were very high, at 1,250,000 phytoliths per cm³ of sediment, which indicates that there was likely an extremely dense strand of grasses and sedges at this particular place and time.

A spike in *Ambrosia* pollen (Figure 3.16 B) in the 4Ab2 sample, along with the presence of *Corylus* pollen, suggests some type of disturbance other than fire, as indicated by low microscopic charcoal values. The disturbance to the surface could have included scenarios such as hurricane force winds and/or flooding. The dramatic spike in grass and sedge phytolith concentrations might also be an outcome of disturbed ground being rapidly colonized by graminoids. Intensive grazing by large herbivores could also simulate an *Ambrosia* bloom, but no sporormella fungal spores were found in the pollen analysis. Low percentages of *Pinus* and *Picea* pollen, greater than 20% Cupressaceae pollen, over 30% *Alnus incana* pollen (Figure 3.16 A), and a diversity of pollen from upland herbaceous plants suggests open canopy woodlands and shrub-lands with standing water at least part of the year (low percentages of pollen from aquatic plants).

In summary for 4Ab2 soil horizon sample, the combined macrofloral, phytolith, and pollen records suggest that regionally, a mixed conifer-hardwood forest with a reduced pine and spruce component predominated. Locally, a dense strand of grasses and sedges may have lined standing or flowing bodies of water, with riparian shrubs and trees like willow, birch, elm, and cedar along the forest margin. The initial AMS bulk charcoal sediment sample of 32,411 ± 298 calibrated calendar years BP (D-AMS 003044: 27,897 ± 171 rcybp) was generated on July 3rd, 2013. The sample, which was rich in carbon, was collected along the shoreline in an area where the 4Ab2 and 5Ab soil horizons merged. As such, the date could represent a mixed average of the ages for both the 5Ab and 4Ab2 surfaces. As the shoreline eroded, a stratigraphic separation of both surfaces became apparent. A second AMS age estimate for the 4Ab2 soil horizon was generated on September 9th, 2013 and produced a result of 29,563 ± 372, 31,846 ± 460, or 32,756 ± 97 calibrated calendar years BP (D-AMS 003532: 25,125 ± 141 rcybp). Two later AMS age estimates for this buried surface on individual charcoal samples reinforce the circa 30,000-year age estimate for the 4Ab2 surface. Two dates generated on individual coniferous charcoal samples in September 5th, 2017 produced ages of 29,058 ± 180 calibrated calendar years BP (PRI-5779: 24,760 ± 71 rcybp) and 29,681 ± 328 calibrated calendar years BP (PRI-5780: 25,367 ± 82 rcybp). The time represented by the 4Ab2 soil (sample 3) is approximately 5,000 years younger than the underlying 5Ab soil. Over this time period, the northern hemisphere has passed through a summer insolation maximum (Figure 3.17). The Greenland and Laurentide ice sheets were growing and air temperatures were on the cusp of a significant downward trajectory (see Hughes and Gibbard 2014). Sea Level at the time would have also dropped in response to the growing ice sheets.

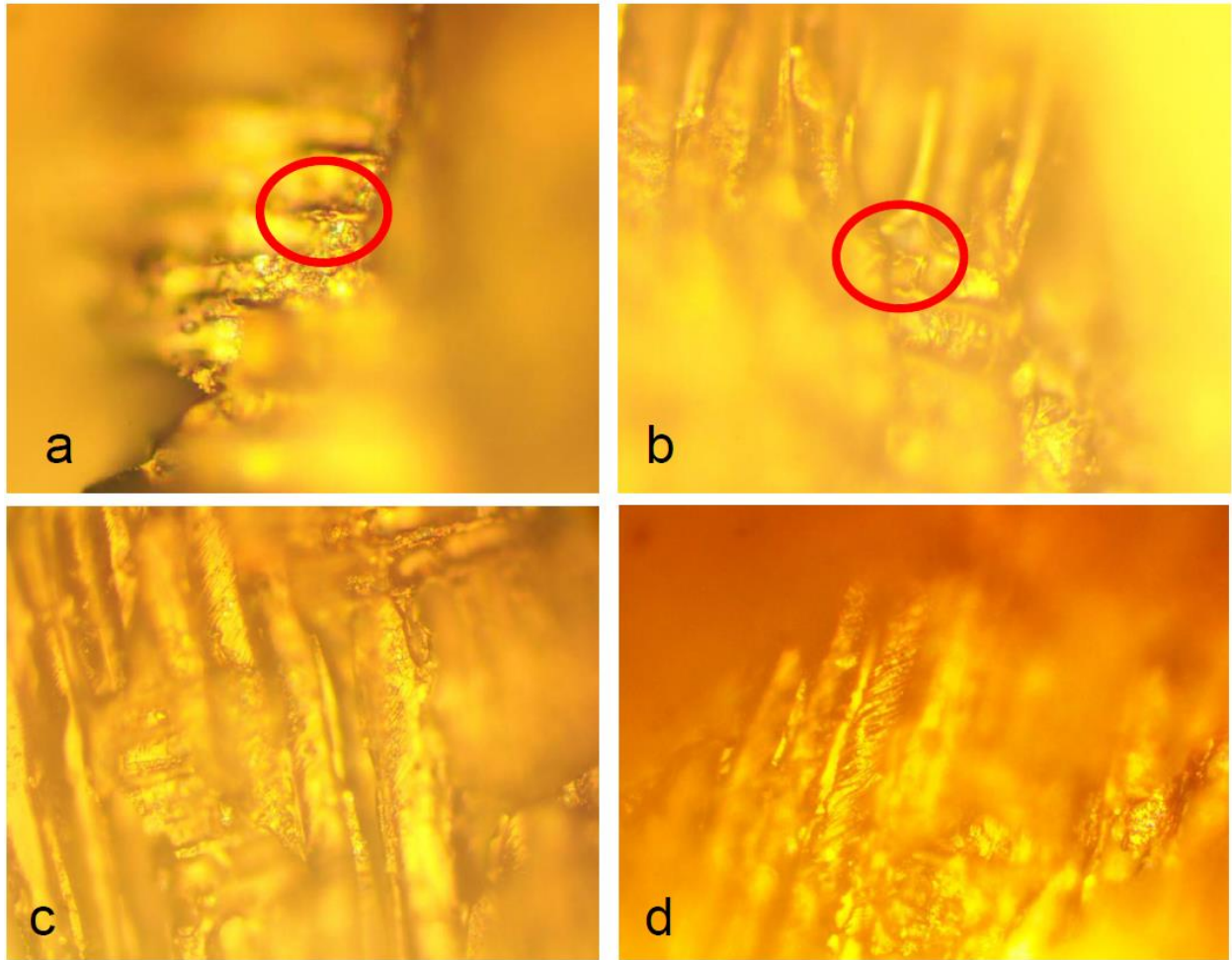


Figure 3.12. The micrographs show selected charcoal images from Parson's Island sample 4, which is associated with the 5Ab soil horizon. All micrographs taken at 600X magnification. The micrographs show A) *Picea* Type 1 ray tracheid pitting, radial view, B) *Picea* Type 1 ray tracheid pitting, radial view, C) helical thickenings on tracheid walls, radial view, and D) helical thickenings on tracheid walls, radial view. Images from Puseman et al. (2014: 27).

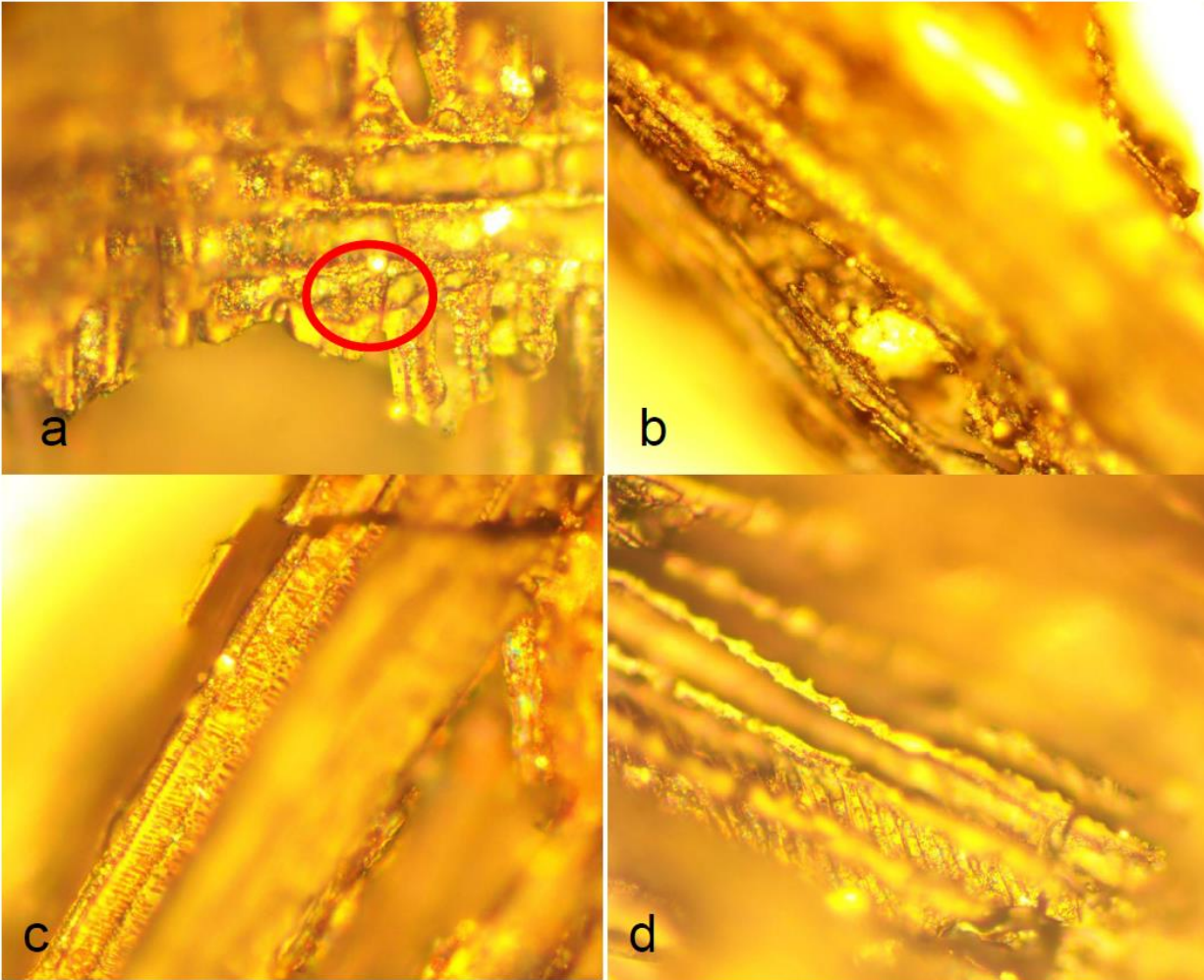


Figure 3.13. The micrographs show selected charcoal images from Parson's Island sample 3 and sample 2 associated with the 4Ab2 and 4Ab1 soil horizons. All micrographs were taken at 600X magnification. One micrograph shows *Picea* Type 1 ray tracheid pitting (A), radial view. Another also shows *Picea* Type 1 ray tracheid pitting (B), radial view. Helical thickenings on tracheid walls, radial view, are evident on charcoal from the 4Ab2 soil horizon (C) and the 4Ab1 soil horizon (D).



Figure 3.14. The micrograph shows a phytolith microfossil recovered from the 4Ab2 soil horizon at Parson’s Island. The micrograph was taken at 500X magnification and shows a bilobate phytolith diagnostic of Panicoideae grasses that may be darkened from exposure to an oxidative fire.

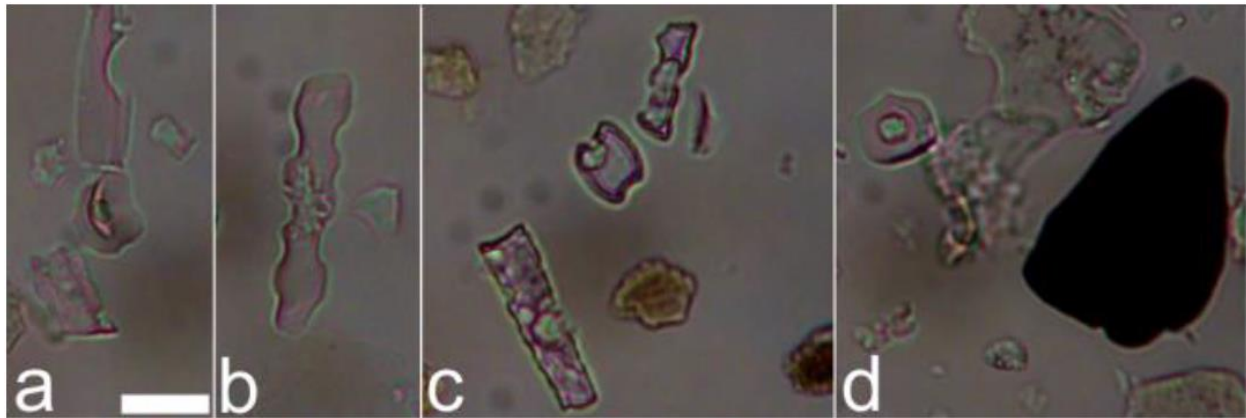


Figure 3.15. The micrograph shows phytolith microfossils recovered from the soil horizons at Parson’s Island. The micrographs were taken at 500X magnification. A keeled rondel phytolith (A) diagnostic of Pooideae grasses was found in the sample from the 5Ab soil horizon at Parsons Island. A trapeziform sinuate phytolith (B) diagnostic of Pooideae grasses was found in the 4Ab2 soil horizon at Parsons Island. A saddle phytolith (C) diagnostic of Chloridoideae grasses was found in the 6Ab soil horizon at Parsons Island. A rondel (D) with angular keel highly distinctive of canarygrass (*Phalaris* sp.) and a microscopic charcoal particle were found in the sample from the 4Ab1 soil horizon at Parsons Island.

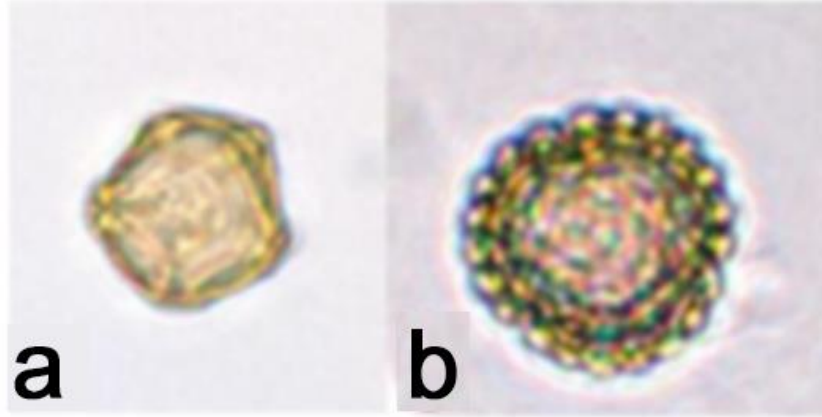


Figure 3.16. The micrographs show speckled alder (*Alnus incana*) pollen and ragweed (*Ambrosia* sp.) pollen from the 4Ab2 soil horizon at Parsons Island, Maryland.

3.1.7. Parsons Island 4Ab1 horizon (20,761 ± 198 cal. yrs. BP D-AMS 003533):

Sample 2, which is associated with the 4Ab1 soil horizon (see Appendix III: 247-248), was collected from above the in-situ biface embedded in the 4Ab1 horizon (North Bank Profile) at a depth of about 225 cm. A date of 17,133 ± 88 RCYBP was returned for this paleosol, with a calibrated age of 20,761 ± 198 CALYBP (D-AMS 003533). Uncharred macrofloral remains in this sample include a few root bark, rootlet, and unidentified organic fragments. A few sclerotia also were noted. The flecks of charcoal present within the 4Ab1 soil horizon were very small. Three pieces of conifer charcoal exhibited helical thickenings (Figure 3.13 D) and might reflect *Pseudotsuga menziesii* (Douglas-fir). One other piece of conifer charcoal did not exhibit any identifying characteristics. Two fragments of hardwood charcoal were too small for further identification. Four pieces of charcoal were too small and vitrified for identification.

Because of its lighter color and high quantity of silt-sized quartz grains, a larger than typical quantity of sediment within the 4Ab1 was selected for phytolith extraction (5 cm³ vs. 2 cm³). The phytolith record is best characterized by a dramatic drop in sedge (Cyperaceae) phytoliths and a dramatic rise in C₃ grass phytoliths. Also significant is the low grass/sedge phytolith concentration of 166,667 phytoliths per cm³. This suggests that either graminoids were much reduced on the landscape or, based on the lithology, the more likely scenario of rapid sediment deposition that significantly outpaced phytolith influx. A few C₄ Panicoideae and Chloridoideae phytoliths were observed, indicating some degree of warmth in the summer. One rondel phytolith that is regionally diagnostic of canarygrass (*Phalaris* sp.) was observed (Figure 3.15 D).

For the pollen record in the 4Ab1 horizon, dominant percentages of Cupressaceae and *Alnus incana* (speckled alder) pollen, significant percentages of pollen from upland herbs, and pollen from a combination of wetland and aquatic species indicate open-canopy forests with standing water during the summer.

In summary of the paleoenvironmental data for the 4Ab1 soil horizon (sample 2), the combined macrofloral, phytolith, and pollen records suggest that regionally, an open canopy forest dominated by

cedar and alder, and with a lesser component of poplar, birch, and elm, existed at this time. Locally, sedges were much reduced and mostly replaced by cool climate C₃ grasses that included *Phalaris*. Members of the Asteraceae and Liliaceae families were more abundant, indicating the presence of some herbaceous plants locally and regionally. The sample is contemporaneous with the later phase of the last glacial maximum (LGM), as well as a period of northern hemisphere summer insolation minimum, summers during this time were likely very cool and short (see Hughes and Gibbard 2014). The Laurentide Ice Sheet (LIS) margin was situated ~250 kilometers to the north, and seasonal runoff from ice melt within the Susquehanna headwaters, and the general dustiness associated with the LGM, may have contributed to the rapid sediment deposition rates suggested by the low phytolith concentrations in the 4Ab1 soil horizon. In essence, aeolian deposition in the region is outpacing phytolith production/accumulation on the landscape surface.

The 4Ab1 soil horizon was later re-dated and the AMS results confirm the overall age range of this buried surface. On July 23rd, 2017, another stone artifact was found along the eroding shoreline within the 4Ab1 soil horizon and associated with charcoal. The date on this charcoal sample provided an age estimate of 22,175 ± 235 calibrated calendar years BP (D-AMS 024724: 18,151 ± 100 RCYBP). On March 9th, 2017, Smithsonian test excavations within the 4Ab1 soil uncovered an undiagnostic quartz flake associated with a fleck of charcoal. The date for this charcoal sample was 22,501 ± 155 calibrated calendar years BP (PRI-5777: 18,515 ± 73 RCYBP). During the same Smithsonian investigation, another charcoal sample was unearthed from the 4Ab1 horizon and submitted for AMS dating. Though unassociated with any stone artifact, the resultant age estimate for this charcoal sample was 23,332 ± 174 and 23,703 ± 106 calibrated calendar years BP (PRI-5778: 19,388 ± 59 rcybp). Combined the ages for the 4Ab1 soil indicate that this surface is between ~23,400 and ~20,100 years old. In sum, the accumulated plant macro-floral, phytolith, and pollen remains from this stratum represent a maximum time span encompassing 3,200 years during the last glacial maximum (see Figure 3.17).

3.1.8. Elliott's Island 5Ab horizon (23,946 ± 318 cal. yrs. BP Beta-286851):

The macro-floral, phytolith, and pollen data for Elliott's Island are important with respect to the comparable-age paleoenvironmental data gleaned from the circa ~23,400 to ~20,100-year-old 4Ab1 soil horizon on Parsons Island. Elliott's Island is located about 70-kilometers (43.5 miles) south of Parsons Island along Fishing Bay in Dorchester County, Maryland. The sample (sample 1) is a peat (50ib soil horizon) extracted from a depth of about 500 cm below the modern ground surface (see Figure 3.18) along the island's northern shore (Table 1). The peat at this location has been dated to 20,020 ± 80 RCYBP, with a calibrated age of 23,946 ± 318 CALYBP (Beta-286851). Along the south shore of the island a comparable buried peat stratum was also dated to 20,400 ± 90 RCYBP, with a calibrated age of 24,342 ± 305 CALYBP (OS-81222). These circa 24,000-year-old peat deposits are contemporaneous with the coldest episode during the northern hemisphere's last glacial maximum.

The macrofloral record for the 50ib peat stratum contained several uncharred *Carex* seeds, an uncharred *Juncus* seed, and three uncharred *Scirpus*-type seeds, reflecting the presence of sedge, rush, and bulrush (Tables 2 and 3). *Scirpus*-type (bulrush) plants are herbaceous aquatic or wetland plants, mostly perennial, with triangular or circular stems. Recent taxonomic studies of the *Scirpus* genus using molecular phylogeny and morphological characteristics resulted in the creation of several new genera, including *Amphiscirpus*, *Bolboshoenus*, *Isolepis*, *Shoenoplectus*, *Schoenoplectiella*, *Trichophorum*, and

others. At one point, the *Scirpus* genus held almost 300 species, but many of the species once assigned to this genus have now been reassigned to the new genera, and it now holds an estimated 120 species (Jung and Choi 2011:409; Muasya et al. 2009:3). The *Scirpus*-type seeds could represent either *Scirpus* or one of the new genera. Sedge, rush, and bulrush are common wetland plants. Several uncharred *Viola* seed fragments most likely reflect *Viola lanceolata* (bog white violet), which can be found growing in bogs, swamps, wet meadows, and along shores. A moderate amount of cf. *Sphagnum* moss stem/branch fragments suggest the presence of sphagnum moss, a common component of bogs. A moderate amount of "Unidentified C" stem fragments exhibited some lightly silicified epidermis, suggesting these stems represent a monocot other than grass or sedge. In addition, the sample yielded numerous unidentified stem/leaf fragments and numerous pieces of unidentified organic material from the partially decayed peat bog plants. Sclerotia also were numerous in this sample. Sclerotia are round, black, smooth balls and range in size from 0.5 to 4+ mm in diameter (Trappe 1969). They are the resting structures of the reproductive organs of fungi such as *Cenococcum*, a mycorrhizal fungus, and were originally identified by Dr. Kristiina Vogt, a professor of Ecology in the school of Forestry and Environmental Studies at Yale University (McWeeney 1989:228). These fungi produce a symbiotic relationship between themselves and the roots of vascular plants, resulting in increased nutrient uptake, expansion of water absorption capabilities, and protection against pathogenic fungi (Harley and Smith 1983). Sclerotia survive at great depths in the soil and in a variety of soil types, from poor to rich, dry woods to bogs, and often are found in areas of deep surface organic accumulation (Mikola 1948:70). *Cenococcum* fungi and their associated sclerotia are found with conifers such as fir (*Abies* spp.), common juniper (*Juniperus communis*), larch (*Larix* spp.), spruce (*Picea* spp.), pine (*Pinus* spp.), and Douglas-fir (*Pseudotsuga menziesii*), as well as deciduous trees including sycamore maple (*Acer pseudoplatanus*), alder (*Alnus* spp.), birch (*Betula* spp.), American hornbeam (*Carpinus caroliniana*), hickory (*Carya* spp.), hazelnut (*Corylus* spp.), oneseed hawthorn (*Crataegus monogyna*), beech (*Fagus* spp.), glossy buckthorn (*Frangula alnus*), cottonwood/aspens/poplar (*Populus* spp.), oak (*Quercus* spp.), willow (*Salix* spp.), mountain ash (*Sorbus* spp.), and basswood (*Tilia* spp.) (Trappe 1962). It is one of the most common and globally abundant genera of ectomycorrhizal fungi, often the dominant mycorrhizal fungus on the roots of trees in arctic, temperate, and subtropical forests (The Regents of the University of California 1997-2014). Experimentation by Trappe (1969) has shown that dead sclerotia will float, resulting in their recovery in archaeobotanic flotation samples.

A few small fragments of *Salix* twig wood in 50ib peat note the presence of willow. A few small fragments of root wood from an unidentified hardwood also were noted. Some of the root wood was compressed, suggesting that this wood was wet, under pressure, and subsequently flattened. The sample also yielded numerous insect chitin fragments.

Phytolith analysis of the peat sample yielded a well preserved and highly concentrated phytolith record which was co-dominated by grass (Poaceae) and sedge (Cyperaceae) phytoliths (Figure 1). One sedge achene phytolith typical of those produced by *Shoenoplectus* and *Scirpus* was observed (Figure 3.19 A). Almost all of the grass phytoliths were derived from cool-climate C3 taxa, with less than 1% relative abundance of warm-climate C4 grasses. One parallelepiped phytolith diagnostic of pine needle/wood tracheid was observed (Figure 3.19 B). Most spruce (*Picea*) and many pines (*Pinus*) do not produce phytoliths. The parallelepiped phytolith is most likely derived from red pine (*Pinus resinosa*), indicating its likely presence nearby or at least within the watershed. The presence of freshwater sponge spicules indicates the occurrence of ponded or flowing water in some proximity to the site. Interestingly,

numerous volcanic glass fragments (tephra) were observed in the phytolith extract (Figure 3.20). Because the phytolith extraction procedure tries to remove particles like tephra, no attempt to quantify the quantity of the tephra material was made. The tephra was subjected to geochemical analyses at the Smithsonian Institution in 2014. Preliminary geochemical sourcing suggests that the tephra could have originated from one of the Brushy Butte shield complex pyroclastic eruptions, which occurred in northern California circa $24,000 \pm 6000$ years (Clynne and Muffler, 2010).

For the pollen record, *Cyperaceae* (sedge) pollen dominated the peat layer on Elliott's Island. Higher percentages of pollen from *Salix* (willow), *Sphagnum* (moss), and at least three species of *Ericaceae* (heath family), as well as a lower percentage of *Cupressaceae* (cedar and cypress) pollen, suggest an open fen with cooler wetland conditions than exist in the area today.

In summary, the combined macrofloral, phytolith, and pollen records indicate the presence of a sedge-dominated habitat with a significant proportion of C₃ grasses that probably has a best-fit modern analog with a boreal wetland or bog. The shrub layer was likely dominated by willow, and spruce and pines were likely growing fairly close to this locality. Looking at this site in the context of northern hemisphere climate records (Figure 3.17), this period of time takes place during an insolation minimum when summers received slightly less incoming solar radiation than today (see Puseman et al. 2014). However, the large northern hemisphere ice sheets were cooling the globe considerably, as evidenced by global mean air temperatures approximately 14° C cooler (Ibid) than today (Figure 3.17 D). With a large quantity of ocean water locked up in ice, global mean sea level was approximately 120 meters (394 feet) lower than present. Because of the weight of the Laurentide Ice Sheet (LIS), the topography of southern New England adjacent to the LIS boundary was depressed anywhere from 35 to 100 meters lower than today (Oakley and Boothroyd 2012). However, Elliott's Island, which was located ~250 kilometers south of the Laurentide Ice Sheet terminus, would have been situated near the crest of maximum glacial forebulge. Thus, relative sea level along the Middle Atlantic coastline may have been 130 meters (425 feet) lower than present. The LIS reached its maximum extent approximately 21,000 CALYBP, and with the Elliott's Island peat sample dated to 23,946 CALYBP and the 4Ab1 soil horizon at Parsons Island dated between ~23,400 and ~20,100 years old, these two Delmarva Peninsula landscapes document the interior terrestrial coastal plain vegetation during the Last Glacial Maximum (LGM). Based on the presence of preserved LGM organics in numerous low depressions, we can conclude that the region had a few scattered interdunal ponds containing perched water. However, the climate was generally cool, influenced by relentless northerly winds, and vast sections of the upland were covered by dry adapted C₃ grass species.

3.1.9. Paleoenvironmental Summary and Conclusions

Identification of macrofloral remains, phytoliths, and pollen in samples from a peat at Elliott's Island and from the buried paleosols at Parson's Island in the Chesapeake Bay, Maryland, reveals much about the Late Pleistocene environments circa 42,000, ~35,000, ~30,000, ~24,000, and ~21,000 years ago.

The phytolith and pollen records were well-preserved for all of the samples analyzed and provide complimentary datasets. Generally, phytoliths record a very localized record, and pollen records both a localized and regional record. Sometimes, the pollen record is overwhelmed with a

particular pollen type that dilutes the signals of taxa with less prolific pollen production. Phytoliths are only produced by certain plants, and thus, do not provide a comprehensive botanical record. However, when taken together, these two approaches in tandem with the macro-floral data provide a comprehensive paleoenvironmental summary.

Very few macrofloral remains were recovered from the paleosol samples. An uncharred *Panicum virgatum* floret in the oldest 6Ab soil horizon at Parson's Island reflects panicgrass growing in the area. The samples yielded very small fragments of charcoal. Pieces of conifer and hardwood charcoal were present in each of the four paleosol samples (6Ab, 5Ab, 4Ab2, and 4Ab1). Fragments of hardwood charcoal were the dominant charcoal type in the 6Ab and the 4Ab2 soil horizons, while conifer charcoal was most abundant in the 5Ab soil horizon. Examination of these charcoal fragments at magnifications of 400-600x revealed a few identifying characteristics. Some of the hardwood charcoal fragments exhibited scleriform intervessel pitting. This type of intervessel pitting is found in only a few types of shrubs/trees, including peppervine, dogwood, American witchhazel, possumhaw, sweetgum, magnolia/sweetbay/cucumber tree, blackgum/tupelo, woodbine/Virginia creeper, currant, blueberry/cranberry, and grape. Recovery of Ericaceae pollen in three of the samples for this project might reflect the presence of blueberry/cranberry and an identification of *Vaccinium* for the charcoal with scleriform intervessel pitting. Pieces of charcoal in the 4Ab2, 5Ab, and 6Ab soil horizons contained Type 1 *Picea* ray tracheid pitting, indicating spruce charcoal. The 5Ab soil yielded charcoal with piceoid cross field pitting and helical thickenings, reflecting Douglas-fir charcoal. Other pieces of conifer charcoal exhibiting helical thickenings in the 4Ab1 and 5Ab soil horizons might also represent Douglas-fir.

Notable regional trends for the Parson's Island and Elliott's records from oldest to youngest include a dominance of deciduous trees in the 6Ab soil horizon (circa 42,000 years ago), followed by coniferous taxa associated with the 5Ab soil (~35,000 years ago), and a rise in shrubs and herbaceous taxa at the LGM (~24,000 to ~21,000 years ago). At the same time, warm season C₄ grasses and sedges dominated the early record and steadily declined as cool climate C₃ grasses increased and then became the dominant feature at the LGM. In sum, the paleoenvironmental record for the region shows a transition from cool wet conditions towards colder dry conditions.

Some researchers (see French et al. 2009, Lemke and Nelson 2004, and Losco et al. 2010) have suggested that during the LGM the region was impacted by permafrost conditions with permanently frozen ground associated with a periglacial "polar-desert-like" climate. The lack of stratigraphic alterations or cryoturbated soil distortions to the buried LGM and pre-LGM strata, as well as the paleoenvironmental indicators (macro-floral carbon, phytoliths, and pollen) from both Parson's Island and Elliott's Island do not support the periglacial conditions put forth by French et al. (2009), Lemke and Nelson (2004), and Losco et al. (2010).

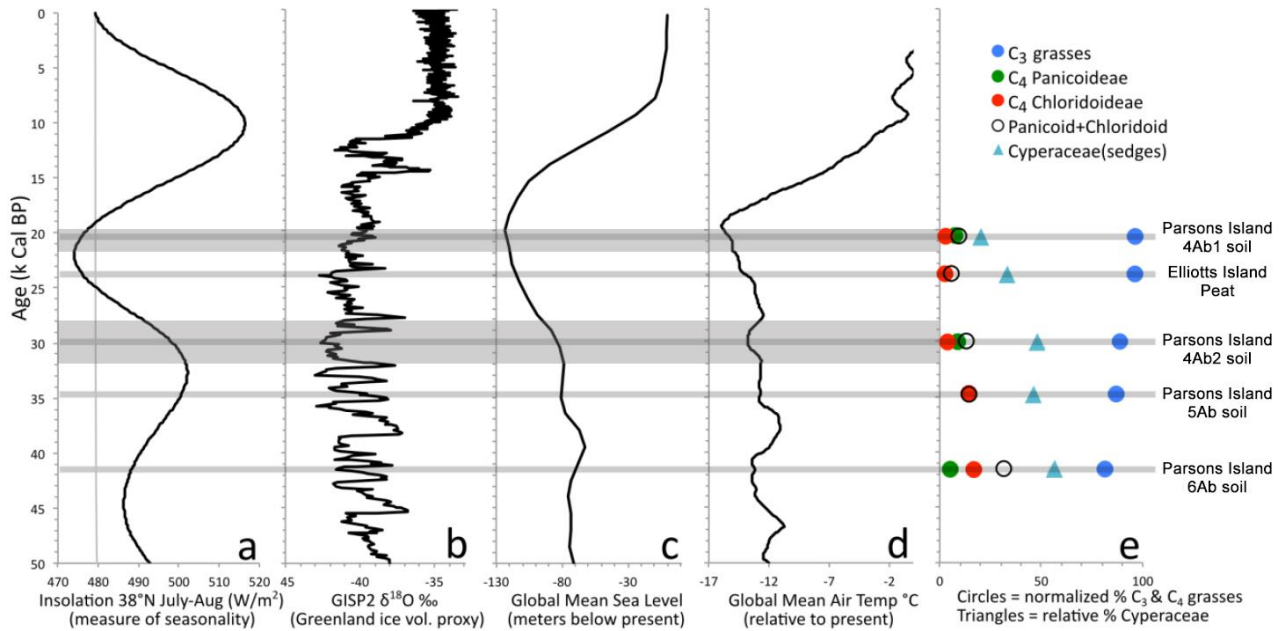


Figure 3.17. The illustration shows a comparison between the grass and sedge phytolith percentages for the 6Ab (circa 41,500-year-old), the 5Ab (circa 34,850-year-old), the 4Ab2 (circa 30,000-year-old), and the 4Ab1 (circa 20,500-year-old) surfaces at Parsons Island with Northern Hemisphere and global climatic records. The grass and phytolith percentages for the circa 24,000-year-old Elliott's Island peat are also included in this illustration. An insolation curve (A) for 21 June – 20 July at 38° N latitude, calculated using Laskar et al., (2004). A gray vertical bar is set to show modern-day insolation value. Changes in insolation (incoming solar radiation) are primarily driven by the earth's changing obliquity and precession of the axis, and is a measure of seasonality. The illustration shows the Greenland Ice Sheet Project (B) stable oxygen isotope curve (Grootes and Stuiver, 1997), which is a proxy for Arctic ice sheet volume (strong negative values = more ice) and generally corresponds with northern hemisphere air temperatures. The illustration also portrays global mean sea level reconstructions (C) relative to today (Waelbroeck et al., 2002). Finally, global mean air temperature reconstruction (D) relative to today (Bintanja, et al., 2005) are also shown. Normalized C₃ and C₄ grass phytolith percentages and overall sedge (Cyperaceae) relative abundance for each buried surface and locality € are depicted. C₃ grasses thrive under cool and mesic conditions, and some are shade tolerant. C₄ Panicoideae grasses thrive under warm conditions with moderate soil moisture, but require full sun. C₄ Chloridoideae grasses thrive under warm, full sun, and dry conditions. Sedges thrive under moist to wet conditions, but have variable temperature and light requirements. The graphic illustration is from Puseman et al. (2014: 24).

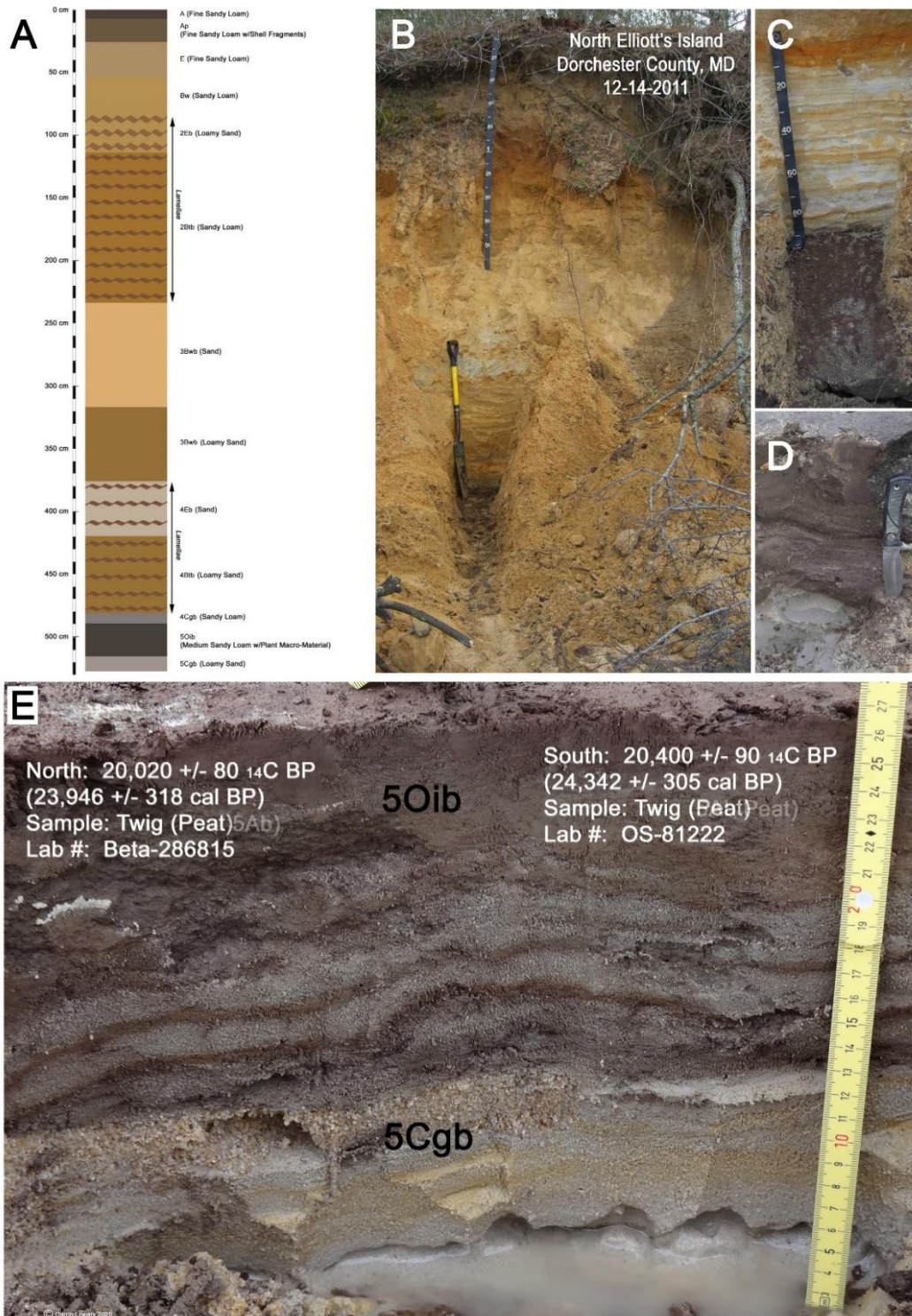


Figure 3.18. The illustration (A) and photo (B) portrays the various soil horizons within the eroded bank profile (B) at Elliott's Island in Dorchester County, Maryland. A distinct peat layer (5Oib) is present at the base of the eroded bank (C and D) along both the northern and southern shoreline. Two AMS dates on macro-floral remains from the buried peat indicate this stratum represents a buried LGM-age (circa 24,000-year-old) interdunal pond/wetland.

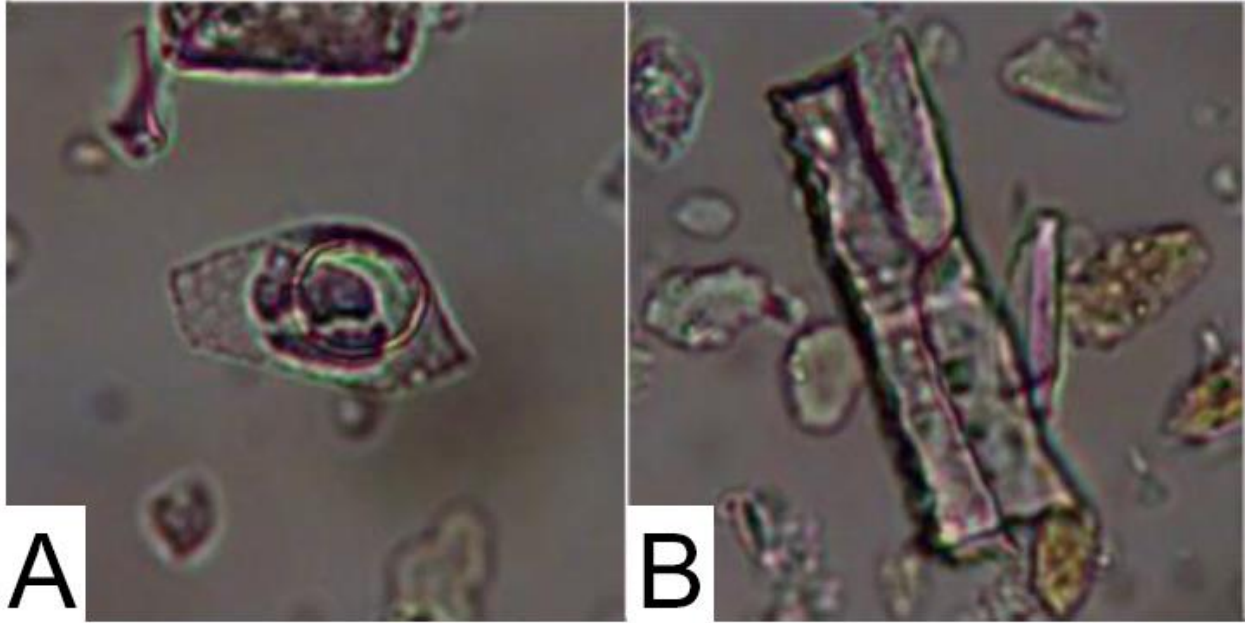


Figure 3.19. The micrographs show various phytoliths within the circa 24,000-year-old peat 50ib stratum at Elliott's Island, Maryland. One micrograph shows a sedge achene phytolith (A) typical of those produced by *Shoenoplectus* and *Scirpus*. A parallelepiped phytolith (B) diagnostic of pine needle/wood tracheid indicate the presence of red pine (*Pinus resinosa*) in the immediate area within the watershed.

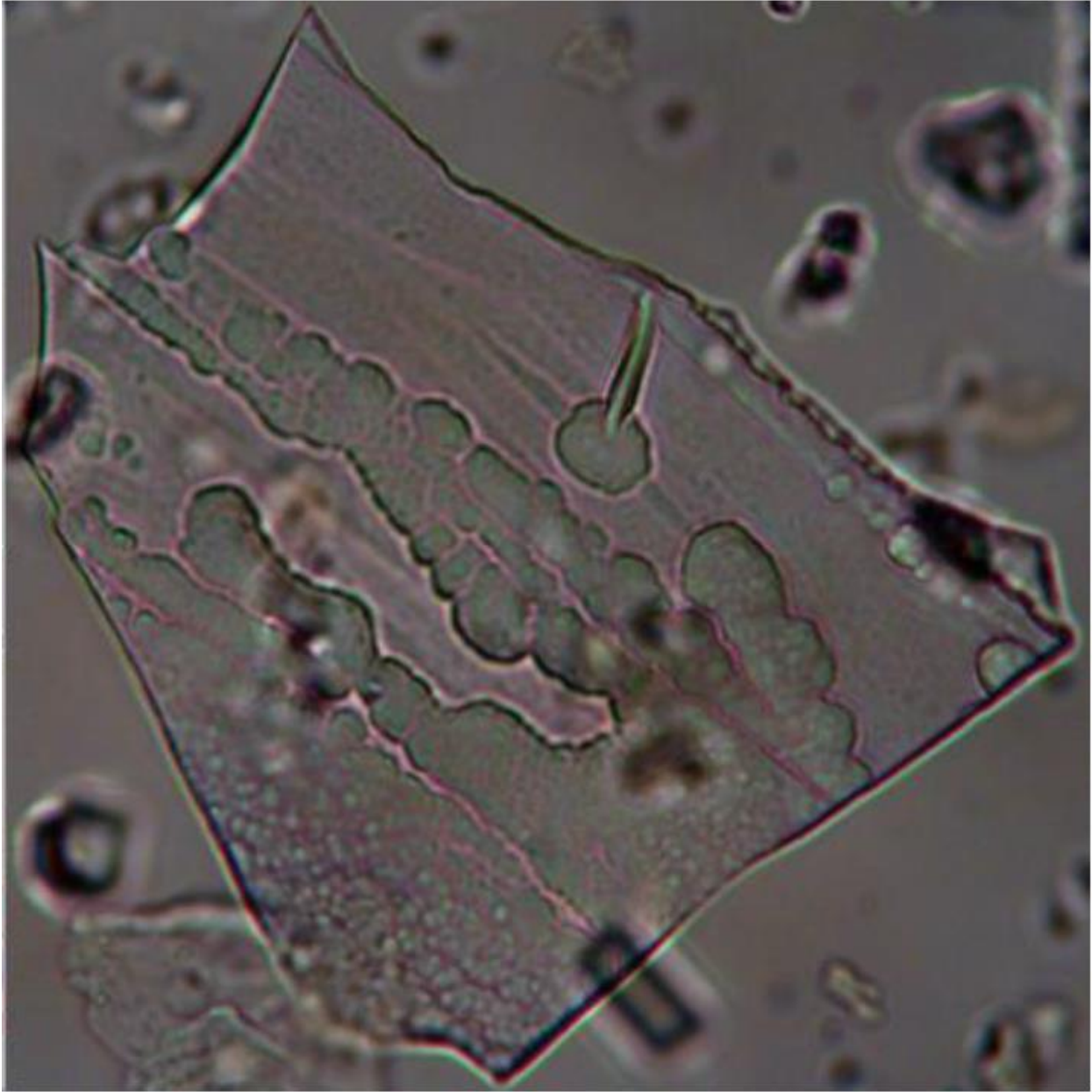


Figure 3.20. The micrograph shows an individual volcanic glass fragment (tephra) found during the phytolith analysis of the circa 24,000-year-old peat 50ib stratum at Elliott's Island, Maryland.

3.2. Synopsis of Archaeological Remains found at Parsons Island

The archaeological record of Parsons Island is scattered along the island's eroding coastal margins. In 1992-1993, when the island was first surveyed, no sites were located and the island encompassed about ~100-acres. As of 2020, four eroding archaeological sites (i.e., 18QU1047, 18QU1065, 18QU1066, and 18QU1067) have been documented and the island now encompasses only ~70-acres (see Figure 3.21). The chronological time frames associated with each of these four sites is different. Each site is summarized below.

3.2.1. Northeast Parsons Island (18QU1065):

The site (see Figure 3.21) encompasses an inundated upland buried beneath a ~1-meter thick layer of tidal marsh peat located along the northeastern margin of Parsons Island. When sea level was lower, the drowned surface represented an upland peninsula wedged between two spring-fed freshwater drainages. The site has revealed 27 Middle Archaic, Late Archaic, and possibly Late Woodland period displaced projectile points (see Figure 3.22). Limited quantities of fire-cracked rock and a few pieces of debitage have also been observed within the drowned upland stratum. The assemblage implies the area was episodically reoccupied as a small hunting-related encampment from 7,000 to 500 years ago. As noted on the 1847 (T-223) U.S. coastal survey (see Figure 2.3), the area inland of the shoreline encompassed a small forested peninsula surrounded by tidal marsh and bounded by Prospect Bay. Today, the site currently maintains a similar unchanged setting. A lengthy stretch of tidal marsh currently envelopes a surface containing a few exposed tree stumps (see Figure 3.22). Tree stumps extend offshore and stumps are completely inundated. The assemblage found along the shoreline imply the artifacts are being eroded from the drowned upland stratum and transgressing inland; via wave activity, onto the present shoreline.

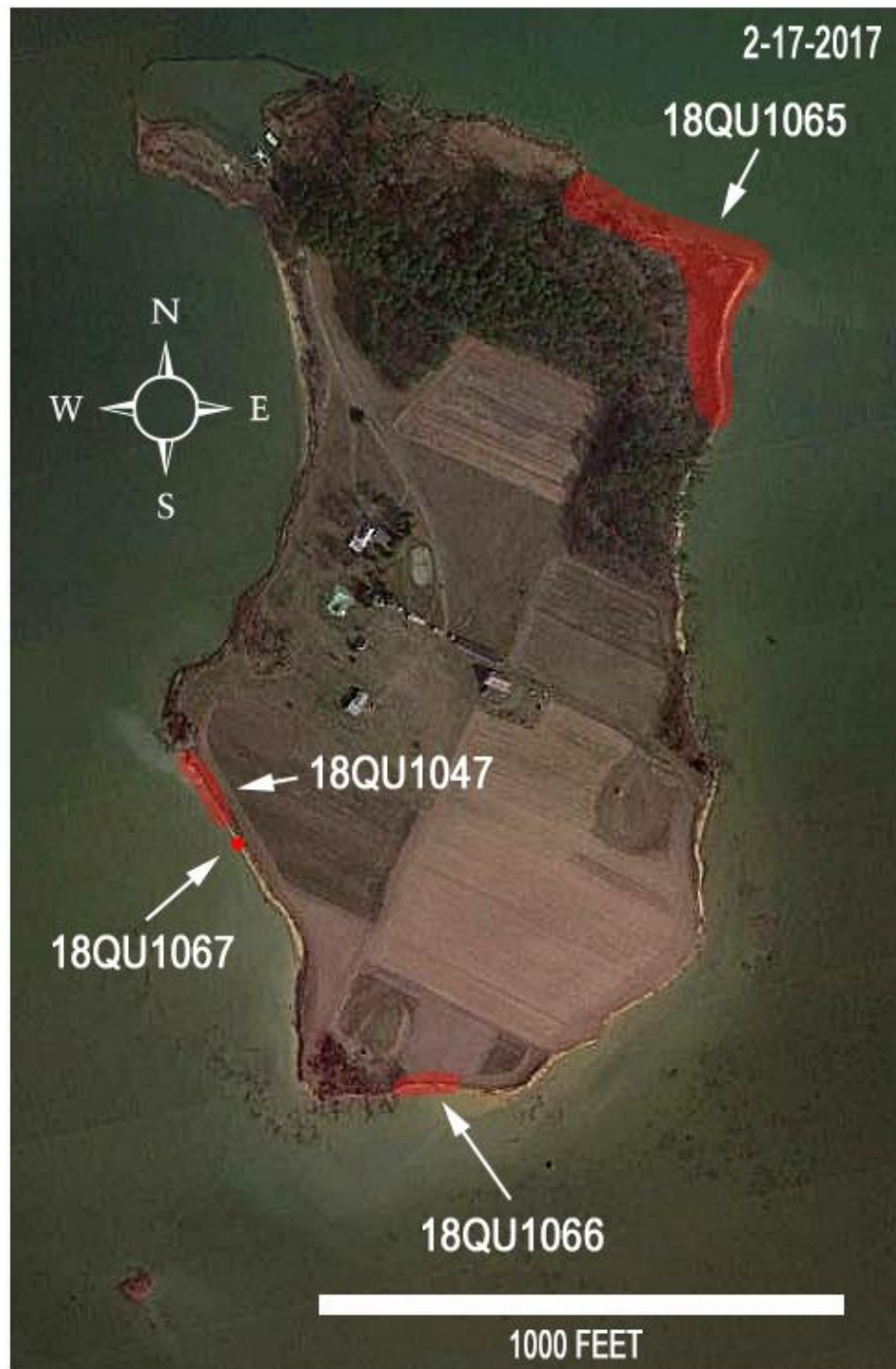


Figure 3.21. The 2017 aerial imagery of Parsons Island shows the Parsons Island site (18QU1047), The Parsons Island Well site (18QU1067), the South Parsons Island site (18QU1066), and the Northeast Parsons Island site (18QU1065).



Figure 3.22. The image shows the tree stumps being exposed by erosion at 18QU1065.



Figure 3.23. The image shows a representative sample of the projectile points found at 18QU1065.

3.2.2. South Parsons Island (18QU1066):

The site (see Figure 3.21) encompasses a steep eroded tilled-field shoreline margin (see Figure 3.24) immediately east of a former topographic swale, which contained a tidal marsh (see Figure 2.3). The site is located along the southeastern margin of Parsons Island. The shoreline has been examined multiple times since 2013 and eight definitive artifacts have been found (see Figure 3.25). The assemblage includes a quartz Late Archaic stemmed point, a damaged rhyolite knife fragment, a three-quarter grooved basalt axe, a basalt adze, a flaked chert adze, a fragmented steatite bannerstone, a pitted nutting stone, and a basalt axe blade fragment. The artifacts are indicative of the Late Archaic period, which brackets a time frame spanning 6,000 to 4,000 years old. All of the artifacts show evidence of agricultural plow scaring and recent plow damage. Before the area was heavily eroded, the site would have been situated along a well-drained westward sloping upland; located east of a small tidal marsh drainage. When sea level was lower, the tidal marsh area (see Figure 2.3) may have consisted of a freshwater spring drainage. Plow damaged fire-cracked rock fragments have also been observed along the shoreline. The scarred fire-cracked rocks and the plow damaged artifacts found along the shoreline originated from the surficial plowzone or Ap-horizon. Unscarred rounded cobbles have also been observed along the shoreline. These cobbles may have derived from the underlying MIS-5 geologic strata. The rounded cobbles may have been naturally-displaced to this location when sea levels were much higher circa 125,000 years ago. A parent lag source for these cobbles can be found east of Parsons Island along the eroded bank margins at Talisman Farms and further north towards Queenstown, Maryland. The lag cobble feature at Talisman Farms represents a former eroded and deflated early Pleistocene circa 1.8 to 2 million-year-old paleochannel deposit (see Schubel and Zabawa 1972).



Figure 3.24. The photograph shows the eroded shoreline associated with 18QU1066.



Figure 3.25. The photograph shows five of the eight artifacts found at 18QU1066. Note the plow scars and iron-metal streaks across the artifacts, which indicates that they had eroded from the historically-plowed surface of Parsons Island.

3.2.3. Parsons Island Well (18QU1067):

The site (see Figure 3.21) encompasses an eroded 19th century well that was found exposed along the shoreline at this location in 2013 (see Figure 3.26). The feature consisted of a ~3-meter high brick well feature located within two stacked wooden (oak) hogs heads (see Figure 3.27). The bricks were hand-made; maybe locally at Parsons Island. Axe hewn wooden planks were used to reinforce the bottom of the well. Hand-wrought iron square-head nails were present in the axe hewn planks. The brick well shaft was initially exposed in August-September 2013. Using the well feature as a benchmark, the rate of shoreline retreat was ~2.5 meters over a 270-day period. The brick well had collapsed by June 21, 2014. By December 2018, the basal portion of the well feature was still present. However, it was situated ~60 feet west of the existing bank margin and inundated by the bay's water at high-tide (see Figure 3.28). Flowing ice along the shoreline during the winter of 2018-2019 effectively removed the remnant wooden hogs head (see Figure 3.29) and dislodged the remaining in-situ bricks. As of 2020, only a pile of coastally-reworked bricks exist at this intertidal location. The artifacts found at the bottom of the well suggest that it was constructed during the late 18th or very early 19th century (see Figure

3.30). A single mold seamed light-green glass cork bottle found in the refuse near the surface of the well implies that it was abandoned and filled by the late 19th century.

From 1992 to 2013, the shoreline had eroded and retreated eastward between ~63.24 meters (207.5 feet) and 72 meters (238 feet); an average erosion of ~67.8 meters (~222.5 feet) over 21 years or 3.23 meters (~10.5 feet) of erosion per year. From 2013 to 2018, the shoreline retreated eastward past the well feature an additional 12 meters (39.5 feet), which equates to an annual erosion rate of ~2.43 meters (~7.9 feet) per year).



Figure 3.26. The dated photographs show the well feature during the period between May 20th, 2013 and March 2nd, 2014, as shoreline erosion gradually exposed the outline and construction aspects of the well.



Figure 3.27. The image shows the well feature on March 2nd, 2014. Note the oyster shell fill near the surface.



Figure 3.28. The image shows the collapsed well feature on December 23rd, 2018.



Figure 3.29. The image shows the bottom portion of the well feature and how it was constructed. The wooden hogs head surrounded the brick shaft. At the bottom a series of hand-hewn wooden planks or timbers were installed to strengthen the well's foundation and possibly serve as a filtering devise.



Figure 3.30. The image shows the artifacts found at the bottom of the well feature exposed along the southwest side of Parsons Island. The assemblage includes a spall or large flake of gunflint (far left), a handle section from a blue/gray stoneware vessel, a small fragment of delftware, a small fragment associated with a manganese-mottled ware vessel, a kaolin pipe stem/bowl fragment, and three small pieces of gunflint (one heavily burned).

3.2.4. Parsons Island (18QU1047):

The site was first recognized in May 2013 during a shoreline analysis conducted by John Wah and Darrin Lowery. Prior to May 2013, the nearby region within Prospect and Eastern Bay had been the focus of late Pleistocene stratigraphic research and geoarchaeological evaluations. These earlier regional investigations focused on Miles Point, Talisman Farms, and Barnstable Farm. The first in-situ artifact found at 18QU1047 was discovered on 8-4-2013 at 10:17am. Between 2013 and 2019, over 200 artifacts, most of which included small lithic debitage, were found at this location. Of these, nine artifacts were found firmly embedded within the 4Ab1 soil-horizon or at the contact between the 4Ab1 and the overlying 3Cgb2 soil-horizons (see Appendix III: 247-248). Most of the artifacts were found directly in front of the eroding bank profile, on the surface of the adjacent beach, or within the nearby inter-tidal zone. Detailed stratigraphic investigations and geochronological analyses were conducted. The archaeological stratum at 18QU1047 and the buried late Pleistocene surface were exposed as a result of the long-term erosion of the shoreline at Parsons Island. The assemblage found at the site includes 286 lithic artifacts, seven (7) late Pleistocene vertebrate mammal teeth, and two wind-polished/silica glazed pebbles. The artifact assemblage is comprised of bi-pointed knives, lanceolate points, unifacial tools, unifacial blades, blade cores, utilized flakes, and debitage, which are clearly distinguished from Clovis Paleoindian assemblages found in North America (see Bradley et al. 2010). However, the bi-pointed knife-forms have been described in a few purported Clovis caches (see Huckell 2014: 133-152). Environmental charcoal associated with three in situ lithic artifacts indicate an extreme age between circa 20,563 and ~22,656 calibrated calendar years before present for this assemblage. Recent OSL-dates (see Appendix II) generated on samples collected from the overlying aeolian strata seem to confirm the antiquity of the assemblage at 18QU1047. However, the large errors inherent with OSL age estimates and the influence that soil moisture content has on perceived OSL age values precludes a direct confirmation of the antiquity of the assemblage.

From 1992 to 2018, the shoreline has eroded and retreated eastward between ~42.56 meters (139.62 feet) and 85 meters (282 feet); (an average ~63.78 meters) or an annual erosion rate of ~2.45 meters (~8 feet) per year over the past 26 years. From 2013 to 2020, the shoreline retreated eastward more so along the southern margin of the 18QU1047 than along the northern boundary of the site. The bank edge retreated 9.93 meters (32.5 feet) eastward over this seven-year period. The rate of erosion varied considerably over this time period. During the first 15-month interval, which spanned May 2013 to October 2014, the shoreline retreated 2.82 meters (9.28 feet). During the next 44-month interval, which covered October 2014 to June 2018, the rate of shoreline bank erosion and retreat decreased to 2.77 meters (9.08 feet). During the timeframe between June 2018 and April 2020, the rate of bank retreat almost doubled to an astounding 4.33 meters (14.2 feet) over this short 22-month period. The episodes of marked erosion at 18QU1047 and other sites in the region can be directly linked to specific years when ice formed (see Zwissler et al. 2014) during the winter months (see Figures 3.31, 3.32, 3.33, 3.34, and 3.35).

The shoreline associated with 18QU1047 was first visited in May 2013 to document the late Pleistocene stratigraphy. The initial recognition that an archaeological site existed at this location did not happen until August 4th, 2013. On that date, a small gray chalcedony bi-pointed knife was found in-situ and embedded within the 4Ab1 soil horizon. After this initial discovery, the site was visited ninety-three (93) times or approximately once a month during the period spanning August 2013 through April 2020. As a result of the ninety-three site visits, 18QU1047 produced 286 lithic artifacts.



Figure 3.31. The photograph shows the shoreline associated with 18QU1047 and 18QU1067 on February 16th, 2014. Fragments of stranded ice can be seen along the shoreline at low tide.



Figure 3.32. On February 16th, 2014, the moist frozen ground along the bank margin has started to melt as a result of solar heating. Thermal slumping has occurred along the eroded bank edge at 18QU1047.



Figure 3.33. The photograph shows the ice that had formed along the shoreline at the Northeast Parsons Island Site (18QU1065) on January 21st, 2019. The photo was taken after most of the ice during the winter of 2019 had melted.



Figure 3.34. The photograph shows the shoreline at 18QU1047 and 18QU1067 on December 23rd, 2018 immediately before the early January 2019 coastal ice formation event. Note the presence of the wooden “Hogs Head” staves associated with the historic well at 18QU1067.



Figure 3.35. The photograph shows the shoreline at 18QU1047 and 18QU1067 on February 6th, 2019 immediately after the coastal ice had melted. Note that the wooden “Hogs Head” staves are no longer present at 18QU1067. Moving ice had dislodged, lifted, and transported the wooden staves over 80-meters south of the brick well feature.

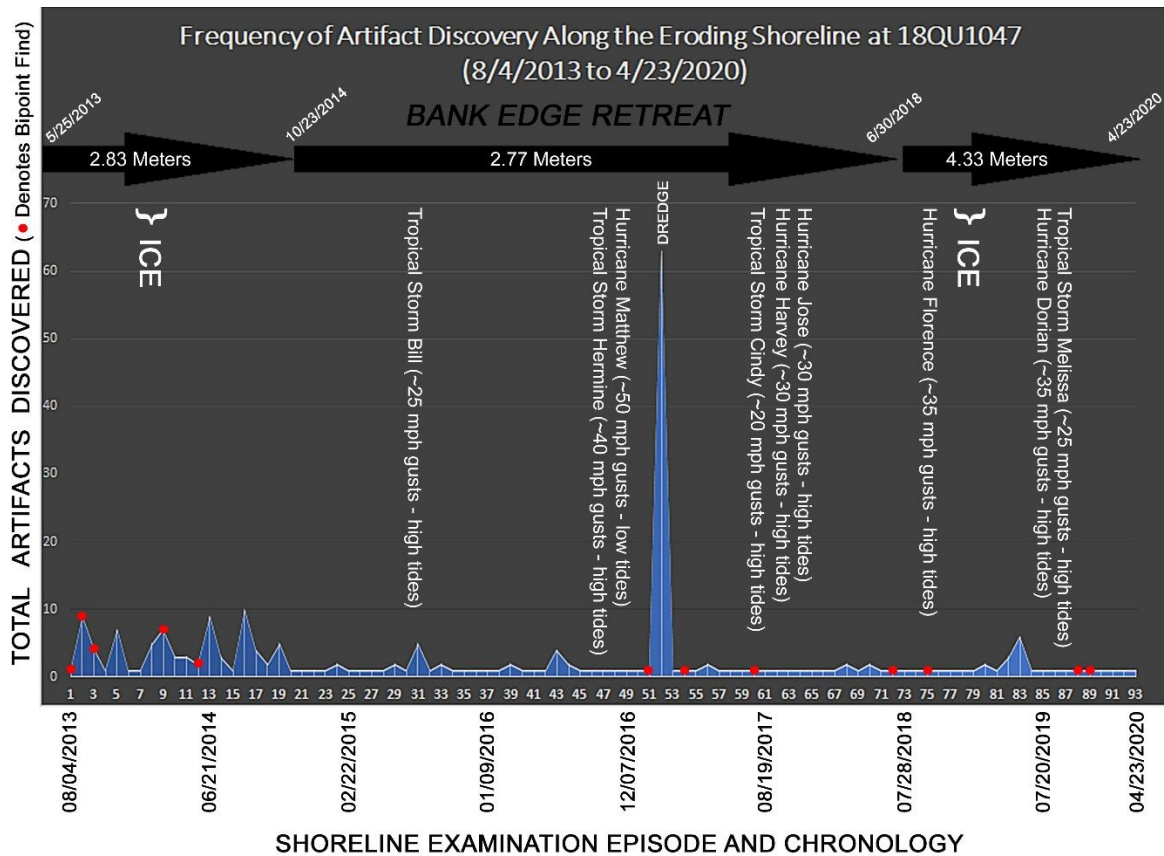


Figure 3.36. The graph shown above portrays the quantity of artifacts found at 18QU1047 over a seven-year period. In total, 286 lithic artifacts were found during this period. The largest number of artifacts from this site were found during the first year (2013 to 2014); a pattern noted at many newly discovered eroding coastal archaeological sites (see Lowery 2003b and Lowery and Stanford 2013). The sixty-three (63) artifacts found on 2/23/2017 were uncovered as a result of systematic dredging and sieving the sediments in the inter-tidal and sub-tidal areas west of the site’s eroding bank profile. The red dots denote the discovery of a bipoint biface at the site. Note the bifaces seem to have been discovered during two distinct episodes separated by a two-and-a-half-year hiatus. Finally, the magnitude of erosion and retreat noted along the site’s bank margin was documented using a hand-held GPS receiver over the seven-year period. Rates of shoreline retreat varied greatly over this period of time and largely depended on the seasonal presence of ice.

Bipoint Bifaces:

The assemblage from Parsons Island includes twelve (12) recognizable bipoint bifaces. These biface forms were found at the site during two distinct separate intervals of time. The first five were found between 8-4-2013 and 6-1-2014. The second grouping was found almost three years later; after the shoreline had eroded and retreated an additional ~3-meters (~10 feet). The second grouping, which contained seven bipoint bifaces, was found between 2-24-2017 and 1-22-2020.

The chronological timing of these discovery episodes seems to imply that erosion may have dislodged two distinct clusters. Field data and observations indicate that these separate erosion/artifact exposure events could represent scattered archaeological caches that were dispersed before being buried (see Deller et al. 2009 and Kilby and Huckell 2013). Considering the completeness and size of these bifaces, their presence at this otherwise ephemeral buried hunting-related locality would imply something more than haphazard or unintentional loss. However, Dr. Stephen Loring (2020: personal communication) has suggested that it is equally probable the knife clusters represent tightly circumscribed winter butchering localities. He has often observed (Ibid) his Innu friends complaining of losing knives while butchering winter caribou kills. When casually placed on the snow covered ground surface, the warmth of the tools melts the snow causing the knives to move downward and disappear, which ultimately results in the knives being overlooked. As such, the two biface clusters noted at 18QU1047 could either represent displaced caches or losses associated with distinct winter butchering areas.

The first grouping, which contained five bipoint bifaces, consisted of two small specimens (see Figure 3.39 A and C) and three large examples (see Figure 3.38 C, E, and G). Of these, two of the bifaces (see Figures 3.38 C and Figure 3.39 A) were found in-situ and firmly embedded within the 4Ab1 soil horizon. Only one (see Figure 3.39 A) was found with flecks of datable charcoal and radiometrically-dated to $17,133 \pm 88$ c14 years old or $20,761 \pm 198$ calibrated calendar years before present (D-AMS 003533). At the time, the 4Ab1 soil was situated approximately 220 centimeters beneath the modern ground surface. The gray chalcedony bi-pointed knife (see Figure 3.39 A) tested positive to bovine antiserum (see Appendix 1). The black chert bi-pointed knife (see Figure 3.38 C) tested positive to camel antiserum. If these analyses are correct, the two in-situ bifaces retain both camelid and bovid blood residue, which may indicate that their use as butchering tools.

The second grouping discovered at the site contained seven bipoint bifaces. Of these, three represent the small variety (see Figure 3.39 B, D, and E) and four consist of the larger variety (see Figure 3.38 A, B, D, and F). Two of the bi-pointed bifaces (see Figure 3.39 B and D) were found in-situ and embedded within the various strata exposed along the eroding bank profile at 18QU1047. One biface (see Figure 3.39 B) was found with flecks of datable charcoal and radiometrically-dated to $18,151 \pm 100$ c14 years old or $22,175 \pm 235$ calibrated calendar years before present (D-AMS 024724). The same biface (see Figure 3.39 B) was found fixed within the upper portion of the 4Ab1 soil, which was ~190-centimeters below the ground surface when it was discovered on July 23rd, 2017. As the shoreline retreated, the buried 4Ab1 soil was higher along the exposed bank profile and situated closer to the modern ground surface. The second in-situ specimen (see Figure 3.39 D) was found embedded at the contact between the 4Ab1 and the overlying 3Cgb2 soil horizon, which was ~175-centimeters below the surface when it was discovered on January 10th, 2020.

Even though the topographic elevation of the modern ground surface remained constant over the entire period of time, the depth of the 4Ab1 soil varied between 190-centimeters below the ground surface in 2017 and 175-centimeters below the ground surface in 2020. When the site was initially discovered in 2013, the 4Ab1 soil was ~220-centimeters below the ground surface. Coastal erosion spanning 2013 and 2020 indicates that the topographic slope/elevation of the buried 4Ab1 soil varied approximately 45-centimeters over a distance of ~9.93 meters or ~32.6 feet. Interestingly, a greater number of artifacts found at 18QU1047 in recent years have revealed evidence of aeolian polish on one or more surfaces with a distinct silica glaze (see Dorn 2012). The small bipoint biface (see Figure 3.39 D), which was found embedded at the interface between the 4Ab1 and the overlying 3Cgb2 soil horizon (see Figure 3.40), has aeolian polish on the one surface (see Figure 3.41 A and B) in contact with the overlying aeolian stratum (i.e., 3Cgb2 soil horizon). The stratigraphic position of this artifact and its post-depositional alteration would imply it was lying exposed on the surface for an unknown protracted period of time, wind polished, silica glazed by water vapor, and then buried by aeolian activity.

Another larger bipoint (see Figure 3.38 F), which was not found in-situ, shows aeolian polish/silica glaze on both faces (see Figure 3.41 C, D, E, and F). The polish/silica glaze observed on several artifacts found in recent years and the depositional circumstances noted for the small orthoquartzite biface found in January 2020 (see Figure 3.40) imply that the upslope portion of the 4Ab1 soil was eroded and deflated before being buried. More importantly some artifacts (see Figure 3.41 C, D, E, and F) may have been dislodged and exposed to aeolian abrasion. A few of the bipoint bifaces (see Figure 3.4 and 3.7) may have even been transported downslope from their primary archaeological contexts along with unassociated charcoal/carbon; reinforcing the concept that the bipoint assemblage from 18QU1047 may represent a singular displaced cache, a series of dislodged caches, or possibly even relocated butchering activity area losses.

The stratum originally containing the archaeological material at 18QU1047 may have been eroded and truncated resulting in an archaeological “lag” deposit. Before being buried by aeolian strata, some of bifaces may have been displaced downslope (see Figures 3.4, 3.7, 3.38C, and 3.39 A). Whereas, other bifaces may have remained on the higher upslope portions of the landscape (see Figure 3.39 B), exposed to aeolian abrasion (see Figures 3.38 F, 3.39 D, 3.40, and 3.41), and then buried. More importantly, the youngest-date of circa $20,761 \pm 198$ calibrated calendar-year-old for the charcoal associated with one of the in-situ bipoint bifaces found at 18QU1047 (see Figure 3.5) may represent a “*terminus post quem*” and indicate the earliest possible age for this lithic assemblage.

Based on the measurements (see Table 3.2), the bipoint bifaces from 18QU1047 seem to represent two distinct types; a small form and a larger form (see Figure 3.37). All of the bipoint bifaces found at 18QU1047 seem to have functioned as knives. Seven specimens have been asymmetrically-sharpened and/or show evidence of torque damage to the edges and distal margins. The lack of hafting wear and the greater width would imply that the larger bifaces were likely hand-held cutting or butchering tools. Wear patterns on the smaller/narrower examples imply these bifaces were hafted or socketed into some sort of handle.

TABLE 3.2. 18QU1047 BIPOINT BIFACE DATA.

DATE:	SMALL BIPOINT BIFACE MATERIAL:	LENGTH:	WIDTH:	THICKNESS:
7/23/2017	Gray/Brown Aquia Orthoquartzite (see Figure 3.39 B)	100.4	24.8	11.6
8/4/2013	Gray Chalcedony (Bovid blood residue, see Figure 3.39 A)	87.8	33.7	11.3
6/1/2014	Patinated Meta-Rhyolite (see Figure 3.39 C)	84.3	32.1	8.6
1/10/2020	Mottled Yellow/Tan Aquia Orthoquartzite (see Figure 3.39 D)	74	30.8	7
3/10/2017	White Quartz (see Figure 3.39 E)	57.6	23.9	11.3
	Average:	80.82	29.06	9.96
DATE:	LARGE BIPOINT BIFACE MATERIAL:	LENGTH:	WIDTH:	THICKNESS:
1/22/2020	Fossiliferous Cream/Tan/Red Chert (see Figure 3.38 A)	152.2	48	12.8
6/21/2018	Argillite (see Figure 3.38 B)	150.5	64.6	11
2/14/2017	Magothy Quartzite (see Figure 3.38 D)	149.1	43.1	12.1
9/25/2013	Black Chert (Camelid blood residue, see Figure 3.38 C)	147	67	8.5
3/2/2014	Silicified Miocene Sandstone (see Figure 3.38 E)	141.6	53.2	16.9
9/20/2018	Banded Chert (see Figure 3.38 F)	129.1	53.1	11.8
9/1/2013	Gray Quartzite (see Figure 3.38 G)	114.6	43.6	16
	Average:	140.5857	53.22857	12.7285714

18QU1047 Bi-Point Biface (Width/Length)

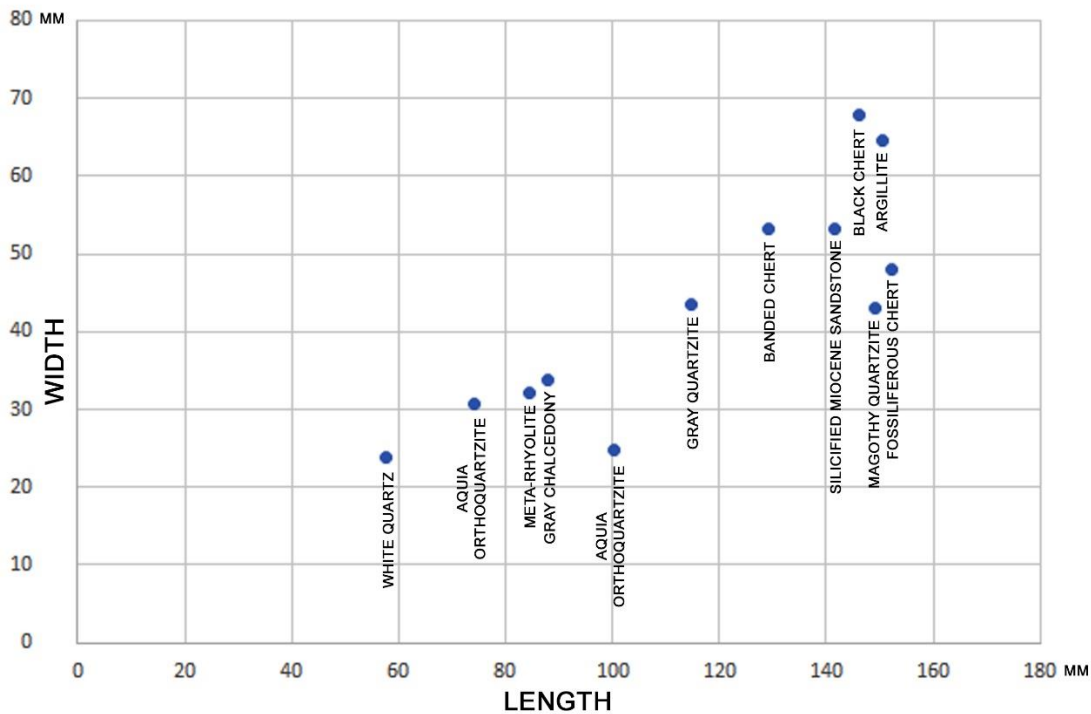


Figure 3.37. The graph portrays the length and width data for all twelve bipoint bifaces found at 18QU1047. Given the diverse suite of lithic materials being used, the biface forms indicate two bipoint varieties; a large and broad type and a small and narrow type. Evidence of sharpening noted on most of the large specimens would imply that they were even bigger when initially manufactured. In contrast, the smaller examples seemed to have been intentionally-made in this size range and are not highly re-tooled or altered versions of the large specimens.

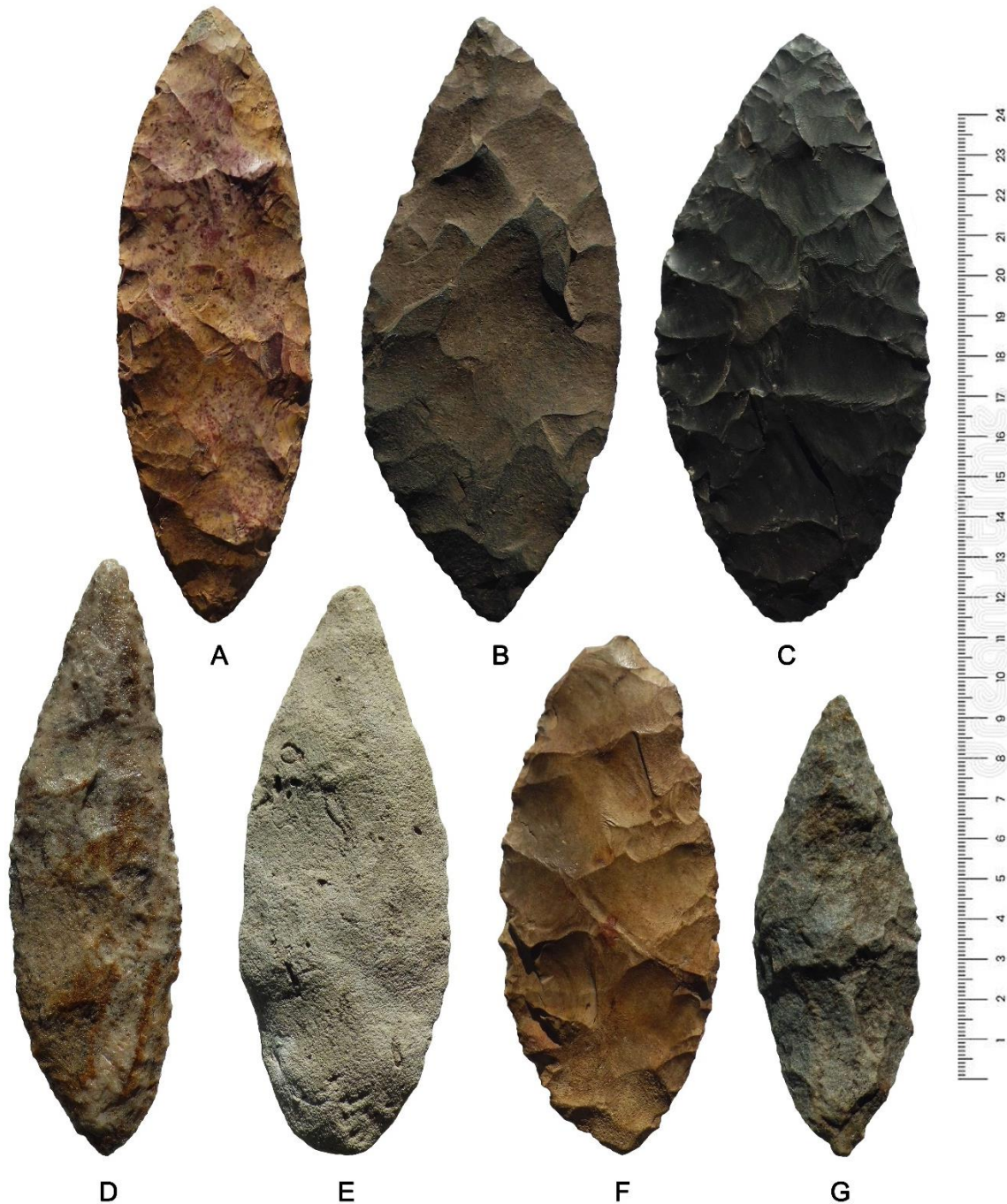


Figure 3.38. The image shows the large bipoint bifaces found at 18QU1047 on Parsons Island, Maryland.

The large fossiliferous tan/red chert specimen (A) was found on January 22nd, 2020. The argillite specimen (B) was discovered on June 21st, 2018. The black chert specimen (C) was exposed along the eroding bank profile on September 25th, 2013 and firmly embedded within the upper portion of the 4Ab1 soil horizon (see Figure 3.7). The Magothy quartzite specimen (D) was discovered on February 14th, 2017. The Miocene silicified sandstone specimen (E) was found on March 2nd, 2014. The banded-chert example (F) was recovered on September 20th, 2018. Finally, the gray quartzite specimen (G) was found at 18QU1047 on September 1st, 2013.

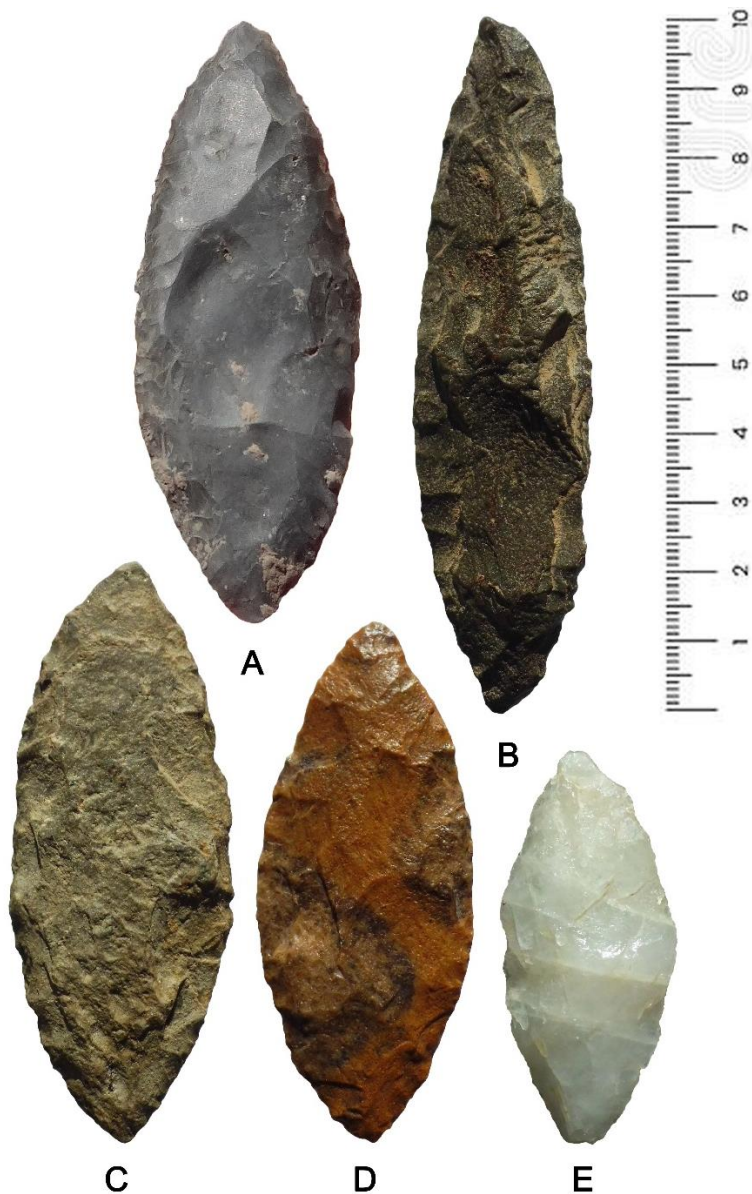


Figure 3.39. The image shows the small bipoint bifaces found at 18QU1047 on Parsons Island, Maryland. The gray chalcedony specimen (A) was exposed along the eroding bank profile on August 4th, 2013 and firmly embedded within the 4Ab1 soil horizon (see Figure 3.4). Charcoal associated with this artifact was radiometrically-dated to $17,133 \pm 88$ c14 years before present or $20,761 \pm 198$ calibrated calendar years before present (D-AMS 003533). The gray/brown Aquia orthoquartzite specimen (B) was found exposed along the bank profile on July 23rd, 2017 and firmly embedded with the 4Ab1 soil horizon. Charcoal associated with this artifact was radiometrically-dated to $18,151 \pm 100$ c14 years before present or $22,175 \pm 235$ calibrated calendar years before present (D-AMS 024724). The patinated meta-rhyolite specimen (C) was found on June 1st, 2014. The mottled yellow/tan Aquia orthoquartzite specimen (D) was found in-situ along the eroded bank profile at 18QU1047 on January 10th, 2020. Finally, the white quartz specimen (E) was recovered on March 10th, 2017.



Figure 3.40. The photograph shows the mottled yellow/tan orthoquartzite bipoint biface (see Figure 3.39 D) found in-situ along the eroded bank profile on January 10th, 2020. The biface is embedded at the contact between the 4Ab1 soil and the overlying 3Cgb2 horizon. The 3Cgb2 stratum represents an aeolian deposit, which buried the underlying 4Ab1 soil.

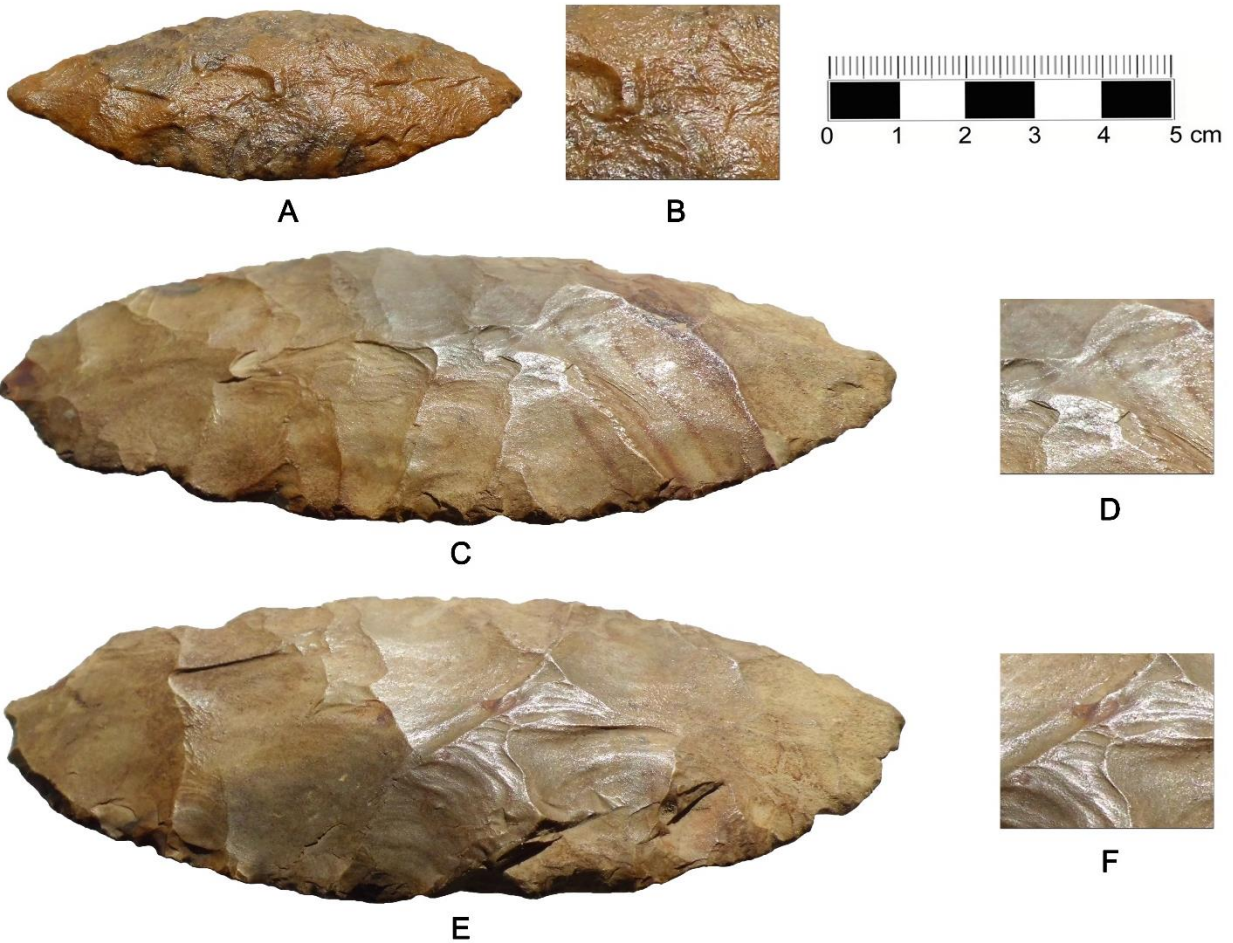


Figure 3.41. The images show slightly oblique views of two bipoint bifaces found at 18QU1047, which have evidence of wind polish and silica glaze. The smaller specimen (A) was found in-situ and embedded at the contact between the 4Ab1 and the overlying 3Cg2 soil horizons at 18QU1047. The side shown (A and B) is polished, silica glazed, and was exposed to the 3Cgb2 horizon. The opposite side of this biface, which was within the 4Ab1 soil, shows no polish or silica glaze. The larger specimen (C, D, E, and F) shows aeolian polish and silica glaze on both faces, which would imply that the artifact had been dislodged from its primary context before being buried. Presumably, this artifact was within the 3Cgb2 soil horizon at 18QU1047. As such, both faces were impacted by intense aeolian abrasion and exposure to water-vapor before being buried by the overlying 3Cgb2 stratum.

Other Bifaces and/or Biface Fragments:

Over the seven-year period spanning 2013 to 2020, fragmented bifaces have been discovered along the eroded shoreline 18QU1047. Some of these fragments seem to represent altered or salvaged biface segments originally associated with damaged or intentionally broken bipoint bifaces. None of these specimens were found in-situ. However, all were found along the shoreface immediately west of the eroded bank profile at 18QU1047. The following summary will describe these bifaces and/or biface

fragments. It will attempt to put them in a context with respect to the lithic technology associated with the archaeological site.

Two segments or fragments (see Figure 3.42 A and B) found at 18QU1047 may represent distal or basal portions of bipoint bifaces that had been accidentally damaged or intentionally broken. The basal segment of a biface (see Figure 3.42 B) seems to have been broken as a byproduct of accidental prying, torque, or twist damage. Intersecting fractures associated with the distal fragment (see Figure 3.42 A) of a biface may indicate that it was intentionally smashed or broken to produce “pie-wedge” segments (see Deller et al. 2009).

Two small bifacial “pie-wedge” segments (see Figure 3.43 and 3.44) found at 18QU1047 show intentional utilization and alteration. One fragment (see Figure 3.43), which is made of tan-colored quartzite, has two burin-flake detachments removed from a fractured margin towards the edge of the biface. The artifact; though crude, is somewhat reminiscent of wedge-shaped micro-blade cores typically found at Upper Paleolithic sites in Alaska and in Siberia (see Hadleigh West 1996). The other bifacial “pie-wedge” fragment (see Figure 3.44) shows extensive utilization along all of the fracture margins, which suggests these sharp angular margins functioned as scraping planes.

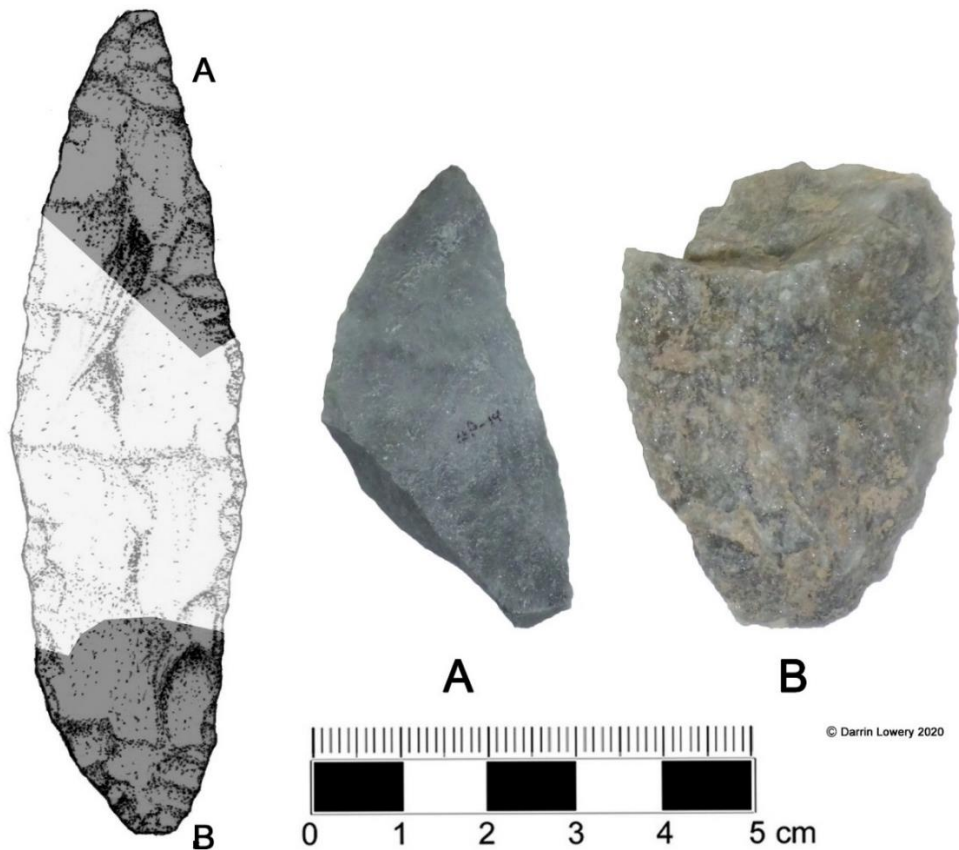


Figure 3.42. The image shows two biface fragments found at 18QU1047. A fragment of a well-made quartzite biface was found at 18QU1047 on 7-10-2016 and it may represent the distal portion of a bipoint biface. The damage to this specimen could represent intentional breakage. Another quartzite biface fragment (B) was found on 1-17-2015 and it may represent the basal section of a bipoint biface, which was broken as a result of twisting or prying actions.

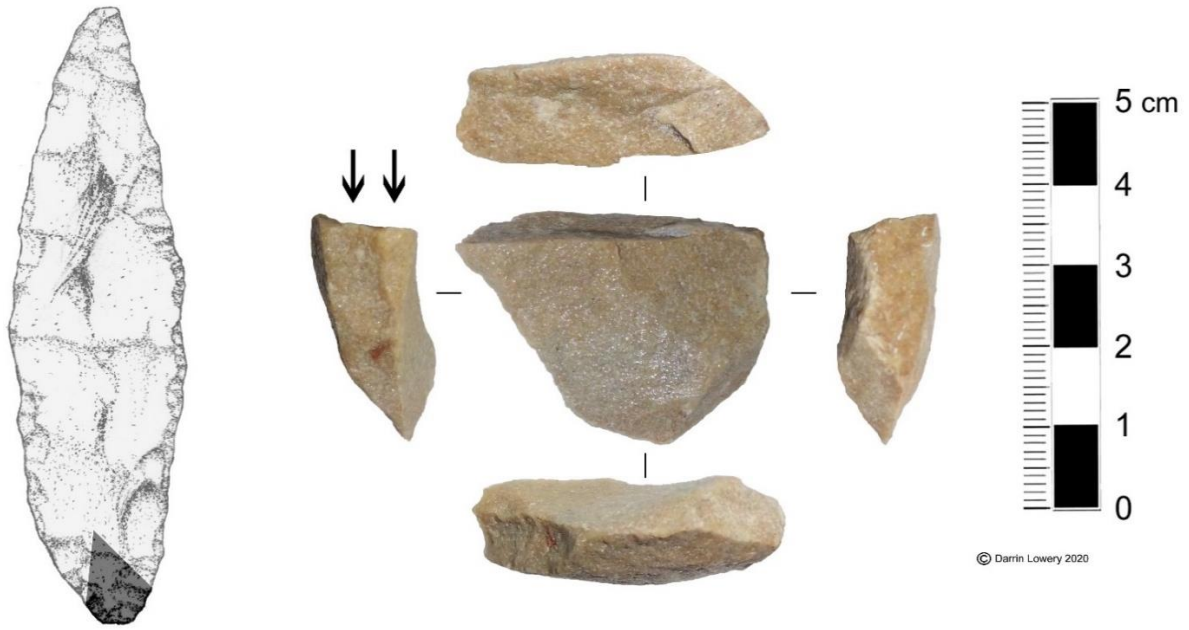


Figure 3.43. A small “pie-wedge” section of a quartzite biface found at 18QU1047 on 6-12-2018 shows intentional “burin-like” flake detachments from the fractured edge margin.

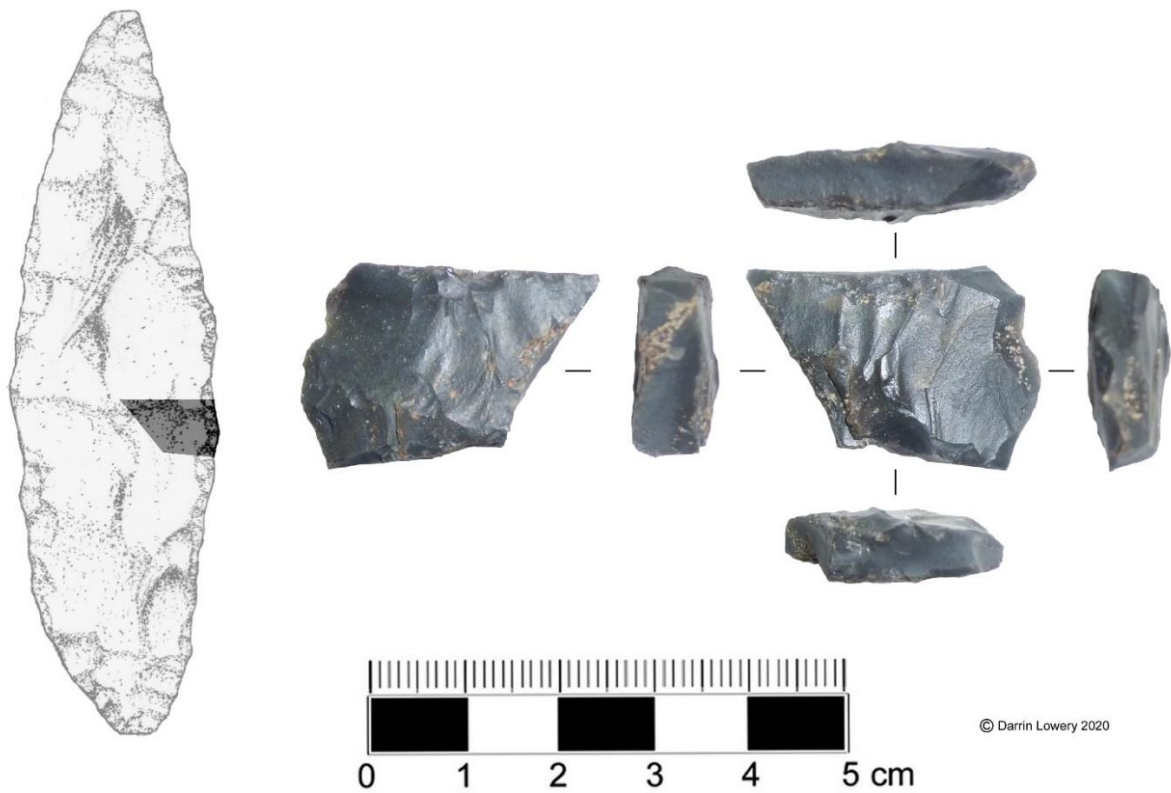


Figure 3.44. A “pie-wedge” section of a gray chalcedony biface found at 18QU1047 on 11-17-2018 shows intentional utilization along all of fractured edges.

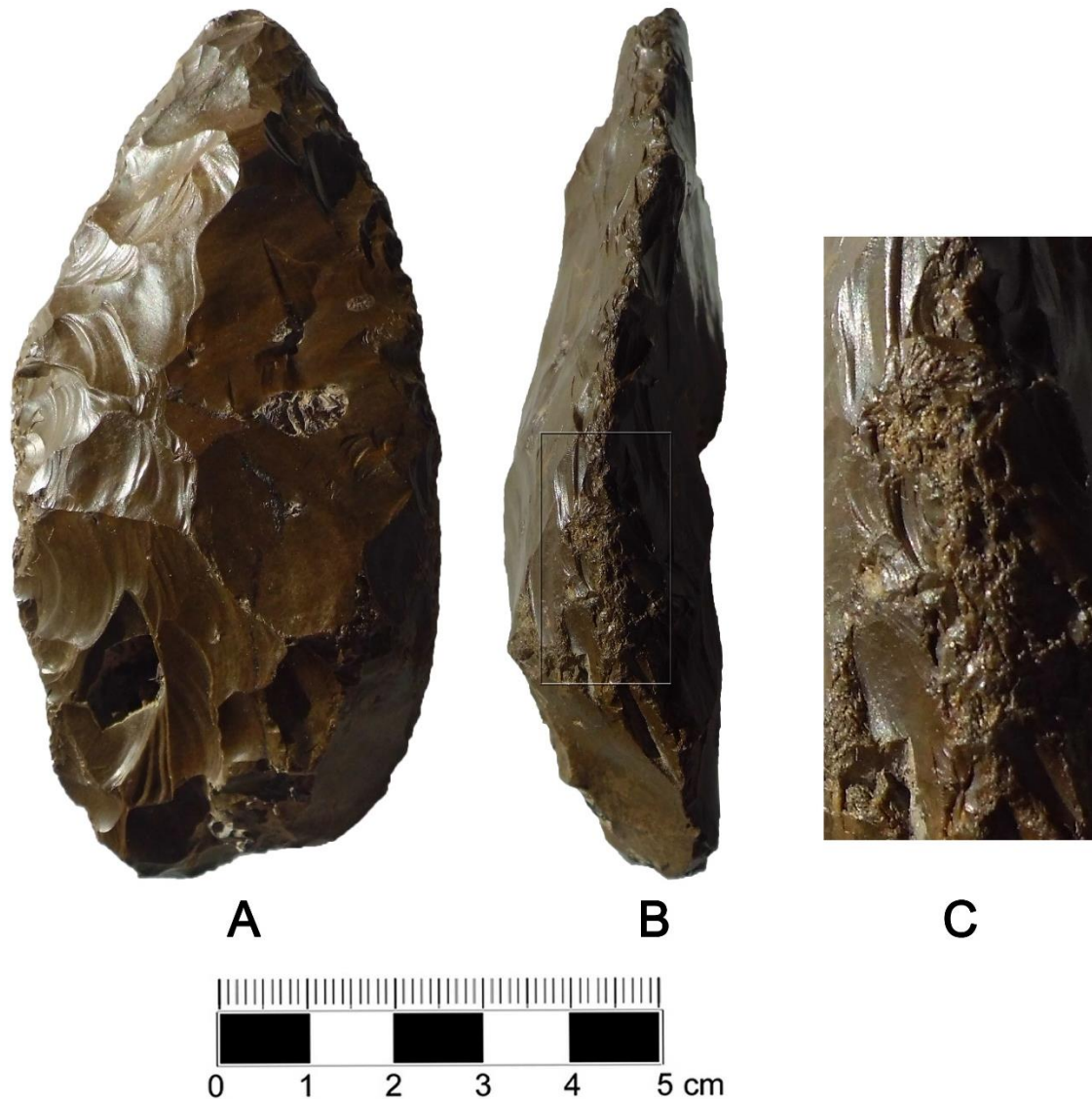


Figure 3.45. The photos show a thick biface made of jasper that was found at 18QU1047 on 8-24-2018. The biface (A) retains evidence of marked battering (B and C) along its lateral edge, which suggests that it may have been used as a hammer.

A single thick jasper biface was also found at 18QU1047 on 8/24/2018. The biface (see Figure 3.45) shows marked battering along one lateral edge with distinct facets indicating that it was subjected to repeated blows. The battering along the right lateral edge (see Figure 3.45 A, B, and C) implies that this artifact may have been used as a hammerstone. The specimen resembles a failed bifacial quarry blank. However, the presence of rounded cobble rind along a small section of this artifact implies it was manufactured from locally-available secondary cobble sources. In sum, the artifact seems to represent a failed attempt to produce a bipoint biface that was expediently deemed suitable as a hammerstone or the edge damage indicates repeated battering associated with failed attempts to thin the biface.

Lanceolate Bifaces:

Eight bifacial lanceolate points have been found at 18QU1047. The lanceolate points can be classified as two distinct types or forms. These types include lanceolate points made from salvaged bipoint bifaces (see Figure 3.46) and those that seem to have been intentionally-made as lanceolate projectile points (see Figure 3.47).

The first type retains some morphological attributes indicating rejuvenation of a pre-existing bifacial artifact. A basalt lanceolate biface (see Figure 3.46 A) uncovered offshore at the site retains a remnant portion of an earlier transverse medial fracture located along its thinned basal edge. The fractured basal margin may indicate that the present lanceolate (see Figure 3.46 A) was originally the distal or basal section of a bipoint biface analogous to several bipoint specimens uncovered at the site (see Figures 3.38 and 3.39). Another chert lanceolate (see Figure 3.46 B) has a marked constriction along its proximal end. The basal edge of this specimen has abrupt steep retouch suggesting it may have also been salvaged from a broken or damaged bipoint biface (see Figure 3.39 B).

The morphology of other lanceolate specimens implies that some examples (see Figure 3.47) were made specifically in a lanceolate shape or outline. These forms are smaller in length and generally narrower (see Table 3.3) than the examples salvaged from broken bipoint bifaces. Some of the smaller lanceolate points (see Figure 3.47 E and F) do show impact trauma suggesting they functioned as projectiles. The assemblage includes six complete lanceolate points (see Figure 3.47 A – F) and five damaged specimens (see Figure 3.47 G – K). Quartz is the dominant lithic material in the sample of both complete and damaged specimens. In the assemblage, the quartz examples have the most evidence of impact trauma. One quartz specimen (see Figure 3.47 G) seems to have shattered upon impact and another (see Figure 3.47 K) snapped immediately above the haft. Finally, it is inferred that a small quartz biface distal fragment (see Figure 3.47 H) found at 18QU1047 may have belonged to a similar lanceolate point, based solely on the fact that it was detached as a result of impact trauma.

The other small lanceolate points and fragments found at 18QU1047 were manufactured from chert (see Figure 3.47 B, D, and J), chalcedony (see Figure 3.47 A and C), and petrified wood (see Figure 3.47 I). All of the materials used to manufacture these points could have easily been derived from nearby secondary cobble sources or coastal plain primary outcrops. One specimen (see Figure 3.47 A) retains rounded cobble cortex along its left lateral edge proving that it was manufactured from a rounded cobble. With respect to the damage petrified wood lanceolate (see Figure 3.47 I), large fragments of petrified wood (see Lowery 2002a) have been observed in outcrops within the coastal plain geologic exposures located in nearby Kent County, Maryland.

The metric data for the lanceolate points found at 18QU1047 are outlined in Table 3.3 and these data (see Figure 3.48) clearly show how similar the small variety lanceolate points (see Figure 3.47) are to each other relative to the marked differences noted in the salvaged examples (see Figure 3.46). Generally speaking, the lanceolate points cluster between 40 and 50 millimeters in length and are approximately 25 millimeters in width. The specimens made from salvaged bipoint bifaces are much longer and greater than 25 millimeters in width.

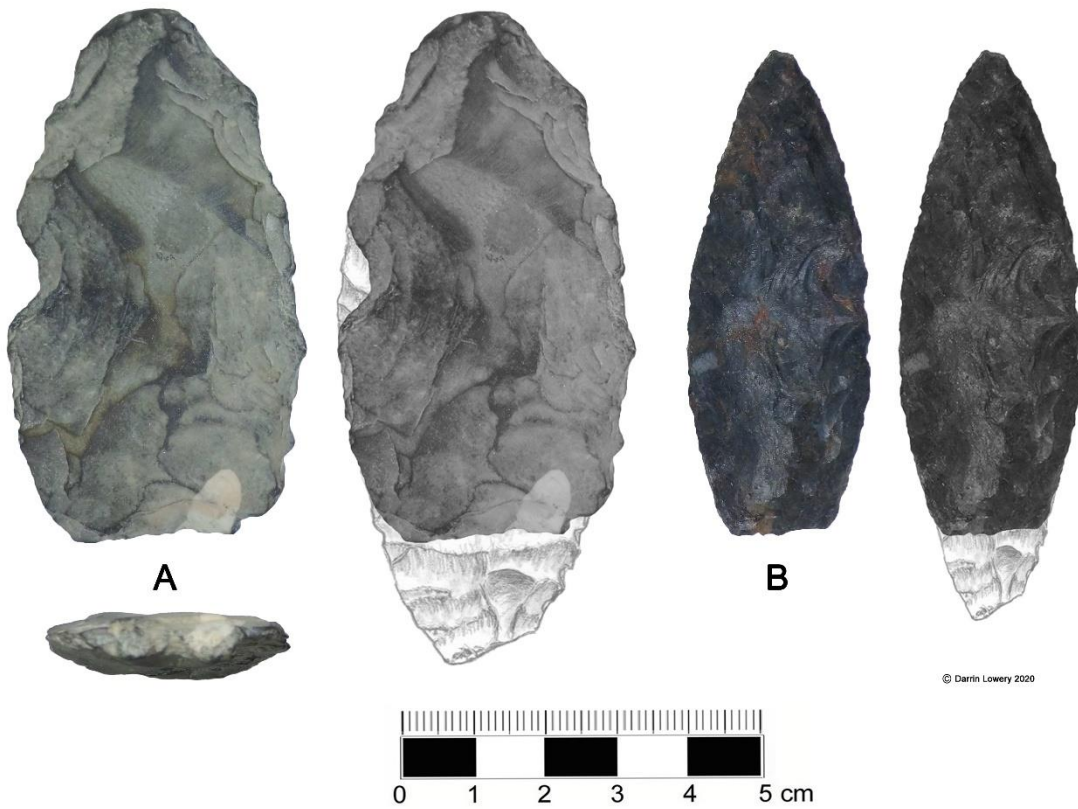
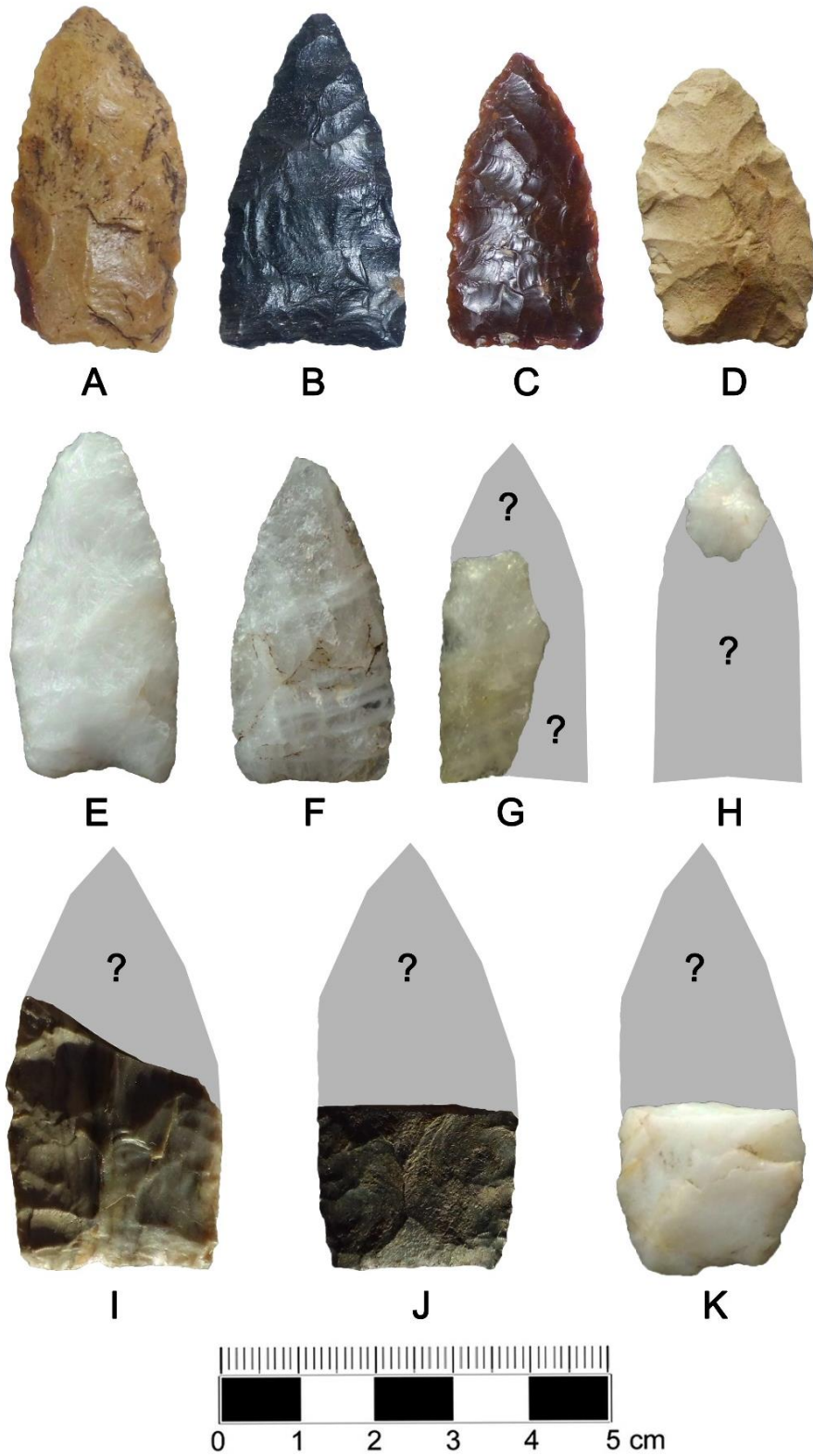


Figure 3.46. The images show two lanceolate bifaces found at 18QU1047. The basal section of one (A) basalt lanceolate is thinned, but retains a remnant transverse medial fracture. The other (B) has a steeply retouched basal edge margin. As implied by the reconstructions, both may have been salvaged from damaged bipoint biface forms.



© Darrin Lowery 2020

Figure 3.47. The image shows both the complete and fragmentary small lanceolate points found at 18QU1047.

TABLE 3.3. 18QU1047 LANCEOLATE POINT DATA.

DATE:	DESCRIPTION:	LITHIC MATERIAL:	LENGTH:	WIDTH:	THICKNESS:
2/16/2014	Lanceolate Point (Salvaged Bi-Point; see Figure 3.46 A)	Basalt	75	42.7	9.7
8/19/2017	Lanceolate Point (Salvaged Bi-Point; see Figure 3.46 B)	Black Chert	69.8	25.9	8.2
6/28/2014	Small Lanceolate Point (see Figure 3.47 C)	Brown Chalcedony	41.8	22.7	6.1
9/26/2014	Lanceolate Point (see Figure 3.47 E)	White Quartz	47.8	23.8	8.3
12/14/2014	Lanceolate Point (see Figure 3.47 F)	White Quartz	42.7	22.4	10.4
2/8/2015	Lanceolate Point (see Figure 3.47 A)	Tan Chalcedony	48.2	23.2	8.5
1/4/2017	Trianguloid Lanceolate Point (see Figure 3.47 B)	Black Chert	46.9	25.4	5.4
6/8/2017	Lanceolate Point (see Figure 3.47 D)	Cream Chert	39.5	24.5	7.5
		AVERAGE:	51.4625	26.325	8.0125

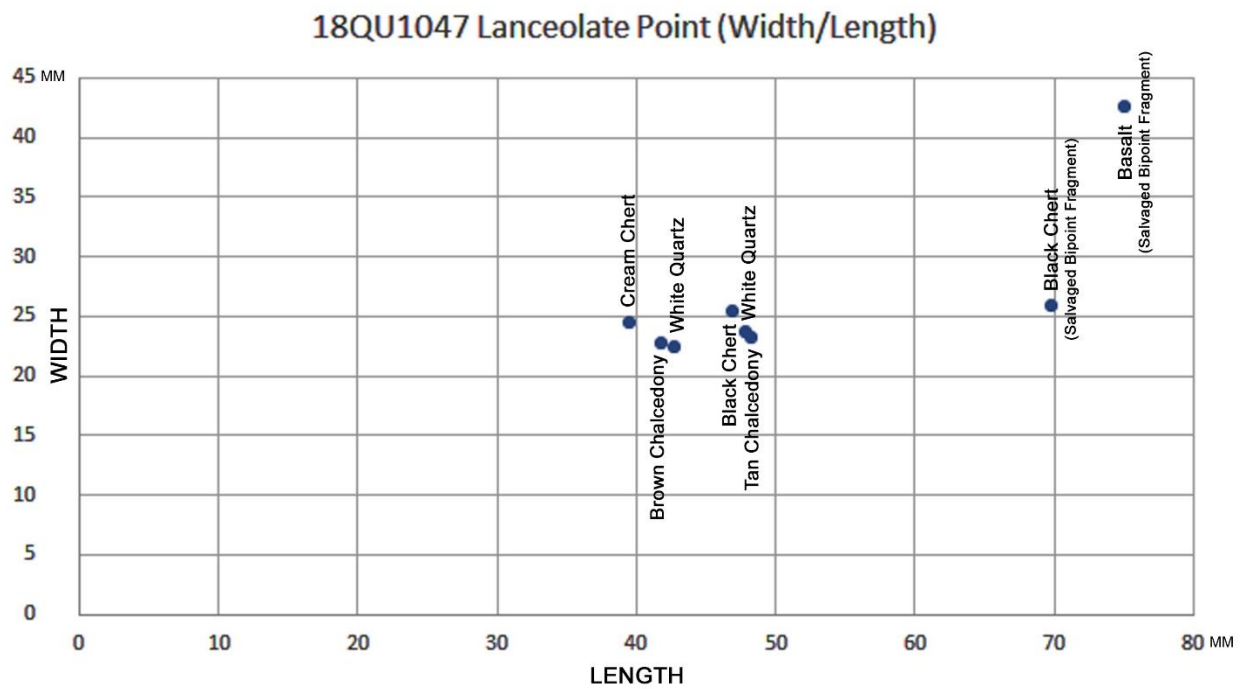


Figure 3.48. The graph portrays the length and width data for all of the complete lanceolate points found at 18QU1047. Note that the small lanceolate forms (see Figure 3.47 A-F) seem to be distinctly different than the salvaged examples (see Figure 3.46).

Blade Cores and Blades:

With respect to the Middle Atlantic's prehistoric archaeological record, the number of blade cores (see Table 3.4 and Figure 3.57) found at 18QU1047 is uncharacteristic and somewhat anomalous. Seven blade cores have been found along the eroding shoreline of 18QU1047 over the past several years. Of these, five have been illustrated (see Figures 3.49, 3.50, 3.53, 3.54, and 3.55). The sixth unillustrated specimen is a small conical core analogous to the example shown in Figure 3.49, but made of white quartz. Another quartz core specimen could not be photographed for this report due to Covid19 pandemic-related restrictions at the Smithsonian Institution where the artifact was on loan. Measurements for this seventh core could only be estimated based on scaled images. As such, it was excluded from the measured sample. The extant quartz core did not lend itself to detailed photography, as such it was not included as a figure in this report, but its measurements were included in the sample.

Three of the cores found at 18QU1047 represent unidirectional blade and/ or flake cores. These include two made of black grainy chert (see Figures 3.49 and 3.50) and the aforementioned white quartz specimen. Two of these specimens are conical (see Figure 3.49) in outline and show a general preference for one margin being selected for blade and/or flake removal. The largest conical core (see Figure 3.49) found at 18QU1047 shows twelve distinct unidirectional blade/flake detachments along the margins. The longest extant blade/flake scar on this core is 75.5 millimeters in length and 25.3 millimeters in width. The small quartz conical core retains six unidirectional blade/flake detachments along its margins. The longest blade/flake scar on the small quartz conical core is 32.2 millimeters in length and 13.5 millimeters in width. The final unidirectional core (see Figure 3.50) can best be described as a blocky flake core. The extant flake scars on the surface of this core are more irregular and reflect less linear control. The longest extant blade/flake scar is 45.3 millimeters in length and 16.2 millimeters in width. In sum, the more irregular flake production reflected by this specimen could be indicative of poor lithic material quality, as well as the fact that the core seems to be exhausted.

The surface conditions of the two unidirectional cores (see Figure 3.49 and 3.50), which were both found eroded out of context, provide some insight into their stratigraphic position within the bank profile at 18QU1047. Both cores have marked wind polish/silica glaze to their platform/tablet areas and around the peripheral margins within some of the blade/flake facets immediately below the platform/tablet corners. Like the in-situ bipoint (see Figures 3.40 and 3.41A) with similar aeolian polish/silica glaze on one face, the lower portions of these cores were presumably embedded in the 4Ab1 soil horizon and protected from wind abrasion. The platform/tablet areas and the upper parts of these cores were clearly exposed to the effects of wind abrasion before and during the deposition of the overlying 3Cg2 soil horizon. The wind polished/silica glazed artifacts found at 18QU1047 offer insights into the deposition, erosion, and aeolian accretion sequence of events at 18QU1047. The suggested sequence is portrayed in Figure 3.51. After the site was abandoned, the 4Ab1 soil horizon encapsulated most of the lithic artifacts associated with the cultural occupation of the site (see Figure 3.51 A). A short-interval of erosion exposed and displaced some of the lithic artifacts. Various portions of these artifacts were made visible on a wind-swept truncated portion of the 4Ab1 surface (see Figure 3.51 B). It was during this interim that uncovered sections of a few artifacts were polished by exposure to protracted wind activity, subsequently glazed by exposure to atmospheric water vapor (see Dorn 2012), and buried by sediment saltation across an otherwise barren landscape (see Figure 3.52). Eventually, the surviving portion of the 4Ab1 soil horizon, as well as any exposed artifacts or artifacts embedded within the 4Ab1 soil were buried by successive aeolian deposition (see Figures 3.51 C and D and 3.52).

These observations imply that the radiometric dates of circa $20,761 \pm 198$ cal. yrs. BP, $22,175 \pm 235$ cal. yrs. BP, $22,501 \pm 155$ cal. yrs. BP, $23,332 \pm 174$ cal. yrs. BP, and $23,703 \pm 106$ cal. yrs. BP for the extant carbon/charcoal within the truncated 4Ab1 soil may predate the human occupation and provide a maximum age estimate or "terminus post quem". Thus, the buried assemblage found at 18QU1047 would have to be $\leq 20,563$ years BP or $\leq 20,761$ minus 198 years BP. The youngest possible OSL age for the overlying pre-Younger Dryas aeolian sediments is 15,130 years BP, which represents a "terminus ante quem". Therefore, the buried assemblage of artifacts at 18QU1047 would be $\geq 15,130$ years BP or $\geq 17,400$ minus 2270 years BP. Without any definitive datable cultural organic remains, the truncated 4Ab1 soil horizon and the aeolian polished/glazed lithic artifacts constrains the period of possible cultural use of this landscape to a large time frame, which spans 5,433 years. Regardless of the significant possible age range, the artifact assemblage from 18QU1047 is definitely a pre-Clovis tool kit.



Figure 3.49. The images show a conical, unidirectional, plain-platform core found at 18QU1047. Marked wind polish and silica glaze are present on the platform/tablet area and around the peripheral margin within some of the flake facets situated immediately below the platform/tablet corners. Note that one face (left and top) shows more polish/glaze along the lip and platform margin than is present along the other margins (center and right). As such, the orientation of this artifact relative to the prevailing northerly wind direction can be established.



Figure 3.50. The images show a blocky, unidirectional, plain-platform core found at 18QU1047. Marked wind polish/silica glaze are present on the platform/tablet area and around the peripheral margin within some of the flake facets immediately below the platform/tablet corners. Note that one face (center and top) shows more polish/silica glaze along the lip and platform margin than is present along the other margins (left and right). As such, the orientation of this artifact relative to the prevailing northerly wind direction can be established.

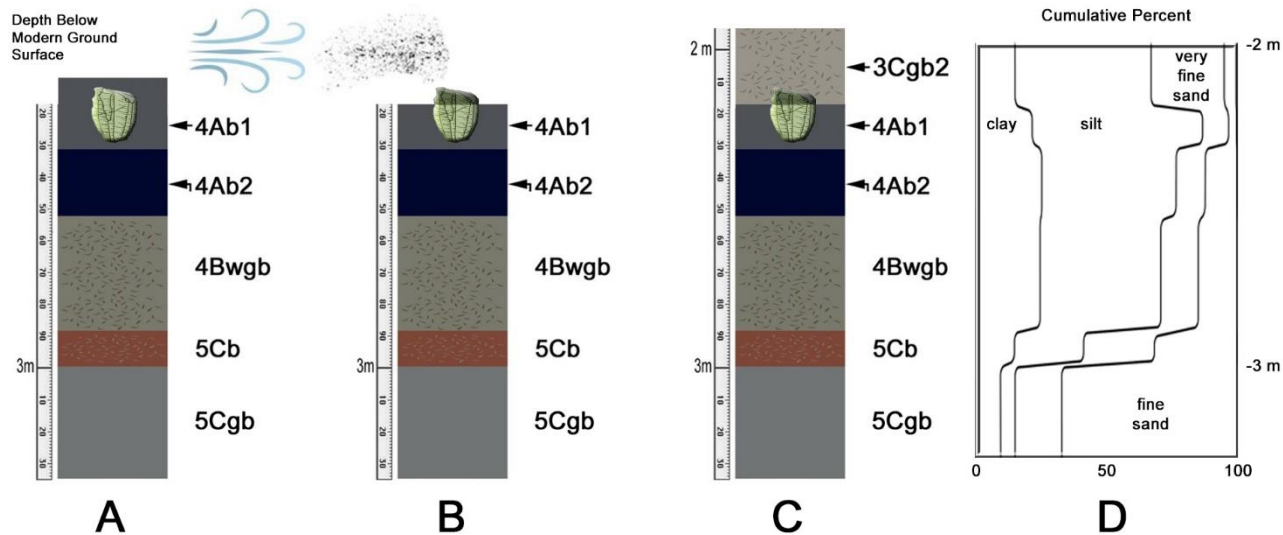


Figure 3.51. The images show the inferred site formation processes at 18QU1047 based on the presence of aeolian polish noted on the faces of some artifacts. After the site was abandoned, the lithic assemblage was initially buried by loess (A). However, erosive actions truncated the 4Ab1 soil and exposed the faces of some artifacts to aeolian activity (B) resulting in an abrasive polished to some artifact surfaces. Water vapor; which could have included snow or ice crystals, resulted in the formation of a silica glaze. The truncated 4Ab1 soil, which contained lithic artifacts, was eventually buried by continued aeolian processes.

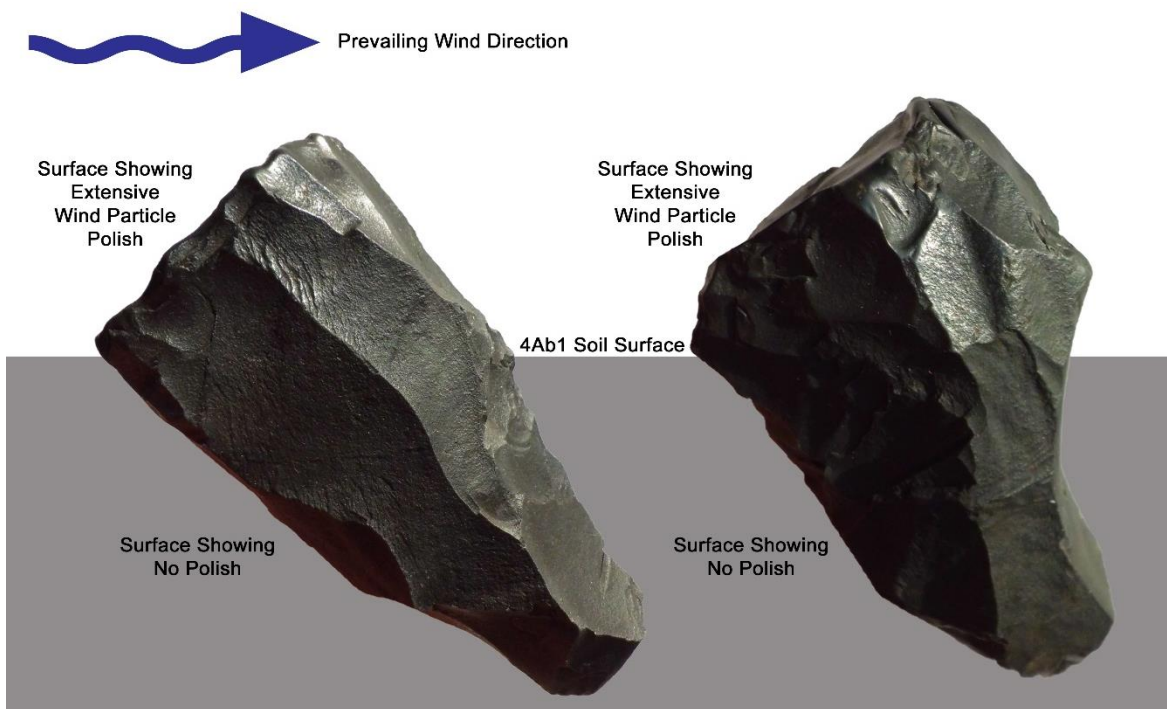


Figure 3.52. The image shows the presumed orientation relative to the prevailing northerly winds and the degree of surface exposure for two wind-polished and silica glazed cores found at 18QU1047.

Additional cores found at 18QU1047 indicate that blades, blade-like flakes, or irregular flakes were intentionally or haphazardly detached from multiple directions. The first (see Figure 3.53) would be classified as a flat-backed core. Aside from a singular small flake detached from the distal section, the core is largely unidirectional and made from red jasper. Another small core (see Figure 3.54) is made from mottled chert and, like the red jasper core, shows the preferential removal of flakes from one end, as well as, two haphazard flake detachments from its distal margin. Both cores retain a singular small section of rounded cortex indicating that they were manufactured from secondary cobbles. The distal flake detachments on each of these cores may simply be the result of indirect impact damage from the use of a supporting stone anvil.

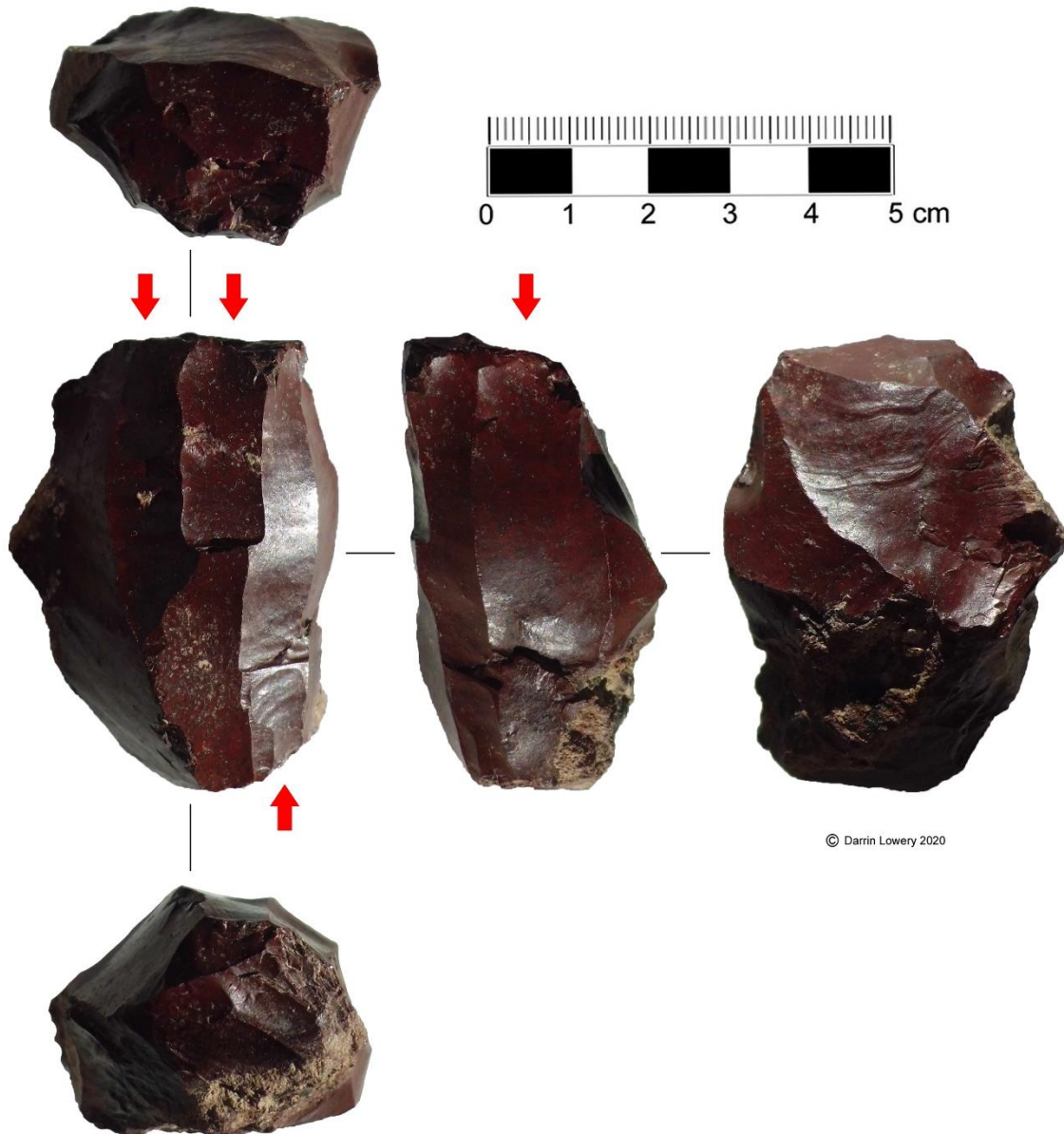


Figure 3.53. The images show a “flat-backed” blade core found at 18QU1047.



Figure 3.54. The images show a small bidirectional blade or blade-flake core found at 18QU1047.

One of the most intriguing cores found at 18QU1047 (see Figure 3.55) would be classified as an opposing platform “crested-back” or keeled bidirectional core. As a type, the crested-back blade core is exceedingly rare in the Middle Atlantic region and the specimen from Parsons Island may be the only known example. The precore or parent form for this type of crested core would have been a large thick biface or bifacial “gigantolith” (see Gira and Bradley 1998: 193-194) and it would have been somewhat analogous to the thick biface already noted at 18QU1047 (see Figure 3.45). The parent thick biface would have been intentionally broken or segmented (see Figure 3.55, top) and the opposing fractured edges would have served as platforms for sequential blade detachments. The initial blade removed from the segmented precore would have consisted of a bifacial edge and it would be classified as a “crested” blade. Consecutive blade detachments would have been derived from both fractured margins until the remnant core consisted of nothing more than the opposing edge (see Figure 3.55 A and B) of the parent bifacial “gigantolith”. Like many of the cores found at Parsons Island, the “crested-back” or keeled core (see Figure 3.55) from 18QU1047 represents an exhausted form.

Like the cores (see Figure 3.52) discussed earlier, the “crested-back” core shows evidence of wind polish/silica glaze. However, the wind polish and glaze on the “crested-back” core is uniformly distributed along all faces. Given the inferred site formation processes (see Figure 3.51), we can conclude that the core had been completely eroded and displaced from the 4Ab1 soil horizon, polished by wind-transported sediment, exposed to water vapor (see Dorn 2012), and then buried by aeolian deposited strata (see Figure 3.51 B and C).

The final core-like artifact (see Figure 3.56) found at 18QU1047 is most-likely a wedge or *pièce esquillée*; rather than a flat-backed unidirectional core. The tan quartzite specimen (see Figure 3.56) is 47.7 millimeters in length, 29 millimeters in width, and 15.2 millimeters in thickness. The rounded

cortex implies it was manufactured from a small cobble. The extant scars indicate the flakes detached from the artifact were derived primarily from one end. However, the cross-section of this artifact is more suggestive of a wedge used to split wood, bone, or ivory; than an actual core. The specimen also has wind polish and silica glaze along one edge (see Figure 3.56, far right).

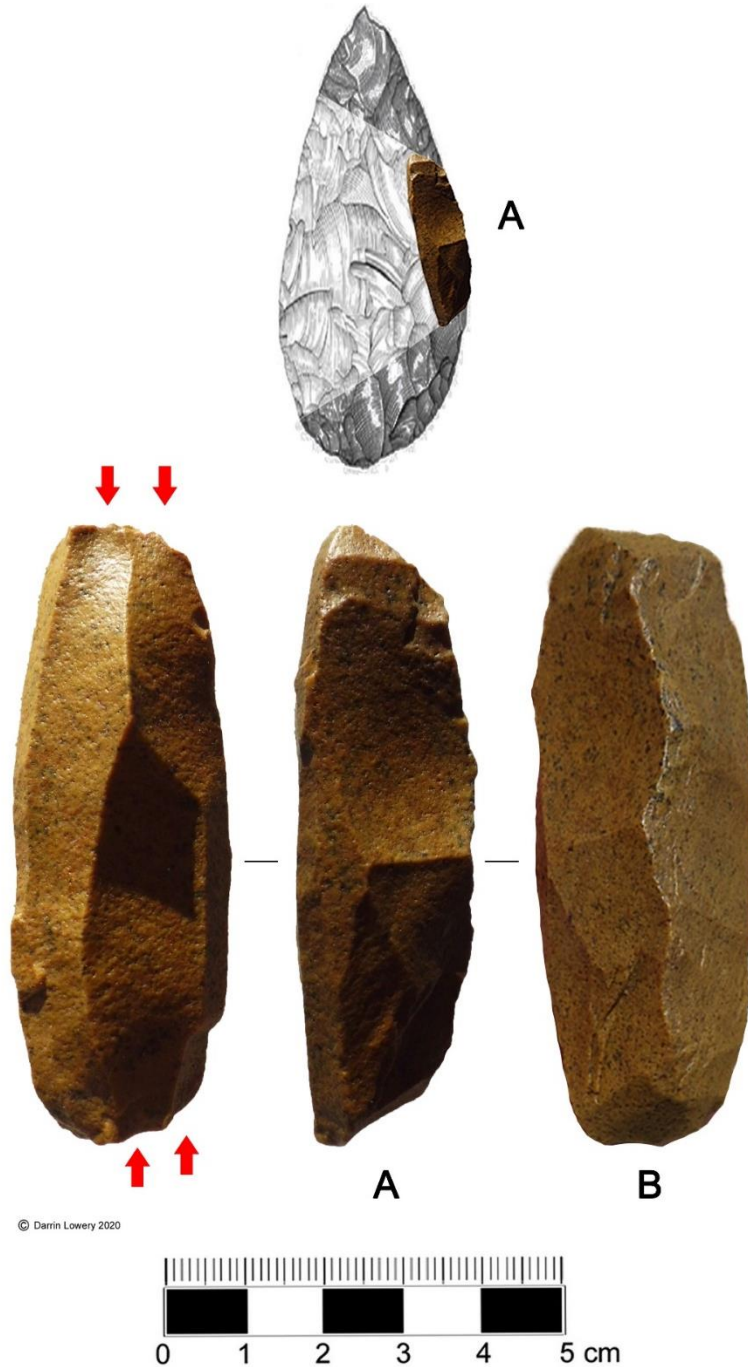


Figure 3.55. The images show a keeled or “crested-back” bidirectional blade core found at 18QU1047. The extant specimen represents the terminal edge of a large thick biface (see A and B) that has been reduced as a result of continued blade or blade-like flake detachments.



Figure 3.56. The image illustrates what is interpreted as a wedge or pièce esquillée; rather than a small “flat-backed” unidirectional core.

TABLE 3.4. 18QU1047 BLADE AND FLAKE CORE DATA.

DATE:	DESCRIPTION:	LITHIC MATERIAL:	LENGTH:	WIDTH:	THICKNESS:
7/26/2014	Exhausted conical unidirectional core	White Quartz	41.8	22.5	22.5
7/9/2017	Conical unidirectional core (aeolian polish; see Figure 3.49)	Black Chert	83.4	35.2	34.7
9/7/2017	Blocky unidirectional core (aeolian polish; see Figure 3.50)	Black Chert	95.8	47.8	47.2
11/2/2017	Bidirectional core with cortex (see Figure 3.53)	Red Jasper	54.7	39.9	28.6
11/23/2019	Bidirectional core with cortex (see Figure 3.54)	Mottled Chert	40	36.5	23.9
6/23/2020	Keeled Bidirectional core (aeolian polish; see Figure 3.55)	Grainy Tan Jasper	80.2	27.7	25.6

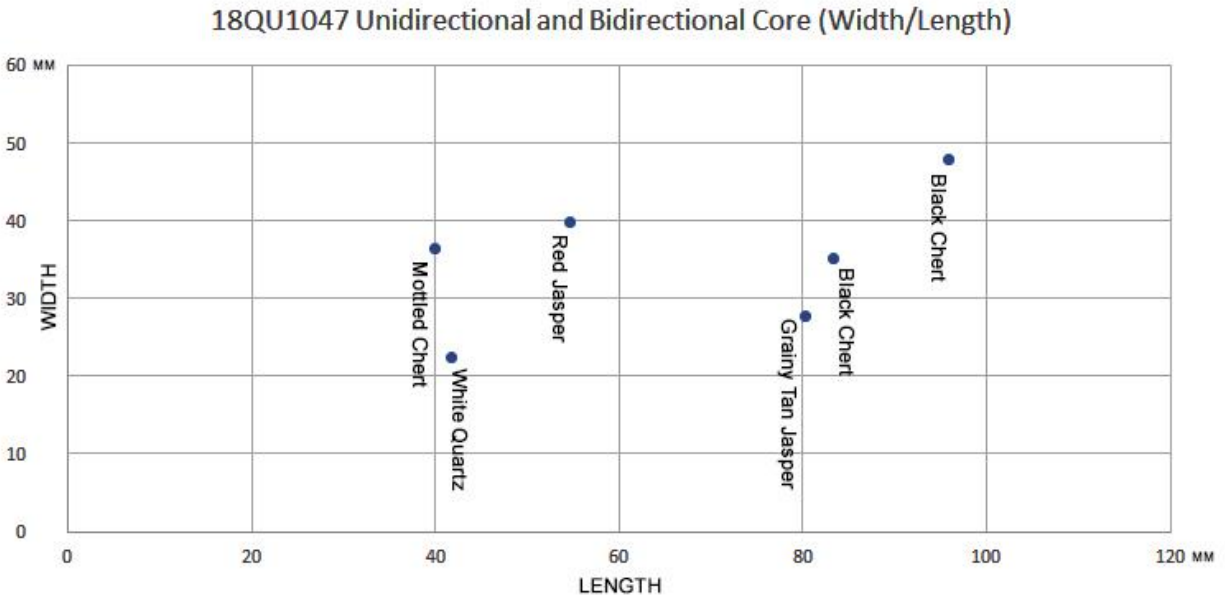


Figure 3.57. The graph portrays the length and width data for all of the cores found at 18QU1047.

Sixteen blade or blade-like flake tools have been found at 18QU1047 (see Figures 3.58, 3.59, and 3.63 A) and they are made from a variety of lithic materials including white quartz, quartzite, petrified wood, jasper, chert, and chalcedony. Several of the specimens (see Figure 3.58 A and 3.59 A) retain a remnant section or portion of rounded cobble cortex; suggesting that they were derived from local secondary cobbles. None of the lithic materials reflected by the extant blade assemblage directly matches or conjoins with any of the cores that have been found at the site.

The blades or blade-like flakes vary in length from 20.3 to 122.2 millimeters (see Table 3.5 and Figure 3.60). However, the majority fall between 45 and 96 millimeters in length. Most of the extant platforms associated with these blades or blade-like flakes are small, isolated, and ground. However, a few (see Figure 3.59 A) have very broad flat platforms and show minimal grinding. Some (see Figures 3.58 C, 3.59 D, and 3.59 B) show minimal utilization damage along their lateral margins implying an expedient knife-like cutting or scraping function. Others (see Figures 3.58 A and B, 3.59 A and C, and 3.63 A) show marked intentional retouch along one or more of their lateral margins. With the exception of one specimen (see Figure 3.58 B), the retouch is confined to the dorsal face. However, all specimens show use-damage to both the dorsal and the ventral faces.

Two blades or blade-like flakes (see Figures 3.59 C and 3.63 A) found at the site show heavy edge retouch, which greatly altered the parent shape and/or outline. The longest blade found at the site (see Figure 3.59 C) has intentional retouch to both lateral edges and the left edge margin has a distinctive “shoulder”. The blade also has a marked pointed distal termination, which has little to no retouch. The dorsal face of the blade in Figure 3.59 C also has noticeable wind polish and silica glaze as indicated by its glossy sheen. In stark contrast, the ventral side of this blade is dull and more indicative of the original parent luster. Like other stone tools found at the site, it is presumed that the blade was

partially exposed as a result of erosion, lying flat on the surface of the 4Ab1 soil horizon, and pelted by aeolian transported silt particles.

The final blade (see Figure 3.63 A) could be categorized as a combination scraper/spokeshave. It is also included under the category of formal flake tools discussed below. Unlike the other blades, the original platform of this artifact has been removed as result of detaching the proximal portion of the blade. Snapping blades into smaller sections has been observed in the assemblage found at 18QU1047 (see Figure 3.61). Most importantly, this blade tool was found in-situ within the 4Ab1 soil horizon and exposed along the eroding bank profile at 18QU1047 (see Figure 3.67). When discovered, it was removed from the eroding bank as a block containing all associated parent sediments. The block sediments containing the artifact were analyzed and excavated in the lab at the Smithsonian Institution. Before it was removed the block was 3-D scanned, x-rayed, and subjected to a CT scanner (see Figure 3.67). These detailed analyses proved that the artifact was indeed in-situ and associated with the sediments accompanying the 4Ab1 soil horizon.

The flake scars along the dorsal faces of each blade provide insight into whether the preceding blades were detached in a unidirectional or bidirectional fashion. Of the sixteen blades, three (see Figures 3.58 D and 3.59 C) suggest the previous blades were removed in a bidirectional alignment. All others indicate a unidirectional orientation.

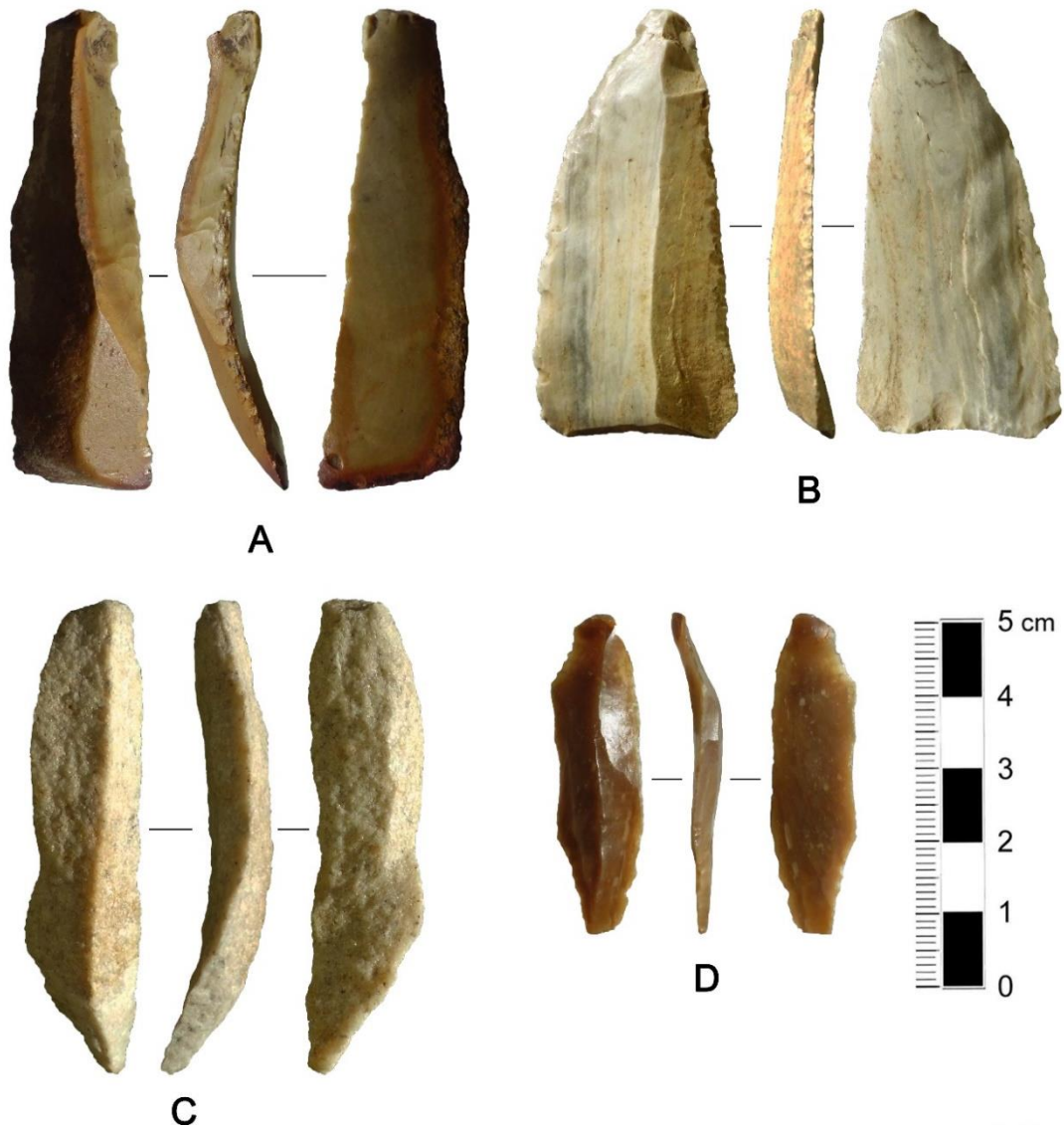


Figure 3.58. The images show four of the blades or blade-like flakes found at 18QU1047. These artifacts are made of a variety of lithic materials, including chert (A), petrified wood (B), quartzite (C), and chalcedony (D).

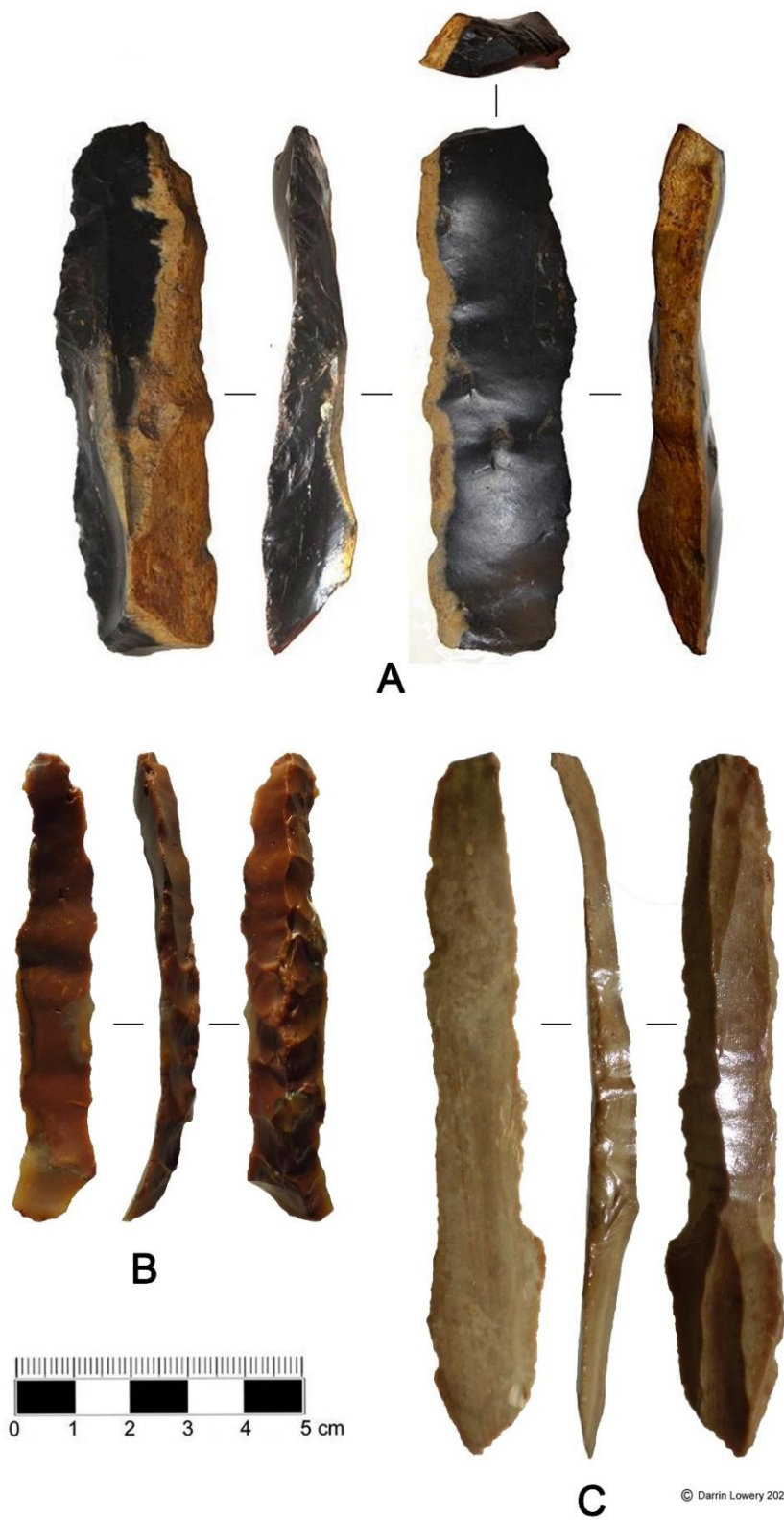


Figure 3.59. The images show three of the blades or blade-like flakes found at 18QU1047. These artifacts are made of a variety of lithic materials, including chert (A) and jasper (B and C).

TABLE 3.5. 18QU1047 COMPLETE BLADE AND BLADE-LIKE FLAKE DATA.

DATE:	DESCRIPTION:	LITHIC MATERIAL:	LENGTH:	WIDTH:	THICKNESS:
9/1/2013	Blade with Rounded Cobble Cortex	White Quartz	66.9	25.9	5.7
9/1/2013	Blade	White Quartz	45.5	22	5.8
9/1/2013	Utilized Blade with Rounded Cobble Cortex (Figure 3.58 C)	Quartzite	68.5	16.6	9.5
4/17/2014	Retouched Blade (Figure 3.58 B)	Petrified Wood	61	29.4	6.2
4/17/2014	Retouched Blade with Rounded Cobble Cortex	Jasper	62	21.6	9
4/17/2014	Retouched Blade with Rounded Cobble Cortex (Figure 3.58 A)	Chert	68.8	20.4	9.1
6/21/2014	Blade-Like Flake with Scraper/Spokeshave (Figure 3.63 A)	Chert	81	30.3	10.8
6/21/2014	Small Prismatic Blade	White Quartz	20.3	13.1	5.9
8/24/2014	Blade with Rounded Cobble Cortex (Figure 3.59 A)	Chert	95.1	27.3	16.1
9/26/2014	Damaged Blade with Possible Spokeshave	Chert	85.9	34.3	15.7
2/22/2015	Utilized Blade-Like Flake with Rounded Cortex	Chert	70.8	29.5	9.5
3/16/2015	Blade	Chert	77.7	16.6	6.5
9/20/2015	Utilized Blade with Aeolian Polish on Dorsal Face (Figure 3.59 C)	Jasper	122.2	20.2	7.4
11/9/2015	Small Prismatic Blade (Figure 3.58 D)	Chalcedony	46.4	12.6	4.1
3/20/2019	Keeled Blade (Figure 3.59 B)	Jasper	83.4	14.9	7.1
10/18/2019	Blade	Chalcedony	54.8	11	4.6

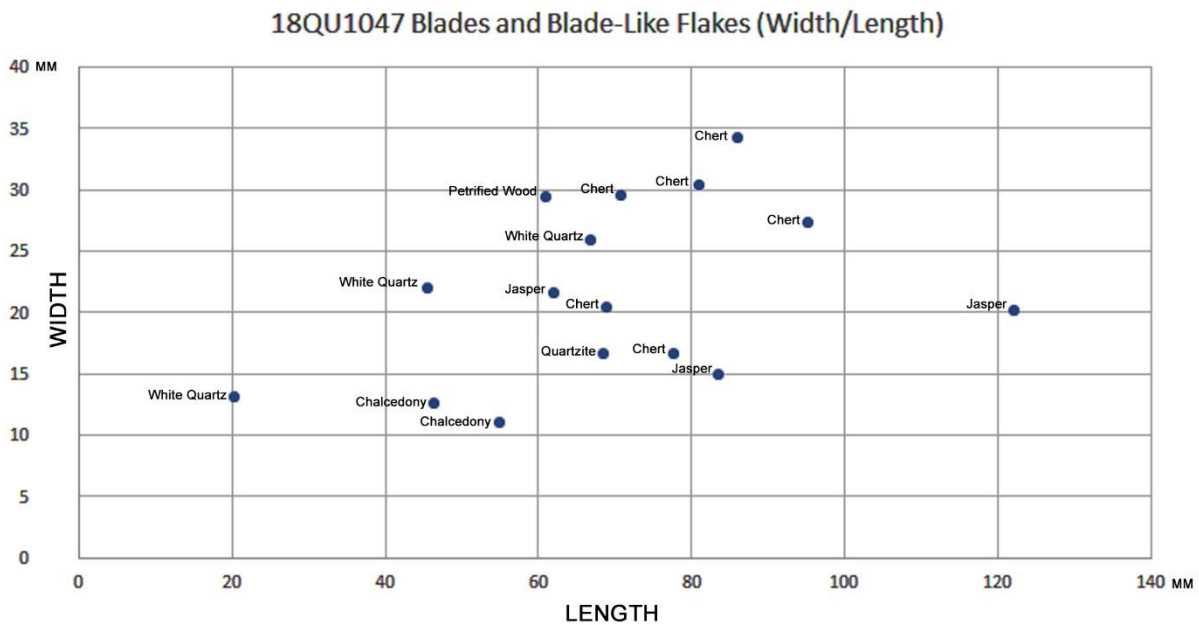


Figure 3.60. The graph portrays the length and width data for the blades and blade-like flakes found at 18QU1047.

Two blade segments (see Figure 3.61 B and C) have been found at 18QU1047 and their original lengths cannot be determined. One (see Figure 3.61 B) represents the proximal end of a jasper prismatic blade. The artifact is 63.4 millimeters in length, 14.5 millimeters in width, and 4.8 millimeters in thickness. As indicated by the scars on the dorsal face, the preceding blades were detached in a unidirectional fashion. The distal end may have been intentionally snapped and removed. The resultant segment is straight. The edges do show some utilization scars scattered along both lateral margins. The specimen was found along the shoreline at 18QU1047 on 4-21-2018. Another jasper prismatic blade

segment was found at 18QU1047 on 4-15-2018. However, it represents the distal end or segment of a longer blade, which seems to have been intentionally detached. The remaining segment is 44.4 millimeters in length, 9.6 millimeters in width, and 3.6 millimeters in thickness. It is slightly curved, shows no evidence of utilization, and the preceding blades were removed in a unidirectional fashion. Finally, an endscraper manufactured from the proximal portion of a larger jasper prismatic blade was found at the site on 9-20-2015. Both lateral edges were retouched along the dorsal face and the margins were subsequently smoothed. The arris ridge also shows deliberate smoothing and/or grinding. The original platform is very small and also has marked grinding. The endscraper is 27.1 millimeters in length, 17.5 millimeters in width, and 8.5 millimeters in thickness. As expected, scraper-like intentional retouch is present along the distal end of this snapped blade section.

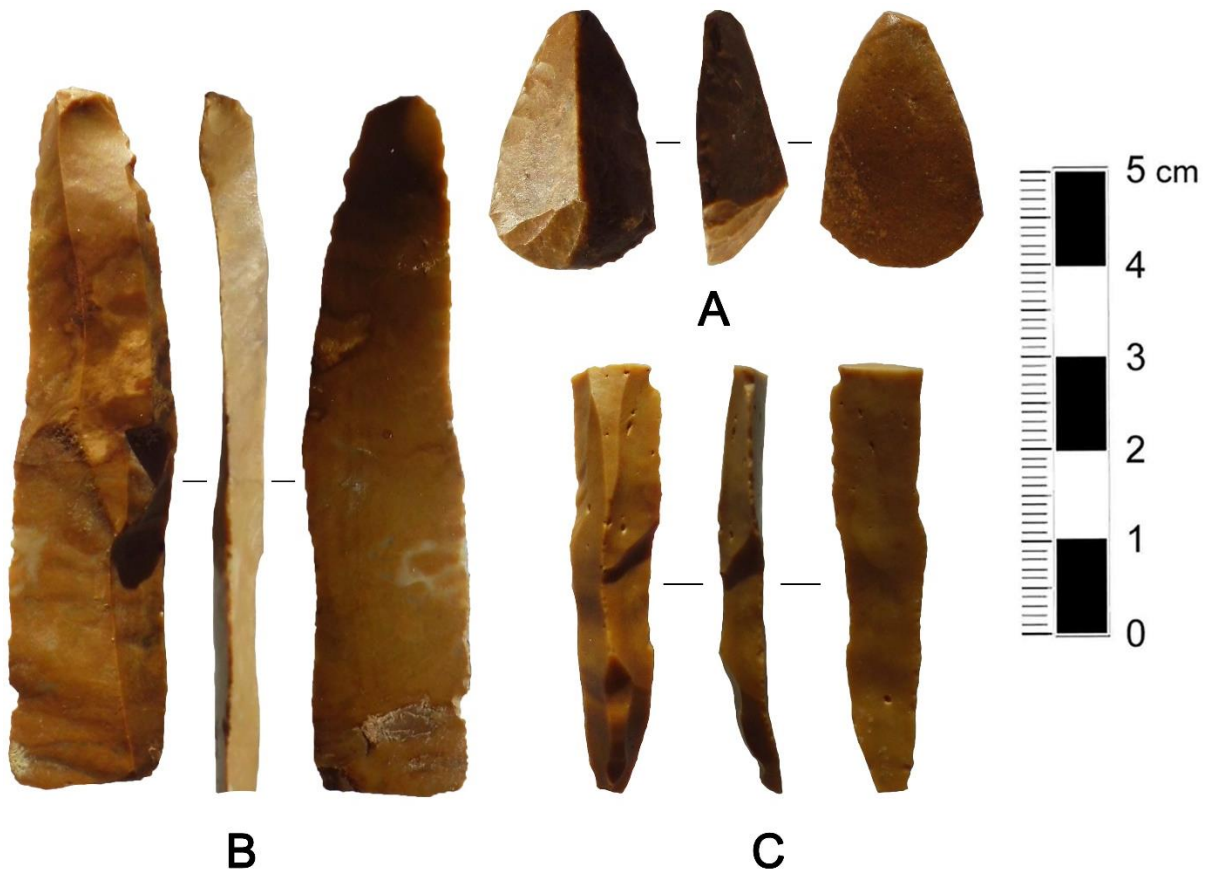


Figure 3.61. The images show three of the intentionally-snapped blades and/or blade-like flake tools found at 18QU1047.

Shouldered Points/Knives on Blades or Blade-Like Flakes:

The most interesting suite of artifacts found at 18QU1047 include a series of utilized and modified blades or blade-like flakes having a distinctive shoulder on one lateral margin (see Figures 3.62, 3.64, and 3.59 C). Specific measurement data for these specimens are outlined in Table 3.6 and Figure 3.65. One example (see Figure 3.59 C) of this tool type has already been discussed under the blade category.

Of the five examples, three specimens retain the original platform and/or bulb of percussion at the proximal end of the flake tool, which corresponds to the “stem” of the flake tool (see Figure 3.62 A, 3.62 D, and 3.59 C). The remaining two examples have conchoidal fracture patterns indicating the platform and/or bulb of percussion was situated at the distal or “point” end of the flake tool (see Figure 3.62 B and 3.62 C). Two of the specimens (see Figure 3.62 A and 3.62 C) have had their original platforms removed as a result of intentional retouch. With the exception of the smallest example in the assemblage (see Figure 3.62 C), retouching and subsequent tool outline alteration is unifacial and confined to the dorsal side of the parent blade or blade-like flake.

The first example found at 18QU1047 (see Figure 3.62 D) is the widest specimen in the assemblage. The artifact is made of mottled black chert. It was found eroded out of context, but adjacent to the site’s steeply eroded bank edge. Retouch on this specimen occurs on both lateral margins and the flake scar patterns on the dorsal face indicate that it was derived from a large bidirectional core. The remnant platform shows intentional grinding. Use-damage/wear occurs on the distal end, as well as both lateral margins. The “stem” area of this specimen shows some slight smoothing or grinding below the “shoulder” towards the remnant platform. With the distal end of the parent blade oriented up, the “shoulder” on this specimen is situated on the left side of the blade’s dorsal face. Use-wear and damage indicates that this stone tool functioned as a hafted unifacial knife.

The second specimen (see Figure 3.62 A), which is made of mottled red/orange chalcedony, was found in-situ and embedded within the upper portion of the 4Ab1 soil horizon. A blocky segment or ped, which had been dislodged from the bank margin, contained the in-situ artifact. Because it had not been tumbled in the surf, the specimen was subjected to use-wear analysis. The use-wear investigation was conducted by Dr. Marvin Kay at the University of Arkansas. His analysis demonstrates that the parent blade was derived from a large unidirectional core and the specimen functioned both as a knife and as a projectile point (see Figure 3.64). Retouch occurs on both lateral margins. Use-wear and/or damage is largely confined to the area above the shoulder towards the artifact’s distal end. To produce the “stem”, it would seem that the artifact’s maker took advantage of the parent blade’s edge curvature, since the concavity below the shoulder shows only minimal retouch. With the distal end of the parent blade oriented up, the “shoulder” on this specimen is also situated on the left side of the blade’s dorsal face. Slight smoothing occurs along the “stem” margins.

A third specimen (see Figure 3.59 C) found at the site is made of jasper and was previously discussed in the blade section of this report. The specimen has some morphological attributes indicating it also functioned as a shouldered knife or point. Unlike the other specimens, the “shoulder” is situated well above the mid-point of the blade. With the distal end of the parent blade oriented up, the “shoulder” is positioned on the right side of the dorsal face, which is also unlike the other examples (see Figure 3.62). The distal end of the parent blade converges towards a point and shows no retouch or alteration. Marked edge retouch occurs along the left lateral edge ~15.4 millimeters down from the

blade's distal terminus. Along the right edge, retouch initially occurs 35.6 millimeters below the blade's distal end and creates the artifact's "shoulder". The retouch noted along both margins is steep and extends to approximately 37 millimeters above the blade's platform. It is conjectured that the artifact's maker may have intended to snap or break the blade along the mid-point, thus shortening the length of the stem of the final "shouldered" knife or point.

A fourth specimen (see Figure 3.62 C) was made from a secondary crested blade (see Gira and Bradley 1998: 198-199) that is somewhat similar to the blade shown in Figure 3.59 B. It is made of a high-quality vitreous honey-colored chalcedony. With the distal end of the artifact oriented up, the "shoulder" on this specimen is located on the left side of the blade's dorsal face. The parent blade was presumably derived from a thick bifacial chalcedony core analogous to the core presented in Figure 3.55. Remnant flake scars on the dorsal surface of this shouldered artifact indicate that two previous bidirectional blades were detached from the parent core. The original blade platform area was retouched forming the distal end of this artifact. Dorsal retouch is largely focused along the "shoulder" and stem area. Retouch along the blade's ventral side is present on the distal end, as well as the left lateral edge margin. Heavy edge smoothing or grinding is evident along the stem margins.

The final shouldered specimen (see Figure 3.62 B) is made of coastal plain orthoquartzite, which originated from local geologic deposits associated with the Paleocene Aquia formation. Again, with the narrow end oriented up, the "shoulder" on this specimen is also situated on the blade's dorsal left edge margin. The ground platform area is still present on this artifact and like the example shown in Figure 3.62 C, it is situated at the artifact's distal end. All retouch and intentional modifications to the parent flake are confined to the dorsal face. Two small concentric flakes are present on the specimen's ventral face and seem to be associated with torque damage. The dorsal face's left lateral edge has retouch along the "stem" area and along the lateral margin above the "shoulder". The dorsal face's right lateral edge has a noticeable constriction to the edge margin at the same overall position of the "shoulder" located on the tool's left edge. Rather than intentional retouch, the constriction area on the right edge shows marked "crushing" as if the damage were created as a result of twisting in a weak haft or a poorly-attached handle. In summation, the orthoquartzite "shouldered" specimen seems to have functioned as a hafted flake knife, rather than a projectile point/knife combination tool.

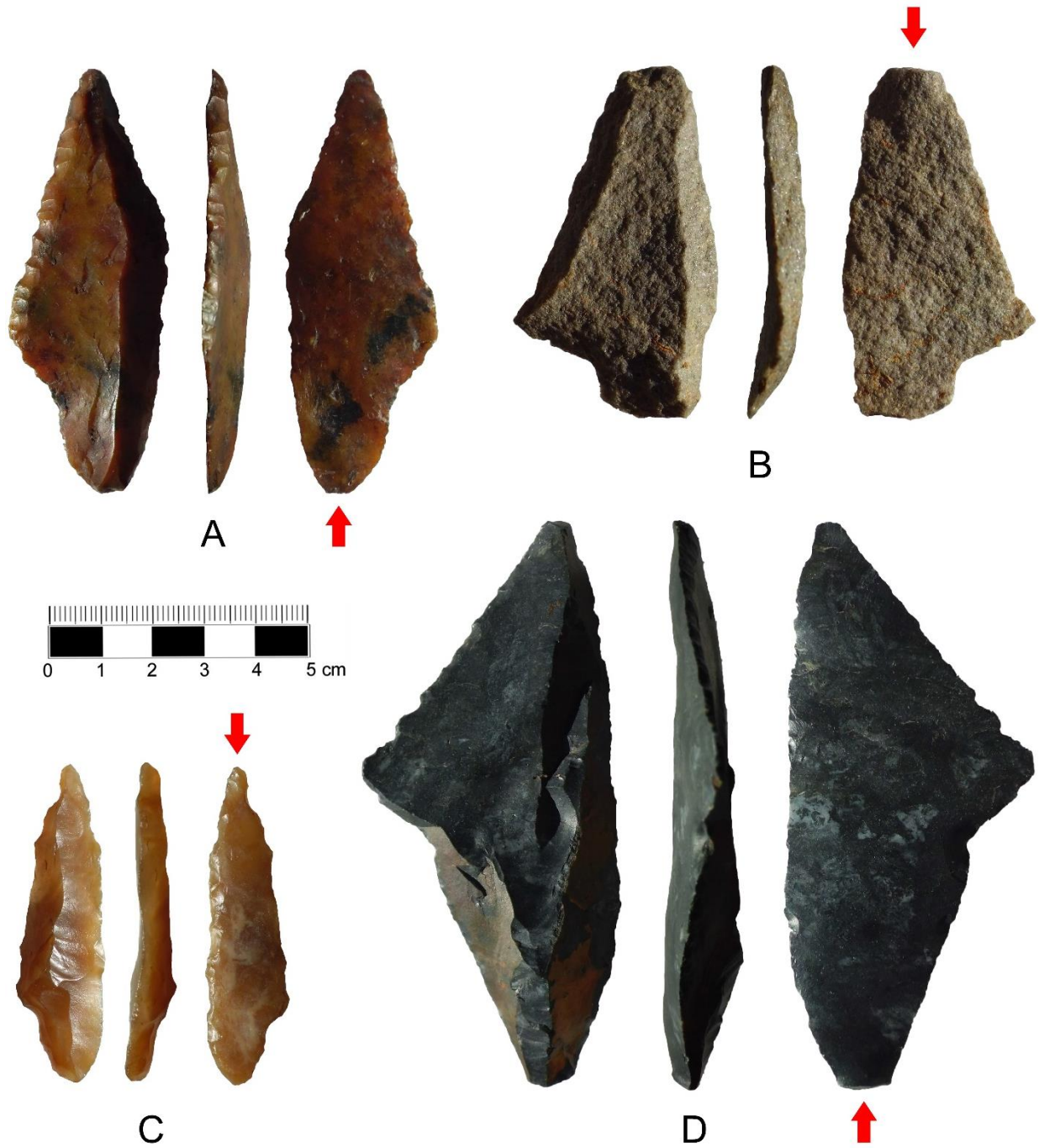


Figure 3.62. The images show four of the shouldered knives/points found at 18QU1047.

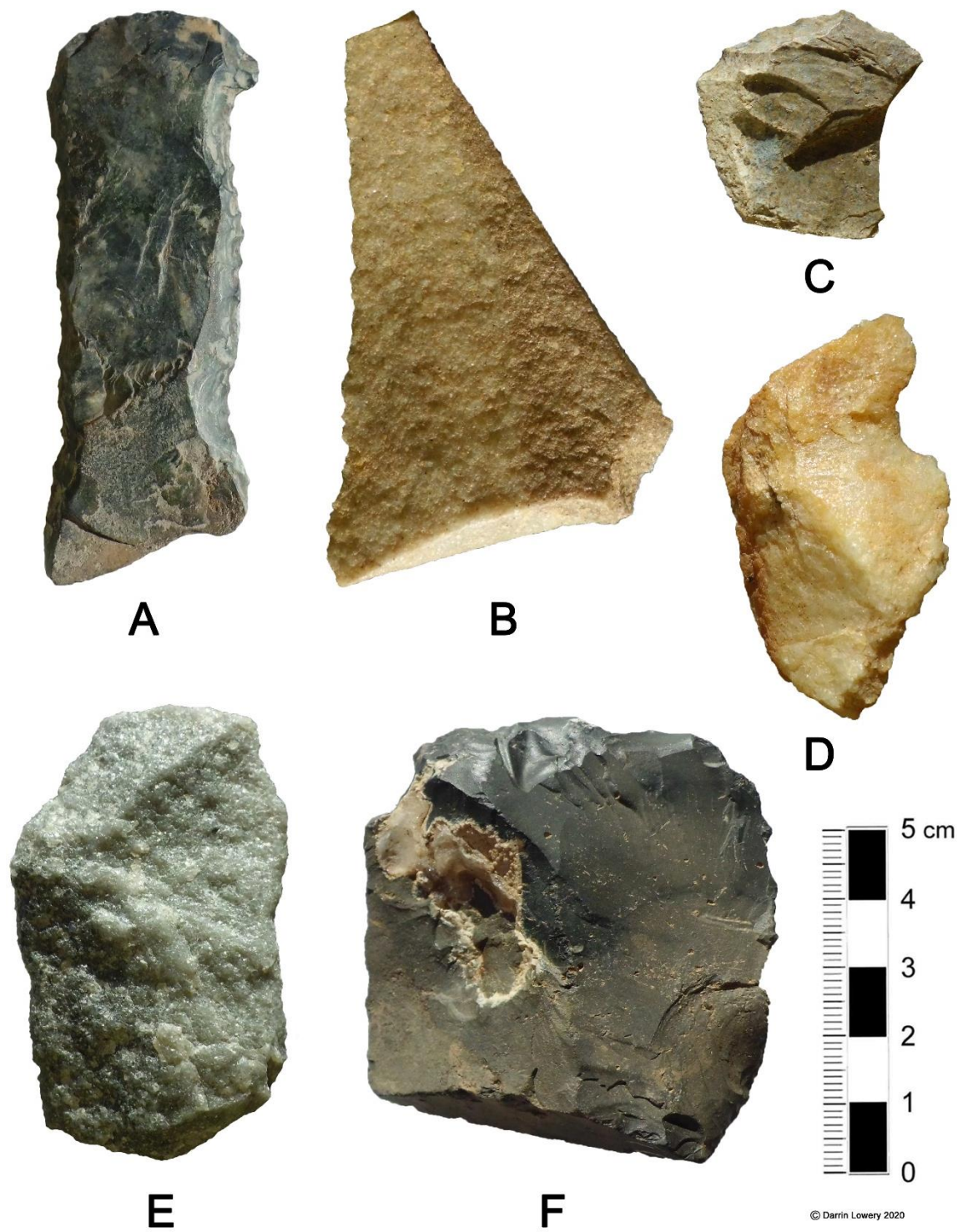


Figure 3.63. The photos portray a representative sample of formal flake tools and utilized flakes found at 18QU1047.

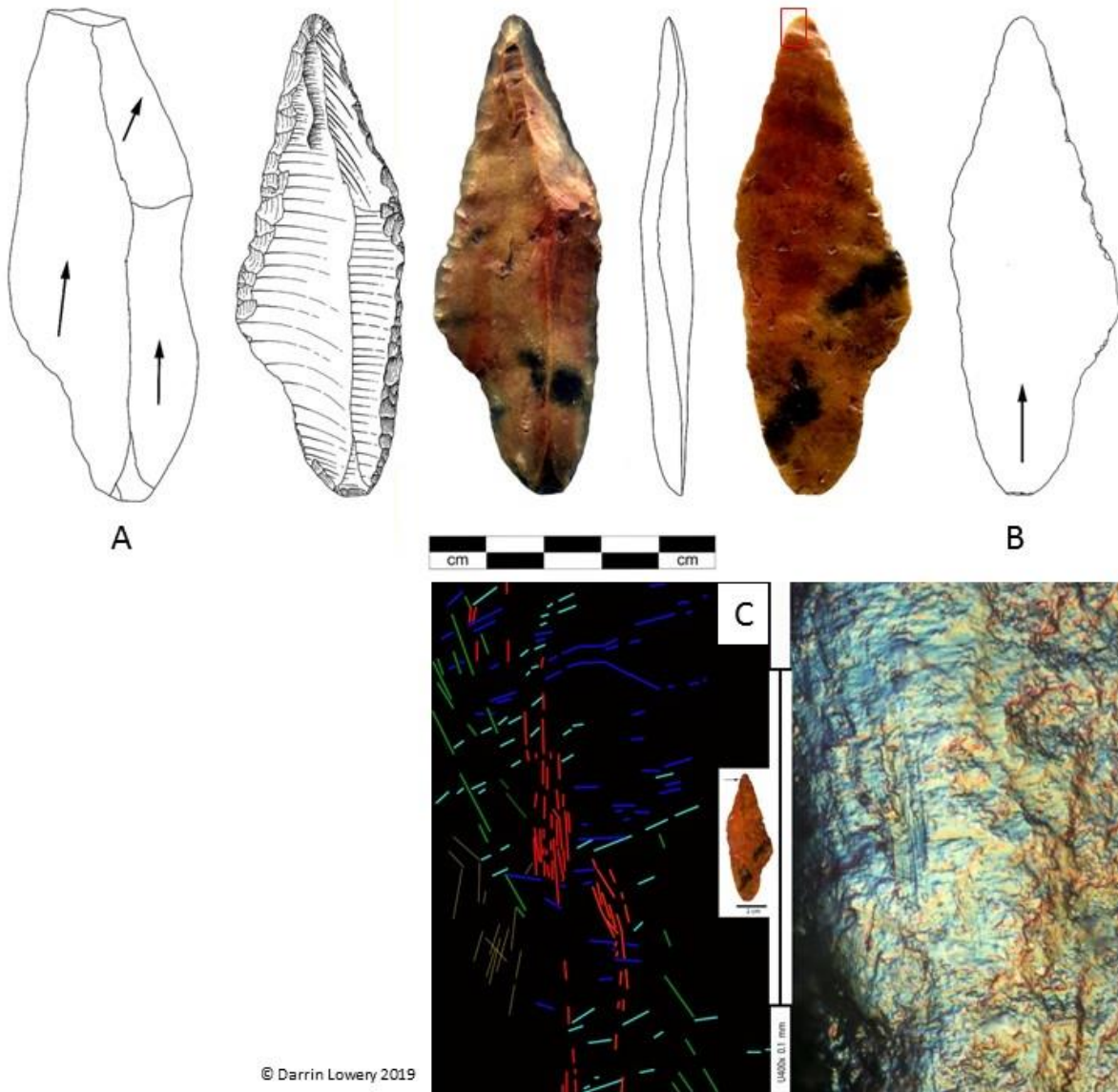


Figure 3.64. The images portray the orientation of the previous flake scars (A and B) and the use-wear (C) present on one of the shouldered knife/points (see Figure 3.62 A) found at 18QU1047.

TABLE 3.6. 18QU1047 BLADE OR BLADE-LIKE FLAKE SHOULDERED KNIFE/POINT DATA.

DATE:	DESCRIPTION:	LITHIC MATERIAL:	LENGTH:	WIDTH:	THICKNESS:
11/17/2013	Large Unifacial Shouldered Knife/Point (Figure 3.62 D)	Chert	100.5	44	13.5
9/26/2014	Unifacial Shouldered Knife/Point (Figure 3.62 A)	Chalcedony	82.9	29.6	7.2
9/20/2015	Utilized Blade (aeolian polish) possible Shouldered Knife (Fig. 3.59 C)	Jasper	122.2	20.2	7.4
5/29/2017	Shouldered Knife/Point (Figure 3.62 C)	Chalcedony	62.3	16.2	8.7
5/27/2018	Unifacial Shouldered Knife (Figure 3.62 B)	Orthoquartzite	65.9	35.5	6.4

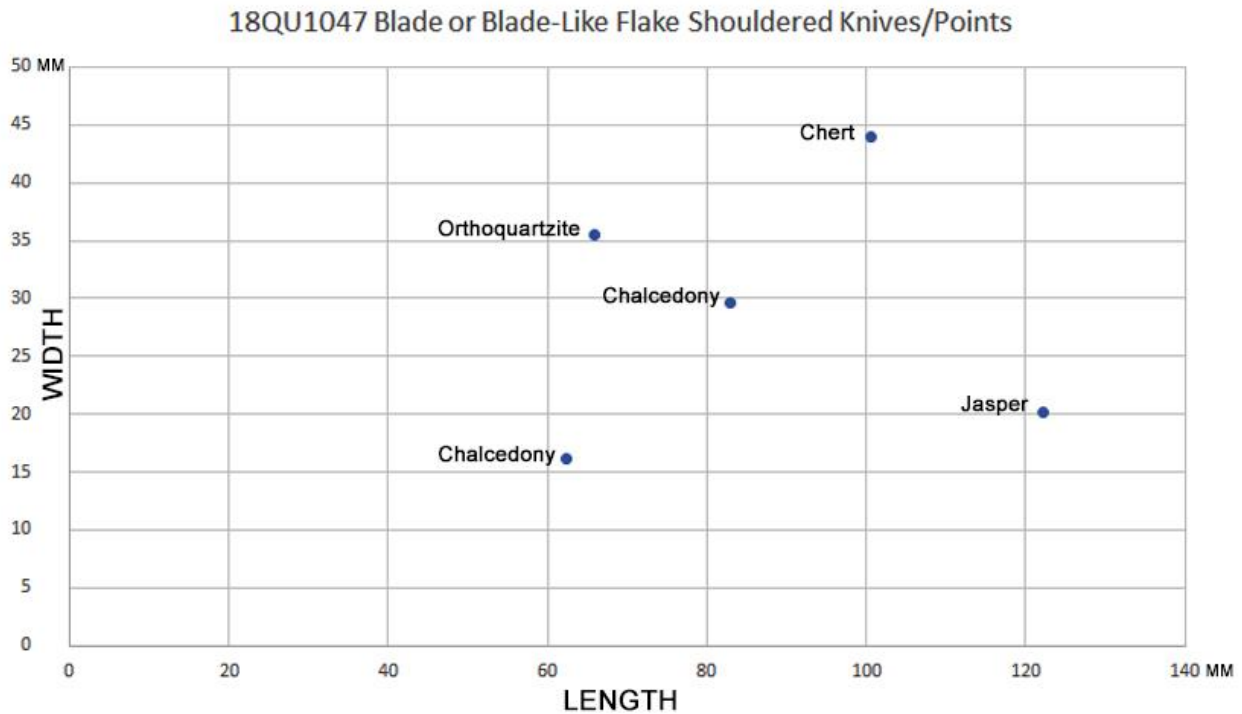


Figure 3.65. The graph portrays the length and width data for the blade or blade-like flake shouldered knives/points found at 18QU1047.

Flake Tools and Utilized Flakes:

Utilized flakes showing intentional retouch and/or damage are present in the assemblage found at 18QU1047. The flake tool assemblage is outlined in Table 3.7 and the length/width data are portrayed in Figure 3.69. The assemblage includes twenty-four (24) formal flake tools and/or utilized flakes. Most of these artifacts show retouch and wear-patterns indicating they functioned as scraping and cutting tools. Three of the artifacts represent incising and/or scoring tools. These include two burins and one graver. The assemblage also includes one modified blade-like flake with impact damage that may have functioned either as a projectile point or as a pointed-scraper with impact trauma (see Figure 3.68). A representative sample of utilized flakes and flake tools found at the site and pictured in this summary include a jasper endscraper fashioned on a blade segment (Figure 3.61 A), a chert

scraper/spokeshave flake tool (Figure 3.63 A), a large utilized flake knife manufactured from local Cretaceous-age Magothy quartzite (Figure 3.63 B), an endscraper made from a secondary cobble chert flake (Figure 3.63 C), a quartzite spokeshave (Figure 3.63 D), a utilized and retouched quartzite flake scraper (Figure 3.63 E), a large chert wedge (Figure 3.63 F), and a blade-like flake projectile point or scraper with impact trauma (Figure 3.68). The flake tools and utilized flakes found at 18QU1047 tend to cluster as three groupings (see Figure 3.69); ten (10) tools <35 millimeters in length, nine (9) tools >45 and <70 millimeters in length, and five (5) tools ~80 millimeters or larger in length.



Figure 3.66. The photograph shows an in-situ utilized blade-like flake tool (see Figure 3.63 A) found along the eroding shoreline at 18QU1047 on 6-21-2014. The artifact was located 201-centimeters beneath the ground surface and situated ~2-centimeters beneath the contact between the 3Cgb2 and the 4Ab1 soil horizons.

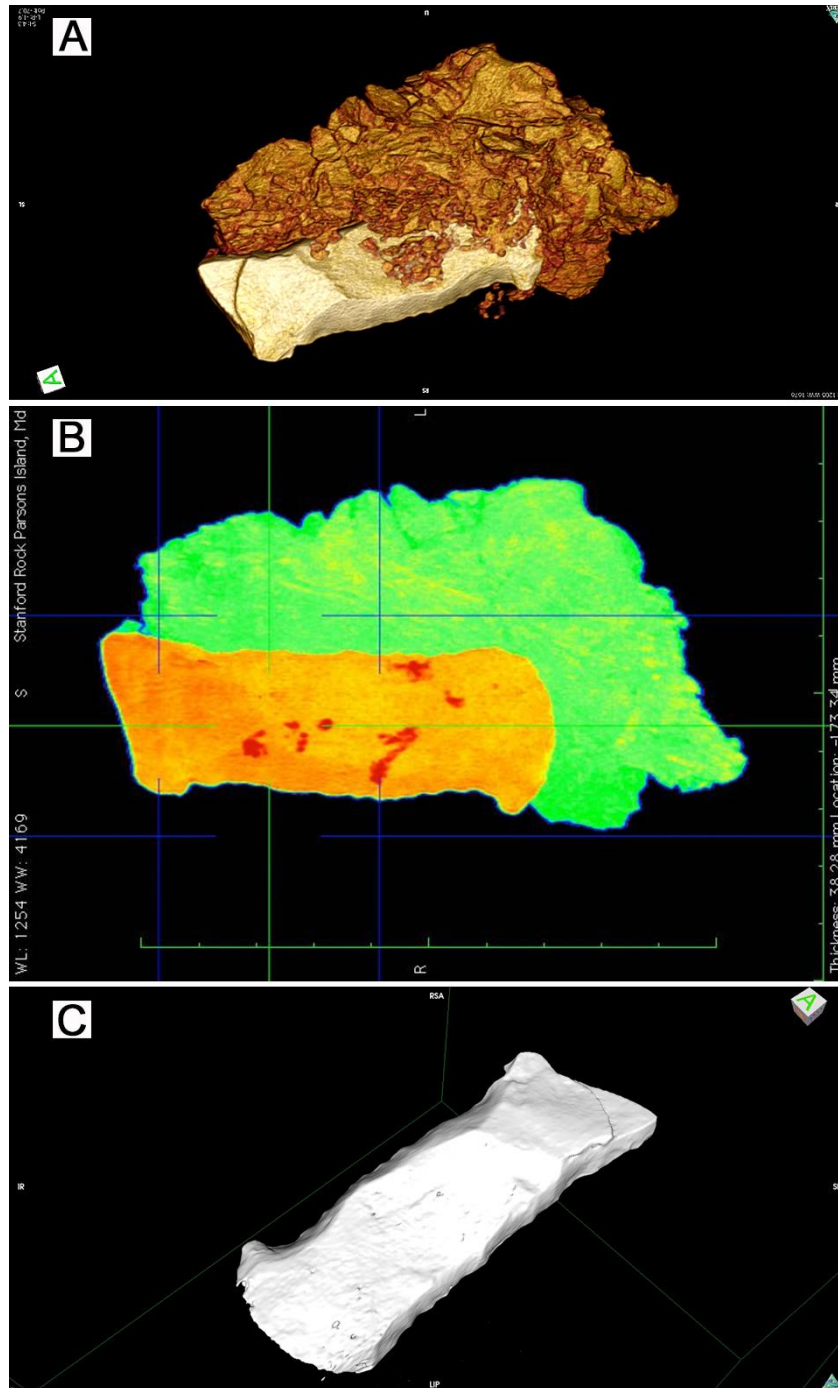


Figure 3.67. The images show various scans of the block removed from the eroding bank profile of 18QU1047 on 6-21-2014, which contained an in-situ stone tool. The sub-angular blocky structure of the parent sediments is visible in the three-dimensional scan (A). The x-ray of the block (B) shows no voids on the interior portion of the in-situ artifact, which would imply that the artifact is in place and was not inserted into the bank profile. Note the red-areas on the surface of the artifact, which represent an accumulation of iron and clay particles indicating a protracted period of in-situ undisturbed burial. Finally, the CT-scan shows the intentional retouch apparent on the interior unexposed portion of the artifact still embedded within the block sediment matrix.



Figure 3.68. The photographs show multiple views of a unifacial projectile point or scraper manufactured from a blade or blade-like flake, which was found at 18QU1047 on 5-29-2017.

TABLE 3.7. 18QU1047 FLAKE TOOLS AND UTILIZED FLAKE DATA.

<u>DATE:</u>	<u>DESCRIPTION:</u>	<u>LITHIC MATERIAL:</u>	<u>LENGTH:</u>	<u>WIDTH:</u>	<u>THICKNESS:</u>
9/1/2013	Utilized Flake (Distal end retouch or flake endscraper)	White Quartz	26	21	7.5
11/17/2013	Unifacial Flake Spokeshave (Figure 3.63 D)	Quartzite	59.1	33.2	17.4
11/17/2013	Utilized Flake (distal and lateral edge retouch)	Quartzite	32.8	25.6	8.5
12/14/2013	Large Retouched and Utilized Flake	Black Chert	86.4	25.8	13.5
1/18/2014	Large Utilized Flake (Scraper with Rounded Cobble Cortex)	Quartzite	65.2	42	14
6/21/2014	Blade-Like Flake with Scraper/Spokeshave (Figure 3.63 A)	Chert	81	30.3	10.8
7/11/2014	Large Flake Wedge (Figure 3.63 F)	Black Chert	65.4	63.7	21
7/26/2014	Burinated Flake (Burin)	Black Chert	28.2	24.6	5.6
7/26/2014	Burinated Flake (Burin)	Quartzite	24.2	22.7	7.3
8/3/2014	Flake Graver	Black Chert	27.8	14.9	8.4
9/26/2014	Cobble Flake Scraper (Scraper with Rounded Cobble Cortex)	Quartzite	79.1	55.8	13.3
1/4/2015	Unifacial Knife/Scraper Fragment	Mottled Chert	68.6	35.7	8.4
4/18/2015	Utilized Flake (Possible Awl or Graver)	Black Chert	25.3	17.6	4.5
5/29/2015	Utilized Flake Scraper (see Figure 3.63 E)	Quartzite	61.7	34.5	9.2
9/20/2015	Endscraper (Figure 3.61 A)	Jasper	27.1	17.5	8.5
1/14/2016	Utilized Flake (Pointed Scraper)	Quartzite	69.5	37.1	19.5
2/27/2016	Utilized Flake (Damaged Edge)	Quartzite	57.5	36	12.3
3/10/2016	Utilized Flake (Retouched Edge)	Black Chert	46.7	18.3	11.1
6/7/2016	Utilized Flake (Backed and Retouched)	Basalt	52.5	25.5	10.2
5/29/2017	Unifacial Blade Point or Scraper (Figure 3.68)	Jasper	53.6	20.6	6.6
2/13/2018	Damaged Unifacial Scraper	Jasper	33.3	31.4	7.9
5/6/2018	Large Utilized Flake (see Figure 3.63 B)	Magothy Quartzite	88.2	48.2	12.7
7/28/2018	Flake Endscraper (Figure 3.63 C)	Mottled Chert	32.2	31.8	7.3
4/3/2019	Utilized Flake	Quartzite	34.2	33.2	9.9

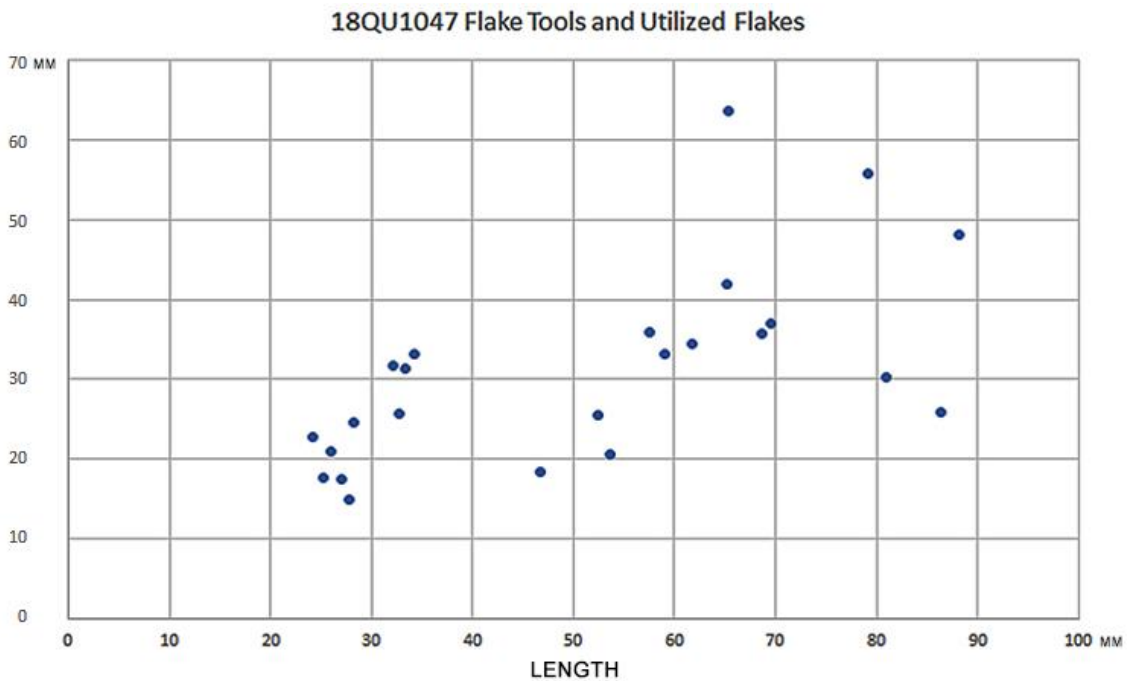


Figure 3.69. The graph portrays the length and width data for the flake tools and utilized flakes found at 18QU1047.

Hammerstones, Anvils, Battered Cobbles, Wind Polished Pebbles, and Rock Features:

Twelve (12) battered cobbles and wind polished/silica glazed pebbles have been found at 18QU1047. Most would be classified as hammerstones and anvils; since they show battering or impact damage along one or more edges (see Figure 3.70). The data for these artifacts are presented in Table 3.8 and the length/width measurement summary is shown Figure 3.73. Four of the twelve rounded lithic artifacts are classified as hammerstones (see Figure 3.70). Five of the specimens are split and battered pebbles and/or cobbles. Two small unaltered flat pebbles, which both have marked aeolian polish and silica glaze on one face, are also included in the sample. Presumably, these manuports were brought to the site by the occupants of the site. Both were found in-situ in 2019 and positioned at the contact between the 4Ab1 and the overlying 3Cgb soil horizons. The pebbles were clearly subjected to similar post-depositional aeolian alterations like the polish/silica glaze noted on a few of the flaked stone tools found at the site (see Figure 3.52). Finally, one rounded artifact is classified as a possible anvil (see Figures 3.71 and 3.72), because it has a few small impact scars on both faces. The specimen was found in-situ (see Figure 3.72) on 8-24-2014 and it has one distinct flake or spall detachment. The conjoining flake, which is listed in Table 3.9, was found along the shoreline approximately three-years later (see Figure 3.71). The stratum containing the possible anvil (see Figure 3.72 A and B) would pre-date the age of the 4Ab1 soil.

The most puzzling combination of non-flaked rounded rock artifacts at 18QU1047 were found as an in-situ cluster on 10-2-2020. Because of the sandier nature of the overlying and underlying strata, these rocks were found embedded within an oxidized stratum 6BCb soil (see Appendix IV: 249) at a depth of 214 to 223-centimeters. The in-situ rocks seem to represent a “feature”; as opposed to an actual artifact clustering. The placement and positioning (see Figures 3.74, 3.75, 3.76, and 3.78) within the bank profile imply the rocks were purposefully arranged by human occupants. The function of this rock feature is largely unknown. Lumps of slightly indurated iron-oxide “powder” within this feature suggest the presence of “red ochre”. Most importantly, it seems very unlikely that natural processes in an otherwise aeolian dominated setting could explain the presence of a sub-angular slab of sedimentary rock perched on top of three rounded quartzite cobbles. One of the cobbles has striations suggesting use as an abrader (see Figure 3.78 A). When the feature was initially discovered, a fourth rounded cobble (see Figure 3.77) had already been dislodged from the eroding bank profile and it was situated within sediment directly beneath the in-situ rock feature.

Debitage and Waste Flakes:

The assemblage found at 18QU1047 contains one-hundred and thirty-two (132) pieces of debitage and/or waste flake debris. A random selection of the flakes found at the site are illustrated in Figure 3.79. Of the sample, only sixty-nine (69) specimens were included in the measurement database summary outlined in Table 3.9 and illustrated in Figure 3.82. As a result of the coronavirus pandemic, the remaining sixty-three (63) flakes could not be analyzed for this report due to Covid19 pandemic-related restrictions at the Smithsonian Institution where the artifacts were on loan. These sixty-three (63) flakes, which were unearthed as a result of dredge-sieving the inter-tidal sediment (see Figure 3.80), are primarily less than 30 millimeters in length and consist largely of white quartz. As a result, the number of small flakes highlighted in Figure 3.82 would increase significantly if the Smithsonian sample were included.

The most significant flake found at 18QU1047 was unearthed as a result of controlled excavations conducted along the eroded bank margin by the Smithsonian Institution in early March of 2017. A single small white quartz flake was found in-situ within the 4Ab1 soil horizon and associated with a lump of charcoal. The charcoal associated with the in-situ quartz flake was subsequently dated to $22,501 \pm 155$ calibrated calBP ($18,515 \pm 73$ ^{14}C -age BP: Lab # PRI-5777). Like most of the flakes found at the site, the excavated specimen is small and fragmented.

The sample of sixty-nine (69) measured flakes provide some interesting insights as to the activities being performed by the site's occupants. The majority of the flakes are small and many of the quartz specimens are highly fragmented (see Figure 3.79 C-F). The morphology, as well as the extant platforms on the complete specimens indicate percussion-related re-tooling and re-sharpening activities were being performed at the site. Only eight of the specimens are greater than 40 millimeters in length or width. Given the dominance of small flakes, we can conclude that stone tool manufacturing was not being conducted at this particular locality; only tool maintenance was being performed. As indicated, the activities seem to be limited to re-tooling and re-sharpening existing stone tools and the occasional use of local cobbles and nearby primary lithic sources to produce expedient cutting/butchering tools.



Figure 3.70. The photograph shows a large hammerstone made from a locally-available rounded cobble of quartzite. The hammerstone was found at 18QU1047 on 6-28-2014.



Figure 3.71. The photograph shows a quartzite anvil found at 18QU1047 on 8-24-2014. The anvil was found in-situ along the eroded bank edge. The conjoining quartzite flake was found three-years later on 10-2-2017.

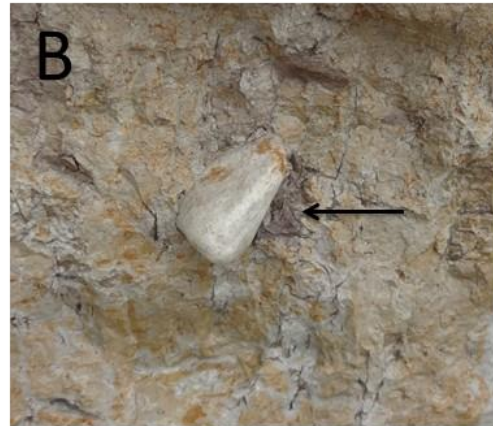


Figure 3.72. The photographs show the in-situ quartzite anvil found at 18QU1047 on 8-24-2014. The anvil is situated at 4Ab1/4Ab2 interface. The flaked edge margin was firmly embedded with the bank profile and could not be seen at the time the artifact was initially discovered. The conjoining quartzite flake was found three-years later on 10-2-2017.

TABLE 3.8. 18QU1047 ROUNDED LITHIC ARTIFACT DATA.

DATE:	DESCRIPTION:	LITHIC MATERIAL:	LENGTH:	WIDTH:	THICKNESS:
11/17/2013	Battered Pebble	White Quartz Cobble	30.8	27.4	22
3/2/2014	Split Pebble	White Quartz Cobble	38.5	22.7	9.7
6/28/2014	Battered Hammerstone (see Figure 3.70)	Quartzite Cobble	89.9	83.1	47
6/28/2014	Heavily Battered Hammerstone	Basalt Cobble	95.1	59.5	45.1
8/24/2014	Battered Cobble Anvil (see Figure 3.71)	Quartzite Cobble	120.3	90.1	57
10/29/2014	Hammerstone	Sandstone Cobble	123	112.4	43.7
5/29/2015	Flake Cobble	Rounded Chert Cobble	57.4	52.4	32.8
1/9/2016	Split Cobble	Quartzite Cobble	67.3	71.9	41.1
5/27/2018	Flaked Hammerstone	Quartzite Cobble	64.2	68.2	35.8
6/12/2019	Aeolian Polished Pebble (Found in situ 4Ab1/3Cgb2)	Brown Jasper Pebble	26.5	21.2	5.6
7/20/2019	Aeolian Polished Pebble (Found in situ 4Ab1/3Cgb2)	Tan Quartzite Pebble	53.9	39.2	10.6
3/12/2020	Battered Pebble	White Quartz Pebble	30.9	28.4	19.1

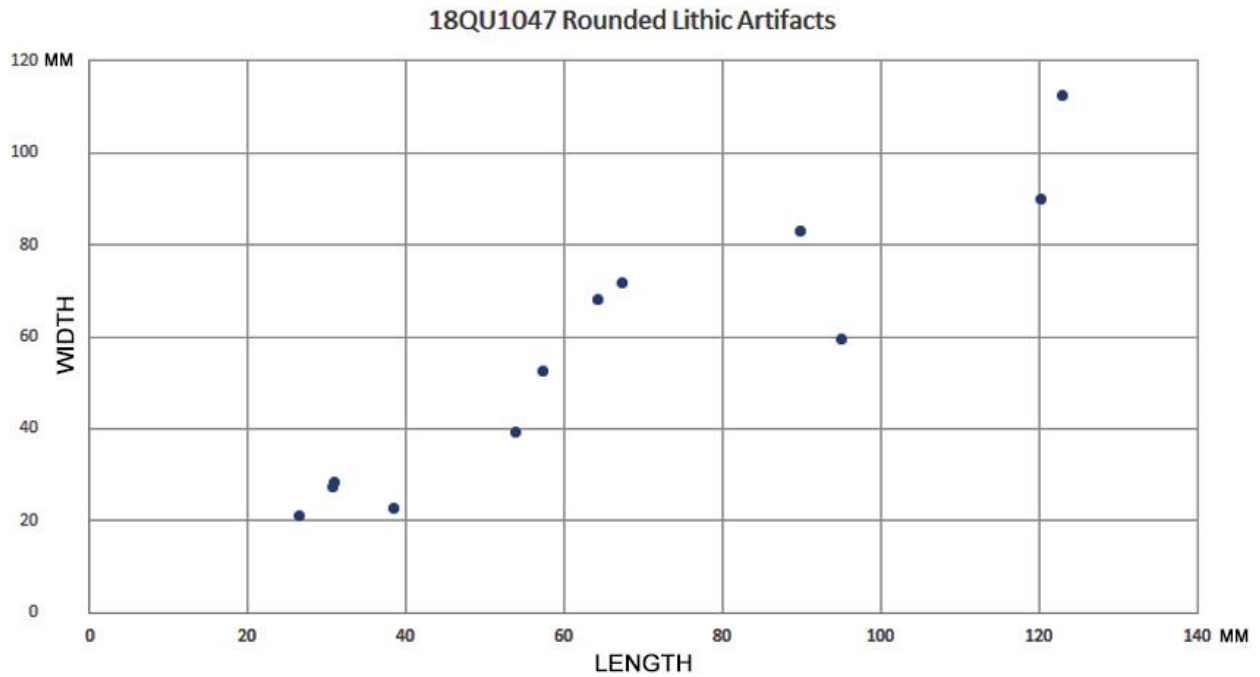


Figure 3.73. The graph portrays the length and width data for the rounded lithic artifacts found at 18QU1047.



Figure 3.74. The photograph shows the eroding bank profile at 10-2-2020. A rock feature was exposed in the bank on that day. The rock feature is located at a depth between 214 and 223-centimeters below the ground surface. The associated soil horizon corresponds with a sandier more oxidized 6BCb horizon.



Figure 3.75. The photograph shows a detailed view of the exposed rock feature within the eroding bank profile at 10-2-2020.



Figure 3.76. The photograph shows the underside of the exposed rock feature found at 18QU1047 on 10-2-2020.



Figure 3.77. The photograph shows a fourth rounded basaltic rock, which has been dislodged. Presumably it was associated with the in-situ rock feature found at 18QU1047 on 10-2-2020.

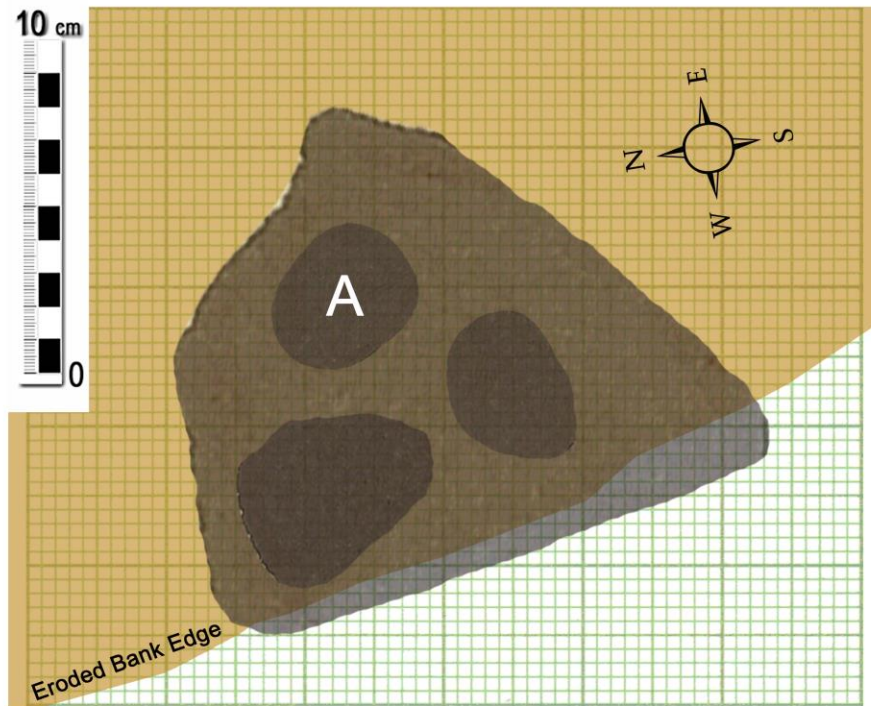


Figure 3.78. The graphic image shows the arrangement of the rock feature found within the 6BCb soil horizon on 10-3-2020. The feature consisted of a flat angular slab of sedimentary rock perched on top of three rounded quartzite cobbles. One of the rounded rocks (A) has striations along one side, which suggests it was used as an abrader.

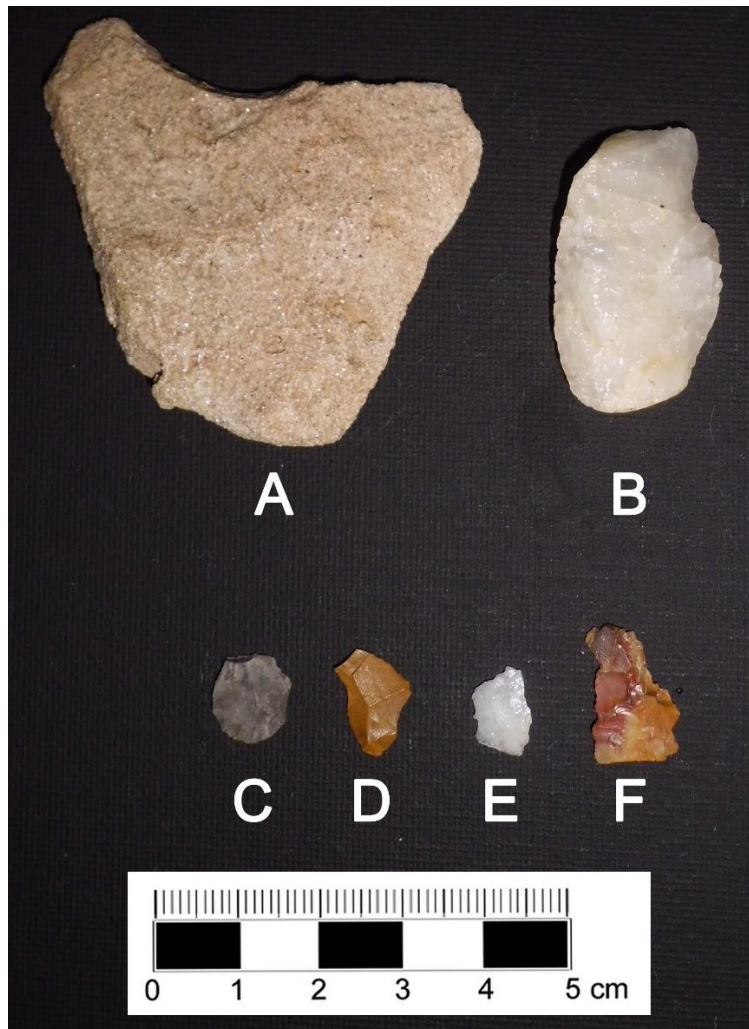


Figure 3.79. The photo shows a representative sample of debitage found at 18QU1047. Large unused flakes are uncommon at the site. The large weathered and degraded Miocene silicified sandstone flake (A) was found on 6-13-2015. The silicified sandstone most likely originated from primary outcrops located on the nearby Wye River; situated about four-miles east of Parsons Island. The same type of lithic material was used to manufactured one of the large bipoint bifaces (see Figure 3.38 E) found at the site. The flake has a broad bifacial platform. White quartz, as noted in the flake derived from a cobble (B), is the most common lithic material found at 18QU1047. The quartz flake (B) seems to have been detached from a small cobble using a hammerstone/anvil and employing a bipolar reduction technique. It was found at 18QU1047 on 3-2-2014. The majority of the flakes found at the site are small; like those shown (see C through F). The chert (C) and jasper (D) flakes are the byproduct of resharpening and they were detached using a soft-hammer percussion. These two flakes were also found at 18QU1047 on 3-2-2014. Small white quartz shatter (E) is the most common type of debitage found at the site. The highly fragmented nature and small size of the quartz debitage may be the consequence of both the fractures in the parent material, as well as, the reduction strategies. The small quartz flake (E) was found at 18QU1047 on 12-3-3018. Some flakes manufactured of other lithic materials also consist of only fragments (F). The photograph shows the distal portion of a jasper flake (F) found at the site on 12-23-2018.



Figure 3.80. The photo images of the dredging activity conducted offshore of 18QU1047 on 2-23-2017. As a result, sixty-three (63) small pieces of debitage and/or waste flakes were found.

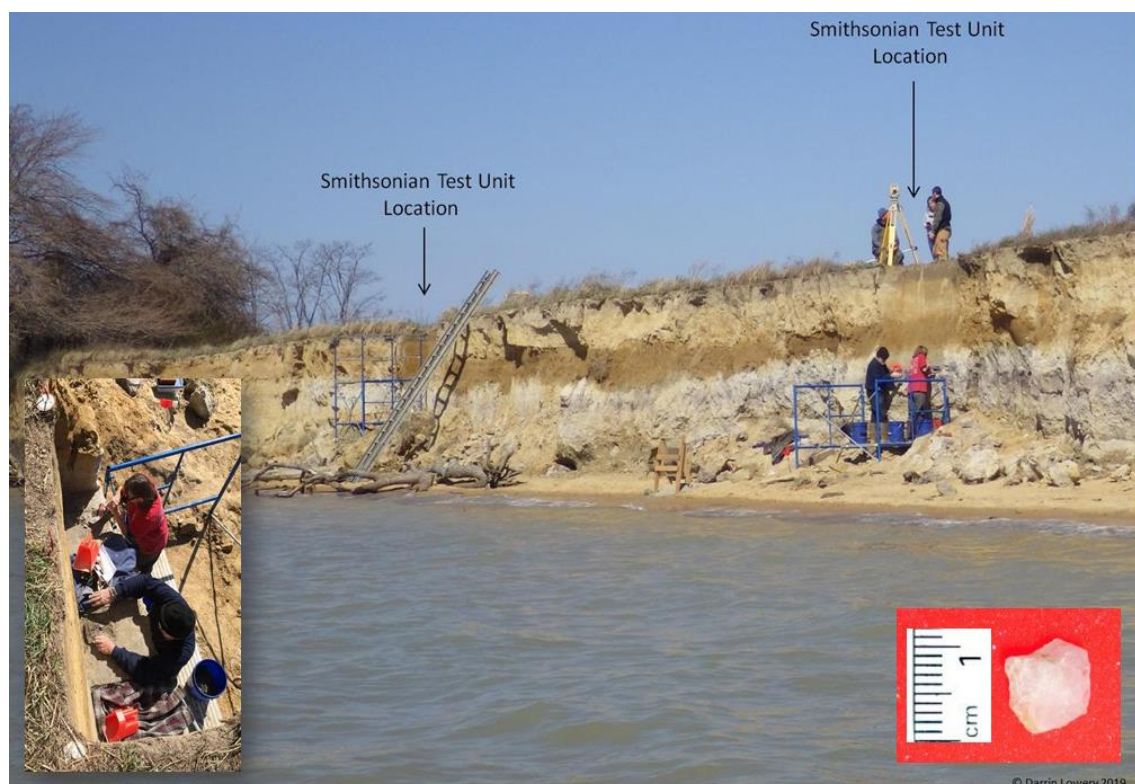


Figure 3.81. The photos, which were taken on March 9th, 2017, show the Smithsonian testing conducted at 18QU1047. A single small white quartz flake (inset) was found in-situ within the 4Ab1 soil horizon associated with the southern test unit.

TABLE 3.9. 18QU1047 DEBITAGE AND WASTE FLAKE DATA.

DATE:	DESCRIPTION:	LITHIC MATERIAL:	LENGTH:	WIDTH:	THICKNESS:
9/1/2013	Flake	White Quartz	33.5	20.5	10.8
9/1/2013	Flake	Brown Quartzite	14.6	14.5	3.5
9/1/2013	Flake	Gray Quartzite	11.2	14.6	3.8
9/1/2013	Flake Fragment	Rhyolite	13.2	26.8	5.9
9/25/2013	Flake	White Quartz	11.2	9.7	4.1
9/25/2013	Flake	White Quartz	13.7	10.1	3.9
9/25/2013	Flake	White Quartz	12	13	4
10/12/2013	Flake	White Quartz	17.3	12.5	4.5
11/17/2013	Flake	Magothy Quartzite	23.4	18	7.9
11/17/2013	Flake	White Quartz	16.5	18.6	5
11/17/2013	Flake	White Quartz	12.6	12.2	4.8
2/16/2014	Flake	White Quartz	22.2	15.9	4.4
2/16/2014	Flake	White Quartz	15.9	12.3	4.6
2/16/2014	Flake	White Quartz	10.4	11.2	2
2/16/2014	Flake	White Quartz	11.4	8.3	2
3/2/2014	Flake	White Quartz	9.1	9	3.4
3/2/2014	Flake	Brown Jasper	14.4	8.9	2.1
3/2/2014	Flake	Grey Chert	12	10.7	2.3
5/12/2014	Spall	White Quartz	35.7	23.5	9.7
5/12/2014	Flake	White Quartz	22.2	17	8.9
5/12/2014	Flake	White Quartz	17.9	11.9	2.9
6/21/2014	Flake	White Quartz	31.1	17.2	7.3
6/21/2014	Flake	White Quartz	20.7	23.1	8.3
6/21/2014	Flake	White Quartz	19.5	13.8	7.2
6/21/2014	Flake	White Quartz	14.6	10.5	10
6/21/2014	Flake	White Quartz	17.7	15.3	3.3
6/21/2014	Flake	Quartzite	16.1	12	7.4
6/21/2014	Flake	White Quartz	18.6	15.4	3
7/26/2014	Flake Fragment	White Quartz	16.5	23.7	6.4
7/26/2014	Flake Fragment	White Quartz	20.5	23	7.2
7/26/2014	Flake	White Quartz	17.5	23.2	11.3
7/26/2014	Flake	White Quartzite	16.4	9.7	3.1
8/3/2014	Spall	Quartzite	80.5	71.1	39.1
8/3/2014	Flake Fragment	Quartzite	24.7	51.7	13
8/3/2014	Flake	Black chert	20	11.1	3.1
5/17/2015	Spall	Black Chert	63.2	33.6	18.7
6/13/2015	Flake	Miocene Silicified S	65.4	59	12.5
7/30/2015	Flake	Jasper	28.5	19.5	8.1
7/30/2015	Flake	White Quartz	23.5	19.2	5.2
7/30/2015	Flake	White Quartz	9	7.5	2.3
7/30/2015	Flake	Basalt	21.8	18.1	5.6
7/30/2015	Flake	Tan/Gray Quartzite	18	13.6	3.2
12/9/2015	Spall	Black chert	70.8	43.7	16.2
2/1/2016	Flake	Quartz	21.5	17.7	6.8
2/1/2016	Flake	Quartz	19.9	17.4	6.1
4/5/2016	Flake	White Quartz	28	22.9	7.6
4/5/2016	Flake	White Quartz	21	14.5	4.1
4/5/2016	Flake	White Quartz	18.4	14.7	5.8
4/5/2016	Flake	Black Chert	42.4	16.1	7.7
5/20/2016	Flake	Quartzite	29.8	19.8	8.6
5/20/2016	Flake	White Quartz	16.8	10.7	8.6
10/10/2016	Flake	White Quartz	26	15.5	4
2/23/2017	63 flakes (dredging)	Various			
3/9/2017	Flake	White Quartz	15	14.1	8.1
4/29/2017	Flake	Miocene Sandstone	21.2	15	6
4/29/2017	Flake	Magothy Quartzite	24.3	15.3	5.8
10/2/2017	Flake	Quartzite	49.5	52.3	13.8
4/5/2018	Flake	White Quartz	18.2	9.5	3.2
12/3/2018	Flake	White Quartz	10.5	7.5	2.6
12/23/2018	Flake Fragment	Tan/Brown Jasper	18.2	11.6	3.6
2/6/2019	Flake	White Quartz	21.5	20.1	6.4
3/8/2019	Flake	White Quartz	8.2	7.9	2.2
3/8/2019	Flake	White Quartz	9.1	6.4	2.2
4/3/2019	Flake	White Quartz	11.1	7.4	2.6
4/3/2019	Flake	White Quartz	11.8	11.6	5.7
4/30/2019	Spall	Basalt	64.3	50.5	37.5
4/30/2019	Flake	Quartz	28.1	20.5	9
4/30/2019	Flake	Quartz	15.5	16.9	6
4/30/2019	Flake	Quartz	21.3	14.7	4.8
4/30/2019	Flake	Quartz	24.2	14.6	6
3/9/2020	Flake	White Quartz	31	19.5	8.2
4/6/2020	Flake	White Quartz	13.9	9.7	3.8

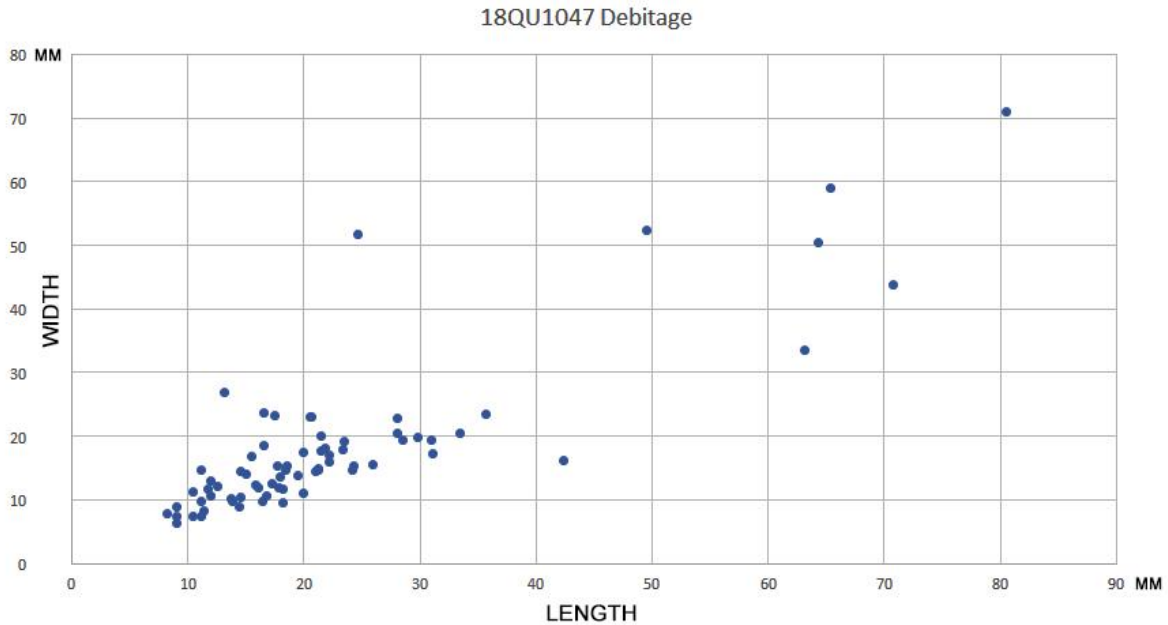


Figure 3.82. The graph portrays the length and width data for the debitage and waste flakes found at 18QU1047.

4. EXCAVATIONS AND ARCHAEOLOGICAL TESTING AT 18QU1047

The area associated with 18QU1047 was subjected to archaeological testing and excavations to determine if artifacts could be found in-situ immediately inland from the shoreline. The following summary outlines the results of these investigations.

4.1. Smithsonian 2017 Archaeological Test Investigation Summary:

The initial testing at Parsons Island was led by Smithsonian investigators; Dr. Dennis Stanford, Dr. Margaret Jodry, and Dr. Bruce Bradley. Currently no fieldwork summary report exists for this excavation. A field-crew, which included Juniata College students and faculty member Dr. Jonathan Burns, provided assistance during the initial testing of 18QU1047. During the week-long investigation, geoarchaeological advisors at the site included Dr. Daniel Wagner and Dr. John Wah.

Fieldwork, which initially began on March 5th, 2017, was concluded on March 10th, 2017. The excavations consisted of two half-meter by two-meter excavation units situated along the steep eroding bank margin. The excavations were conducted using a combination of natural and arbitrary levels. For example, the plowzone was removed as a singular unit and screened using ¼-mesh. Whereas, the ~40-centimeter thick 2Bt2 soil horizon, which seems to represent a singular aeolian depositional stratum, was excavated and screened in arbitrary 10-centimeter levels. The units were placed in areas where in-situ artifacts had been observed along the retreating bank escarpment. The objectives of this preliminary investigation were to determine if in-situ artifacts could be found inland of the eroding bank margin and to attempt to resolve some of the reported age-estimates established for the buried 4Ab1 soil stratum.



Figure 4.1. The photograph shows Dr. Bruce Bradley affiliated with the University of Exeter and Dr. Pegi Jodry of the Smithsonian Institution meticulously excavating the 4Ab1 soil horizon along the exposed bank profile associated with the Southern Test Unit. The Southern Test Unit revealed a single in-situ small white quartz flake at a depth of ~198-centimeters. Charcoal associated with this lithic artifact produced a two-sigma age estimate of $22,501 \pm 155$ cal. yrs. BP (PRI-5777: $18,515 \pm 73$ rcybp). Another fragment of charcoal found in the same stratum in this unit and not associated with a lithic artifact produced a two-sigma age estimate of $23,332 \pm 174$ cal. yrs. BP and $23,703 \pm 106$ cal. yrs. BP (PRI-5778: $19,388 \pm 59$ rcybp).



Figure 4.2. The scaled 2-17-2017 satellite image shows the shoreline associated with 18QU1047. The georeferenced 2017 Smithsonian test units are positioned along the bank edge. The location of a bipoint biface (see Figure 3.39 E) found offshore of the site during the fieldwork has also been plotted.



Figure 4.3. The scaled 11-5-2019 satellite image shows the shoreline associated with 18QU1047 almost two years after the Smithsonian testing had been completed. The placement and position of the Smithsonian test units were evident along the eroding bank profile in archival photos taken as late as November 2018. The current positions of the 2017 Smithsonian test units have been plotted on the 11-5-2019 satellite image. During this short 20-month interval spanning March 9, 2017 to 11-5-2019, the bank edge receded approximately 4.17 to 4.92 meters (13.68 to 16.14 feet). The extreme erosion and eastward bank retreat noted during this short interval can be directly correlated with the January 2019 formation of ice in the Chesapeake Bay region (see Figures 3.33 and 3.36).

All of the sediments from the various strata overlying and beneath the 4Ab1 soil horizon at 18QU1047 were screened during the test excavations conducted by the Smithsonian in 2017. The excavations extended from the current ground surface to a depth of ~220-centimeters and stopped at the bottom of the 4Ab2 soil horizon. In both test areas, no lithic artifacts were found in the strata overlying or beneath the 4Ab1 soil horizon. The northern Smithsonian test unit (see Figures 3.81 and 4.2) produced no lithic artifacts. However, the southern test unit (see Figures 3.81, 4.1, and 4.2) revealed one lithic artifact. At a depth of ~198-centimeters, a single white quartz flake (see Figure 3.81, inset) was found within firmly embedded in the 4Ab1 soil. A fragment of charcoal associated with this lithic artifact produced a two-sigma age-estimate of 22,501 ± 155 calibrated calendar years BP (PRI-5777: 18,515 ± 73 rcybp). Another fragment of charcoal from the 4Ab1 soil and not directly associated with the lithic artifact produced a two-sigma age-estimate which calibrates to 23,332 ± 174 calendar years BP and 23,703 ± 106 calendar years BP (PRI-5778: 19,388 ± 59 rcybp).

An extreme low tide event, which occurred on March 10th, 2017, and associated with the last day of fieldwork revealed a white quartz bipoint biface (see Figure 3.39 E) that had been displaced out of primary context and deposited offshore of the eroding site (see Figures 4.2 and 4.1). The initial Smithsonian test excavations demonstrated that lithic artifacts are undeniably embedded within the 4Ab1 soil horizon and are not present within any of the overlying strata at 18QU1047. The testing also independently verified that the 4Ab1 soil horizon is indeed 20,000 to 23,000 years old.

4.2. CWAR 2020 Archaeological Test Investigation Summary:

The recent fieldwork and testing at Parsons Island began in December 2019. These investigations were funded by a non-capital grant from the Maryland Historical Trust. The objectives of this investigation were to conduct a complete archaeological survey of the island and test the area associated with 18QU1047. Contrary to Bradley-Lewis (2021), the testing at 18QU1047 was to consist of four (4) one-by-one meter test units and represent a formal archaeological investigation. These units were to be excavated from the surface to the base of 4Ab1 soil horizon and determine if any in-situ archaeological remains were present inland from the bank edge. Like the previous 2017 testing, the sediments, which were screened using a ¼-mesh, were excavated using a combination of both natural and arbitrary stratigraphy. The objectives were to also find any possible associated charcoal to evaluate and assess the age or ages of any in-situ archaeological remains. The investigation also included a comprehensive ground-penetrating radar (GPR) survey of the island conducted by Ms. Neeshell Bradley-Lewis (see Bradley-Lewis 2021) and Dr. Michael O'Neal of the University of Delaware (see Figure 4.4). The GPR investigation evaluated the effectiveness of GPR remote sensing to document the relic topographic undulation of the buried 4Ab1 paleosol (see Appendix IV) and assess its effectiveness in locating any associated archaeological features. The outcomes of the GPR investigation and aerial survey at Parsons Island have been prepared at this time (see Bradley-Lewis 2021) and the results of these investigations are not included in this monograph.



Figure 4.4. The photograph shows the ground penetrating radar sled being deployed in the interior of Parsons Island on 12-21-2019.

An in-situ artifact (see Figures 3.40 and 4.5) exposed along the eroding bank profile provided a base for establishing the location and position of the four test units. In the early spring 2020, the fields had been tilled and the field areas were subjected to an intensive pedestrian survey on April 6th, 2020. Like the results generated in 1992 (see Lowery 1993), no prehistoric artifacts or lithic debris were found on the surface within the tilled fields at Parsons Island. The four one-by-one-meter excavation units were clustered in an area located approximately 1.53 meters inland of the eroded bank edge and positioned directly east of the in-situ biface found on 1-20-2020.

The excavations began on May 13th, 2020 (see Figures 4.6 and 4.7). On this date, the plowzone or Ap-soil horizon was removed and screened as a single unit. The only artifacts found in the plowzone included a plastic shotgun shell wad and a small highly degraded fragment of oyster shell. The regional data would imply the underlying silts to a depth of 67-centimeters represent the Younger-Drays age Paw Paw loess. As such, the underlying E, BE, and Bt soil-horizons were excavated as seven arbitrary 5-centimeter layers. Because no artifacts were found, the lower 2-centimeter section of the Bt-horizon was included with the overlying excavation stratum. The complete removal of the Paw Paw loess had been completed by 6-3-2020 (see Figure 4.8). The underlying 53-centimeters associated with the 2Btb1 and 2Btb2 soil-horizons were excavated as ten individual 5-centimeter excavation layers and completed on 6-8-2020 (see Figures 4.9, 4.10, and 4.11). Again, no artifacts were found. The 50-centimeter stratum associated with the 3Cgb1 and 3Cgb2 horizons (see Figures 4.12 and 4.13) were excavated as ten individual 5-centimeter excavation layers and completed on 6-29-2020. On June 29th, the initial 5-centimeter upper portion of the ~14-centimeter thick 4Ab1 soil-horizon was excavated and screened (see Figure 4.14). On this date, three lithic artifacts were uncovered near the far southwestern corner of the four one-by-one-meter excavation block (see Figures 4.15, 4.17, and 4.23). At the end of the day,

these artifacts were initially covered and left in-situ with the anticipation that the unit block area could be scanned using a 3-D imagery scanner. Most importantly, it was thought that the cultural stratum could be sampled for biomarkers and the overlying strata could be subjected to OSL-dating. From July through October, the region experienced consecutive episodes of marked rain, wind, and tropical storms. The units were completely filled with water and portions of the side walls collapsed. The late summer through the fall of 2020 was the wettest on record. As such, the removal of the remaining portion of the 4Ab1 and underlying 4Ab2 horizons was postponed until the Spring of 2021. In the Spring of 2021, the in-situ artifacts were removed for photography (see Figure 4.23). In sum, the archaeological investigations conducted at Parsons Island in 2020 had been plagued by both a pandemic and marked cyclonic-precipitation events. However, the original objective of evaluating the presence of in-situ archaeological remains at 18QU1047 had been achieved.



Figure 4.5. The eroded bank profile at 18QU1047 as it appeared on January 10th, 2020. Note the in-situ bipoint biface (see Figure 3.39 D) situated at the contact between the 4Ab1 soil horizon and the overlying 3Cgb2 soil horizon.



Figure 4.6. The photo shows the field crew, which consisted of Mr. Norm Brady, associated with the first day of excavation at 18QU1047. The testing on May 13th, 2020 consisted of the removal of the plowzone exposing the underlying sub-soil. Importantly, this work began during the height of the COVID-19 pandemic and travel/work restrictions had been imposed within the State of Maryland.



Figure 4.7. The photo, which is looking due west, shows the amount of progress made during the initial day of testing on May 13th, 2020 with a two-person crew. The crew included Mr. Norman K. Brady and Darrin Lowery.



Figure 4.8. The photo, which is looking towards the southwest, shows the excavation progress made at 18QU1047 by June 3rd, 2020.



Figure 4.9. The photograph shows the field crew involved with the excavations conducted on June 3rd, 2020. The crew included Neeshell Bradley-Lewis, Michael O’Neal, and Darrin Lowery.



Figure 4.10. The photo, which is looking towards the northeast, shows the excavation of the units as they appeared on June 8th, 2020. The field crew included Jack Lowery, David Thompson, Norman Brady, and Darrin Lowery.



Figure 4.11. The photo, which was taken at the completion of the excavations on June 8th, 2020 shows the west wall of the excavation area. Note the moisture content clearly delineates the surficial Younger Dryas-age Paw Paw loess, which includes the Ap through Bt soil-horizons, from the underlying 2Btb1 and 2Btb2 soil-horizons. The circular hole in the unit is an auger hole used to determine the soil horizon thicknesses in the underlying strata.



Figure 4.12. The photo, which was taken during the excavations at 18QU1047 on June 16th, 2020 shows the west wall of the excavation area. The crew included Neeshell Bradley-Lewis, Michael O’Neal, Norm Brady, and Darrin Lowery.

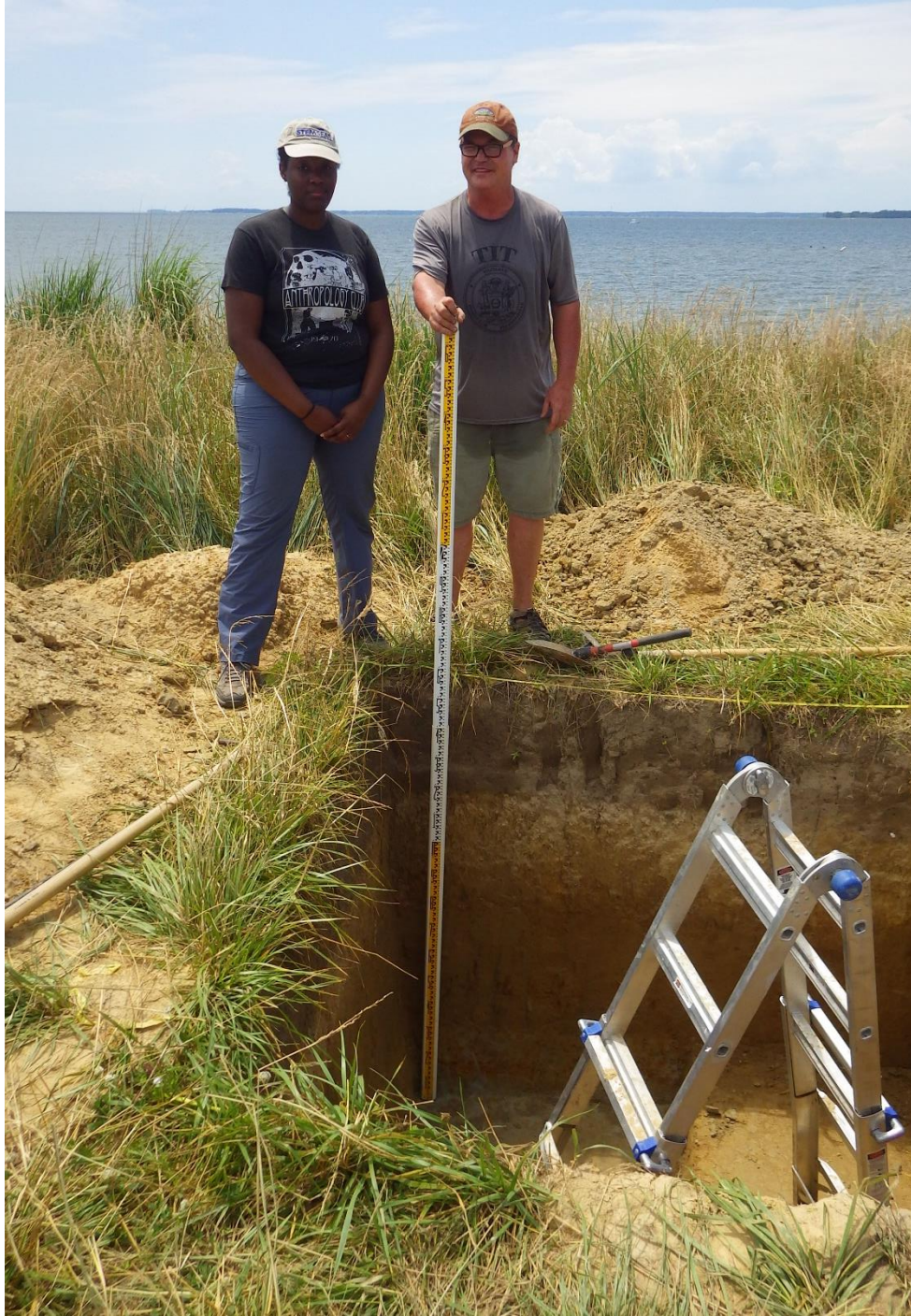


Figure 4.13. The photo, which was taken after the completion of the excavations at 18QU1047 on June 25th, 2020 shows the southwest corner of the excavation area. The crew included Neeshell Bradley-Lewis, Michael O’Neal, Joseph Clemens, and Darrin Lowery.



Figure 4.14. The photo, which was taken after the completion of the excavations at 18QU1047 on June 29th, 2020 shows the southwest corner of the excavation area. At this time, the excavation units were 1.75 meters (175-centimeter or 5.741-feet) below the current ground surface. The crew included Norm Brady and Darrin Lowery.

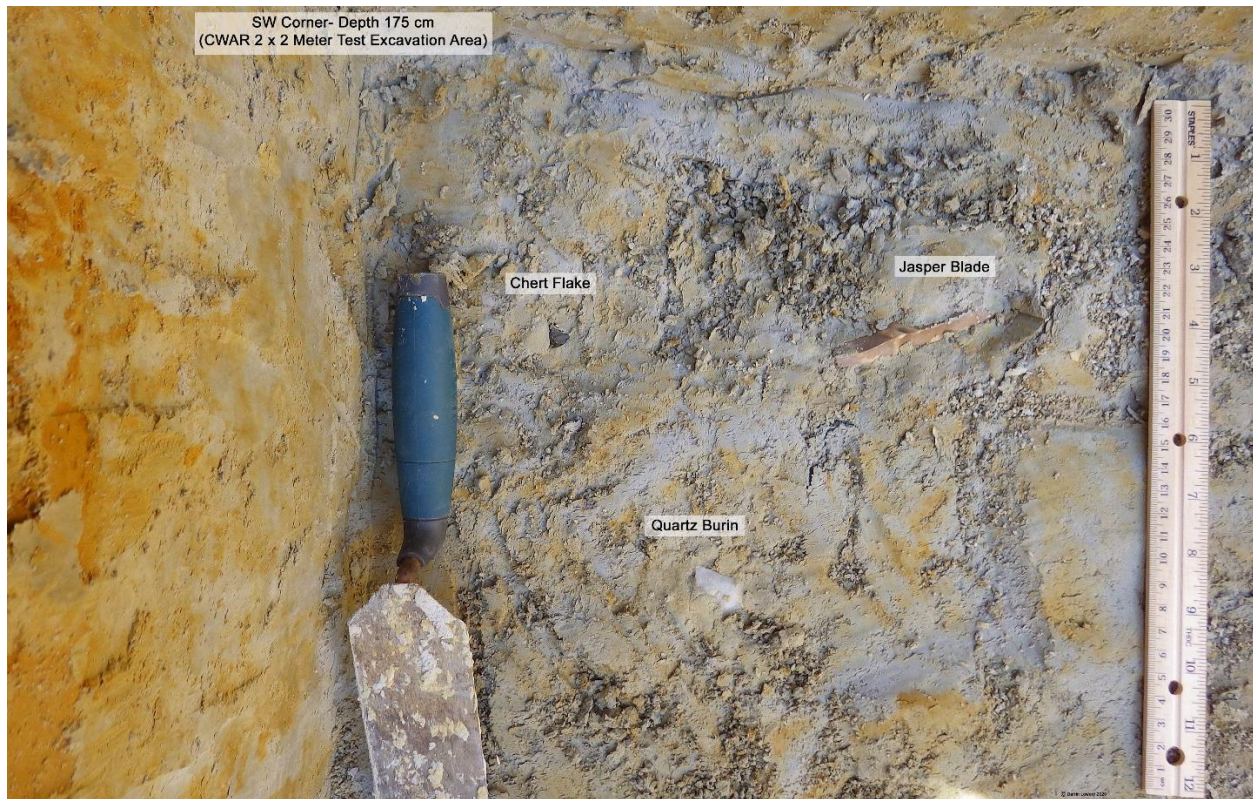


Figure 4.15. The photo, which was taken after the completion of the excavations at 18QU1047 on June 29th, 2020 shows the three in-situ lithic artifacts exposed within the southwest corner of the excavation area. These three artifacts were situated in the upper portion of the 4Ab1 soil horizon.

4.4. CWAR 2020 Geoarchaeological Summary at 18QU1047:

In 1992 when Parsons Island was initially surveyed (see Lowery 1993), the western edge of the excavation units positioned at 18QU1047 in 2020 was situated 64.27 meters (210.8 feet) inland of the eroding shoreline. Twenty-eight years later, the actively eroding shoreline at 18QU1047 had retreated 62.74 meters (~205.78 feet) eastward. When the area was first re-examined in May of 2013, the actively eroding shoreline was positioned 11.13 meters (36.5 feet) due west of the 2020 excavation units. Between 2013 and 2020, the shoreline at 18QU1047 retreated 9.6 meters (31.49 feet). Over this seven-year period, the shoreline at 18QU1047 was re-examined ninety-three times. As a result, 286 lithic artifacts, 7 late Pleistocene vertebrate teeth, and two aeolian polished/glazed pebbles were found. Of the 286 lithic artifacts, only nine artifacts were found in-situ; which does not include the three (see Figures 4.15 and 4.17) found during the 2020 excavation. Minus the sixty-three (63) artifacts found during the dredging/sieving fieldwork conducted on 2/23/2017 (see Figures 3.36 and 3.80), the longitude/latitude positions for most of the formal tools found at 18QU1047 were amassed during each shoreline re-examination episode. These GPS measurements are <12-inch accuracy. Collectively, these data have allowed us to better understand how the dislodged artifacts are being naturally-transported by seasonal wind and wave actions (see Figure 4.16). Given the recorded locations of all in-situ artifact finds (see Figure 4.16), we can conclude some of the artifacts could have been displaced ~50-meters

(~165 feet) south and ~20-meters (~66 feet) north of the observed in-situ artifact cluster. However, if there are multiple loci are being eroded the lateral movement may be slightly less. The meticulous spatial documentation of each artifact at 18QU1047 provides a better understanding about where in-situ archaeological remains may be located east of the actively retreating eroding bank margin. More importantly, it illustrates how site-specific coastal geometries in tandem with wind and wave actions can rework eroded and displaced artifacts.

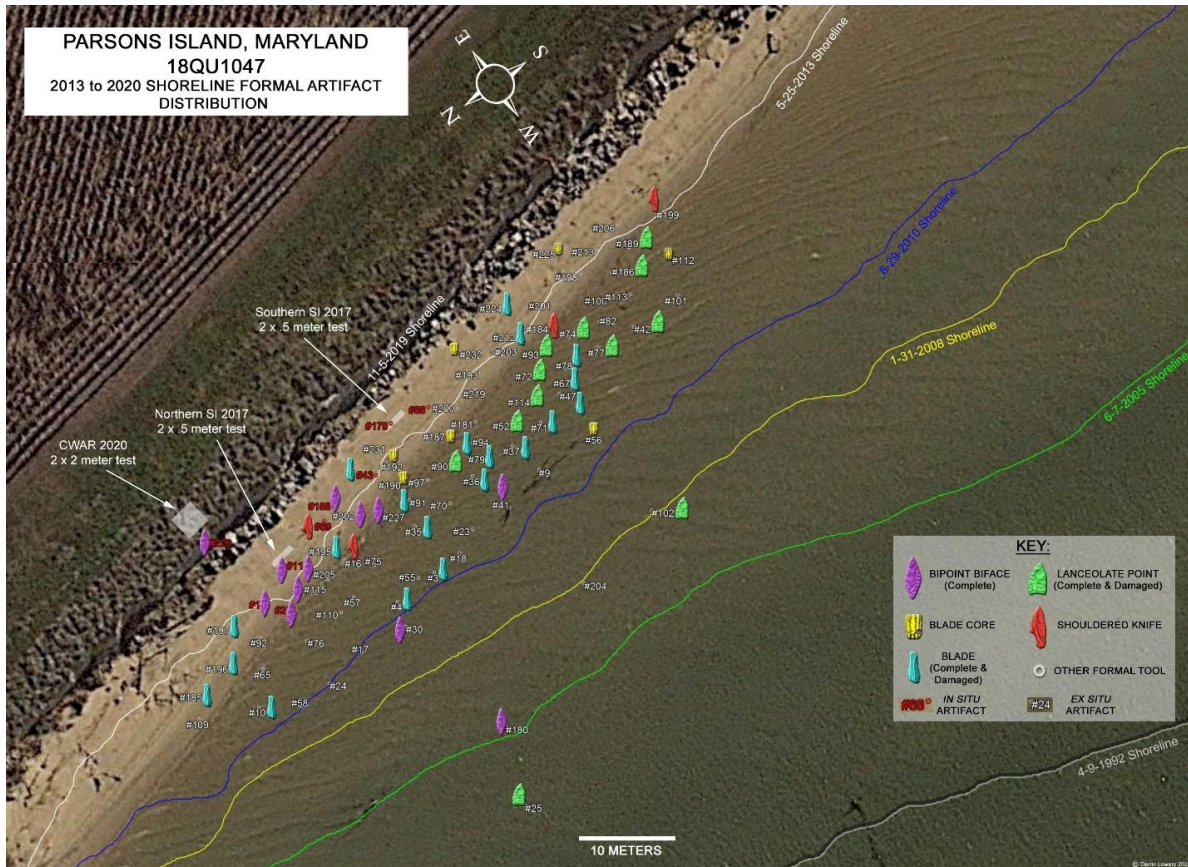


Figure 4.16. The image shows the 11-9-2019 satellite view of 18QU1047. The graphic also plots the longitude/latitude recorded positions of all formal tools found along the shoreline at the site between 2013 and 2020. The key designates each type of artifact. Other formal tools include formal scraping implements, utilized flakes, and hammerstones. The distribution of the debitage has not been included in this plot. Note that each artifact is sequentially numbered. Artifacts #1 through #23 were found in 2013, artifacts #24 through #74 were found in 2014, artifacts #75 through #95 were found in 2015, artifacts #96 through #113 were found in 2016, artifacts #114 through #192 were found in 2017, artifacts #193 through #208 were found in 2018, artifacts #209 through #225 were found in 2019 and artifacts #226 through #232 were found in 2020. The eastward eroding bank margins spanning the period between 1992 to 2019 have been positioned. The 2017 Smithsonian excavation units (see Figures 3.81 and 4.1), which were originally situated along the bank face have also been plotted. Note that these test units are currently located >5 meters (>16.4 feet) west of the 2019 bank edge. Finally, the 2020 excavation units have also been plotted. The trending northwesterly and southwesterly winds, which regularly impact the shoreline, may have transported some of the displaced artifacts ~50-meters (~165 feet) south and ~20-meters (~66 feet) north of the observed in-situ artifact cluster.

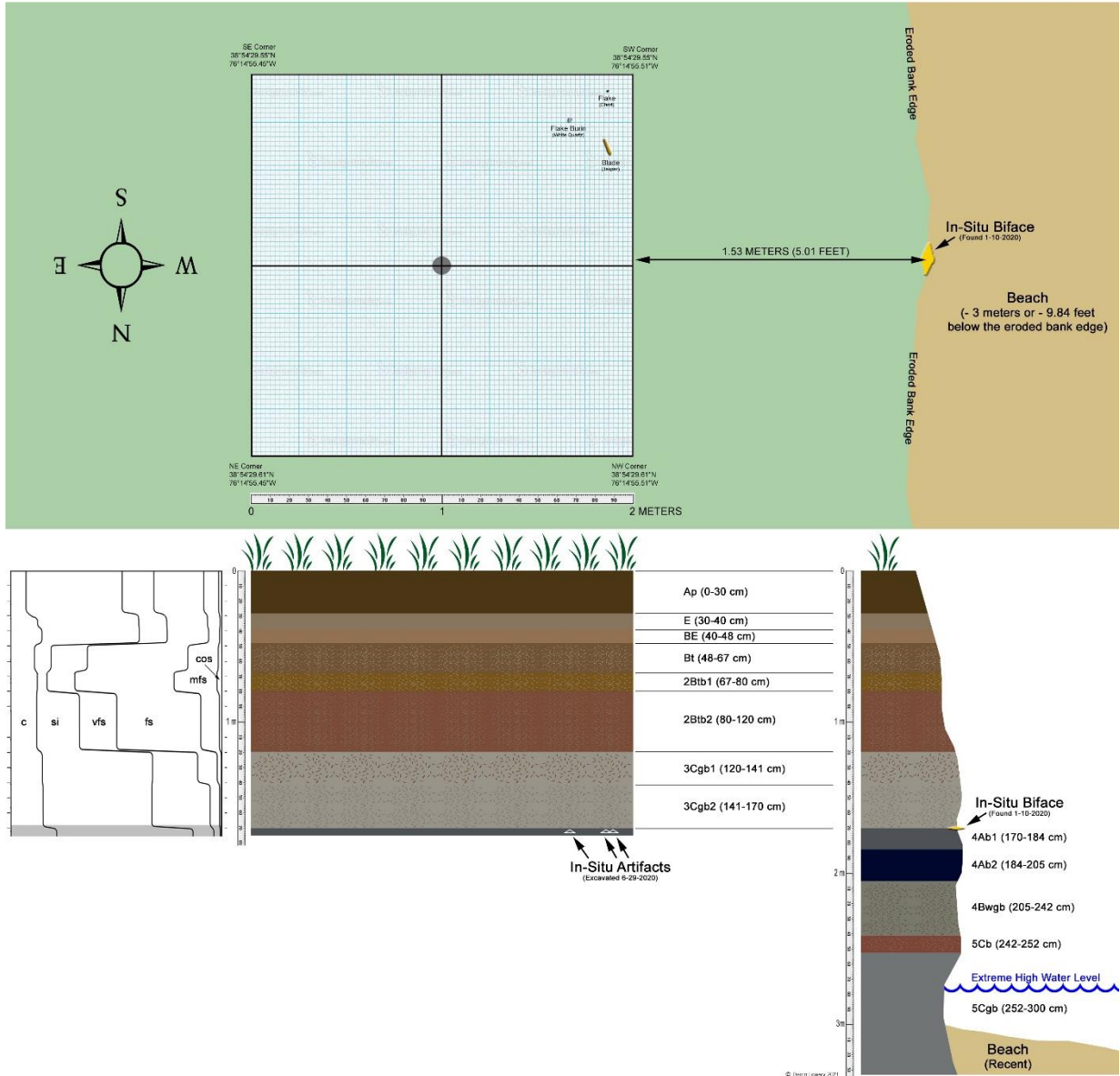


Figure 4.17. The graphics show the 2020 excavation units relative to the eroding bank profile. The position of the three in-situ artifacts, which were located in the far southwest section, have also been plotted. The location of the in-situ biface found on 1-10-2020 has also been positioned. The various soil horizons and sediment particle sizes within the test units and along the eroded bank margin are also portrayed.

The collective long-term investigation of 18QU1047 has provided a higher resolution understanding of the regional late Pleistocene-age upland site formation processes, as well as providing a detailed assessment of the negative impacts that recent coastal erosion is having on archaeological deposits (see Figures 4.16 and 4.18). Because of the vertical and horizontal bank shifts over time, episodic re-examinations offer inexpensive and detailed insights into site stratigraphy, chronology, as well as the impacts of recent coastal erosion.

The late Pleistocene stratigraphic sequence and chronological data gleaned from 18QU1047 (see Figure 4.19) has greatly increased our understanding of the region. Earlier research (see Lowery et al. 2010) indicated a circa 12,300-year gap and/or missing package of sediments between an LGM/pre-LGM-age Tilghman soil and the overlying YD-age Paw Paw loess (see Figure 2.31). The previous age estimate generated on the Tilghman soil suggested it dated between ~25,000 and ~32,000 years old (ibid). With the data now assembled from Parsons Island (see Figure 4.19), the previous AMS-age estimates on the Tilghman soil may actually represent the collective averaging of the circa 20,000- to 23,000-year-old vitrified carbon within the 4Ab1 soil horizon and the circa 29,000- and 32,000-year-old vitrified carbon associated with the 4Ab2 soil horizon. In sum, the Parsons Island data imply environmental carbon is persisting and not decaying during this era of colder climates. Also, much of the regional upland stratigraphy may be dominated by a “singular” Tilghman soil overwhelmed by mixtures of persistent vitrified environmental carbon (see Figure 2.31). Finally, the data from Parsons Island (see Figures 4.18 and 4.19; A1 and B) imply that bioturbation in the surface soils was comparatively low between 42,000 to 20,000 years ago or MIS-3 through MIS-2. In sum, continued geoarchaeological investigations at earlier site locations (see Figure 2.31) may have resulted in a gamut of averaged AMS-age estimates, which may or may not correlate with the “true” age of any associated archaeological remains. The same assertion may apply at Parsons Island.

Our research at 18QU1047 indicates the vitrified carbon within the 4Ab1 soil spans approximately ~3000 years; which encompasses a very large time frame when compared with the Middle Atlantic’s recognized prehistory. The Parsons Island research also demonstrates (see Figures 3.40, 3.41, 3.51, 3.52, and 4.5) that some unknown portion of the 4Ab1 soil is missing and has been eroded. Flecks of carbon within this missing portion may have provided a better age for the embedded archaeological remains. The current AMS ages would imply that the artifacts within the 4Ab1 soil are $\leq 20,761 \pm 198$ cal. yrs. BP (D-AMS 003533: $17,133 \pm 88$ rcybp), which represents the youngest age for this buried paleosol. As such, the *terminus post quem* age estimate for the archaeological remains at Parsons Island would be $\leq 20,563$ years old. The youngest OSL-age on the overlying aeolian sediments situated immediately beneath the YD-age Paw Paw loess is $17,400 \pm 2,270$ OSL years old (UW3800). The *terminus ante quem* estimate for the buried archaeological remains would be $\geq 15,130$ years old. Thus, the archaeological assemblage found at 18QU1047 can be confined to a broad time frame spanning almost 5,500 years encompassing ~20,500 to ~15,000 years old. Needless to say, a high-resolution reconciliation as to the “true” age of the Parsons Island assemblage and other similar lithic assemblages (see Figures 2.30, 2.31, 2.34, 2.36, 2.37, and 2.39) is sorely lacking at this time. Stratigraphically, we can, however, conclude that these lithic assemblages are indeed a “pre-Clovis lithic tool kit”. Future investigations may eventually unearth anthropogenic features containing datable charcoal, which will reconcile the “true” age of these assemblages. Unfortunately, the stone feature recently found eroding from the shoreline at Parsons Island (see Figure 3.74 through 3.78) contained no associated charcoal.

The retreating and eroding shoreline at Parsons Island (see Figure 4.18) does provide some insights into the topographic relief of the 4Ab1 surface, as well as some potential information about the archaeological site formation processes associated with 18QU1047. In 2013 when the bank edge was ~10 meters (~32 feet) further west, the top of the 4Ab1 surface was located 220-centimeters (~7.2 feet) below the ground surface (see Figure 4.20). Over the ensuing seven years, the contact between the 3Cg2 and the 4Ab1 soil horizons is now located 172-centimeters (~5.6 feet) beneath the ground surface (see Figure 4.20) and is ~50-centimeters shallower. At ~335-centimeters (~10.9 feet) in overall height,

the elevation of the modern ground surface has remained consistent since 2013. Given the combined stratigraphic datasets, we can conclude that the 4Ab1 surface, which has revealed several in-situ lithic artifacts, had a westward trending slope of approximately five percent (5%). The in-situ artifacts found exposed along the bank profile during the initial three years of examination were thoroughly encapsulated beneath a veneer of sediments associated with the 4Ab1 soil. As the 4Ab1 surface rises in the profile, some recent in-situ finds are at or near the contact between the 4Ab1 and the overlying 3Cgb2 soil horizons. Notably, several artifacts discovered in recent years show evidence of aeolian polish and silica glaze to one or more faces (see Figures 3.49, 3.50, 3.51, and 3.52).

Collectively, it is suggested that some of the lithic artifacts currently within the 4Ab1 soil horizon were displaced shortly after being discarded/lost and naturally transported downslope. The downslope movement preceded the partial erosion/truncation of the 4Ab1 surface. The partial truncation exposed a few of the artifacts to aeolian abrasion, which incompletely polished various faces. Subsequently, these artifacts were exposed to water vapor; which resulted in a distinct silica glaze. Finally, the 4Ab1 surface horizon, which contained artifacts in primary contexts, displaced contexts and partially wind polished/glazed conditions, was rapidly buried as a result of the aeolian deposition of the overlying 3Cgb stratum. After burial, the archaeological remains at 18QU1047 remained largely undisturbed until the combined effects of late Holocene sea level and fetch-related wave erosion gradually encroached upon the island. At the time 18QU1047 was occupied, sea levels were approximately >120 to ~78 meters (>400 to ~256 feet) lower than present and Parsons Island was an arid interior upland setting (see Faure et al. 2002) far removed from the Atlantic coastline. A few discoveries (see Stanford et al. 2014) offer equivocal indications that the Paleo-Americans who once occupied 18QU1047 may have also been interested in coastal environments circa 20,500 and 15,000 years ago.

Additional sites in the local area (see Lowery et al. 2010) indicate that the Miles River, Eastern Bay, and Prospect Bay watersheds may have been attractive to these early Paleo-Americans. The only surviving extant landscapes in the coastal plain associated with this early era are the interior uplands. All of the 20,000 to 15,000-year-old lowland settings, floodplain environments, river confluences, and coastal locations are now inundated as result of post-last glacial maximum sea level rise. The significance of Parsons Island to these early settlers may be hidden in the island's stratigraphy. The eroded southwest shoreline (see Figure 4.21, top) has exposed a continuous expression of the buried landscape, which provides a better understanding of the local physiographic setting at the time of occupation. A buried interdunal pond or wetland is located along the southern end of the island. The interdunal pond (see Figure 4.19 B) has produced a stratified sequence with four dated wetland surfaces spanning 27,000 to 42,000 years in age. The buried interdunal pond/wetland has also revealed several late Pleistocene vertebrate teeth (see Figure 3.8). A contemporaneous elevated dune (i.e., south dune crest) landform separates the pond/wetland area from the buried archaeological site located further to the north (see Figure 4.21, bottom). The archaeological landscape is positioned within a trough or swale immediately south of a topographically higher dune (i.e., north dune crest), which may have originally served as a wind-break. Like today, the dominant wind directions would have included strong NW-winds (see Markewich et al. 2009) associated with the onset of a high-pressure system followed by strong SW-winds preceding a low-pressure system. In summation, the location and position of the site seems to have taken advantage of the relic topography, the prevailing winds, and the presence of a nearby game-attractive wetland meadow. Unfortunately, the continuation of these relic late glacial landscapes situated north, south, east, and west of the current island landmass have been obliterated

by several centuries of coastal erosion, as well as Holocene sea level rise. Multi-decadal archaeological examinations (see Lowery 2016) along eroding coastlines of the Middle Atlantic have failed to locate any similar settings. As such, late glacial landscapes like the situation observed at Parsons Island may have been relatively rare. Therefore, the local physiographic and geologic conditions associated with Parsons Island may have made it extremely attractive to Paleo-Americans. As an analogy, the setting circa 20,500 to 15,000 years ago may have resembled the conditions portrayed in Figure 4.22.



Figure 4.18. The satellite image shows the shoreline at 18QU1047 on 5-25-2013 and on 11-5-2019. The A2 location (see Figure 4.17; lower right) represents the current bank profile. The 5-25-2013 shoreline (red) denotes the positions of two prior bank profile localities described in 2013. The specifics associated with the two 2013 profile descriptions are portrayed in Figure 4.19.

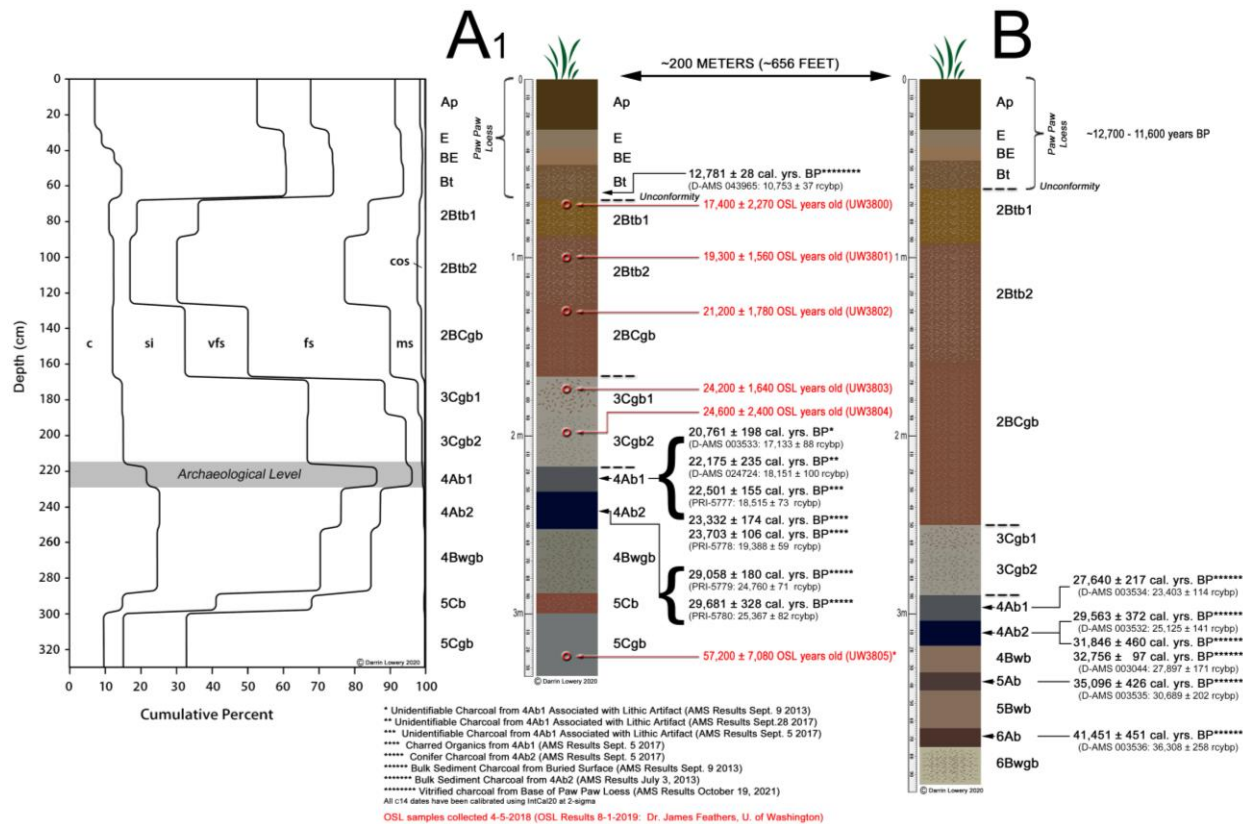


Figure 4.19. The illustrations portray the bank profiles described at Parsons Island in 2013. The associated particle-sizes, AMS-age estimates, and OSL chronological values are also noted. The locations of these two profile spots are represented in Figure 4.18.

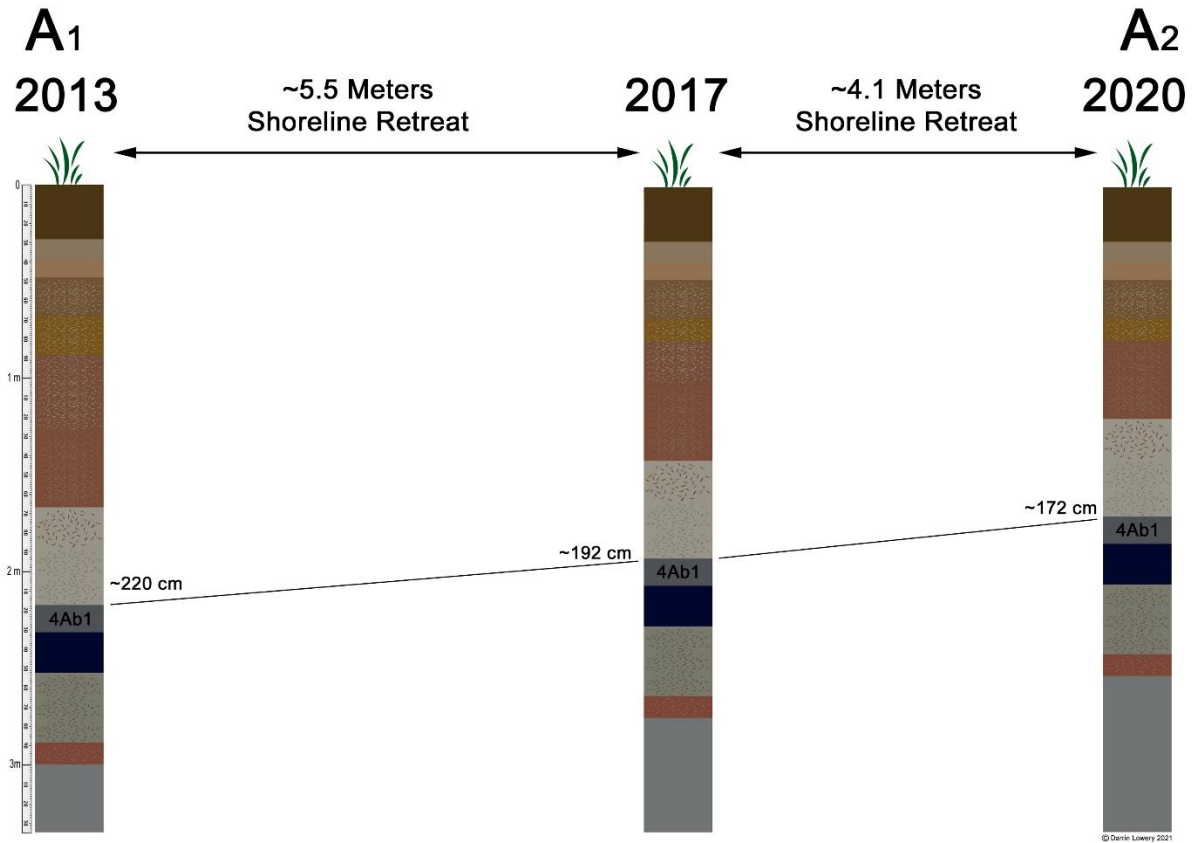


Figure 4.20. Relative to the shoreline datum as well as the ground surface elevation, the three images portray the idealized soil profile thickness changes over the period between 2013 and 2020 as the shoreline eroded. Note that the upper package of aeolian sediments situated immediately beneath the Younger-Dryas Paw Paw loess stratum has become more truncated as the shoreline retreated from west (A1) to east (A2). Also, note that the underlying paleosol (4Ab1) has become topographically higher and closer to the YD-onset unconformity as the shoreline eroded and retreated eastward. As the shoreline continues to retreat eastward, the buried 4Ab1 paleosol surface will, presumably, be situated immediately beneath the Younger-Dryas Paw Paw loess stratum. Hypothetically, the intervening aeolian sediments will have been completely stripped away by the regionally-recognized initial YD-onset surface erosion event.

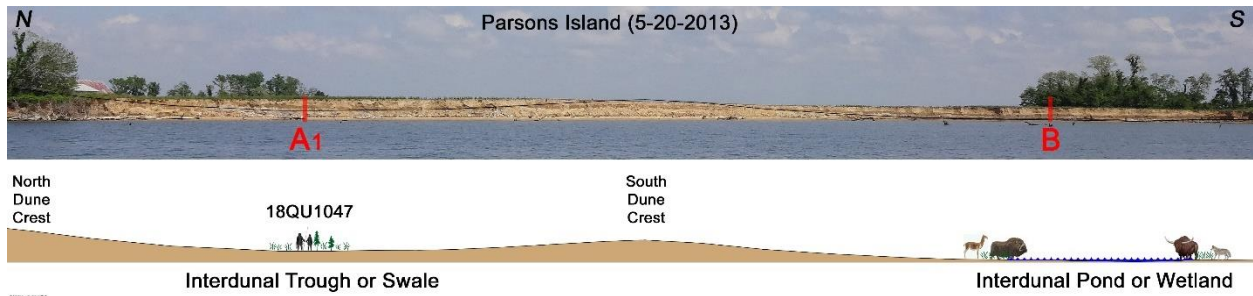


Figure 4.21. The photograph (above) shows the bank profile along the southwest side of Parsons Island as it appeared on 5-20-2013. The underlying buried paleosol is clearly evident along the eroding shoreline. The bank profile description areas associated with 18QU1047 (see Figure 4.19; A1), and the interdunal pond/wetland (see Figure 4.19; B) have been designated. The buried topographic relief of the underlying paleosol is clearly evident and it offers a better understanding of the local stratigraphic variation along a north to south transect spanning ~200 meters (656 feet). The archaeological site (18QU1047) was situated within an interdunal trough or swale between two relic dune crests (below). When the area was exposed, 18QU1047 encapsulated zone containing loess (silt-loam), which retained some moisture and augmented the long-term preservation of vitrified charcoal. The buried interdunal pond situated further south also accumulated silt-loam and was topographically ~70-centimeters lower than the archaeological site area (below).



Figure 4.22. The photograph portrays a hypothetical view showing what the buried landscape at 18QU1047 may have look like sometime between ~20,500 to ~15,000 years ago.

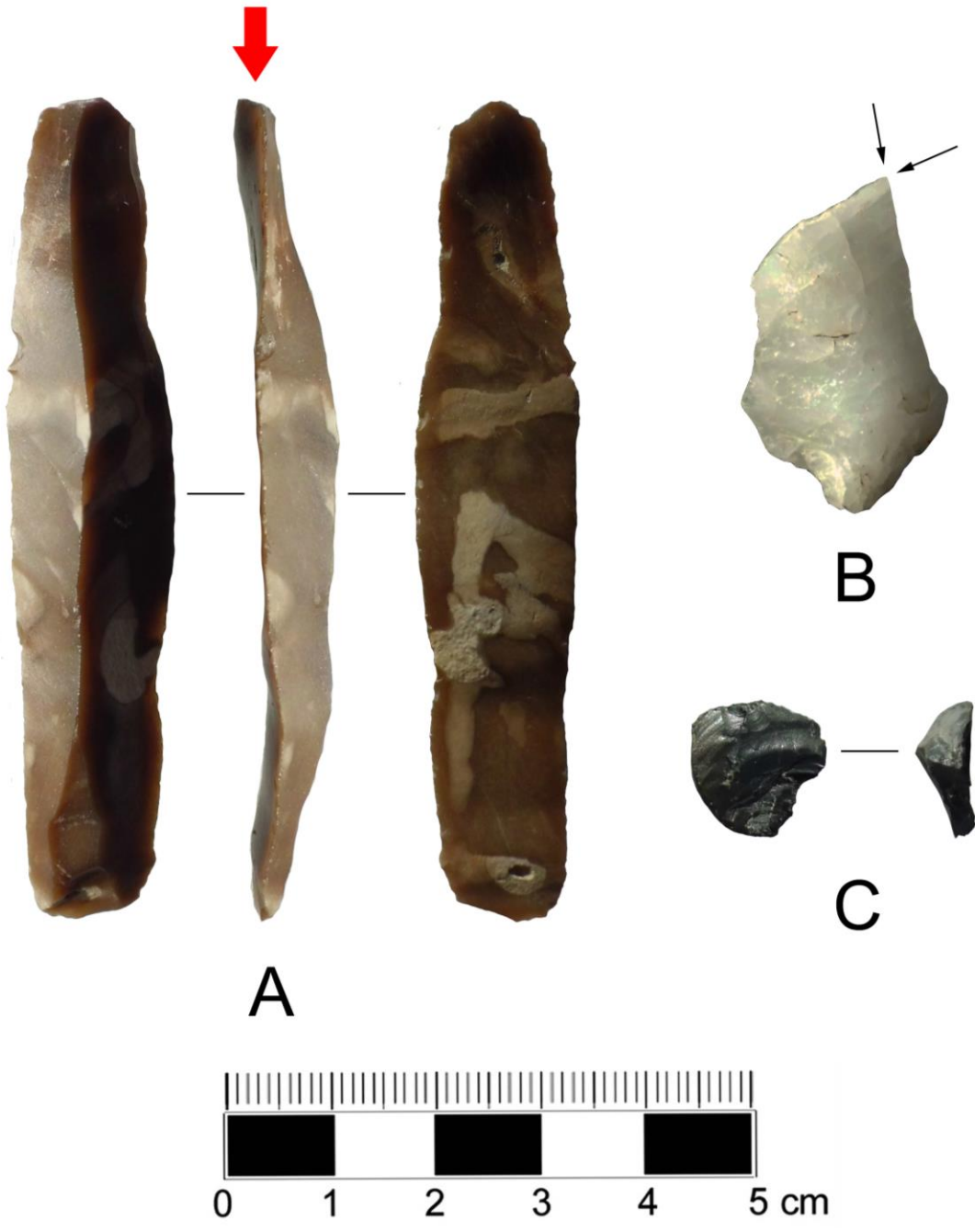


Figure 4.23. Images show multiple views of the various artifacts found at the 18QU1047 during the 2020 excavations.

5. PARSONS ISLAND ARCHAEOLOGICAL SURVEY AND EXCAVATIONS SUMMARY AND CONCLUSIONS

Coastal landscapes containing archaeological sites are a common feature throughout the Middle Atlantic region. Many of these nearshore landscapes are rapidly vanishing and the associated sites with their unique geologic record are disappearing. The collective research highlighted in this monograph illustrates the quality of the data that can be gleaned if individuals are willing to invest the time, effort, and money towards these vanishing island landscapes. For example, many nearby islands in the Chesapeake Bay, like Sharps Island, Nelson's Island, Bodkin Island, Opossum Island, Little Island, Phil Potts Island, Long Island, Little Fox Island, and Herring Island have vanished without a single archaeological survey or geoarchaeological investigation. Some islands, like Watt's Island in Virginia (see Lowery 2016: 41-53), have been surveyed and significant sites were documented. However, the archaeological sites documented at Watt's were never tested or partially salvaged and the island will disappear as a result of coastal erosion within the next decade.

Many individuals who have little or no experience in coastal settings blame the loss of coastal landscapes on either "climate change" or "sea level rise" and sometimes both (see Horton et al. 2020). Sea level rise is a factor that has impacted archaeological sites in the region (see Lowery 2020a). However, the interplay between the normal daily tidal range, seasonal wind directions, the local geology, and the hourly wind-wave actions, as well as, localized shoreline geometries have a far greater impact on coastal erosion than millennial-scale sea level rise (see Lowery 2016). Individuals touting that "climate change" and/or "sea level rise" are the factors (see Horton et al. 2020) for coastal land loss should be reminded that not all islands in the Middle Atlantic are eroding (see Lowery 2016). For example, Fisherman's Island near the mouth of the Chesapeake Bay has accreted well over 1500 acres of land within the past 55 years (Ibid: 244). Other islands; like Mockhorn Island, Myrtle Island, Wreck Island, and Shipshoal Island, have had significant gains in land area over the past four centuries (Ibid). In sum, many islands in the region are eroding and some islands are accreting.

Parsons Island is an eroding landscape. It was once an attached peninsula containing ~340 acres. It is now an island containing ~68 acres of land; a loss of 272 acres of land over the past 370 years. Parsons became an island sometime in the early 19th century when a natural tidal marsh causeway was breached by erosion. The gap separating the island from the mainland widened rapidly as the daily tidal actions expanded and scoured a deep channel where the natural causeway once existed (see Lowery 2019: 149). Having tried to salvage as much information from various vanishing island-archaeological landscapes over the past two decades (see Lowery 2002a, 2004, 2010, 2015a, and 2015b), each project concluded with a statement indicating "*it is hoped that cultural resource managers and academicians will heed the need and urgency of addressing the rapid loss and disappearance of these significant coastal archaeological sites.*" So far, the suggestions have largely "*fallen on deaf ears*".

With 4,479 square miles of water area and 11,684 linear miles of coastline, which is more shoreline than the entire west coast, the Chesapeake Bay is the largest estuary in the United States. The Chesapeake is, therefore, uniquely different than any other archaeological-cultural resource zone in the United States. As such, cultural resource managers and academicians need to apply a different set of management parameters to the coastal archaeological resources adjacent to the Chesapeake. When significant archaeological sites are exposed by erosion cultural resource managers and academicians need to "seize the day". The Parsons Island monograph demonstrates what you can learn from an eroding island landscape if you "seize the day". In sum, nearshore and inter-tidal archaeological sites;

like those at Parsons Island, are neither terrestrial nor underwater archaeological resources. The Parsons Island sites; like many other sites along the margins of the Chesapeake Bay, encompass a markedly different suite of site formations processes that are not addressed by any “classic” academic training program. If you manage nearshore coastal sites in the Chesapeake Bay like you would terrestrial or underwater archaeological resources, the sites will suffer, erode, and eventually disappear. Contrary to news “media” assertions (see Montgomery 2013 and Bass et al. 2018), erosion of coastal landscapes containing archaeological sites is not “sinking” (see Lowery 2018 and 2020b). Over the past four centuries, most nearshore coastal archaeological sites within the Chesapeake have been truncated, scoured, dismantled, disarticulated, and reworked by nothing more than the normal daily wind, wave and tidal actions of the bay.

An initial archaeological survey of Parsons Island was conducted in 1992 (see Lowery 1993). At the time, the island encapsulated ~99 acres of land and no archaeological sites were discovered along the shoreline or on the surface of the island’s agriculturally tilled fields. Twenty-one years later in 2013, Parsons Island had been reduced to ~78 acres; at loss of about 1-acre of land per year since 1992. In 2020, the island currently encompasses ~68 acres of land; a loss of about 1.42-acres of land per year since 2013.

During the re-examination of Parsons Island between 2013 and 2020, four archaeological sites were documented. These sites include 18QU1047, 18QU1065, 18QU1066, and 18QU1067. 18QU1065, which is positioned on the island’s far northeastern margin, represents an inundated upland setting consisting of an in-situ Middle to Late Archaic period occupation; as well as a possible Early and Late Woodland-era settlement. 18QU1066, which is located along the island’s heavily eroded southeastern margin, seems to have succumbed to erosion sometime before 2013. The few Late Archaic period artifacts uncovered at 18QU1066 were found in displaced intertidal contexts and all show evidence of plow-damage indicating these stone artifacts were once within an active plowzone or Ap-horizon. Circa 1992 aerial photos indicate that the area associated with 18QU1066 was fallow and contained a young forest. As such, the site was not discovered during the initial survey of Parsons Island because of the fallow field conditions. During the intervening twenty-one years, 18QU1066 eroded away. The site designated as 18QU1067 clearly illustrates the ephemeral nature of archaeological features along active shorelines. In August 2013, erosion exposed an historic late 18th through early 19th century well feature along the southwestern shore of the island. Given the feature’s age, it was undoubtedly excavated by slaves or tenant-help working on the property two centuries ago. By June 2014, the well-feature had collapsed. Over a four-year period, erosion continued and the bank edge retreated an additional 12-meters (42-feet). Flowing ice along the shoreline in early 2019 dislodged the remnant wooden hogs head once situated at the base of the well. Currently, only a pile of coastally-reworked hand-made brick exists at the intertidal location once associated with 18QU1067. Like 18QU1067, the in-situ Paleo-American stratum and assemblage noted at 18QU1047 has and is actively being threatened by coastal erosion. If left alone, 18QU1047 will eventually succumb to the deleterious effects of wind, wave, and tidal actions. Given the significance and rarity of Paleo-American sites (see Water 2019), the current investigation conducted at 18QU1047 was focused on determining if in-situ archaeological remains are still present inland of the actively eroding shoreline. Like the 2017 Smithsonian investigation, the recent excavations indicate that some in-situ remains are indeed present. How much of the Paleo-American site actually remains inland of the active shoreline is still largely unknown. Most importantly, the collective synthesis of the work already conducted at Parsons Island proves that significant

archaeological data can be gleaned from eroding sites. The Parsons Island investigations conducted between 2013 and 2020 should serve as a template demonstrating how to effectively investigate eroding coastal archaeological landscapes.

After our investigation of Miles Point (18TA365) and leading up to 2013, several exposed shoreline settings were subjected to varying degrees of testing, evaluation, and dating with the hope of rectifying the late Quaternary upland geoarchaeology along the western margins of the Delmarva Peninsula (see Table 2.1). Ultimately, the discovery and subsequent investigations conducted at Parsons Island indicate that during the period between circa 42,000 and 20,000 years ago, vitrified carbon persisted and endured in the region's cooler/colder climate. The bulk soil ages and the amalgamation of individual charcoal flecks from the 2ABtxb "Tilghman Soil", which provided an adequate dateable sample-size, resulted in AMS-age averaging at Miles Point. Thus, the true antiquity of archaeological assemblage exposed at Miles Point (see Figure 2.30) may never have been rectified even if controlled excavations had been conducted.

In many ways, the same age estimate problems plague the in-situ archaeological assemblage found at 18QU1047 on Parsons Island. However, the overlying aeolian strata, which pre-date the Younger Dryas onset, do offer some time constraints. The stone tools found at 18QU1047 are uniquely different than the types of lithic artifacts found at regional circa 13,000-year-old Clovis-age archaeological sites (see Figures 2.17, 2.18, 2.19, 2.21, 2.23, 2.24, 2.26, and 2.27). However, like the environmental settings associated with the extant regional Clovis age sites, 18QU1047 is positioned within an interior upland interfluvial area accompanying a poorly drained wetland area.

Purported comparable age Paleo-American sites (see McAvoy and McAvoy 1997 and 2015) have revealed similar types of lanceolate points (see Figures 2.28, 2.29, 2.30, and 2.35) like those found at Parsons Island. Some of these alleged Paleo-American sites have also revealed blade tools, blade cores, small prismatic blade flakes, utilized flakes, as well as, shouldered-flake knives; like the Mungai Knife found at Meadowcroft Rockshelter (see Adovasio et al. 1978). However, bipoint bifaces are absent in all of the above assemblages.

The assemblage found in-situ and along the shoreline at 18QU1047 is similar to specimens found at several Paleo-American site, but it is also different. Collectively, the tool kit at 18QU1047 consists of many complete bifaces. Several are damaged and others have been re-tooled to the point of exhaustion; a pattern noted at a few local Clovis sites; like Paw Paw Cove (see Figure 2.17). Formal flake tools and utilized flakes are common at 18QU1047. Debitage, however, is limited largely to small waste flakes indicative of re-tooling and/or re-sharpening activities. Collectively, the tool kit found at 18QU1047 is similar to many small episodically reused interior-upland hunting-related butchering encampments, like Paw Paw Cove (see Lowery 2002a). The similar overall character of these assemblages may simply represent parallel adaptations to comparable environmental/ecological settings over a very long period of time.

The assemblage found at 18QU1047 does, however, have some differences with respect to the assemblages noted at both the Paleo-American (see McAvoy and McAvoy 1997 and 2015), as well as the Paleoindian sites, such as Paw Paw Cove. The bi-pointed bifaces (see Figures 3.38 and 3.39) found at 18QU1047 are not present at the other sites. The 18QU1047 bipoint bifaces are largely complete and still useful. Comparable bipoint knife forms have been reported at ambiguous Paleo-American

inundated site contexts (see Stanford et al. 2014), as well as supposed Clovis caches (see Huckell 2014: Figure 8.3 A).

The bipoint assemblage from 18QU1047 is somewhat indicative of a cache or series of caches that may have been deposited at this locality, displaced, and ultimately buried by continued aeolian activity. The bipoint bifaces are complete, have significant remaining use-life, many examples show little evidence of resharpening, and several are very large in size. All of these aspects suggest these bifaces represent something more than haphazard losses or intentional discards. These bipoint bifaces were discovered over two distinct episodes (see Figure 3.36); the first occurred between 8-4-2013 and 6-1-2014 and the second occurred between 2-14-2017 and 1-22-2020. Between 2013 and 2020, the ~three-meter-high bank retreated approximately 10-meters or ~32-feet and the elevation of the buried 4Ab1 surface changed, which suggests the buried surface had a 5% percent slope (see Figure 4.18 to 4.20). As postulated, it seems that the cache or caches at 18QU1047 may have been scattered across the westward sloping 4Ab1 surface before being buried by continued aeolian activity. It is conceivable that some of the blades (see Figure 3.58, 3.59, and 3.61), shouldered knives (see Figure 3.62), cores (see Figures 3.52 and 3.53), and even a few of the formal tools were also included within the cache or caches. As noted earlier, the remaining assemblage found at 18QU1047 seems to imply the presence of a hunting-related encampment.

An analog to the assemblage found at Parsons Island has been observed at a nearby Middle Woodland-age archaeological site (i.e., 18TA228). A cache containing forty (40) large bifaces exposed as a result of coastal erosion was found at this site (see Lowery 1992). Aside from the notable cache, the contemporaneous assemblage found at 18TA228 included a little collection of highly exhausted and resharpened points, a few utilized flakes, and lithic waste debris. Similar limited habitation debris has been observed at other cache localities throughout the region (see Lowery 1995). If this were the situation at 18QU1047, the cache or caches may have simply been utilitarian hoards (see Deller et al. 2009). The limited re-use and/or re-occupation of these localities may explain why the caches were overlooked and never exhumed. In other words, the memory of these utilitarian caches may have been simply forgotten. The cache or caches noted at 18QU1047 could also represent mortuary or symbolic/ceremonial hoards. However, the presence of human bone or skeletal remains in a setting like Parsons Island would have vanished long ago with its low pH (~4.9 to 4.8) soils. The “perched” rock feature (Figure 3.76 and Figure 3.78), which seems to have a cultural origin, implies the buried landscape at 18QU1047 was of some importance. The construction of this “perched” rock feature may have served at the time as some sort of marker (i.e., mortuary, navigational, or ceremonial) on a landscape dominated by low lying vegetation. The significance of this buried landscape may never be known.

In the Chesapeake Bay region, bipoint biface forms are very rare. However, some researchers have professed that the bipoint biface style is common and can be found in good Archaic though Woodland-period contexts (see Boulanger and Eren 2015). Most of the purported local examples that these authors illustrate are not bipoint forms and are nothing more than rounded-base ovoid cache bifaces. The additional illustrated specimens (Ibid: Figure 3 D and E) shown by these authors are made of Ohio Valley lithic materials and associated with the regionally-recognized Delmarva Adena-Hopewell complex. Most importantly, Boulanger and Eren (Ibid) never examined the two specimens they illustrate. The authors simply looked at low-resolution blurry photos. More than a decade prior to their publication, I have personally examined both specimens and the two examples they show are not

bipoint bifaces. Both specimens have continuous rounded basal margins that do not converge to a point, like the examples from Parsons Island.

Bipoint bifaces analogous to the examples found at Parsons Island have been found at a few regional archaeological sites (see Figure 5.1). These specimens, however, all lack datable contexts (see Figure 5.2) and only one (i.e., the Cinmar biface) has any potential chronological time constraints. The time constraints for the Cinmar biface are estimated based solely on radiometrically-dated isostatic sea level positions for the Middle Atlantic coast (see Stanford et al. 2014). Bifaces analogous to the Cinmar example are extremely rare. Joseph McAvoy; excavator of the famous Cactus Hill site in Virginia (see McAvoy and McAvoy 1997 and 2015), noted that he has “*not observed any of the large, thin, Cinmar-like bifacial bipoints*” within “*the western coastal plain of southeastern Virginia and northeastern North Carolina.*” He commented that he has “*personally been interested in the archaeology of this area for over 50 years,*” and has “*not found one*” nor has he “*seen a single example in the numerous collections*” that he has examined “*between Richmond, Virginia and Raleigh, North Carolina.*” (McAvoy: personal communication, 2021). Prior to the discoveries made at Parsons Island, I personally had only found one single bipoint biface (see Lowery 2016: 125). A quartz specimen was found at 44AC464 in 1999 along Back Creek in Accomack County, Virginia, while conducting a shoreline survey for the Commonwealth of Virginia (see Lowery 1999: Appendix B 44AC464 site data form). Importantly, the Smithsonian Institution, which houses hundreds of thousands of artifacts from the Middle Atlantic region, has only two examples (see Figure 5.3) and both were collected during the 19th century.

From a global perspective, bipoint biface forms occur in later period archaeological contexts (see Brehm 1981), as well as much earlier archaeological contexts (see Villa et al. 2009). Whether the bipoint examples plotted in Figure 5.1 are chronologically-related or were the byproduct of multiple prehistoric cultural entities will never be known. Most importantly, the bipoint biface form in the regional archaeological record is extremely rare. For example, twenty-five (25) recorded specimens are plotted in Figure 5.1 and associated with a 64,299-square-mile area of the Chesapeake Bay watershed. Notably, fifty-five (55) Paleoindian period fluted points have been documented for the miniscule 398-square-mile area of lower Northampton County, Virginia (see Figure 2.22). Boulanger and Eren (2015) imply that bipoint forms are common and recognizably associated with Archaic and Woodland period contexts; specifically, the Terminal Archaic. In the area shown in Figure 5.1, there are literally tens of thousands of Archaic and Woodland period affiliated sites and only twenty-five bipoint bifaces are currently known for this same region. The collective data for regionally-recognized biface forms analogous to the examples shown in Figure 3.38 and 3.39 stand in stark contrast to the assertions made by other scholars; namely Boulanger and Eren (2015).

Is it possible to have Paleo-Americans in the Chesapeake Bay region between 15,000 and 20,000 years ago? Some researchers (Stanford and Bradley 2012) have proposed an Atlantic crossing at a time when ice was at its maximum extent during the LGM. Others (Erlandson et al. 2007) have suggested a coastal migration following a “kelp highway” along the Pacific margin. Is it feasible to have Paleo-Americans circa 20,000 years ago migrating through the traditional “corridor” (see Tamm et al. 2007) wedged between the Laurentide and Cordilleran ice sheets?

Recent genetic studies have implied that the separation between ancient Siberian populations and the early Native American populations (ANE, APS, AB) occurred approximately 23,000 or 24,000 years ago (see Raghavan et al. 2014 and Raghaven et al. 2015), which correlates well with the time when

geneticists also think dogs were domesticated (see Perri et al. 2021). Other genetics studies (see Kivisild 2017) infer that the separation between these two human populations may have occurred slightly later or sometime between 20,000 and 15,000 years ago. However, neither of these studies specify a geographic area where the split between these two populations may have occurred (i.e., western Beringia, eastern Beringia, or someplace else in Siberia). Finally, the calibrated genetic chronology may also be somewhat biased by the use of the archaeological record (see Moa et al. 2021). Therefore, the “accepted” archaeological sites may serve as benchmarks to rectify the timing, spread, and direction of these early human migrants. Recent genetic research implies there have been many failed human migrations (see Moa et al. 2021: Figure 3) into northern Asia and Siberia. These migrations did indeed leave an associated archaeological record. However, the archaeological record is not connected with later more prosperous migrants who successfully colonized the region. In essence, the successful “genetic clock” cannot be directly linked with the “accepted” archaeological record and vice versa.

The Laurentide Ice Sheet reportedly attained its maximum extent approximately 21,000 to 22,000 years ago (see Dyke et al. 2002). In contrast, the Cordilleran Ice Sheet did not reach its maximum extent until about 16,000 to 13,000 years ago (see Hendy 2009 and Lacelle 2013). In sum, the Laurentide Ice Sheet had retreated eastward and northward for approximately 6000 years as the Cordilleran was advancing eastward into the Canadian plains. The retreat of the Laurentide Ice Sheet from western Canada began sometime prior to circa 15,700 years ago (Munyikwa et al. (2017). Their work on deglacial aeolian landforms within the corridor does not preclude the emergence of a wide corridor between the Laurentide and the Cordilleran Ice Sheet earlier than 15,700 years ago. A few OSL-age estimates (see Munyikwa et al. 2017: Table 2) indicate that an opening between the two ice sheets existed $18,300 \pm 1200$ and possibly even earlier around $20,300 \pm 1,800$ years ago. Some researchers (see Dawe and Kornfeld 2017) have suggested that an ice-free corridor was not required for a successful human migration between the Cordilleran and Laurentide ice sheets. They (Ibid: 68) have suggested that people could have easily traveled from Asia through the corridor, even during the LGM. If humans traversed an early gap between these two imposing ice sheets, they would have developed an adaptation to a cold, interior aeolian environmental setting containing interdunal meltwater ponds and freshwater lakes (see Dawe and Kornfeld 2017 and Munyikwa et al. 2017). This environmental setting is analogous to that observed at Parsons Island (see Figure 4.22) circa 20,000 years ago.

In addition to the OSL-dated aeolian landforms, fossil remains unearthed at Natural Trap Cave in Wyoming indicate a gap may have existed between the two ice sheets at various intervals during the LGM. Discoveries in the cave include Beringian wolf remains dated to circa 25,800-years ago (see Meachen et al. 2016). The Beringian wolf is an extinct sub-species that was largely confined to Siberia and Alaska, and its movement southward into North America was largely restricted by the ice sheets. Meachen et al. (Ibid: 3435) state “the extinct Beringian haplotype, which is distinct from extant Alaskan and Canadian wolf populations” migrated through a corridor separating the Laurentide and Cordilleran ice sheets from Alaska through Canada and south of the ice sheets during the LGM. Stable isotope values in the bone collagen of pre-LGM Alaskan Beringian wolves suggest the Woodland Musk Ox (*Bootherium bombifrons*) was a significant part of their diet (Fox-Dobbs et al. 2008). Meachen et al. (2016: 3435) have proposed that *Bootherium* may have been the impetus for the initial Beringian wolf migration south of the ice sheet. Coincidentally, *Bootherium* has been found in the late Pleistocene faunal assemblage from Parsons Island (see Figure 3.8). If four-legged predators, like the Beringian wolf, could traverse a 1500-mile opening between the Laurentide and Cordilleran ice sheets during the LGM,

it is conceivable that two-legged predators (i.e., humans) and their dogs could have followed the same path.

The only indications that humans may have existed in Alaska during this early time frame are largely equivocal (see Bourgeon et al. 2017 and Vachula et al. 2020). These data consist of circa 24,000-year-old “human” cut-marked bones from Bluefish Caves and human fecal sterols extracted from circa 34,000- to 16,000-year-old lake sediments in eastern Beringia. Arguably, the presence of humans in Siberia during the LGM is also negligible. If humans were in Alaska during the LGM as some ambiguous data would imply (see Bourgeon et al. 2017 and Vachula et al. 2020), why would people rapidly move south through an unexplored narrow glacial corridor not knowing what, if anything, existed on the other side? The answer to this question may be simple. To survive in the high arctic, we can assume that hunter/gatherers were very observant about the world around them. They were also attuned to any information migrating species might provide. Fiedel (2007) has suggested that migratory birds might have played a significant role in the peopling of the Americas. A significant portion of the human diet consisted of waterfowl; including swan at some Paleo-American sites in Alaska, like Swan Point and Broken Mammoth (see Holmes 1996 and Holmes et al. 1996). Representations of swan (see Figure 5.4 A and B) have been found at the circa 24,000-year-old site of Mal'ta near Lake Baikal (see Medvedev et al. 1996). The mammoth ivory carvings from Mal'ta resemble both flying swan and swan situated in defensive postures (see Figure 5.4 C and D). Most importantly, the Mal'ta boy shares strong genetic ties with extant Native Americans (see Raghavan et al. 2014).

People have long observed animals for signs of impending hazards or evidence of potential environmental threats (see National Research Council 1991). Like the seasonal migrations of Berwick's swan in Siberia (see Vangeluwea et al. 2018: Figure 1), the summer nesting areas and southward wintering holdovers (see Ely and Meixell 2016: Figure 1) of tundra swan (*Cygnus columbianus*) correlate very well with unglaciated regions, as well as the boundaries of glacial ice during the last maximum (see Figure 5.5). The eastern Beringian Tundra swan may also have functioned as a sentinel species to early Paleo-American explorers. If humans were present in eastern Beringia circa 20,000 years ago, the southward migrations of tundra swan may have provided important environmental data. Thus, the late summer/fall migrations of tundra swan south of the Laurentide and Cordilleran ice sheets would designate that warmer conditions and milder environments existed on the other side of the ice. Only a single season would be required to assess or evaluate the contexts of these southerly unexplored regions.

Tundra swans breeding and nesting along the arctic ocean and north of the Brooks Range in Alaska now seasonally migrate (see Ely and Meixell 2016) and winter over in the Middle Atlantic and Chesapeake Bay region (see Figure 5.5). Concomitantly, the Middle Atlantic has also revealed five archaeological site locations, which suggest an early human presence in North America prior to 14,500 years BP. The archaeological data from sites like Mal'ta, Broken Mammoth, and Swan Point imply swans were important to Ancient North Eurasians (ANE), Ancient Paleo-Siberians (APS), as well as Ancient Beringians (AB). Like the idea proposed by Fiedel (2007), it is conceivable that migrating waterfowl species like the tundra swan served as the catalyst that initiated and expedited the early human migration south from Alaska, across North America south of the ice sheets in a northwest to southeast direction, to the Middle Atlantic (see Figure 5.6). It is also plausible that the genetic separation between ancient Beringian populations and early Native Americans occurred south of North America's ice sheets.

The “story” outlined above, which attempts to explain the presence of humans at Parsons Island and other sites in the Middle Atlantic between 15,000 and 20,000 years ago, is nothing more than a series of “what if” and “could be” scenarios. Linking all of these disjointed facts will require additional research and further analyses, both of which are far beyond the confines of this project. However, researchers and academicians living in areas unaffiliated with the Middle Atlantic might question why the modern Chesapeake Bay encapsulates a region containing several anomalously early archaeological sites. With the above “story”, I have provided a credible explanation. Compared with the many published and “accepted” migration scenarios (see Raff and Bolnick 2014), the “story” presented above is equally plausible. Alternatively, variations on all of the published migration themes (see Stanford and Bradley 2012 and Erlandson et al. 2007) could also be correct and selecting one “story” over another may not be rational at this particular moment in time.

With the ever-expanding paleogenetic database (see Moa et al. 2021), it is clearly becoming evident there are instances where there is no direct affiliation between the earliest archaeological record, successful colonizers, and extant native populations. The colonization of the planet by *Homo sapiens* is far more complicated than we ever thought. If the assemblage and geoarchaeological record discovered at 18QU1047 were situated along some island near the Alaskan-side of the Bering Sea, most North American Paleoindian scholars would not question it. Matter of fact, I would predict most would embrace it. Under the current situation, these same scholars would say that 18QU1047 is on the wrong side of the continent and it’s too old. The assertion would imply an inherent North American Paleo-American or Paleoindian scholarly colonization bias. In many ways, 18QU1047 may be somewhat analogous to the archaeological data discovered at Yana RHS (see Pitulko et al. 2004); which is presently the only isolated pre-LGM site situated within the Arctic Circle whose inhabitants did not genetically contribute to later successful Arctic colonizers (see Moa 2021). Only time and continued research will expound upon the meaning of 18QU1047.

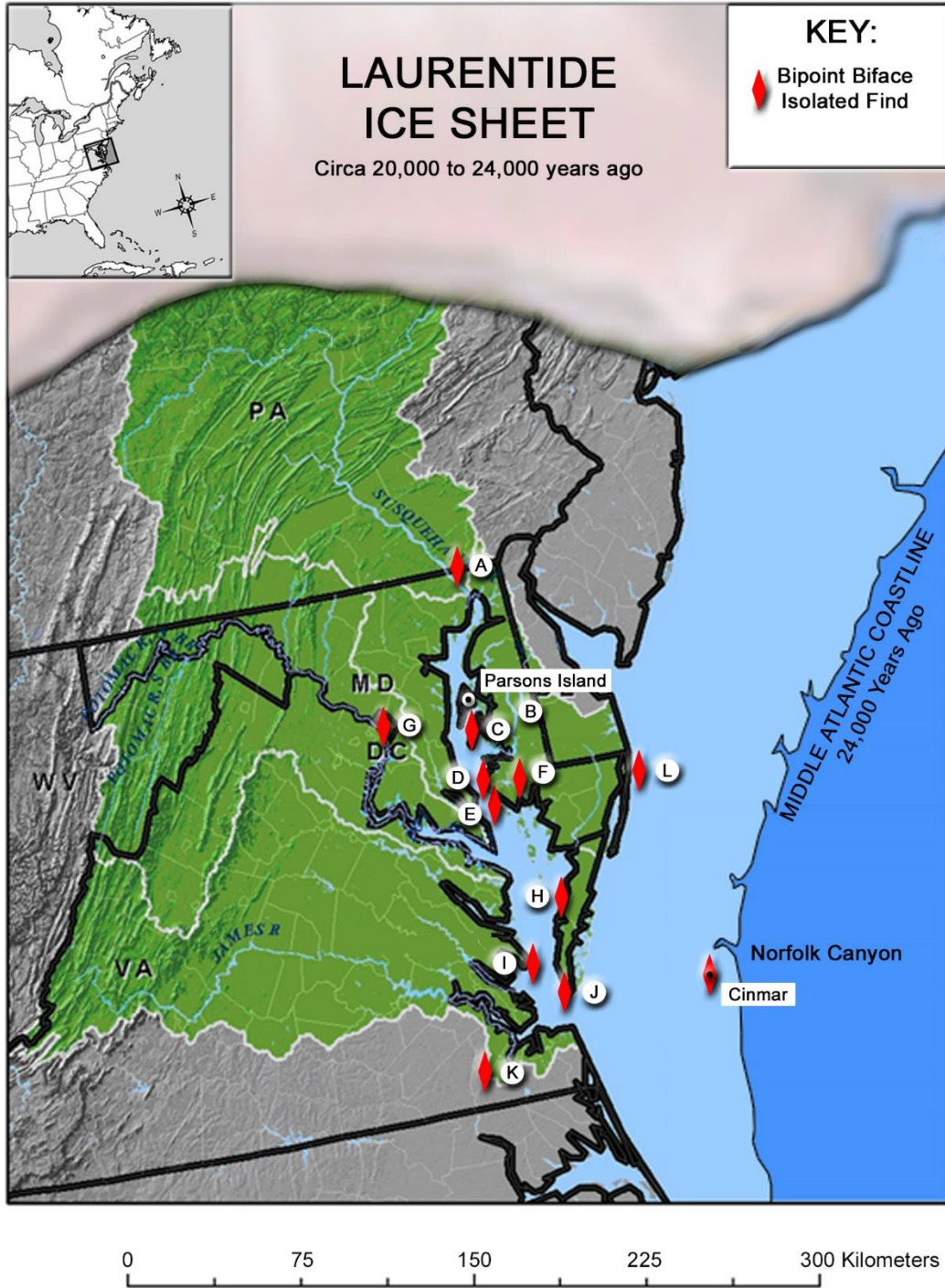


Figure 5.1. The map shows the approximate location of thirteen isolated bipoint bifaces similar to the twelve specimens found at 18QU1047 on Parsons Island. Most of the specimens lack both primary archaeological and ge archaeological contexts. The locations are shown primarily to illustrate how rare bipoint bifaces are in the regional archaeological record. As a comparison, the same watershed has revealed >1000 Paleoindian fluted points and most would be classified as Clovis type points.



Figure 5.2. The photograph shows one of the isolated bipoint bifaces (see Figure 5.1 K) found at an archaeological site within the Chesapeake Bay watershed. The specimen was unearthed while digging a basement near Suffolk, Virginia.

Wilson
(1899: Fig. 90)



Figure 5.3. The photograph shows a quartzite bipoint biface found during the 19th century in Northampton County, Virginia (see Figure 5.1 J). The specimen currently resides in the collection of the Smithsonian Institution's Museum of Natural History and was initially reported in 1899 (see Wilson 1899: Figure 90).

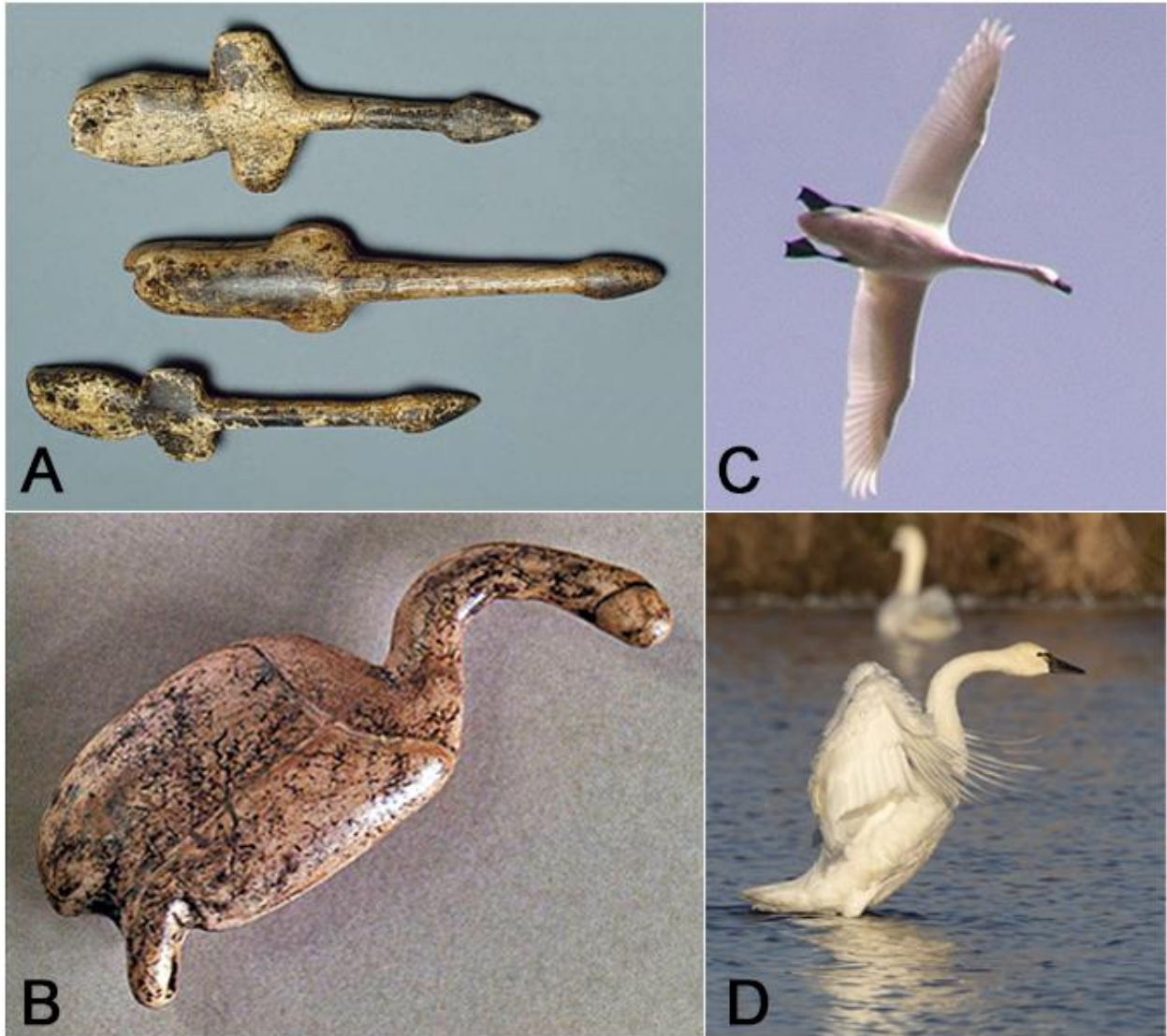


Figure 5.4. The images show mammoth ivory “bird” carvings (A and B) found associated with the circa 24,000-year-old Mal'ta near Lake Baikal. The thirteen or fourteen representations of stylized flying birds (A) were found during the 1956 – 1957 excavations (see Delporte 1979). The flying bird carvings (A) are interpreted as representations of flying tundra swan (C) observed from beneath. The other carved bird (B) has been interpreted as showing a ground perspective of a tundra swan in a defensive posture (D).

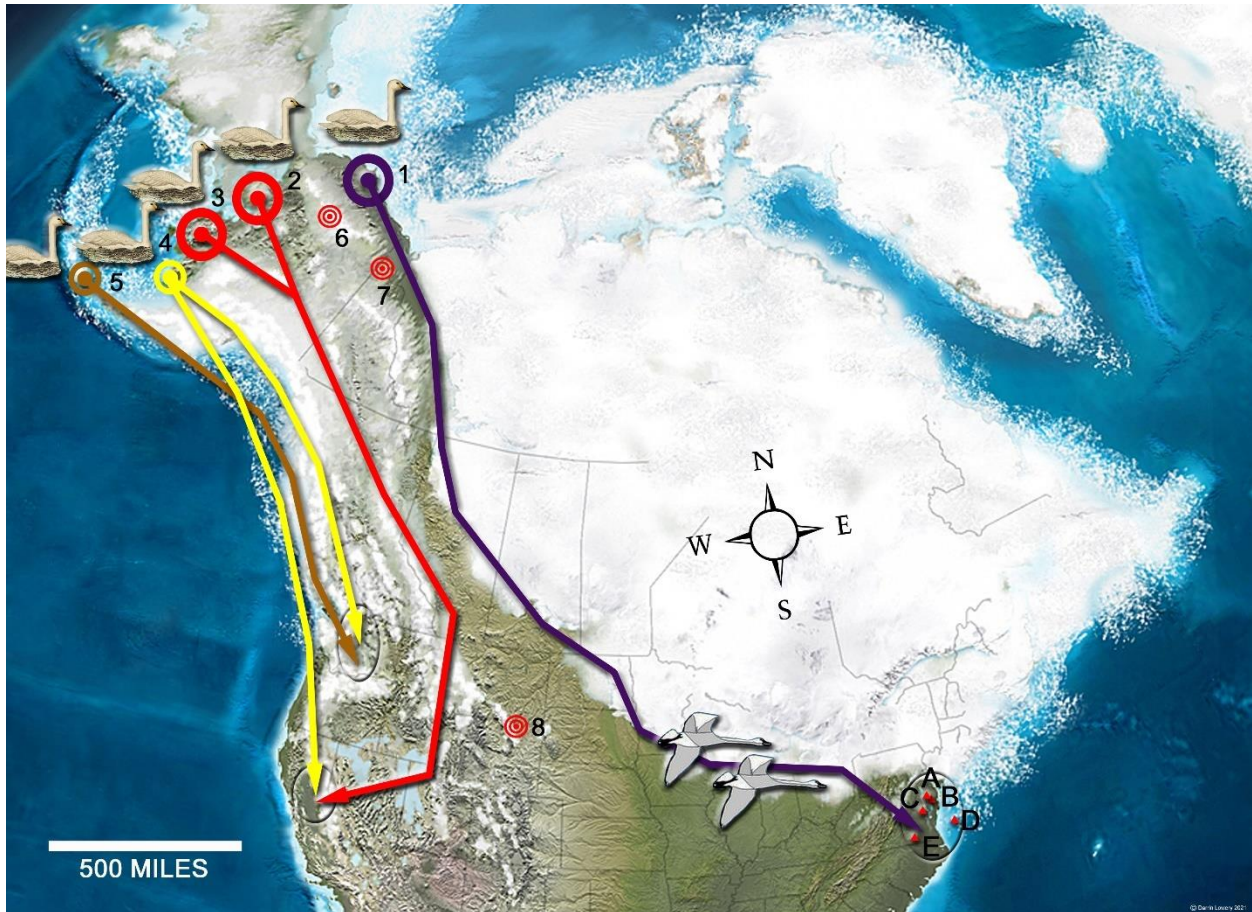


Figure 5.5. The graphic shows the North American ice sheets as they appeared circa 20,000 years ago. The five recognized summer tundra swan nesting areas in Alaska (see Ely and Meixell 2016: Figure 1) are noted on the map (1-5). After the young swan have fledged, tracking devices document their southward winter migratory paths. Note how the present tundra swan migratory flights clearly define the former maximum extent of both the Cordilleran and Laurentide ice sheets. The nesting tundra swan situated along the arctic ocean and well north of the Brooks Range seasonally migrate solely to the Middle Atlantic and Chesapeake Bay region. The graphic also denotes Burial Lake (6) in Alaska where researchers have reportedly found human fecal sterols dated between 32,000 and 16,000 BP. The location of Bluefish Cave (7) in the Yukon, which has reportedly revealed 24,000-year-old human cut-bone, is also denoted. The approximate location of Natural Trap Cave (8) is positioned and shows where researchers have found circa 25,800-year-old Beringian wolf remains, which implies that predators could easily traverse the corridor between the ice sheets during the LGM. Finally, note that Parsons Island (A), Miles Point (B), Patuxent River (C), Cinmar (D), and Cactus Hill (E) are all located within the Middle Atlantic tundra swan wintering area. During the LGM, the seasonal southward migrating tundra swan would have served as the "canary in a coal mine" to early hunter/gatherers unfamiliar with the North American continent. Unlike other migratory land-species, the swan would have indicated to these early colonizers that warmer conditions existed south of the ice.

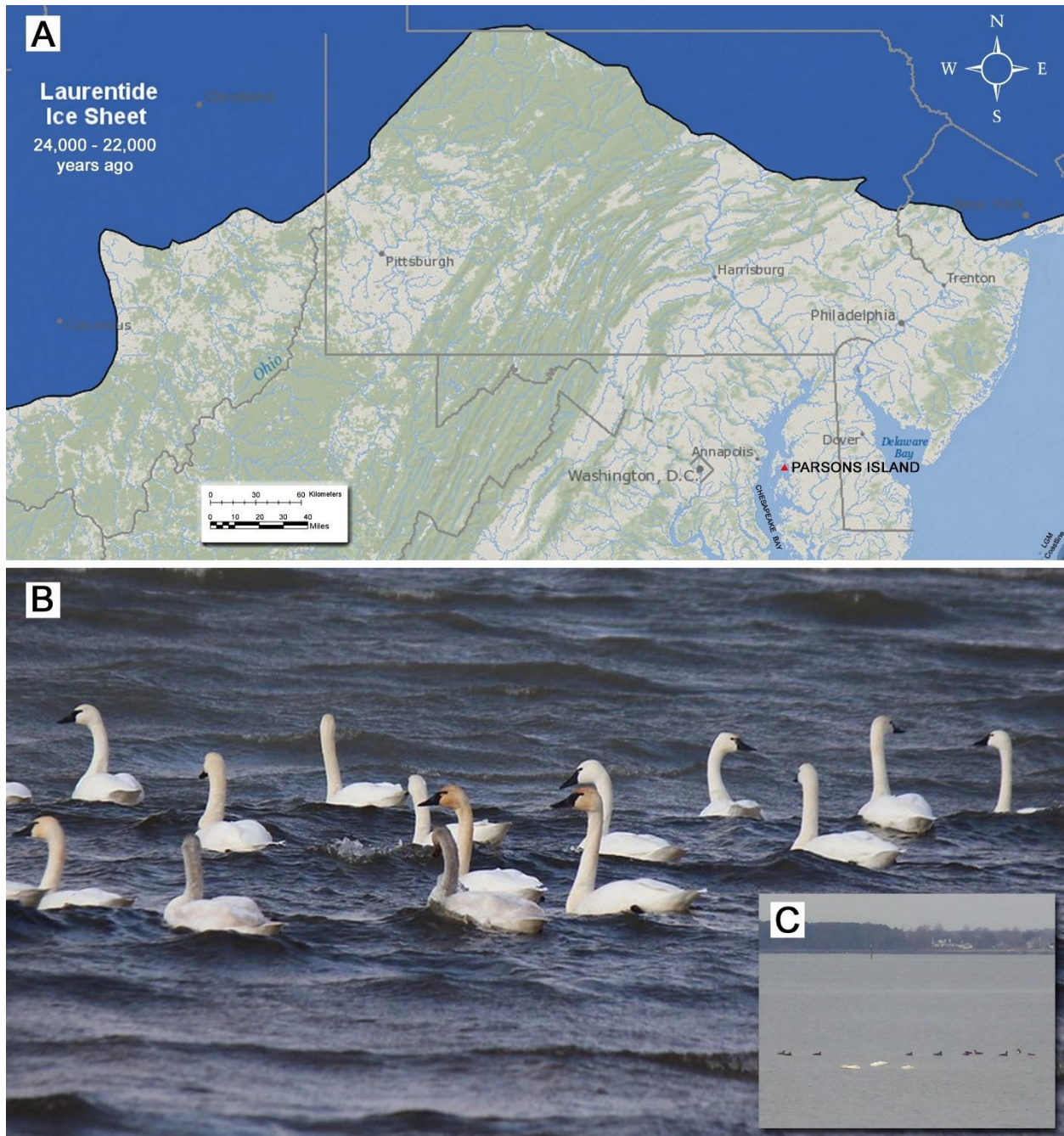


Figure 5.6. The location of Parsons Island relative to the Laurentide ice sheet maximum boundary (A) is shown. A small flock of wintering tundra swan (B) are shown within the Chesapeake Bay near Parsons Island. During the initial day of fieldwork, feeding tundra swan within a grouping of Canada geese were observed offshore of Parsons Island on December 21st, 2019.

Over the years, I have been regularly confronted with statements made by a few academic archaeologists indicating that coastal shoreline surveys and testing at eroding coastal archaeological sites offer little or no important information. Recently for example, Custer (2018: 202) published that *“if site location data are to be useful . . . they need to be carefully integrated into larger regional programs and will require better controls for various sources of biases than are currently seen in the opportunistic shoreline surveys and alleged tests of intuitive and anecdotal predictive models currently in vogue in archaeological studies undertaken in the coastal areas of the central and southern Eastern Shore”*.

In response, coastal erosion and late Holocene sea level rise do not discriminate in what they destroy. If anything, these two natural agents will comprehensively extinguish all archaeological sites in their wake. If left, unchecked, unrecorded, and unevaluated (see Lowery 2018), there will be no archaeological record, or even a biased record along many coastal margins. If in 2013, 18QU1047 were situated on the southern end of Parsons Island (see Figure 4.18), the site would have been completely eroded and destroyed within the first year.

Academicians, like Custer (2018), need to be continually reminded that SHPO offices were established to create an inventory of cultural (i.e., archaeological and architectural) sites and to evaluate the significance of these resources before they disappear, not merely to develop and expand upon predictive models. Some data (see Lowery 2020a and 2020b) have now been published illustrating that a significant proportion of the region’s archaeological record has been inundated, eroded, or some combination of both natural processes. Predictive models in the coastal area may well represent an “investment in futility” in terms of ultimate preservation. Mother nature, after all, is an inexorable force. But recordation and evaluation of significant coastal cultural resources, before they disappear, remains an important facet in evaluating the true archaeological record. Predictive models, based upon the demonstrated history of disappearing resources, may offer useful guidance to SHPO offices in weighing the allocation of present and future fiscal economic resources (see Reeder-Myers 2015).

Various archaeologists have cited the cost prohibitive aspects of conducting shoreline salvage archaeology. As an example, a recent state/federally-funded survey and geoarchaeological evaluation of ~1000 acres of coastal southern New Jersey had a pre-defined budget of \$380,000.00 (Stuart Fiedel, Personal Communication 11-28-2018). Another project in the Middle Atlantic, which surveyed ~5 linear miles of shoreline had a budget of \$90,000.00 (Ibid). Arguably, these examples represent greatly overinflated fiscal resources and probably indicate a misunderstanding of nearshore and/or intertidal settings. As a field of research, archaeology typically encompasses either terrestrial and/or underwater academic concentrations. However, nearshore intertidal zones are geologically dynamic and require a unique suite of geoarchaeological skills. These nearshore intertidal skillsets are not part of a typical academic educational curriculum. The requirements mandated for terrestrial archaeologists; focus on upland site formation processes. Underwater archaeologists typically specialize in shipwrecks and the variables impacting vessel preservation. As such, archaeological investigations in nearshore coastal settings seem somewhat “foreign” and daunting because of the interplay between both long-term and short-term geologic variables. The various time scales and the dynamic processes associated with archaeological sites along shorelines can be somewhat intimidating. In sum, each coastal scenario is unique, requiring an innate understanding of the issues manipulating archaeological sites within their exclusive setting.

Parsons Island contains four unique coastal and/or intertidal archaeological sites that are being impacted by their own complement of geologic and anthropogenic processes. 18QU1065, for example, represents a drowned upland forest situated beneath a veneer of tidal marsh peat that formed as a result of late Holocene marine transgression. Of the sites on the island, the survival and perseverance of 18QU1065 are largely byproducts of its position relative to the island's fetch regime, the prevailing wind directions, and the overall resistance of tidal marsh to erosion. If 18QU1065 had not been inundated, it might have been plowed as a result of recent agricultural land-disturbance activities; like its neighbor 18QU1066. The topographic position, the soil type, the fetch-regime, and the location of 18QU1066 played a role in its longevity. As a result of recent coastal erosion (see Figure 2.3 to 2.5), the site no longer exists and the few plow-scarred artifacts found at this location represent nothing than the reworked tailings associated with a former tilled and deflated prehistoric occupation. The loss of 18QU1066 to coastal erosion occurred sometime prior to 2013. Most importantly, the situation postulated for 18QU1066 is not uncommon along the shoreline margins of the Chesapeake Bay.

The historic well recorded as 18QU1067 clearly illustrates coastal erosion in action (see Figures 3.26 to 3.29 and 3.34 to 3.35). The loss of 18QU1067 as a result of fetch, wave, and tidal processes are analogous to what must have occurred at 18QU1066 sometime prior to 2013. Finally, the survival and perseverance of 18QU1047 throughout the Holocene represents nothing more than a geologic accident. Numerous island and nearshore landscapes have disappeared within the Chesapeake Bay (see Lowery 2018 and 2020b) over the past century-and-a-half. Many of these vanished landscapes may have once contained archaeological remains and/or features equivalent to those documented at 18QU1047. Even the persistence of 18QU1047 over the past several years is largely a fluke of both natural and anthropogenic variables. As elucidated above, developing archaeological site predictive models for coastal areas may be an "investment in futility". However, the research and investigations at 18QU1047 focusing on its eroding Paleo-American and geoarchaeological remains represent an "investment in opportunity". As a low-visibility eroding archaeological deposit, the seven-year study of 18QU1047 should clearly illustrate the fiscal value of systematic and episodic shoreline re-examinations.

The collective study of Parsons Island between 2013 and 2020 demonstrates what can be learned if resources are focused towards an eroding coastal landscape. It also exemplifies the fiscal investments required to conduct this type of long-term project. Over the seven years, the amount of donated time, expenditures, and efforts put forth to complete this research were monitored. Including financial contributions, the total budget allocated towards the Parsons Island project would be \$170,710.00; less than half the total budget allocated for the New Jersey project cited above. Of this total, only \$61,000.00 (36%) consisted of grant funded cash resources; which is only 67% of the budget allocated to conduct aforementioned five-mile coastal archaeological survey. The remaining \$109,710.00 represents the collective value of donated efforts, which includes 2576 man-hours of labor (\$91,110.00), as well as donated equipment value (\$18,600.00). Considering the budgets allocated for similar coastal-oriented projects, the total cost to complete the Parsons Island study is relatively inexpensive.

The future of 18QU1047, like countless other sites in the Chesapeake Bay, depends largely on the concerted efforts of others and the immediacy of salvage actions. Considering the odd series of unforeseen circumstances that occurred in 2020, our original testing plans were greatly hindered by travel restrictions, social distancing, and a variety of other COVID-related factors. However, we did achieve the goal of determining if in-situ archaeological remains were located inland of the existing bank

profile. Now that we know this, what do we do next? If left alone, 18QU1047 and 18QU1065 will both eventually be lost to erosion. Of the two extant archaeological sites, 18QU1047 is easily one of the most significant prehistoric archaeological sites in Maryland and arguably one of the most important prehistoric sites in North America. If left to its own devices, the site will disappear. Ultimately, the coastal erosive actions that exposed it will eventually erase it. Over the past 30 years, I have seen this process happen time and time again. The laundry list of “extinct” archaeological sites once located along the margins of the Chesapeake Bay and its tributaries is rather extensive. As an example, 35 of the 243 archaeological sites along the margins of Accomack and Northampton counties in coastal Virginia were lost to erosion over a short fifteen-year period between 2000 and 2015 (see Lowery 2016). A similar study which was conducted within the Honga River watershed of Dorchester County, Maryland noted that 12 of the original 72 archaeological sites had vanished in recent decades as a result of coastal erosion (see Lowery 2019: 153). Other significant nearshore archaeological sites have disappeared with barely a mention in the published and/or written record (see Lowery 2017 and 2019: 63-64). It is analogous to someone dying without having a published obituary.

Why record these threatened coastal sites if you are only going to let them erode away? If site data “*need to be carefully integrated into larger regional programs*” as some have professed (see Custer 2018: 202), you would assume that vigilant episodic re-evaluations of archaeological sites threatened by erosion and ultimate destruction be mandated by state agencies. 18QU1047 is a very low visibility site and has revealed less than 300 artifacts over the past seven years. Other high visibility eroding sites; like 44NH440 (see Lowery 2016: 294-297), have produced a vast array of diagnostic artifacts, contain numerous in-situ features, and offer a wealth of information if continually monitored. The continued re-analysis of both low and high visibility archaeological sites threatened by imminent loss to erosion should be vital when trying to integrate or improve archaeological site predictive models along coastal margins.

Over the past two decades, I have reiterated statements and observations about coastal erosion and archaeological site loss at various public and/or professional forums. I have seen significant and irreplaceable archaeological resources (see Lowery 2017) simply vanish. The loss of archaeological sites to coastal erosion is analogous to a hypothetical infestation of silverfish, booklice, and biscuit beetles consuming important documents in the National Archives, which under these circumstances would be mitigated. I have been told by various agency heads that they have no jurisdictional mandates relegating any responsibility towards addressing archaeological site loss along dynamic shorelines. However, I disagree. The Annotated Code of Maryland, Environment Article, Title 16-Wetlands and Riparian Rights (§16-10l) defines “State wetlands” as any land under the navigable waters of the State below the mean high tide and affected by the regular rise and fall of the tide. Maryland became a “mean high tide” state in 1958. Prior to that date, Maryland was a “mean low tide” state, like neighboring Virginia. Of course, there are some discrepancies in the defined “high tide” boundary. However, other laws decree jurisdictional responsibility for land immediately inland of the shoreline’s high tide mark. Maryland’s Critical Area Act requires the establishment of a protective 100-foot buffer within the critical area (COMAR 27.01.09.01). The critical area as defined by this act is 100-foot landward of the mean high-water line and regulates any disturbance within this buffer. Notably, the greatest disturbance along any raw unprotected shoreline is coastal erosion induced by tidal water; owned, managed, and regulated by the State of Maryland. These laws and acts do imply that

jurisdictional mandates already exist relegating some State responsibility for the loss of archaeological resources along eroding shorelines.

Exceptions to “mean high tide” State ownership include riparian rights, which means the State does not own the land within the intertidal zone because of some valid grant or historical land patent description. The legality of riparian rights was tested in Maryland’s court in 1992 (see Baltimore Sun 1992) in the legal case of Becker vs. Litty, (318 Md. 76). Because early land patent descriptions for some properties bordering the Chesapeake noted the owner has “rights to the water”, those rights transferred to succeeding owners, unless an eroding property was resurveyed and the reduced acreage officially recorded. In sum, I think there is some legal responsibility of state agencies; especially in Maryland, to address the loss of archaeological sites as a result of erosion. Like many archaeological features and sites bordering the Chesapeake Bay, it is not a matter of “if” 18QU1047 will be destroyed by coastal erosion; it’s a matter of “when” 18QU1047 will be destroyed by erosion.

The research and investigations, which were funded by the Smithsonian, the Chesapeake Watershed Archaeological Research Foundation, and the Maryland Historical Trust’s Non-Capital Grant Program, offer a glimpse into what can be gleaned if some fiscal resources are allocated towards archaeological resources threatened by coastal erosion. In sum, it really does not take much effort! It simply takes a restructuring about how certain state and federal agencies prioritize their programs.

REFERENCES CITED:

Adovasio, J., J. Donahue and R. Stuckenrath

1990 The Meadowcroft Rockshelter Radiocarbon Chronology 1975-1990. *American Antiquity* 55:348-354.

1991 Never Say Never Again: Some Thoughts on Could Haves and Might Have Beens. *American Antiquity* 57:327-331.

Adovasio, J., J. D. Gunn, J. Donahue and R. Stuckenrath

1977 Meadowcroft Rockshelter: Retrospective 1976. *Pennsylvania Archaeologist* 47(2-3):1-93.

1978 Meadowcroft Rockshelter, 1977: An Overview. *American Antiquity* 43 (4): 632

Adovasio, J., J. D. Gunn, J. Donahue, R. Stuckenrath, J. E. Guilday and K. Volman

1980 Yes Virginia, It Really is that Old: A Reply to Haynes and Mead. *American Antiquity* 45:588-595.

Baltimore Sun

1992 *Lawsuit over little bridge still cuts wide chasm in Shore town.* July 31st, 1992, Baltimore, Maryland.

Bass, J., B. Espinola, K. Sheesley, J. Grannis, and M. Scott

2018 *Mainstreaming Sea Level Rise Preparedness in Local Planning and Policy on Maryland's Eastern Shore.* A report prepared for the Eastern Shore Climate Adaptation Partnership by Eastern Shore Land Conservancy.

Bradley, B., M. Collins, and A. Hemmings

2010 *Clovis Technology.* Archaeological Series 17. International Monographs in Prehistory, Ann Arbor.

Brehm, H. C.,

1981 *The History of the Duck River Cache.* Miscellaneous Paper No. 6, Tennessee Anthropological Association, pp. 1-24.

Bintanja, R., R. S. van de Wal and J. Oerlemans

2005 Modelled Atmospheric Temperatures and Global Sea Levels over the Past Million Years. *Nature* 437(7055):125-128.

Boulanger, M. and M. Eren

2015 On the Inferred Age and Origin of Lithic Bi-Points from the Eastern Seaboard and Their Relevance to the Pleistocene Peopling of North America. *American Antiquity* 80(1): 134-145.

Bourgeon, L., A. Burke, and T. Higham

2017 Earliest Human Presence in North America Dated to the Last Glacial Maximum: New Radiocarbon Dates from Bluefish Caves, Canada. *PLOS ONE* 12(1): e0169486.

<https://doi.org/10.1371/journal.pone.0169486>.

- Carlquist, Sherwin
1988 *Comparative Wood Anatomy*. Springer-Verlag, Berlin, Heidelberg.
- Clyne M A, Muffler L J P,
2010 *Geologic Map of Lassen Volcanic National Park and vicinity, California*. United States Geologic Survey Science Investigation Map, SIM-2899, 1:50,000 scale, 3 sheets and 110 pp. & text.
- Colman, S. M., J. P. Halka, and C. H. Hobbs, R. B. Mixon, and D. S. Foster
1990 Ancient Channels of the Susquehanna River Beneath the Chesapeake Bay and the Delmarva Peninsula. *Geological Society of America Bulletin*, 102: 1268-1279.
- Core, H. A., W. A. Cote, and A. C. Day
1976 *Wood Structure and Identification*. Syracuse University Press, Syracuse, New York.
- Custer, J.
2018 Sea Level Rise and the Cultural Paleoecology of Woodland Settlement Patterns in the Delaware and the Central Middle Atlantic Coastal Zone: Retrospect and Prospect. *Archaeology of Eastern North America* 46: 191-214.
- Davis, E.
2020 *A Reassessment of the Late Quaternary Surficial Geology of the Lower Delmarva Peninsula, Virginia*. Unpublished thesis submitted to the Faculty of the University of Delaware in partial fulfillment of the requirements for the degree of Master of Science in Geological Sciences. Newark, Delaware.
- Davis, L.
1993 *Weed Seeds of the Great Plains A Handbook for Identification*. University Press of Kansas, Lawrence.
- Dawe, R., and M. Kornfeld
2017 Nunataks and Valley Glaciers: Over the Mountains and through the Ice. *Quaternary International* 444: 56-71.
- DeJong, B., P. Bieman, W. Newell, T. Rittenour, S. Mahan, G. Balco, and D. Rood
2015 Pleistocene Relative Sea Levels in the Chesapeake Bay Region and Their Implications for the Next Century. *GSA Today*, August 2015: 4-10.
- Deller, B., C. Ellis, and J. Keron
2009 Understanding Cache Variability: A Deliberately Burned Early Paleoindian Tool Assemblage from the Crowfield Site, Southwestern Ontario, Canada. *American Antiquity* 74 (2): 371 – 397.
- Delorit, R.
1970 *An Illustrated Taxonomy Manual of Weed Seeds*. Wisconsin State University Agronomy Publications, River Falls, Wisconsin.

Delporte H.

1979 *L'image de la femme dans l'art préhistorique*, Paris, Picard.

Dorn, R.

2012 Formation of Silica Glaze Rock Coatings through Water Vapor Interactions. *Physical Geography* (33-1): 21–31.

Dyke, A., Andrews, J.T., P.U, C., England, J., Miller, G., Shaw, J., and Veillette, J.

2002 The Laurentide and Inuitian Ice Sheets during the Last Glacial Maximum. *Quaternary Science Reviews*, 21: (1-3): 9-33.

Ely, C., and B. Meixell

2016 Demographic Outcomes of Diverse Migration Strategies assessed in a Metapopulation of Tundra Swans. *Movement Ecology* 4(10): 1-15.

Erlandson, J., M. Graham, B. Bourque, D. Corbett, J. Estes and R. Steneck

2007 The Kelp Highway Hypothesis: Marine Ecology, the Coastal Migration Theory, and the Peopling of the Americas, *The Journal of Island and Coastal Archaeology*, 2:2, 161-174.

Fægri, K. and J. Iversen

1989 *Textbook of Pollen Analysis*. Fourth Edition. John Wiley and Sons, Great Britain.

Faure, H., R. C. Walter, D. R. Grant

2002 The Coastal Oasis: Ice Age Springs on Emerged Continental Shelves. *Global and Planetary Change* 33: 47-56.

Fiedel, S.

2007 Quacks in the Ice: Waterfowl, Paleoindians, and the discovery of America. In: Walker RB, Driskell BN (eds) *Foragers of the terminal Pleistocene in North America*. University of Nebraska Press, Lincoln/London, pp 1–14.

Foss, J.E., Fanning, D.S., Miller, F.P., Wagner, D.P.

1978 Loess Deposits of the Eastern Shore of Maryland. *Soil Science Society of America Journal* 42, 329–334.

Fox-Dobbs, K., J. A. Leonard, and P. L. Koch

2008 Pleistocene megafauna from eastern Beringia: Paleoecological and paleoenvironmental interpretations of stable carbon and nitrogen isotope and radiocarbon records. *Palaeogeography. Palaeoclimatology. Palaeoecology*. 261:30–46.

French, H.M., Demitroff, M. and Newell, W.L.

2009 Past Permafrost on the Mid-Atlantic Coastal Plain, Eastern USA. *Permafrost and Periglacial Processes*, 20: 285-294.

Giria, Y., and B. Bradley

1998 Blade Technology at Kostenki 1/1, Avdeevo, and Zaraysk. In *The Eastern Gravettian*, edited by H. A. Amirkhanov. Russian Academy of Natural Sciences, Institute of Archaeology, Moscow.

Grootes, P. M. and M. Stuiver

1997 Oxygen 18/16 Variability in Greenland Snow and Ice with 10³ to 10⁵-Year Time Resolution. *Journal of Geophysical Research* 102(C12):26455.

Harley, J. and S. Smith

1983 *Mycorrhizal Symbiosis*. Academic Press, New York.

Haury, E. W.

1953 Artifacts with Mammoth Remains, Naco, Arizona: Discovery of the Naco Mammoth and the Associated Projectile Points. *American Antiquity* 19: 1–14.

Hayden, H.

1820 *Geological Essays; or An Inquiry into Some of the Geologic Phenomena to be Found in Various Parts of America, and Elsewhere*. 8vo. 412 pp. Baltimore, MD.

Hendy, I.

2009 A Fresh Perspective on the Cordilleran Ice Sheet. *Geology* 37- 1: 95–96.

Hoadley, R. B.

1990 *Identifying Wood: Accurate Results with Simple Tools*. The Taunton Press, Inc., Newtown, Connecticut.

Holmes, C. E.

1996 Broken Mammoth. In *American Beginnings: The Prehistory and Palaeoecology of Beringia*, edited by Frederick Hadleigh West, pp. 312-317. The University of Chicago Press, Chicago and London.

Holmes, C. E., R. Vanderhoek, and T. Dilley

1996 Swan Point. In *American Beginnings: The Prehistory and Palaeoecology of Beringia*, edited by Frederick Hadleigh West, pp. 319-323. The University of Chicago Press, Chicago and London.

Horton, T., D. Harp and S. Cannon-Brown

2020 *High Tide in Dorchester County*. Bay Journal Films (see <https://www.bayjournal.com/films/>).

Huckell, Bruce H.

2014 But how do we know if it's Clovis? An examination of Clovis overshoot flaking of bifaces and a North Dakota cache. *Clovis Caches: Recent Discoveries & New Research*. Edited by Bruce B. Huckell and J. David Kilby. University of New Mexico Press, Albuquerque.

Hughes, P., and P. Gibbard

2014 A Stratigraphical Basis for the Last Glacial Maximum (LGM). *Quaternary International* 383: 174-185.

InsideWood

2004 *InsideWood Database*. Electronic document, <http://insidewood.lib.ncsu.edu/search>, accessed October, 2013.

Jung, J. and Hong-Keun Choi

2011 Taxonomic Study of Korean Scirpus L. s.l. (Cyperaceae) II: Pattern of Phenotypic Evolution Inferred from Molecular Phylogeny. *Journal of Plant Biology* 54:409-424.

Kilby, D., and B. Huckell

2013 Clovis Caches: Current Perspectives and Future Directions. In *Paleoamerican Odyssey*, edited by Kelly Graf, Caroline Ketron, and Michael Waters, pp. 257-272. Center for the Study of the First Americans, Texas A&M University, College Station, Texas.

Kivisild, T.

2017 The Study of Human Y Chromosome Variation through Ancient DNA. *Human Genetics* 136(5): 529–546.

Lacelle, D., B. Lauriol, G. Zazula, B. Ghaleb, N. Utting, and I. D. Clark

2013 Timing of advance and basal condition of the Laurentide Ice Sheet during the last glacial maximum in the Richardson Mountains, NWT. *Quaternary Research* 80:274–283.

Lambeck, K., H. Rouby, A. Purcell, Y. Sun, and M. Sambridge

2014 Sea level and Global Ice Volumes from the Last Glacial Maximum to the Holocene. *Proceedings of the National Academy of Sciences*, v. 111 (43): 15,296–15,303.

Laskar, J., P. Robutel, F. Joutel, M. Gastineau, A. C. M. Correia and B. Levrard

2004 A Long-Term Numerical Solution for the Insolation Quantities of the Earth. *Astronomy and Astrophysics* 428(1):261-285.

Laub, R.

2002 The Paleoindian Presence in the Northeast: A View from the Hiscock Site, pp. 105–121, In Kurt W. Carr & James M. Adovasio (eds.), *Ice Age Peoples of Pennsylvania*, Pennsylvania Historical and Museum Commission, Harrisburg.

Lemke, M. and F. Nelson, F.E.

2004 Cryogenic Sediment-Filled Wedges, Northern Delaware, USA. *Permafrost and Periglacial Processes*, 15: 319-326.

Leonhardy, F.

1966 *Domebo: A Paleo-Indian Mammoth Kill Site in the Prairie-Plains*. Lawton, Oklahoma: Great Plains Historical Association.

Losco, R., W. Stephens, and M. Helmke

2010 Periglacial Features and Landforms of the Delmarva Peninsula. *Southeastern Geology*, 47(2): 85-94.

Lothrop J., D. Lowery, A. Spiess, and C. Ellis

2016 Early Human Settlement of Northeastern North America. *PaleoAmerica: A Journal of Early Human Migration and Dispersal*, Vol. 2 (3): 192-251.

Lowery, D.

1992 The Distribution and Function of Prehistoric Sites within the Lower Bay Hundred District, Talbot County, Maryland. *Journal of Middle Atlantic Archaeology* 8, pp. 11-40.

1993 *An Archaeological Survey of the Chester River, Prospect Bay and Wye River Drainages, Queen Anne's County, Maryland*. Manuscript on file at the Maryland Historical Trust, Crownsville, Maryland.

1995 The Amy's Marsh Broadspear Cache and Its Implications for the Barker's Landing Complex on Maryland's Eastern Shore. *Maryland Archaeology* 31, No. 1-2.

1999 *A Survey of Selected Prehistoric Artifact Collections Associated with the Choptank River Watershed, Maryland*. Manuscript prepared for the Maryland Historical Trust in cooperation with Dr. R. Michael Stewart of the Department of Anthropology at Temple University.

2002a *A Time of Dust: Archaeological and Geomorphological Investigations at the Paw Paw Cove Paleo-Indian Site Complex in Talbot County, Maryland*. Maryland Historical Trust, In cooperation with the Department of Anthropology at Temple University and the Chesapeake Bay Watershed Archaeological Research Foundation.

2002b The Distribution of Miocene Silicified Sandstone in the Archaeological Record and Interpretations Based on the Observed Patterns: A Test of GIS in Archaeology. *Journal of Middle Atlantic Archaeology* 14.

2003a *Archaeological Survey of the Atlantic Coast Shorelines Associated with Accomack County and Northampton County, Virginia*. Survey and Planning Report Series No. 7. Virginia Department of Historic Resources, Richmond, Virginia.

2003b *A Landscape Sculpted by Wind and Water: Archaeological and Geomorphological Investigations at the Upper Ridge Site (44NH440) on Mockhorn Island in Northampton County, Virginia*. Manuscript prepared for the Virginia Department of Historic Resources, Richmond, Virginia.

2004 *A Landscape Sculpted by Wind and Water: Additional Archaeological and Geomorphological Investigations on Mockhorn Island in Northampton County, Virginia*. Manuscript prepared for the Virginia Department of Historic Resources, Richmond, Virginia.

2007 *Phase I Terrestrial Archaeological Survey at Miles Point in Talbot County, Maryland*. Manuscript prepared for the Midland Companies.

2010 *The Late Quaternary Geology and Archaeology of Mockhorn Island, Virginia. A Summary of 2009 and 2010 Research*. Virginia Department of Historic Resources, Richmond, Virginia.

2015a *Archaeological Shoreline Survey of the Lower York River Islands in Coastal Virginia*. Virginia Department of Historic Resources, Richmond, Virginia.

2015b *Archaeological Shoreline Survey of Back Bay along Coastal Virginia*. Virginia Department of Historic Resources, Richmond, Virginia.

2016 *A Coastal Archaeological Survey, Shoreline Erosion, and Sea Level Assessment of Accomack and Northampton Counties, Virginia*. Virginia Department of Historic Resources, Richmond, Virginia.

2017 *Erosion and Archaeological Site Loss Adjacent to the Chesapeake Bay and Atlantic Coast. At the Water's Edge: Our Past on the Brink*. Maryland Archeology Month Bulletin.

2018 *Sea Level Rise, Shoreline Erosion, and Their Impact on Archaeological Interpretation: A Delmarva Case Study*. *Journal of Middle Atlantic Archaeology*, 34: 1-22.

2019 *Recent Coastal Erosion and Late Holocene Sea Level Rise Impacts on Archaeological Resources within the Honga River, Dorchester County, Maryland*. Maryland Historical Trust, Crownsville, Maryland.

2020a *Recent Coastal Erosion and Late Holocene Sea Level Impacts on Archaeological Resources within the Fishing Bay Watershed, Dorchester County, Maryland*. Maryland Historical Trust, Crownsville, Maryland.

2020b *Making the Most of Chance Submerged Finds: Offshore and Inshore*. *Archaeology of Eastern North America*, 48: 1-22.

Lowery, D., M. A. O'Neal, J. S. Wah, D. P. Wagner, and D. J. Stanford

2010 *Late Pleistocene Upland Stratigraphy of the Western Delmarva Peninsula, USA*. *Quaternary Science Reviews* 29 (11- 12): 1472-1471.

Lowery, D., and D. Stanford

2013 *A Paleoindian Encampment at 44NH233: An Inundated Coastal Paleoindian Site along the Atlantic Seashore of the Delmarva Peninsula*. Smithsonian Research Reports, Washington, D.C.

Lowery, D., and D. Wagner

2012 Geochemical Impacts to Iron-Rich Lithic Artifacts in the Nearshore Coastal Zone. *Journal of Archaeological Science* 39 (3): 690-697.

Lowery, D., J. Wah, and T. Rick

2012 Post-Last Glacial Maximum Dune Sequence for the "Parsonburg" Formation at Elliott's Island, Maryland. *Current Research in the Pleistocene* 28: 134-135.

Mao, X. H. Zhang, S. Qiao, J. Olsen, E. A. Bennett, and Q. Fu

2021 The Deep Population History of Northern East Asia from the Late Pleistocene to the Holocene. *Cell* 184, 1–11. <https://doi.org/10.1016/j.cell.2021.04.040> .

Marguerie, D. and J. Y. Hunot

2007 Charcoal Analysis and Dendrology: Data from Archaeological Sites in Northwestern France. *Journal of Archaeological Science* 34:1417-1433.

Markewich, H., R. Litwin, M. Pavich, and G. Brook

2009 Late Pleistocene Eolian Features in Southeastern Maryland and Chesapeake Bay region indicate Strong WNW–NW Winds accompanied Growth of the Laurentide Ice Sheet. *Quaternary Research* 71 (3): 409-425.

Markewich, H., R. Litwin, D. Wysocki, and M. Pavich

2015 Synthesis on Quaternary Aeolian Research in the Unglaciaded Eastern United States. *Aeolian Research* 17: 139–191.

Martin, Alexander C. and William D. Barkley

2000 *Seed Identification Manual*. The Blackburn Press, Caldwell, New Jersey. Reprint of the 1961 Edition by the Regents of the University of California.

Medvedev, G., Cauwe, N., Vorobyeva, G., Coupe, D., Claes, L., Lipnina, E., and Khenzykhenova, D.

1996 *The Mal'ta Paleolithic Locality*. ARCOM Press (in Russian). Google Scholar.

McAvoy, J., and L. McAvoy

1997 *Archaeological Investigations of Site 44SX202, Cactus Hill, Sussex County, Virginia*.

Commonwealth of Virginia Department of Historic Resources, Research Report Series No. 8. Richmond, Virginia.

2015 *Nottoway River Survey, Part II: Cactus Hill and Other Excavated Sites*. The Dietz Press, Petersburg, Virginia.

McAvoy, Joseph

2021 Personal Communication; E-mail received Thursday, January 28th, 10:01AM.

McCary, Ben C.

1985 Survey of Virginia Fluted Points, Nos. 707-732. *Archaeological Society of Virginia Quarterly Bulletin* 40 (1): 1-11.

McConaughy, M.

1999 Meadowcroft Rockshelter.

(<http://people.delphiforums.com/MCCONAUGHY/meadowcroft/meadow.htm>)

McParland, Laura C., Margaret E. Collinson, Andrew C. Scott, Gill Campbell and Robyn Veal

2010 Is Vitriification in Charcoal a Result of High Temperature Burning of Wood?

Journal of Archaeological Science 37:2679-2687.

McWeeney, Lucinda

1989 What Lies Lurking Below the Soil: Beyond The Archaeobotanical View of Flotation Samples.

North American Archaeologist 10(3):227-230.

Mikola, P.

1948 On the Physiology and Ecology of *Cenococcum graniforme* Especially as a

Mycorrhizal Fungus of Birch. *Institutie Forestalis Fenniae Communicationes* 36:3,

pp. 1-104.

Mixon, R.B.,

1985 *Stratigraphic and Geomorphic Framework of Uppermost Cenozoic Deposits in the Southern Delmarva Peninsula, Virginia and Maryland*. U.S. Geological Survey Professional Paper., Vol. 1067-G.

Montgomery, D.

2013 The Future of Crisfield, MD. *The Washington Post*, October, 24, 2013.

Muasya, A. Muthama, David A. Simpson, G. Anthony Verboom, Paul Goetghebeur, Robert F. C. Naczi, Mark W. Chase and Erik Smets

2009 Phylogeny of Cyperaceae Based on DNA Sequence Data: Current Progress and

Future Prospects. *The Botanical Review* 75:2-21.

Munyikwa, K., Feathers, J.K., Rittenour, T., Shrimpton, H.K.,

2011 Constraining the retreat of the Laurentide Ice sheet using luminescence ages from postglacial eolian dunes. *Quaternary Geochronology* 6, 407–422.

Munyikwa, K., T. Rittenour, J. Feathers

2017 Temporal constraints for the Late Wisconsinan deglaciation of western Canada using eolian

dune luminescence chronologies from Alberta. *Palaeogeography, Palaeoclimatology, Palaeoecology*

470: 147-165.

National Research Council (U.S.).

1991 Committee on Animals as Monitors of Environmental Hazards. *Animals as Sentinels of Environmental Health Hazards: Committee on Animals as Monitors of Environmental Hazards*. National Academy Press, Washington, D.C.

Niekus, Marcel J., Paul R. B. Kozowyk, Geeske H. J. Langejans, Dominique Ngan-Tillard, Henk van Keulen, Johannes van der Plicht, Kim M. Cohen, Willy van Wingerden, Bertil van Os, Bjørn I. Smit, Luc W. S. W. Amkreutz, Lykke Johansen, Annemieke Verbaas, Gerrit L. Dusseldorp
2019 Middle Paleolithic complex technology and a Neandertal tar-backed tool from the Dutch North Sea. *Proceedings of the National Academy of Sciences*, 116 (44) 22081-22087.

Oakley, Bryan A. and Jon C. Boothroyd

2012 Reconstructed Topography of Southern New England Prior to Isostatic Rebound with Implications of Total Isostatic Depression and Relative Sea Level. *Quaternary Research* 78(1):110-118.

Owens, J., and C. Denny

1979 *Upper Cenozoic Deposits of the Central Delmarva Peninsula, Maryland and Delaware*. U.S. Geologic Survey, Professional Papers, vol. 1067-A. 28 pp.

Panshin, A. J. and Carl de Zeeuw

1980 *Textbook of Wood Technology*. McGraw-Hill Book Co., New York.

Pastor, A., S. Poblador, L. Skovsholt, and T. Riis

2020 Microbial carbon and nitrogen processes in high-Arctic riparian soils. *Permafrost and Periglacial Processes*, 31(1): 223-236.

Pavich, M., H. Markewich, and G. Brook

2006 Significance of Kent Island Formation to Geomorphic History of the mid-Atlantic Region. *Geological Society of America Abstracts with Programs* 38 (7), 226.

Perria, A., T. Feuerborn, L. Frantz, G. Larsoni, R. Malhi, D. Meltzer, and K. Witt

2021 Dog Domestication and the Dual Dispersal of People and Dogs into the Americas. *Proceedings of the National Academy of Sciences*, 118 (6), <https://doi.org/10.1073/pnas.2010083118> .

Pitulko, V., P. Nikolsky, E. Girya, A. Basilyan, V. Tums koy, S. Koulakov, S. Astakhov, E. Pavlova, and M. Anisimov

2004 The Yana RHS Site: Humans in the Arctic Before the Last Glacial Maximum. *Science*, 303 (5654): 52-56.

Puseman, K., C. Yost, and A. Nurse

2014 *Macrofloral, Phytolith, and Pollen Analysis of Peat from Elliott's Island and Paleosol Samples from Parson's Island, Maryland*. Technical report 13006 prepared for Chesapeake Bay Watershed Archaeological Research Foundation, and Smithsonian Institution, Washington, D.C.

Raff, J. and D. Bolnick

2014 The Genetic Roots of the First Americans. *Nature* 506: 162–163.

Raghavan, M., P. Skoglund, K. Graf, M. Metspalu, A. Albrechtsen, I. Moltke, S. Rasmussen, T. Stafford Jr., L. Orlando, E. Metspalu, M. Karmin, K. Tambets, S. Rootsi, R. Mägi, P. Campos, E. Balanovska, O. Balanovsky, E. Khusnutdinova, S. Litvinov, L. Osipova, S. Fedorova, M. Voevoda, M. DeGiorgio, T. Sicheritz-Ponten, S. Brunak, S. Demeshchenko, T. Kivisild, R. Villems, R. Nielsen, M. Jakobsson, and E. Willerslev

2014 Upper Palaeolithic Siberian Genome Reveals Dual Ancestry of Native Americans. *Nature* 505: 87–91.

Raghavan, M., M. Steinrucken, K. Harris, S. Schiffels, S. Rasmussen, M. DeGiorgio, A. Albrechtsen, C. Valdiosera, M. C. Avila-Arcos, and A. Malaspina, A.-S.

2015 Genomic evidence for the Pleistocene and recent population history of Native Americans. *Science* 349, aab3884.

Ramsey, K.W.

2010 *Stratigraphy, correlation, and depositional environments of the middle to late Pleistocene interglacial deposits of southern Delaware*. Delaware Geologic Survey Report of Investigations 76.

Reeder-Myers, L.

2015 Cultural Heritage at Risk in the Twenty-First Century: A Vulnerability Assessment of Coastal Archaeological Sites in the United States. *Journal of Island and Coastal Archaeology* 10(3): 436-445.

Schubel, J. R.; and C. F. Zabawa

1972 *A Pleistocene Susquehanna River Channel Connects the Lower Reaches of the Chester, Miles, and Choptank Estuaries. Special Report 24: Reference 72-8*. Chesapeake Bay Institute, The Johns Hopkins University. Baltimore, Maryland.

Scott, T., D. Swift, G. R. Whittecar, and G. Brook

2010 Glacioisostatic Influences on Virginia's Late Pleistocene Coastal Plain Deposits. *Geomorphology* 116: 175-188.

Stanford, D. and B. Bradley

2012 *Across Atlantic Ice*. University of California Press, Berkeley.

Stanford, D., D. Lowery, M. Jodry, B. Bradley, M. Kay, T. Stafford, and J. Speakman

2014 New Evidence for Paleolithic Occupation of the Eastern North American Continental Shelf at the Last Glacial Maximum, pp. 73-94. In *Prehistoric Archaeology of the Continental Shelf: A Global Review*, edited by Amanda Evans, Joseph Flatman, and Nicholas Flemming, Springer.

Stanford, D., D. Lowery, M. Jodry, and M. Frank

2018 Mockhorn Island Clovis Site: An Intertidal Locality from Coastal Virginia, pp. 16-37. In *the Eastern Fluted Point Tradition*, Volume II, edited by Joseph A. M. Gingerich, University of Utah Press.

Tamm, E., T. Kivisild, M. Reidla, M. Metspalu, D. Glenn Smith, C. Mulligan, C. Bravi, O. Rickards, C. Martinez-Labarga, E. Khusnutdinova, S. Fedorova, M. Golubenko, V. Stepanov, M. Gubina, S. Zhadanov, L. Ossipova, L. Damba, M. Voevoda, J. Dipierri, R. Villems, and R. Malhi
2007 Beringian Standstill and Spread of Native American Founders. *PLOS ONE* 2(9): e829.
<https://doi.org/10.1371/journal.pone.0000829> .

The Regents of the University of California
1997-2014 *Cenococcum geophilum* 1.58 v2.0. Electronic document,
<http://genome.jgi-psf.org/Cenge3.home.html>, accessed February 19, 2014.

Trappe, J.
1962 Fungus Associates of Ectotrophic Mycorrhizae. *The Botanical Review*, U.S. Department of Agriculture, Washington, D.C.

1969 Studies on *Cenococcum graniforme*. I. An Efficient Method for Isolation from Sclerotia. *Canadian Journal of Botany* 47, pp. 1389-1390.

Vachula, R., Y. Huang, J. Russell, M. Abbott, M. Finkenbinder, and J. O'Donnell
2020 Sedimentary Biomarkers Reaffirm human impacts on northern Beringian ecosystems during the Last Glacial period. *BOREAS*, 49-3: 514-525.

Vandergoes, M. J.
2000 *High Resolution Record of Late Quaternary Vegetation and Climate Change, South Westland, New Zealand*. Unpublished Ph.D. thesis, University of Otago, New Zealand.

Vangeluwea, D., S. Rozenfeldb, S. Volkovb, S. Kazantzidisc, V. Morosovd, D. Zamyatine, and G. Kirtaev
2018 Migrations of Bewick's Swan (*Cygnus Bewickii*): New Data on Tagging the Migration Routes, Stopovers, and Wintering Sites. *Biology Bulletin*, 45 (7): 90–101.

van Vliet-Lanoe, B., A. Magyarib, and F. Meilliez
2004 Distinguishing between Tectonic and Periglacial Deformations of Quaternary Continental Deposits in Europe. *Global and Planetary Change*, 43: 103–127

Villa, P., M. Soressi, C. Henshilwood, and V. Mourre
2009 The Still Bay points of Blombos Cave (South Africa). *Journal of Archaeological Science* 36: 441–460.

Waelbroeck, C., L. Labeyrie, E. Michel, J. Cl Duplessy, J. F. McManus, K. Lambeck, E. Balbon and M. Labracherie
2002 Sea-Level and Deep-Water Temperature Changes Derived from Benthic Foraminifera Isotopic Records. *Quaternary Science Reviews* 21(1):295-305.

Wagner, D.

2013 *Geoarchaeology of the Patuxent River Naval Ais Station, St. Mary's County, Maryland*. Louis Berger Group, Inc., Washington, D.C.

Wagner, D., D. Lowery, and J. Clemens

2019 *Geoarchaeology of the Higbee Beach Wildlife Management Area, Cape May, New Jersey*. Louis Berger U.S., Inc.

Wah, J.

2003 *The Origin and Pedogenic History of Quaternary Silts on the Delmarva Peninsula in Maryland*, Unpublished Ph. D. dissertation. University of Maryland, College Park.

Wah, J., D. Lowery, and D. Wagner

2014 Loess, Landscape Evolution, and Pre-Clovis on the Delmarva Peninsula, pp. 32-48. In *Pre-Clovis in the Americas: International Science Conference Proceedings*, edited by Dennis Stanford and Alison Stenger, Smithsonian Institution, Washington, D.C.

Wah, J., D. Wagner, and D. Lowery

2018 Loess in the Middle Atlantic, USA. *Quaternary Research*, 89 (3): 786-796.

Waters, M.

2019 Late Pleistocene Exploration and Settlement of the Americas by Modern Humans. *Science* 365 (138).

West, Frederick H. (editor)

1996 *American Beginnings: The Prehistory and Palaeoecology of Beringia*. University of Chicago Press: Chicago and London.

Wilson, Thomas

1899 *Arrowpoints, Spearheads, and Knives of Prehistoric Times*. U.S. Government Printing Office, Washington, D.C.

Wright, J., R. Sheridan, K. Miller, J. Uptegrove, B. Cramer, J. Browning

2009 Late Pleistocene Sea level on the New Jersey Margin: Implications to Eustasy and Deep-Sea Temperature. *Global and Planetary Change* 66: 93–99.

Zwissler, B., T. Oommen, and S. Vitton

2014 A Study of the Impacts of Freeze–Thaw on Cliff Recession at the Calvert Cliffs in Calvert County, Maryland. *Geotechnical and Geological Engineering* 32: 1133–1148.

APPENDIX I:

Blood Residue Analysis Report for Two In-Situ Artifacts found along the
Eroded Bank Profile at Parsons Island, Maryland.



Archaeological Investigations Northwest, Inc.

3510 N.E. 122nd Ave. • Portland, Oregon 97230
Phone (503) 761-6605 • Fax (503) 761-6620

Vancouver Phone (360) 696-7473
E-mail: ainw@ainw.com
Web: www.ainw.com

March 13, 2014

Dennis Stanford, Ph.D.
Smithsonian Institution, NMNH/MRC 112
10th & Constitution Ave. NW
Washington, D.C. 20560-0001

Re: Results of Blood Residue Analysis on Two Artifacts from Parson's Island, Maryland
AINW Report No. 3248

Dear Dr. Stanford:

At your request, Archaeological Investigations Northwest, Inc. (AINW) analyzed two artifacts from Parson's Island. The analysis was done to identify possible blood residues using cross-over immunoelectrophoresis (CIEP). There were two positive reactions to two of the four antisera used in the analysis. Positive reactions were noted on both artifacts.

The CIEP technique has been widely used in forensic laboratories to determine the origin of bloodstains as evidence in criminal investigations, and has fairly recently been adapted for use in archaeology to detect protein residues on prehistoric artifacts. The CIEP technique is based on the immune (antigen-antibody) reaction. Extracts of protein residues from artifacts in an ammonia solution are tested against antisera from known animals. The solutions are placed on a gel substrate and exposed to an electric current, which causes the proteins to flow together. An immune reaction between the extract and the antiserum causes a precipitate to form, which is visible after being stained. A brief overview of the CIEP technique and an outline of AINW's laboratory procedures are included with this report.

The CIEP tests were conducted between February 14 and March 3, 2014, by laboratory director Dr. Cameron Walker. The extracts from the two artifacts were tested against bovine, camel, deer, and horse antisera. The bovine, deer, and horse antisera are forensic-grade antisera manufactured by MP Biomedicals, LLC. The camel antiserum is manufactured by Bethyl Laboratories. A chart included with this report shows the antisera that were used in the tests and the species found to react with each antiserum.

Standard analysis procedures began with extracting residues from the two artifacts in a 5% ammonia solution. The artifact extracts were then placed singly into gels, and tested against the antisera selected for these tests with the CIEP technique. In addition to the artifact extracts, positive and negative control sera were run with each gel. This was done to determine if there were any contaminants or extraneous proteins that may give false positive results. If an anomalous result such as an extract reacting with multiple antisera or to a negative control serum is obtained, the extract solution is mixed with an equal volume of a 1% solution of a non-ionic detergent to increase chemical bonding specificity, and is run through the CIEP process again. If a reaction still occurs after the addition of the non-ionic detergent, any reactions of those specimens to the antisera are discounted. None of the extracts analyzed for this project reacted with the negative control or with multiple antisera.

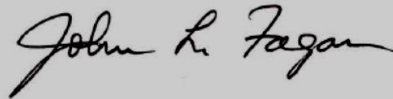
As shown on the attached table, there were positive reactions for both artifacts. Artifact #1 tested positive to bovine antiserum; Artifact #2 tested positive to camel antiserum. The

bovine antiserum reacts with species within the family Bovidae, which includes domestic cattle and bison. The camel antiserum reacts most strongly with camelids, but will also react more broadly within the Order Artiodactyla. Because two other families within the Order Artiodactyla were tested during this analysis (Bovidae and Cervidae), the positive result of Artifact #2 to camel antiserum suggests the presence of camelid residue, or possibly residue from an artiodactyl not classified within the families of Bovidae or Cervidae.

These positive reactions were confirmed by repeat analysis. It should be noted that the negative results from testing against the selected antisera do not preclude the possibility of the specimens retaining residues from other animals. The liquid extracts obtained from the artifacts have been frozen for storage and will be retained for one year should you wish any additional tests. Please call us if you have any questions about the analysis or this report.

Thank you for providing us the opportunity to run these tests. The results have proven to be of great interest to us.

Sincerely,



John L. Fagan, Ph.D., R.P.A.
President/Senior Archaeologist



Cam Walker, Ph.D.
Supervising Archaeologist/
Laboratory Director

Attachments

**ARCHAEOLOGICAL INVESTIGATIONS NORTHWEST, INC.
BLOOD RESIDUE ANALYSIS COMPARATIVE RESULTS**

Project: Parson's Island

RAL #	TYPE OF ANTISERUM			
	Bovine	Camel	Deer	Horse
1	+	-	-	-
2	-	+	-	-
GEL # (Artifact #1)	14/2175-1	14/2175-1	14/2175-2	14/2175-2
GEL # (Artifact #2)	14/2175-3	14/2175-3	14/2175-4	14/2175-4

Key: + = Positive; - = Negative

**ARCHAEOLOGICAL INVESTIGATIONS NORTHWEST, INC.
RESIDUE ANALYSIS LABORATORY
ANTISERUM CHART**

COMPANY	ANTISERUM	HOST	REACTS WITH
BLI*	BOTTLENOSE DOLPHIN	rabbit	Family Delphinidae: dolphins, less strongly with porpoises and toothed whales
	WHITE WHALE	rabbit	Family Monodontidae: belugas and narwhals, porpoises
	CAMEL	rabbit	Order Artiodactyla: camelids, bovids, cervids
BYT*	PIGEON	rabbit	Order Columbiformes: pigeons, doves
	DUCK	rabbit	Family Anatidae: swans, geese and ducks
CBI*	TROUT	rabbit	Subfamily Salmoninae: salmon, steelhead, rainbow trout, char
MP*	BEAR	goat	Family Ursidae: black bear, brown bear, grizzly
	BOVINE	goat	Family Bovidae: domestic cow, bison
	CAT	goat	Family Felidae: cat, mountain lion, lynx, bobcat
	CHICKEN	rabbit	Order Galliformes, Order Anseriformes, Order Columbiformes
	DEER	goat	Family Cervidae: white-tail and mule deer, elk, moose
	DOG	rabbit	Family Canidae: domestic dog, coyote, wolf
	GUINEA PIG	goat	Order Rodentia: guinea pig, porcupine, beaver
	HORSE	goat	Family Equidae: horse, donkey, mule, extinct equids
	MOUSE	goat	Order Rodentia: mice, rats
	RABBIT	goat	Family Leporidae: rabbit, jackrabbit
RAT	goat	Order Rodentia: rats, mice, squirrels	
SHEEP	goat	Genus Ovis: domestic sheep, bighorn sheep	
SIGMA*	HUMAN	goat	Order Primates: humans, apes, monkeys
	SHEEP	rabbit	Sheep and goat, bighorn sheep; less strongly with pronghorn, cervids, and bovids
	GOAT	rabbit	Bovoid Subfamilies Bovinae and Caprinae, less strongly with cervids

*Notes: BLI = Bethyl Laboratories, Inc., BYT = Biorbyt Laboratories, Inc., CBI = Cocalico Biologicals, Inc., MP = MP Biomedicals, LLC, Sigma = Sigma Chemical Laboratories.

ARCHAEOLOGICAL INVESTIGATIONS NORTHWEST, INC.
RESIDUE ANALYSIS LABORATORY
METHODS AND PROCEDURES

Blood protein residue analysis performed at the Archaeological Investigations Northwest, Inc. (AINW) Residue Analysis Laboratory uses the technique of cross-over immunoelectrophoresis (CIEP) to analyze protein residues extracted from the surface of stone artifacts and other objects. This technique has been widely used in forensic laboratories to determine the origin of bloodstains as evidence in criminal investigations, and has fairly recently been adapted for use in archaeology to detect protein residues on stone tools. The CIEP method used by the AINW Residue Analysis Laboratory is based on techniques developed by the Royal Canadian Mounted Police Serology Laboratory in Toronto, Ontario (Culliford 1971; Newman 1990; Williams 1990). The CIEP technique uses the immune (antibody-antigen) reaction, the principle that all animals produce immunoglobulin proteins (antibodies) that recognize and bind with foreign proteins (antigens) as part of the body's defense system. The ability of antibodies to precipitate antigens out of solution is the basis of CIEP analysis (Newman 1990:56). CIEP indicates the presence or absence of a particular antigen, and is not designed as a quantitative test. While other types of immunoassay have been used effectively to analyze blood protein residues under various conditions, the CIEP test is particularly suitable in that it is sensitive (able to detect protein in concentrations of about two parts per million), does not require expensive or bulky equipment, is relatively fast (about 48 hours per test), and can easily and efficiently accommodate multiple samples (Newman 1990:52).

BLOOD PROTEIN RESIDUES

Blood is composed of red and white blood cells and serum, which is composed of about 150 different proteins including albumin, alpha, and beta globulins. Immunoglobulins are large, Y-shaped proteins with antigen binding sites located on the V portion of the Y. There are several immunoglobulin molecules of different weight, size, and function. The most common type (and the most pertinent for CIEP) is immunoglobulin G (IgG). Other less common varieties are immunoglobulin A (IgA), immunoglobulin D (IgD), immunoglobulin E (IgE), and immunoglobulin M (IgM). Some of these proteins can survive in the environment in a nonfunctional but immunologically identifiable form for long periods of time by forming a "covalently cross-linked proteinaceous mass with a high molecular weight" (Marlar et al. 1995:30). This combination of protein, fatty tissues and soil particles is resistant to microbes and is markedly insoluble in water. It seems probable that porosity and surface roughness of the artifact also aids in the preservation of protein residues. Experiments by AINW and others have identified blood residues from mammoth, bison, musk ox, horse, caribou, bear, duck, and trout on Paleoindian artifacts that may be as old as 11,500 years (Forgeng 1998; Loy and Dixon 1998; Williams 1993). Other studies suggest that protein residues can survive in recognizable form for as long as 40,000 years (Prager et al. 1980).

Artifacts can be examined under a binocular microscope (at around 240 x maximum magnification) to identify probable residues, as well as cells, hair and other tissues. Microscopic examination is not always effective as a screening technique as CIEP can still detect otherwise invisible residues. A common medical test for occult blood is sometimes effective when used to screen the extracted residue solution. However, the CEIP technique can detect residues in more dilute concentrations than is possible with the commonly available occult blood test.

THE IMMUNE REACTION

Immunological forensic tests owe their effectiveness to the antigen-antibody reaction, which allows very specific recognition and identification. Essentially, any molecule that can bind to an antibody is an antigen. For archaeological purposes, the antigen is an unknown protein adhering to an artifact after its use. Antigens are foreign proteins that, when introduced into the blood stream of an animal, stimulate the immune system of the animal to produce antibodies (most commonly IgG protein molecules) with specific binding sites that match corresponding sites on the foreign antigen. Polyclonal antibodies, which bind to multiple sites on the antigen and therefore have a high rate of successful matching to unknown proteins, are the most commonly used reactants in CIEP. The meeting of antigen and antibody forms a very strong bond between the two proteins. The visible line formed in a positive CIEP reaction occurs when an antigen with multiple binding sites matches a group of polyclonal antibodies, binds with them, and causes the proteins to precipitate out of solution (Marlar et al. 1995:28).

Antigen-antibody reactions can be highly specific, although proteins from closely related species share enough of the same binding sites on the immunoglobulin molecule to react in similar ways. More distantly related species react less strongly. The purity of the antiserum used in the analysis is thus of primary importance in determining what species of animal is represented. Quantified analyses have been performed using more sophisticated techniques to test the similarity of immune reactions between related animal species, largely to determine relationships between living and extinct species (Lownstein 1980, 1985). These results and CIEP experiments performed by AINW and others indicate that CIEP can generally distinguish between blood proteins at approximately the taxonomic family level.

ANTISERA

The antisera used in AINW's CIEP analysis are obtained from commercial laboratories. A forensic antiserum is made by injecting a host animal, typically a goat or rabbit, with a protein solution obtained from another animal. The immune system of the host animal produces antibodies (mainly IgG) in reaction to the foreign antigen. Blood serum drawn from the host animal is purified and tested to determine the range of reactivity of the antiserum. The purified antiserum is then freeze-dried for storage and shipment. After receipt of a new lot of antiserum, the AINW laboratory routinely tests each antiserum against representative specimens from up to 32 different animal species.

AINW obtains forensic-grade bear, bovine, cat, chicken, deer, dog, guinea pig, horse, mouse, rabbit, rat, and sheep antisera from MP Biomedicals, LLC (MPB). Human and goat, antisera are manufactured by Sigma Chemical Corporation (Sigma). Bethyl Laboratories manufactures Camel antiserum, which will also react with pronghorn antelope residue. Duck and pigeon antiserum is obtained from Biorbyt Laboratories. Trout antiserum is manufactured by Cocalico Biologicals, Inc. (CBI). The bear, bovine, cat, deer, dog, horse, pigeon, and rabbit antisera react well within their own taxonomic family (Ursidae, Felidae, Cervidae, Canidae, Equidae, Columbidae, and Leporidae respectively) but do not react with blood proteins from animals from other taxonomic families. Experiments have shown that the deer antiserum reacts well with other cervids such as white-tail deer, mule deer, elk, and moose, but does not react with other artiodactyls such as domestic cows, bison, antelope, goat, or sheep. The MPB chicken antiserum reacts with members of four families of three orders of Superorder Neognathae. These include Phasianidae (pheasants, partridges and quail) and Tetraonidae (grouse) of Order Galliformes, Columbidae (doves and pigeons) of Order Columbiformes and Anatidae (geese, ducks, and swans) of Order Anseriformes. The MPB rat antiserum also reacts broadly at the level of Order Rodentia with many species of rats, mice, and squirrels. The MPB guinea pig antiserum also reacts with many rodents including beaver and porcupine. The MPB

sheep antiserum reacts with members of the Subfamily Ovidae including domestic sheep and bighorn sheep. Goat antiserum (Sigma) reacts strongest with sub-family Caprinae, which includes goat, sheep, chamois, and muskox. It will react more subtly with other artiodactyls within the Infraorder Pecora, specifically the families of Cervidae (deer) and Bovidae (cattle, goats, sheep, and antelope). The Sigma sheep antiserum reacts with members of Subfamily Ovidae, and less strongly with other bovids, cervids, and antilocaprids. The MPB and CBI trout antiserum reacts with members of the Genus *Oncorhynchus*: salmon, steelhead, rainbow trout. A chart included with this report shows the species found to interact with each antiserum.

THE AINW RESIDUE ANALYSIS LABORATORY

Ancient protein residues are often difficult to extract from the artifacts that have preserved them. The AINW Residue Analysis Laboratory uses a 5% ammonia solution, which has been used for similar applications in forensic medicine (Dorrill and Whitehead 1979; Kind and Cleevly 1969). Ammonia is generally more effective in lifting old and partially denatured blood proteins than other solvents (Newman 1990). A small amount of the ammonia solution is applied to the artifact in a plastic tray, and the tray and artifact are placed in an ultrasonic bath (Branson 2200) for 30 minutes or longer. The artifact in solution is then placed on a mechanical rotator (Thermolyne Rotomix) for an additional ten minutes. Artifacts too large for the ultrasonic extraction may be placed on the rotator for 30 minutes or longer. Residues from soil samples can also be extracted using variations of these methods. The extraction solution is then drawn off and stored in an airtight microcentrifuge tube. The extracts are centrifuged to clarify the sample, refrigerated, and the CIEP test is run as soon as possible after extraction. The extracts may be frozen immediately if testing is to be delayed for more than one week.

AINW's CIEP method uses an agarose gel as a substrate. Standard analysis procedures begin with extracting residues from the artifacts with a 5% ammonia solution. The artifact extracts are then placed singly into gels, and tested against the antisera selected for these tests with the CIEP technique. In addition to the artifact extracts, positive and negative control sera are run with each gel. This is done to determine if there are any contaminants or extraneous proteins that may give false positive results. If an anomalous result such as an extract reacting with multiple antisera or to a negative control serum is obtained, the extract solution is mixed with an equal volume of a 1% solution of a non-ionic detergent to increase chemical bonding specificity, and is run through the CIEP process again. If a reaction still occurs after the addition of the non-ionic detergent, any reactions of those specimens to the antisera are discounted. Experiments at AINW have implicated plant pitch used in hafting prehistoric stone tools as a possible cause of some cross or non-specific reactions.

Electrophoresis is used to drive the antigens and antibodies together. The gel substrates are placed in acrylic electrophoresis tanks filled with barbital buffer solution, then attached to the regulated H.V. power source. The antibodies move toward the cathode because of the overall negative charge on the molecule, while the antigens move toward the anode. A precipitate is formed where the proteins meet and bond in the area between the wells, visible as a white line or arc (Culliford 1971). The gel is soaked overnight in saline to stabilize the reaction, then dried and stained with a standard protein stain as a permanent record of the CIEP results. The dried and stained gel is then backlit on a light table, and examined under magnification for the presence of precipitate lines, indicating positive reactions.

After testing the extracts are refrozen and stored for one year in case additional testing is requested.

HINTS FOR ARTIFACT COLLECTION AND TREATMENT FOR RESIDUE ANALYSIS

For optimum results, the following suggestions are provided for archeologists considering submitting artifacts for blood residue analysis (see also Marlar et al. 1995:36)

1. Handle artifacts as little as possible in the field. Avoid contamination by using latex gloves, the tip of a clean trowel, or other careful methods similar to the treatment of radiocarbon samples.
2. Do not brush off, spit clean, or wash the artifact. Since proteins are known to bind to soil particles, loss of adhering dirt may result in loss of blood antigen.
3. Place the artifact in a clean ziplock bag with as little loose dirt as possible.
4. Submit a small amount (about one tablespoon) of soil from the area adjacent to the artifact. As bacteria or animal excreta in the soil may cause false positive reactions, soil controls are useful for cross checking results from artifacts.
5. Positive results have been obtained from projectile points, scrapers, flake tools, debitage, bone, burned bone, fire-cracked rock, cobble tools, ground stone tools, and soil samples from features and general site contexts. Surface artifacts are also good candidates for residue preservation. Obsidian, CCS, and basalt artifacts are equally likely to preserve residues, although some more porous materials may contain more proteins.
6. When selecting the type of antisera for analysis, consider allowing for a broad range of testing supplemented by more specific testing of positive results (for example, testing positives for chicken against duck and pigeon to narrow the results). If an artifact tests negative for all of the selected antisera, it may still contain preserved residues from other species.

REFERENCES

Culliford, Bryan J.

1971 *The Examination and Typing of Bloodstains in the Crime Laboratory*. National Institution of Law Enforcement and Criminal Justice, U.S. Printing Office, Washington, D.C.

Dorrill, Marion, and P. H. Whitehead

1979 The Species Identification of Very Old Human Bloodstains. *Forensic Science International* 13:111-116.

Forgeng, Eric

1998 *Blood Residue Analysis of Seven Crescents from Sonoma County, California*. Archaeological Investigations Northwest, Inc. Residue Analysis Report No. 97/399. Prepared for the Anthropological Studies Center, Sonoma State University, California.

Kind, S. S., and Rosalynd Cleevy

1969 The Use of Ammoniacal Bloodstain Extracts in ABO Groupings. *Journal of Forensic Sciences* 9:131-139.

Loy, Thomas, and E. James Dixon

1998 Blood Residues on Fluted Points from Eastern Beringea. *American Antiquity* 63(1):21-46.

Marlar, Richard A., Kathryn Puseman, and Linda Scott Cummings

1995 Protein Residue Analysis of Archaeological Materials: Some Comments on Criticisms and Methods. *Southwestern Lore* 61(2):27-37.

Newman, Margaret E.

1990 *The Hidden Evidence from Hidden Cave, Nevada: An Application of Immunological Techniques to the Analysis of Archaeological Materials*. Ph.D. Dissertation, Department of Anthropology, University of Toronto, Ontario, Canada.

Prager, E. M., A. C. Wilson, J. M. Lowenstein, and V. M. Sarich

1980 Mammoth Albumin. *Science* 209:287-289.

Williams, Shirley B.

1990 *Immunology and Archaeology: Blood Residue Analysis of Three Sites*. Unpublished Masters Thesis, Department of Anthropology, Portland State University, Portland, Oregon.

1993 *Blood residue Analysis of a Clovis Point from the Needles, California Resource Area*. Archaeological Investigations Northwest, Inc. Residue Analysis Laboratory Letter Report No. 93/144. Prepared for the USDI Bureau of Land Management, Needles, California.

APPENDIX II:

Luminescence Dating of Sediments from Parsons Island, Chesapeake Bay.

LUMINESCENCE DATING OF SEDIMENTS FROM PARSON'S ISLAND, CHESAPEAKE BAY

13 May 2021
James Feathers
Luminescence Dating Laboratory
University of Washington
Seattle, WA 98195-3412
jimf@uw.edu

Six sediment samples from a sandy bluff overlooking Chesapeake Bay on Parson's Island, Maryland, were submitted for luminescence dating by Christopher Moore, University of South Carolina. This is part of a project directed by Derrin Lowery of the Smithsonian Institution. The samples are from pedogenically modified loess and sand deposits. A buried paleosol has yielded artifacts and radiocarbon dates of 20-21 ka. Sample information is given in Table 1. The paleosol is located just under horizon 3Cgb2. Laboratory procedures are given in the appendix.

Table 1. Samples

Lab sample #	Soil horizon	depth (m)	C-14 age (calibrated BP)
UW3800	Base of Bt	0.65	
UW3801	2Btb2	1.00	
UW3802	2BCgb	1.30	
UW3803	3Cgb1	1.60	
UW3804	3Cgb2	1.80	20525 ± 341
UW3805	5Cgb	3.65	> 30196 ± 264

Dose Rate

Dose rate was measured as described in the appendix. Table 2 gives the concentration of the major radionuclides, and the beta dose rate calculated in two ways. The beta dose rate is calculated from flame photometry and alpha counting, assuming secular equilibrium, and also is derived directly from beta counting. These are within 1-sigma error terms for the top four samples, but there is a discrepancy for the bottom two samples, with the beta counting giving a lower value. A possible reason is disequilibrium in the U decay chain. The K contents are low, so a large portion of the beta dose rate is coming from the decay chains. In cases of disequilibrium, the alpha counting can be in error. The radionuclide concentration also increases with depth, perhaps because of downward movement of clay. The water carrying the clay could also be carrying soluble radionuclides from the U decay chain, perhaps leading to disequilibrium. Because beta counting is a more direct measure of dose rate, the beta counting results were used in age calculation for these two samples.

If radionuclides have moved through time, then it is possible for the dose rate to have changed through time. If radionuclides are moving down the effect on lower samples will be to make them older.

Measured moisture contents for all samples ranged from 8.7 to 20.2%. An average of $15 \pm 5\%$ was used for all samples. Total dose rates are given in Table 3..

Table 2. Radioactivity

Sample	^{238}U (ppm)	^{233}Th (ppm)	K (%)	Beta dose rate (Gy/ka)	
				β -counting	α -counting/ flame photometry
UW3800	2.53±0.19	8.29±1.19	0.82±0.02	1.25±0.10	1.28±0.05
UW3801	2.02±0.15	6.34±0.93	0.33±0.01	0.82±0.07	0.74±0.04
UW3802	1.58±0.15	8.76±1.10	0.44±0.07	0.83±0.09	0.84±0.07
UW3803	2.50±0.21	11.25±1.38	1.02±0.03	1.62±0.18	1.51±0.06
UW3804	3.16±0.23	10.98±1.39	1.60±0.14	1.68±0.17	2.08±0.13
UW3805	0.88±0.16	13.78±1.53	1.03±0.06	1.00±0.09	1.35±0.07

Table 3. Total dose rates

Sample	alpha	beta	gamma	cosmic	total
UW3800	0.01±0.01	0.93±0.06	0.76±0.06	0.18±0.04	1.87±0.09
UW3801	0.01±0.01	0.52±0.04	0.52±0.05	0.16±0.03	1.22±0.07
UW3802	0.01±0.01	0.59±0.06	0.60±0.06	0.16±0.03	1.36±0.09
UW3803	0.01±0.01	1.10±0.07	0.91±0.07	0.15±0.03	2.18±0.11
UW3804	0.01±0.01	1.34±0.12	0.78±0.08	0.15±0.03	2.27±0.15
UW3805	0.01±0.01	0.81±0.06	0.43±0.07	0.12±0.03	1.36±0.10

Equivalent dose

Equivalent dose was measured using OSL on 180-212µm single grains of quartz. Table 4 gives the number of grains measured, those rejected for various reasons, the number of accepted grains, and the ratio of accepted to measured. The samples were relatively insensitive, the average acceptance rate being only 6.4%. More than 7000 grains were measured to achieve a statistically acceptable number of good grains.

Table 4. Acceptance rates*

Sample	N	No signal	Failed Recycle	Too high	Feldspar	Recuperation/ Zero dose	Accepted	Rate (%)
UW3800	1274	1115	25	5	34	15	80	6.3
UW3801	1182	1031	25	6	24	10	86	7.3
UW3802	1479	1338	26	8	25	14	68	4.6
UW3803	1179	863	23	6	28	12	81	6.9
UW3804	987	856	20	9	18	19	65	6.6
UW3805	1182	1005	34	10	38	10	85	7.2
Total	7283	6208	153	44	167	78	465	6.4

* “No signal” refers to grains that lacked a measurable signal, as judged by an error greater than 30% on the test dose or a natural signal that was not at least three standard deviations above background. The other criteria for rejection were for those grains where the designated criterion was the only problem. “Failed recycle” refers to grains where the recycle ratio did not fall within 0.8 and 1.2. “Feldspar” refers to grains that were deemed to be feldspars due to loss of signal from an infrared stimulation after two regeneration points. “Recuperation” refers to grains where the signal from a zero dose was more than 10% of the natural signal and the decay curve showed a definite downward slope. “Too high” refers to grains where the natural signal was larger than the signal from the highest regeneration dose and thus did not intersect the growth curve. “Zero dose” refers to grains where the derived equivalent dose was not significantly different from zero. All grains falling under these criteria were rejected for analysis.

A dose recovery test was done on 200 grains from UW3803 and UW3804. In this test, grains are first set to zero by exposure to the laser and then given a known dose. The SAR procedure (see appendix) is then applied to see if this known dose can be obtained. Only 57 grains produced a measurable signal, but the ratio of derived to given dose was 0.98 ± 0.03 , which is satisfactory. Over-dispersion was 8%.

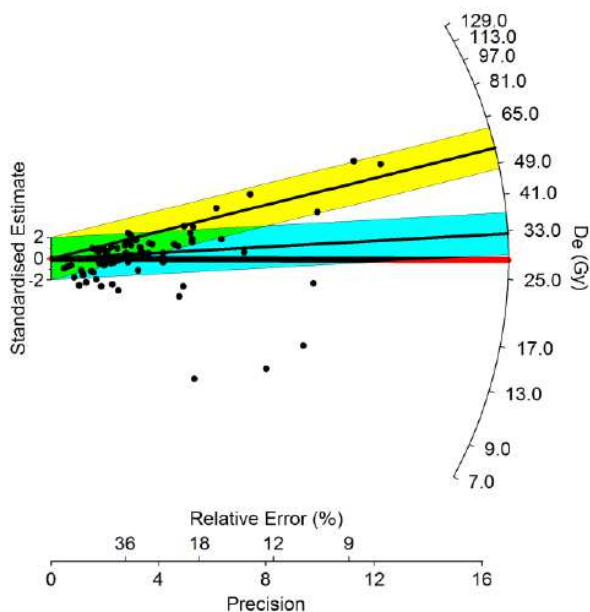
Table 5 gives the equivalent dose in terms of the central age model and the finite mixture model, as explained in the appendix. The central age model is used for samples that are well-bleached and unmixed. Also given in the table is the over-dispersion (spread in values beyond that which can be explained by differential precision). Because the over-dispersion for most samples is higher than what is likely typical for a single-aged sample, a finite mixture model was applied. This is appropriate for mixed samples and provides structure by dividing the distribution into single-aged components. Specifying an over-dispersion value considered typical of a single age sample is required. The over-dispersion from the dose recovery test can be used as a minimum for the typical over-dispersion since all grains in the test received the same dose. It is only a minimum for a single-age, however, because all grains in the natural sample may not have received the same dose due to micro-variations in the beta dose rate. A likely cause of such variation in these samples is the distribution of potassium feldspars that provide beta irradiation from ^{40}K . The K-feldspars cannot be assumed to provide a uniform dose through the deposit because they are relatively rare (see Table 2). Mayya et al. (2006) provide a model, based on the K content, for determining possible differences in dose rates to different grains. A 10% over-dispersion, somewhat higher than from dose recovery, was applied in the finite mixture model. The samples divided into from two to four components. Table 5 gives the values and proportions for the two most abundant. Considering the Mayya model, all components in each sample were too far apart in value to be explained by micro-dosimetry. They must represent some kind of mixture, which is not uncommon for sandy deposits along the Atlantic coast. By increasing the over-dispersion for the finite mixture model to 15%, the number of components and the value for each component changed little. The one exception was for UW3801, where three components were defined instead of four. The second and third components at 10% over-dispersion (values given in Table 5) were combined into one component at 15% with a value of 22.1 ± 1.22 Gy representing 82% of the grains.

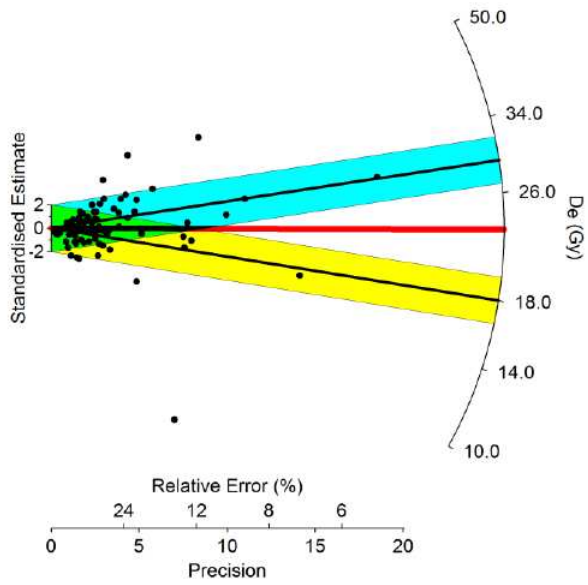
Table 5. Equivalent dose

Sample	N	Central age Model (Gy)	Over-dispersion (%)	Finite Mixture Model Model (Gy)	
				Largest component (%)	Next largest component (%)
UW3800	80	28.2±2.20	57.0±6.4	32.7±3.80 (60.4)	53.7±7.55 (21.5)
UW3801	86	22.8±1.75	55.4±6.5	28.7±1.96 (50.1)	17.6±1.36 (40.7)
UW3802	68	28.4±1.74	30.0±5.9	28.9±1.21 (97.8)	74.5±11.9 (2.2)
UW3803	81	33.0±3.39	82.7±7.9	52.7±1.89 (74.0)	13.4±0.75 (23.2)
UW3804	65	13.3±2.55	145.2±14.3	55.9±3.65 (43.4)	2.59±0.18 (38.0)
UW3805	85	26.2±2.06	55.2±6.7	19.3±1.39 (49.5)	33.1±2.18 (35.9)

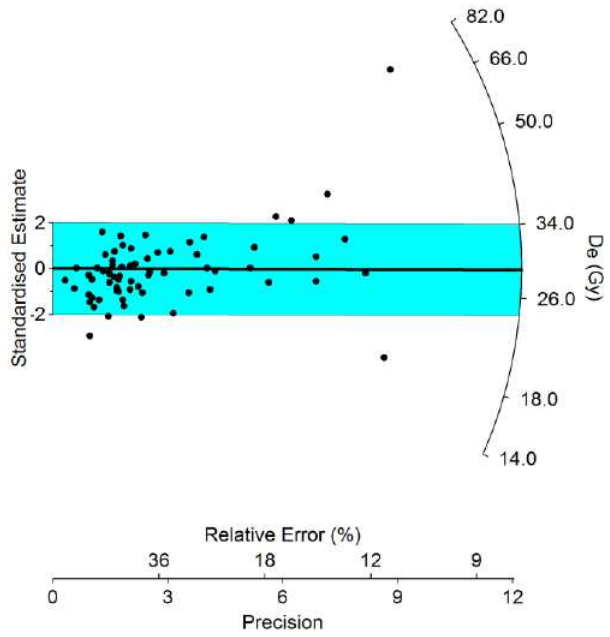
The equivalent dose values for each sample are displayed in radial graphs (Figure 1). Radial graphs plot precision against equivalent dose, the latter normalized by the number of standard errors the value is from some reference. More precise points are plotted toward the right. The measured doses are scaled on the right axis and can be determined for any point by the intersection of a line drawn from the origin through the point. The references used are the two most abundant components of the finite mixture model, with blue (most abundant) and yellow (next most abundant) shading, and the central age model (red line). The shading encompasses all points within two standard errors of the reference. An exception is for UW3802 where only the most abundant component (98% of grains) is referenced because it is nearly a single-aged sample. No over-dispersion typical for a single aged sample is assumed in these graphs

Figure 1

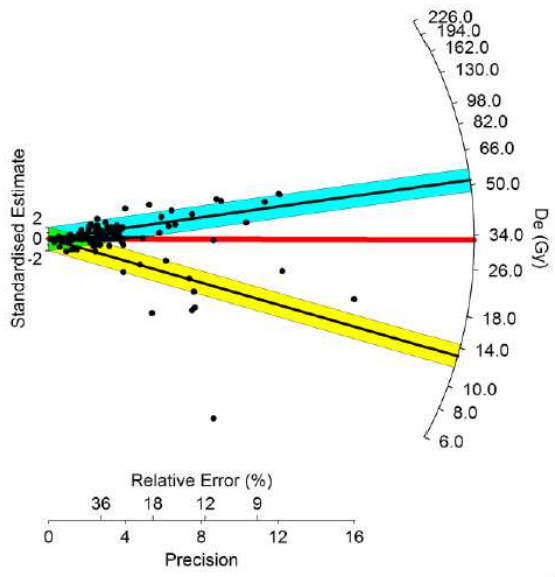




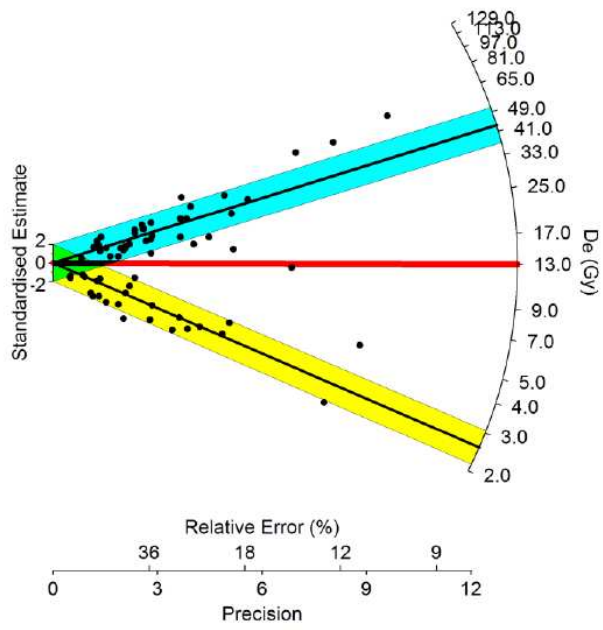
UW3801



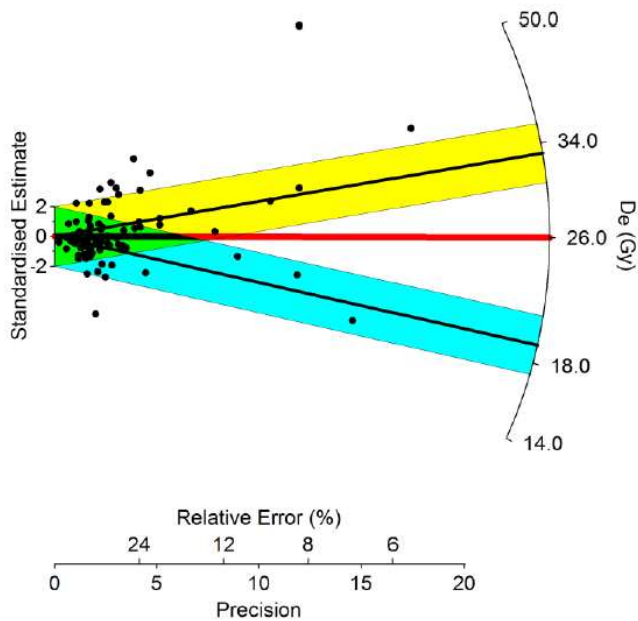
UW3802



UW3803



UW3804



UW3805

Ages

Best estimates of the ages are given in Table 6.

The most straightforward sample is UW3802, which is nearly single-aged, with 98% of the grains consistent with a single-value. It can be used as a stratigraphic benchmark to evaluate the other samples. Next best is UW3801. Although the radial graph shows some bimodality, close examination shows that all but one of the grains in the yellow-shaded reference are close to the blue shading. If using an over-dispersion of 15% for the finite mixture model, both of these referenced components combine into a single component. The two components together account for 90% of the grains, so this sample is also nearly single-aged. Both UW3800 and UW3803 are dominated by one component but contain a smattering of younger grains. If this component is used for the age, then all of the top four samples (UW3800-UW3803) are in the right stratigraphic order and are consistent with the radiocarbon ages. The highest sample, UW3800 is 15-20 cm below a Pt anomaly which has been dated in other places to 12.8 ka, so the ages are also consistent with that.

There are more problems with the bottom two samples. UW3804 has a very low central age equivalent dose value. If this was used for the age, a value of 5.8 ka would be obtained, much too young for its stratigraphic position and inconsistent with the radiocarbon ages. So there appears to be a lot of anomalously young grains in this sample. There is one component, the 3rd, however, that yields an age of 24.6 ± 2.40 ka, which is stratigraphically consistent and in agreement with the radiocarbon ages obtained near this sample. But this component contains only 43% of the grains. A look at the radial graphs shows a strongly bimodal distribution. If the very young component is discounted, then the 3rd component contains 70% of the remaining grains. The central age model would certainly be a bad choice for the age in this sample because very few grains are consistent with it. The 3rd component therefore represents the most likely estimate for the age, but the question arises of where all those young grains came from. They are not present to any large degree in the upper samples. A possibility is that a portion of the sample was inadvertently exposed to light either during collection or in lab preparation, but there is no clear evidence for either. Another possibility is that a burrowing animal brought some young grains down, but this sample is quite deep, nearly 2 m. The young grains appear anomalous.

UW3805 also has a lot of young grains. The second component, which contains 50% of the grains, gives an age less than 15 ka. The third component (with only 38% of the grains) gives an age in agreement with the age from UW3804, but UW3805 is nearly 2 m deeper. Unless there was a very fast deposition, much faster than what is apparent for the upper part of the deposit, this age is likely an under-estimate. There is a small proportion of older grains, which make up component 4. This contains only 13% of the grains, but it does yield a perhaps more realistic age of 57 ka. Because only a few grains are consistent with this age, not much confidence can be placed in it. Like UW3804 this sample raises the question of where all the young grains came from – in this case most of the grains.

The dose rate for the deeper samples could also be over-estimated if radionuclides have been transferred downward, making the measured dose rate now higher than the average dose rate. An over-estimated dose rate will result in an under-estimated age. Because the ages for the upper samples and also for the 3rd component of UW3804 are consistent with independent dating evidence, it is not likely this is a major factor

Table 6. Ages

Sample	Age (ka)	Basis for age
UW3800	17.4±2.27	2 nd Component -- 60% of grains
UW3801	19.3±1.56	2 nd &3 rd components – 90% of grains
UW3802	21.2±1.78	1 st component – 98% of grains
UW3803	24.2±1.64	3 rd component – 74% of grains
UW3804	24.6±2.40	3 rd component – 43% of grains
UW3805	57.2±7.08*	4 th component – 13% of grains

* This age is not reliable

Procedures for Luminescence Analysis of Coarse-grained Quartz from Sediment Samples

Sample preparation

Sample material is removed from the collection container, leaving aside any portions (such as the ends of tubes) that may have been exposed to light. The latter may be used for dose rate information. From the unexposed portions, about $\frac{1}{4}$ is set aside as a voucher (material that can be used at a latter date if necessary). If separate samples for measuring moisture content have not been collected, the voucher can be used for this. For moisture the sample is simply weighed wet, and then dried for several days at 50°C before weighing again. The wet minus the dry weight divided by the dry weight gives the percent moisture by weight.

Remaining unexposed material is separated into size fractions by sieving. If the material contains abundant silt or clay, the sample is wet sieved through a 90 μ m screen. Otherwise it is sieved dry. The greater than 90 μ m fraction is treated with HCl and H₂O₂, rinsed three times with water and dried. It is then dry sieved to retrieve the 180-212 μ m fraction (or any other fraction deemed appropriate). This fraction is density separated using a lithium metatungstate solution of 2.67 specific gravity, saving the light fraction. This is then etched for 40 minutes in HF and then rinsed with water, HCl and water again. After drying, it is passed through the 180 μ m screen to remove any degraded feldspar.

Equivalent dose

Grains are placed in specially-manufactured disks for single-grain measurement. Luminescence is measured on a Risø TL/OSL-DA-20 reader with single-grain attachment. Stimulation is by a 532nm laser delivering 45 W/cm². Detection is through 7.5 mm U340 (ultraviolet) filters. Exposure is for 0.8s on each grain at 125°C. The first 0.06s is used for analysis and the last 0.15s for background. A preheat of 240°C for 10 seconds follows each dose, except for the calibrating test doses after which a 200°C for 1 second preheat is employed. The test dose employed is about 5 Gy. Doses are delivered by a ⁹⁰Sr beta source which provides about 0.1 Gy per second to coarse-grained quartz.

Equivalent dose (D_e), which is a measure of the total absorbed dose through time, is determined using the single-aliquot regenerative dose (SAR) protocol (Murray and Wintle 2000, Wintle and Murray 2006). The SAR method measures the natural signal and the signal from a series of regeneration doses on a single aliquot. The method uses a small test dose to monitor and correct for sensitivity changes brought about by preheating, irradiation or light stimulation. SAR consists of the following steps: 1) preheat, 2) measurement of natural signal (OSL or IRSL), L(1), 3) test dose, 4) cut heat, 5) measurement of test dose signal, T(1), 6) regeneration dose, 7) preheat, 8) measurement of signal from regeneration, L(2), 9) test dose, 10) cut heat, 11) measurement of test dose signal, T(2), 12) repeat of steps 6 through 11 for various regeneration doses. A growth curve is constructed from the L(i)/T(i) ratios and the

equivalent dose is found by interpolation of $L(1)/T(1)$. A zero regeneration dose and a repeated regeneration dose are employed to insure the procedure is working properly.

An advantage of single-grain dating is the opportunity to remove from analysis grains with unsuitable characteristics by establishing a set of criteria grains must meet. Grains are eliminated from analysis if they (1) had poor signals (as judged from errors on the test dose greater than 30 percent or from net natural signals not at least three times above the background standard deviation), (2) did not produce, within 20 percent, the same signal ratio (often called recycle ratio) from identical regeneration doses given at the beginning and end of the SAR sequence, suggesting inaccurate sensitivity correction, (3) yielded natural signals that did not intersect saturating growth curves, (4) had a signal larger than 10 percent of the natural signal after a zero dose, (5) produced a zero D_e (within 1-sigma of zero), or (6) contained feldspar contaminates (judged visually on growth curves by a reduced signal from infrared stimulation before the OSL measurement; done on two doses to lend confidence the reduction in signal is due to feldspar contamination).

A dose recovery test is performed on some grains. The luminescence of the grains is first removed by exposure to the laser (using the same parameters mentioned earlier). A dose of known magnitude is then administered. The SAR procedure is then applied to see if the known dose can be obtained. Successful recovery is an indication that the procedures are appropriate.

A D_e value is obtained for each suitable grain. Because of varying precision from grain to grain, the same value is not obtained for each grain even if all are of the same age. Instead a distribution is produced. The common age model and central age model of Galbraith (Galbraith et al. 1999, 2005) are statistical tools used in evaluation of D_e distributions. These models are used in reference to D_e and not “age” per se, although dividing the D_e values by the bulk dose rate provides an “age” for each grain (not accounting for differential dose rates for individual grains). The common age model controls for differential precision by computing a weighted average using $\log D_e$ values. The central age model is similar except rather than assuming a single true value it assumes a natural distribution of D_e values, even for single-aged samples, because of non-statistical sources of variation. It computes an over-dispersion parameter (σ_b) interpreted as the relative standard deviation (or coefficient of variance) of the *true* D_e values, or that deviation beyond what can be accounted for by measurement error. Empirical evidence suggests that σ_b of between 10 to 20 percent are typical for single-aged samples (Olley et al. 2004, Jacobs et al. 2006). For samples of mixed ages, either a minimum age model or a finite mixture model is employed for evaluation. The minimum age (Galbraith et al. 1999) calculates a statistical minimum using a truncated normal distribution and is suitable for partially bleached samples. Finite mixture model (Roberts et al. 2000) uses maximum likelihood to separate the grains into single-aged components based on the input of a given σ_b value and the assumption of a log normal distribution of each component. The model estimates the number of components, the weighted average of each component, and the proportion of grains assigned to each component. The model provides two statistics for estimating the most likely number of components, maximum log likelihood (l_{lik}) and Bayes Information Criterion (BIC). The finite mixture model is appropriate for samples that have been post-depositionally mixed (although with limitations).

APPENDIX III:

Soil Profile Descriptions for Parsons Island, Maryland.

During the period between 2013 and 2020, the stratigraphy at five locations along the eroded margins of Parsons Island were described in detail by Dr. Dan Wagner. A sixth location was described by Dr. John Wah at the location of the Smithsonian Institution's 2017 test excavation. However, Wah's profile description has not been transcribed and submitted at the time of this publication.



Appendix III; Figure 1: The original locations of the bank profile descriptions at Parsons Island have been plotted on the 2019 satellite image of the region.

NORTH PROFILE (10-10-2016): The GPS location is 38°54'30.39"N; 76°14'56.33"W and as of 6-20-2021, the original profile location is currently located ~3 meters (~10 feet) offshore.

Parsons Island Soil Profile Description, ~40 Meters North of 18QU1047 (10-10-2016)

Horizon	Depth (cm)	Properties
Ap	0-20	Brown (10YR 4/3) loam; weak, medium granular structure; friable consistence; abrupt, smooth boundary
E	20-27	Yellowish brown (10YR 5/4) fine sandy loam; weak, medium platy structure; friable consistence; clear, smooth boundary
BE	27-40	Dark yellowish brown (10YR 4/6) fine sandy loam; weak, medium subangular blocky structure; friable consistence; clear, smooth boundary
Bt	40-80	Strong brown (7.5YR 4/6) and dark yellowish brown (10YR 4/6) fine sandy loam to loam; weak to moderate, medium to coarse subangular blocky structure; nearly continuous clay films; friable consistence; clear, smooth boundary
2Btxb	80-137	Strong brown (7.5YR 4/6) and dark yellowish brown (10YR 4/6) silt loam; many, large distinct depletions of light brownish gray (10YR 6/2); moderate, coarse prismatic parting to weak, medium platy structure; nearly continuous clay films of brown (7.5YR 4/4) on prism and plate faces; firm consistence; gradual, smooth boundary
2Btxgb	137-165	Light brownish gray (2.5Y 6/2) loam; many, large distinct concentrations of brownish yellow (10YR 6/6); moderate, very coarse prismatic parting to weak, medium platy structure; patchy clay films; very firm consistence; clear, smooth boundary
2BCb	165-180	Dark yellowish brown (10YR 4/6) loam; common, large distinct depletions of light brownish gray (10YR 6/2); weak, very coarse prismatic parting to weak, medium platy structure; friable consistence; abrupt, smooth boundary
4C	180-195	Dark yellowish brown (10YR 4/4) loamy fine sand; weak, coarse platy structure; very friable consistence; abrupt, smooth boundary
5Bwb1	195-215	Dark yellowish brown (10YR 4/6) fine sandy loam to loamy sand; weak, very coarse prismatic parting to weak, very coarse platy structure; friable consistence; clear, smooth boundary
5Bwb2	215-235	Strong brown (7.5YR 4/6) fine sandy loam; weak, very coarse prismatic parting to weak, very coarse platy structure; friable consistence; clear smooth boundary

6C	235-257	Yellowish brown (10YR 5/6) fine sandy loam; structureless, massive; very friable consistence; clear smooth boundary
6Cg	257-297+	Grayish brown (2.5Y 5/2) fine sandy loam to loamy sand; structureless, massive; very friable consistence

Other comments: Profile was described ~ 40 m north of the location where bipoints were retrieved from a 4Ab horizon at the depth of 231 cm; from that location the buried surface horizon rises northward to eventual extinction and is not morphologically present in this profile; compositionally and stratigraphically, it may correlate with the 2Btxgb horizon at the depth of 137 cm; surficial Paw Paw Loess of Younger Dryas age has only a meager presence limited to some mixing in the plow zone; tillage-induced deflation is likely a factor; the 4C horizon is possibly a buried surface that has lost the typical dark coloration; described and sampled by D.P. Wagner and J.E. Clemens, 10/10/16

18QU1047 PROFILE (8-8-2013): The GPS location is 38°54'28.93"N; 76°14'55.81"W and as of 6-20-2021 the original profile location is currently located ~17 meters (~56 feet) offshore.

Parsons Island (18QU1047) Soil Profile Description (8-8-2013)

Horizon	Depth (cm)	Properties
Ap	0-28	Dark brown (10YR 3/3) silt loam; weak, medium granular structure; friable consistence; abrupt, smooth boundary
E	28-39	Brown (10YR 5/3) silt loam; weak, fine subangular blocky structure; friable consistence; clear, smooth boundary
BE	39-48	Dark yellowish brown (10YR 4/4) and brown (10YR 5/4) silt loam; weak, medium subangular blocky structure; friable consistence; clear, smooth boundary
Bt	48-67	Dark yellowish brown (10YR 4/4) silt loam to loam; many, medium distinct iron concentrations of strong brown (7.5YR 4/6), and few, fine distinct depletions of light brownish gray (10YR 6/2); moderate, medium subangular blocky structure; nearly continuous clay films; friable consistence; clear, smooth boundary
2Btb1	67-88	Dark yellowish brown (10YR 4/6) loam to fine sandy loam; many, large distinct depletions of light brownish gray (10YR 6/2); moderate, coarse platy parting to weak to moderate, coarse subangular blocky structure; patchy clay films; few small pebbles; friable consistence; clear, smooth boundary
2Btb2	88-127	Strong brown (7.5YR 4/6) fine sandy loam; moderate, coarse platy parting to moderate, coarse angular blocky structure; nearly continuous clay films of brown (7.5YR 4/4); pockets of light brownish gray (10YR 6/2) fine sand; friable consistence; clear, wavy boundary
2BCgb	127-168	Yellowish red (5YR 4/6) and strong brown (7.5YR 4/6) degrading B-bodies of fine sandy loam to loamy fine sand (~60%), and grayish brown (10YR 5/2) loamy fine sand (~40%); weak, coarse angular blocky structure; patchy clay films; friable and very friable consistence; clear, wavy boundary
3Cg1	168-189	Gray (5Y 6/1) silt loam, many, large prominent iron concentrations of strong brown (7.5YR 4/6); moderate, medium platy sediment structure; friable consistence; clear, smooth boundary
3Cg2	189-217	Gray (5Y 6/1) silt loam; common, medium faint concentrations of grayish brown (2.5Y 5/2); structureless, massive; friable consistence; clear, smooth boundary

4Ab1	217-231	Dark gray (2.5Y 4/1) heavy silt loam; moderate, very coarse prismatic breaking to weak, coarse platy structure; prism faces are dark yellowish brown (10YR 4/4); friable to firm consistence; clear smooth boundary
4Ab2	231-252	Black (2.5Y 2.5/1) heavy silt loam; moderate, very coarse prismatic structure; prism faces are dark yellowish brown (10YR 4/4); firm consistence; clear smooth boundary
4Bwgb	252-288	Gray (5Y and 2.5Y 5/1) heavy silt loam; common, large distinct iron concentrations of olive (2.5Y 4/4); moderate, very coarse prismatic structure; firm consistence; abrupt, wavy boundary
5C	288-299	Yellowish red (5YR 4/6) and gray (5Y 5/1) fine sandy loam; weak, coarse platy sediment structure; several gravels; variable cementation; friable and firm consistence; abrupt, wavy boundary
5Cg	299-330+	Gray (2.5Y 5/1) loamy fine sand; structureless, massive; friable consistence

Other comments: Profile was described ~ 5 m north of the location where a bipoint was retrieved from the 4Ab1 horizon; upper 67 cm are interpreted to be Younger Dryas in age (Paw Paw Loess); from laboratory particle size analyses visibly high mica contents in the very fine sand fractions of the 3Cg and 4Bwgb horizons suggest these materials are earlier loess deposits likely derived from the Susquehanna paleofloodplain; also, an increase in silt and some mica in the 2BCgb horizon may indicate partial mixing with the underlying stratum; thickness of the 2Bb sequence varies along the beach exposure in relation to the level of the 4Ab horizon, and is as much as 1.75 m thick where the buried surface is the lowest; described and sampled by D.P. Wagner, 8/8/13

ROCK FEATURE PROFILE (10-2-2020): The GPS location is 38°54'25.66"N; 76°14'52.73"W and as of 6-20-2021, the original profile location is currently located ~2 meters (~7 feet) offshore.

Parsons Island Soil Profile Description, Rock Feature (Cairn) Location (10-2-2020)

Horizon	Depth (cm)	Properties
Ap	0-29	Dark brown (10YR 3/3) silt loam to loam; weak, medium granular structure; friable consistence; abrupt, smooth boundary
E	29-37	Brown (10YR 5/3) silt loam to loam; weak, fine subangular blocky structure; friable consistence; clear, smooth boundary
BE	37-42	Dark yellowish brown (10YR 4/4) and brown (10YR 5/4) silt loam to loam; weak, medium subangular blocky structure; friable consistence; clear, smooth boundary
Bt	42-53	Dark yellowish brown (10YR 4/4) silt loam to loam; moderate, medium subangular blocky structure; nearly continuous clay films; friable consistence; clear, smooth boundary
2Btb	53-88	Strong brown (7.5YR 4/6) fine sandy loam; very coarse prismatic breaking to moderate, coarse platy and moderate, coarse angular blocky structure; nearly continuous clay films of brown (7.5YR 4/4); friable consistence; clear, smooth boundary
3BCb	88-138	Light olive brown (2.5Y 5/3) silt loam to very fine sandy loam; very coarse prismatic breaking to moderate, fine platy structure; friable consistence; clear, smooth boundary
4BCb	138-168	Strong brown (7.5YR 5/6) silt loam; many, medium prominent depletions of light olive brown (2.5Y 5/3); very coarse prismatic structure; friable consistence; clear, smooth boundary
5BCb	168-190	Light yellowish brown (2.5Y 6/3) very fine sandy loam; common, medium distinct concentrations of dark yellowish brown (10YR 4/4); very coarse prismatic structure; friable consistence; clear, smooth boundary
6BCb	190-230	Strong brown (7.5YR 5/6) very fine sandy loam to silt loam with bands of light olive brown (2.5Y 5/3); very coarse prismatic structure; friable consistence; clear, smooth boundary
7BCb	230-245+	Light olive brown (2.5Y 5/3) very fine sandy loam; very coarse prismatic structure; friable consistence

Other comments: The profile is located ~103 m south of the test unit location; the upper 5 horizons have properties similar to those in the vicinity of the test unit, but the sequence is compressed from a thickness of 168 cm to 88 cm; the underlying sequence of BC horizons with alternating textures of very fine sandy loam and silt loam are somewhat unique compared to much of the island, but are still readily consistent with an eolian origin; minimum pedogenetic alteration suggests that even the uppermost BC horizon may have been significantly deeper beneath a former paleolandscape, and that this landscape was possibly truncated as much as a meter or more prior to deposition of the Younger Dryas Paw Paw Loess; the artifact-bearing stratum (rock-feature) is ~214 to 223 cm beneath the modern ground surface and associated with the 6BCb soil horizon; the location is thus more favorably drained, and what originally were former surfaces no longer exhibit dark colorations; in such circumstances buried surfaces can actually appear light in color; described by D.P. Wagner, 10/2/20

SOUTH PROFILE (8-8-2013): The GPS location is 38°54'23.23"N; 76°14'53.52"W and as of 6-20-2021, the original profile location is currently located ~32 meters (~105 feet) offshore.

Parsons Island Soil South Profile Description (8-8-2013)

Horizon	Depth (cm)	Properties
Ap	0-28	Dark brown (10YR 3/3) silt loam; weak, medium granular structure; friable consistence; abrupt, smooth boundary
E	28-37	Brown (10YR 5/3) silt loam; weak, fine subangular blocky structure; friable consistence; clear, smooth boundary
BE	37-46	Dark yellowish brown (10YR 4/4) and brown (10YR 5/4) silt loam; weak, medium subangular blocky structure; friable consistence; clear, smooth boundary
Bt	46-61	Dark yellowish brown (10YR 4/4) silt loam to loam; many, medium distinct iron concentrations of strong brown (7.5YR 4/6), and few, fine distinct depletions of light brownish gray (10YR 6/2); moderate, medium subangular blocky structure; nearly continuous clay films; friable consistence; clear, smooth boundary
2Btb1	61-93	Dark yellowish brown (10YR 4/6) loam to fine sandy loam; many, large distinct depletions of light brownish gray (10YR 6/2); weak to moderate, coarse subangular blocky structure; patchy clay films; few small pebbles w/varnish; friable consistence; clear, smooth boundary
2Btb2	93-160	Strong brown (7.5YR 4/6) fine sandy loam; moderate, coarse angular blocky structure; nearly continuous clay films of brown (7.5YR 4/4); pockets of light brownish gray (10YR 6/2) fine sand; friable consistence; clear, wavy boundary
2BCb	160-249	Yellowish red (5YR 4/6) and strong brown (7.5YR 4/6) degrading B-bodies of fine sandy loam to loamy fine sand; weak, coarse angular blocky structure; patchy clay films; friable and very friable consistence; clear, wavy boundary
3Cgb1	249-264	Gray (5Y 6/1) silt loam, many, large prominent iron concentrations of strong brown (7.5YR 4/6); moderate, medium platy sediment structure; friable consistence; clear, smooth boundary
3Cgb2	264-290	Gray (5Y 6/1) silt loam; common, medium faint concentrations of grayish brown (2.5Y 5/2); structureless, massive; friable consistence; clear, smooth boundary

4Ab1	290-303	Dark gray (2.5Y 4/1) heavy silt loam; moderate, very coarse prismatic breaking to weak, coarse platy structure; prism faces are dark yellowish brown (10YR 4/4); friable to firm consistence; clear smooth boundary
4Ab2	303-318	Black (2.5Y 2.5/1) heavy silt loam; moderate, very coarse prismatic structure; prism faces are dark yellowish brown (10YR 4/4); firm consistence; clear smooth boundary
4Bwb	318-332	Yellowish red (5YR 4/6) heavy silt loam; common, large distinct iron concentrations of olive (2.5Y 4/4); moderate, very coarse prismatic structure; firm consistence; abrupt, wavy boundary
5Ab	332-343	Black (2.5Y 2.5/1) heavy silt loam; moderate, very coarse prismatic structure, prism faces are dark yellowish brown (10YR 4/4); firm consistence; clear smooth boundary
5Bwb	343-364	Yellowish red (5YR 4/6) heavy silt loam; common, large distinct iron concentrations of olive (2.5Y 4/4); moderate, very coarse prismatic structure; firm consistence; abrupt, wavy boundary
6Ab	364-375	Black (2.5Y 2.5/1) heavy silt loam; moderate, very coarse prismatic structure, prism faces are dark yellowish brown (10YR 4/4); firm consistence; clear smooth boundary
6Bwgb	375-396	Gray (5Y and 2.5Y 5/1) heavy silt loam; common, large distinct iron concentrations of olive (2.5Y 4/4); moderate, very coarse prismatic structure; firm consistence; abrupt, wavy boundary
6Cgb	396-400+	Gray (2.5Y 5/1) silt loam; structureless, massive; friable consistence

Other comments: Profile was described ~ 110 m south of the location where a bipoint was retrieved from the 4Ab1 horizon at 18QU1047; upper 61 cm are interpreted to be Younger Dryas loess. Samples were collected in a stratigraphic column from the 4Ab1, 4Ab2, 5Ab, and 6Ab soil horizons for AMS dating. The 4Ab1 at this location is ~70-centimeters lower than the comparable surface at 18QU1047. The location is interpreted as an interdunal wetland or pond. Samples were also collected in for plant macro and micro analyses. Described and sampled by D.P. Wagner, 8/8/13

SOUTHEAST PROFILE (3-12-2020): The GPS location is 38°54'22.61"N; 76°14'41.90"W and as of 6-20-2021, the original profile location is currently located ~1 meters (~4 feet) offshore

Parsons Island Soil Profile Description, Southeast (3-12-2020)

Horizon	Depth (cm)	Properties
Ap	0-29	Brown (10YR 4/3) loam to silt loam; structureless, massive; friable consistence; abrupt, smooth boundary
BE	29-39	Dark yellowish brown (10YR 4/6) and yellowish brown (10YR 5/4) loam to silt loam; weak, medium subangular blocky structure; friable consistence; clear, smooth boundary
2Btb	39-78	Strong brown (7.5YR 4/6) fine sandy loam; weak, coarse subangular blocky structure; nearly continuous clay films; friable consistence; clear, smooth boundary
3Btb	78-110	Strong brown (7.5YR 4/6) silt loam; many, medium distinct depletions of light brownish gray (10YR 6/2); weak, coarse prismatic platy parting to moderate, medium subangular blocky structure; continuous clay films; friable consistence; clear, smooth boundary
3BAtb	110-125	Brown (10YR 4/3) and dark grayish brown (2.5Y 4/2) silt loam; common, large distinct depletions of light brownish gray (10YR 6/2); moderate, coarse prismatic parting to weak, coarse subangular blocky structure; nearly continuous clay films; firm consistence; clear, smooth boundary
4Ab	125-140	Very dark gray (2.5Y 3/1) and very dark grayish brown (2.5Y 3/2) silt loam; moderate, coarse prismatic parting to weak, coarse subangular blocky structure; patchy clay films mainly on prism faces; firm consistence; clear, smooth boundary
4Btb	140-155	Light olive brown (2.5Y 5/3) heavy silt loam; many, large distinct depletions of light brownish gray (2.5Y 6/2); moderate, coarse prismatic parting to weak, coarse subangular blocky structure; nearly continuous clay films mainly on prism faces; firm consistence; clear, smooth boundary
4Btgb	155-200	Light brownish gray (2.5Y 6/2) heavy silt loam; common, medium distinct iron concentrations of dark yellowish brown (10YR 4/4); moderate, coarse prismatic platy parting to weak, coarse subangular blocky structure; nearly continuous clay films mainly on prism faces; firm consistence; gradual, smooth boundary

4BCgb 200-220 Light brownish gray (2.5Y 6/2) very fine sandy loam; common, medium distinct iron concentrations of dark yellowish brown (10YR 4/4); moderate, coarse prismatic parting to weak, coarse subangular blocky structure; friable consistence

Other comments: Soils exposed along the southeastern bank express greater short-distance variability than those in the vicinity of 18QU1047 on the southwest side of the island, particularly with respect to the 2Btb horizon which ranges in texture from sandy loam to nearly silt loam; overall stratigraphy is similar to the southwestern profile, but is compressed; Paw Paw Loess of Younger Dryas age comprises the upper 39 cm; subsoil development in the Tilghman Paleosol (4Btb horizons) here is much more advanced, as overlying deposits are not thick enough to have isolated the buried soil from continuing pedogenesis; the age of the 4Ab horizon is expected to be correlative to the 4Ab horizons in the southwestern soil; all deposits are interpreted to be either loess or eolian sand; admixtures of the two likely account for the above noted variability; moderately well drained; described by D.P. Wagner, 3/12/20

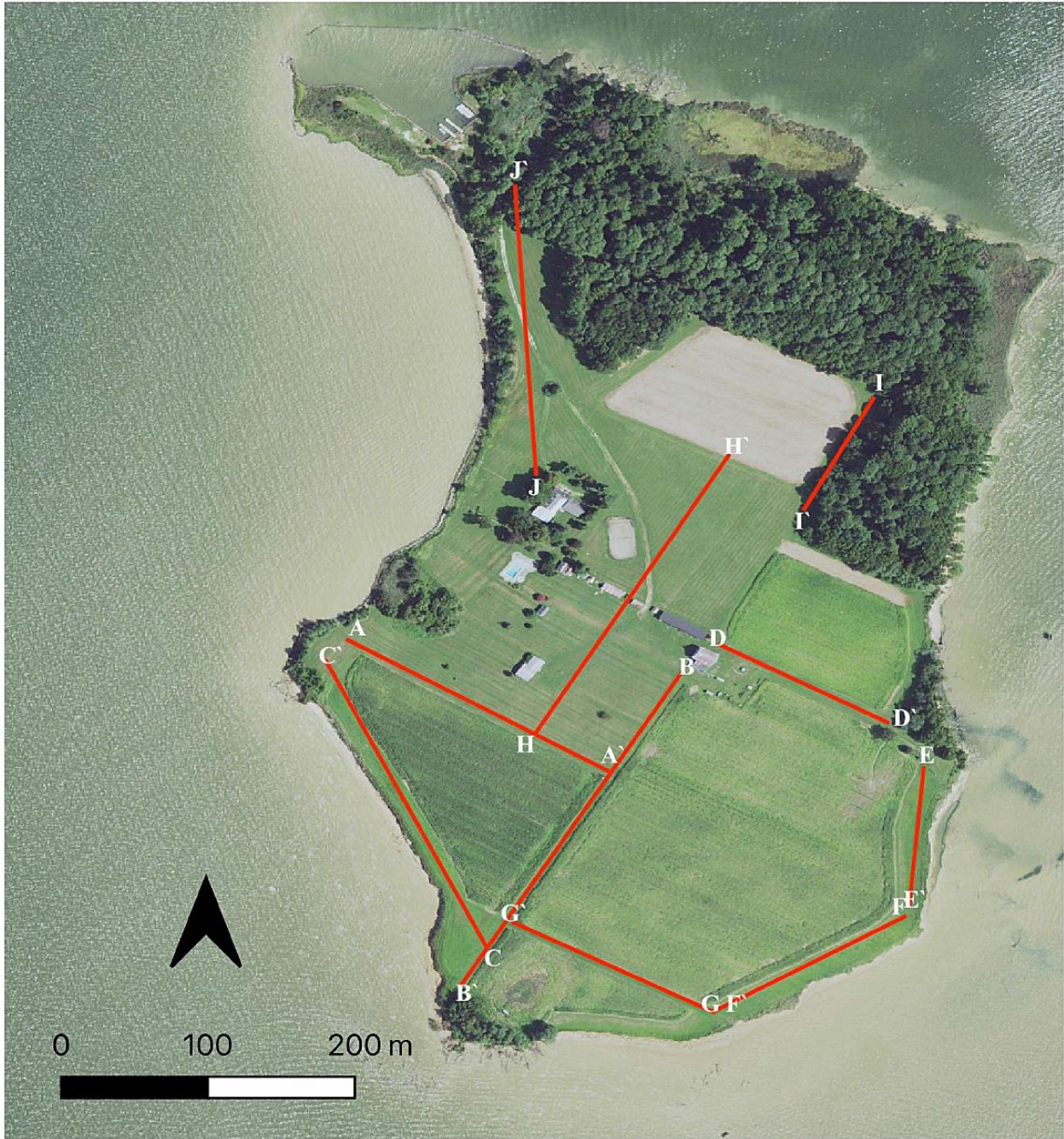


Appendix III; Figure 2: The image shows the eroded bank margin associated with the Southeast Profile soil description area on Parsons Island.

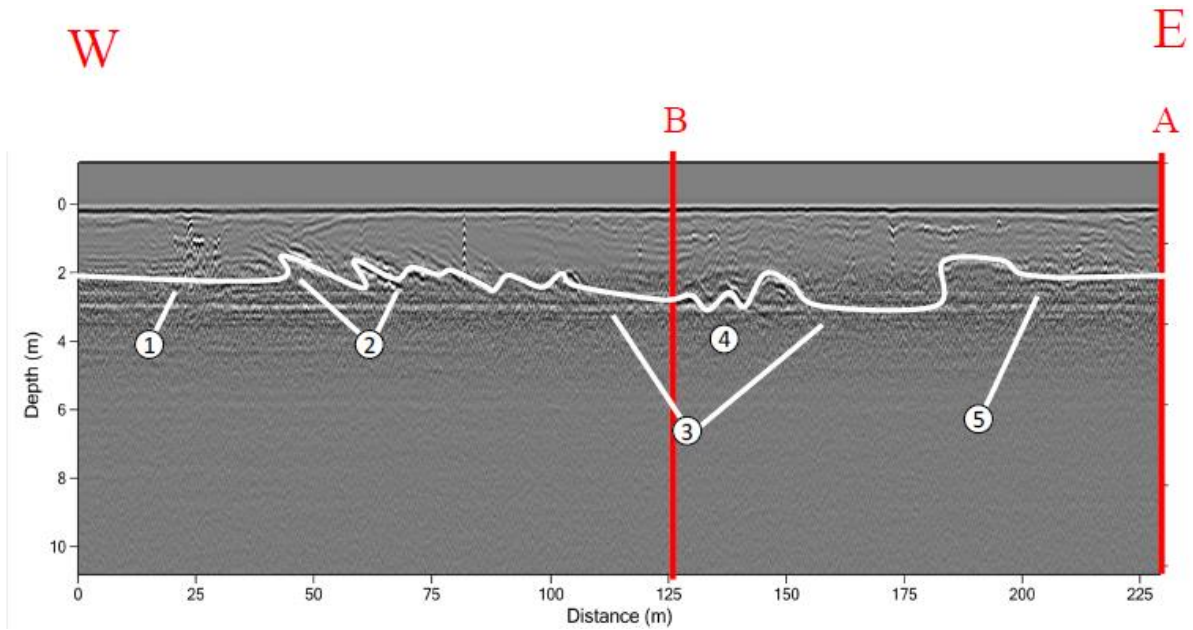
APPENDIX IV:

GPR Data for Parsons Island, Maryland.

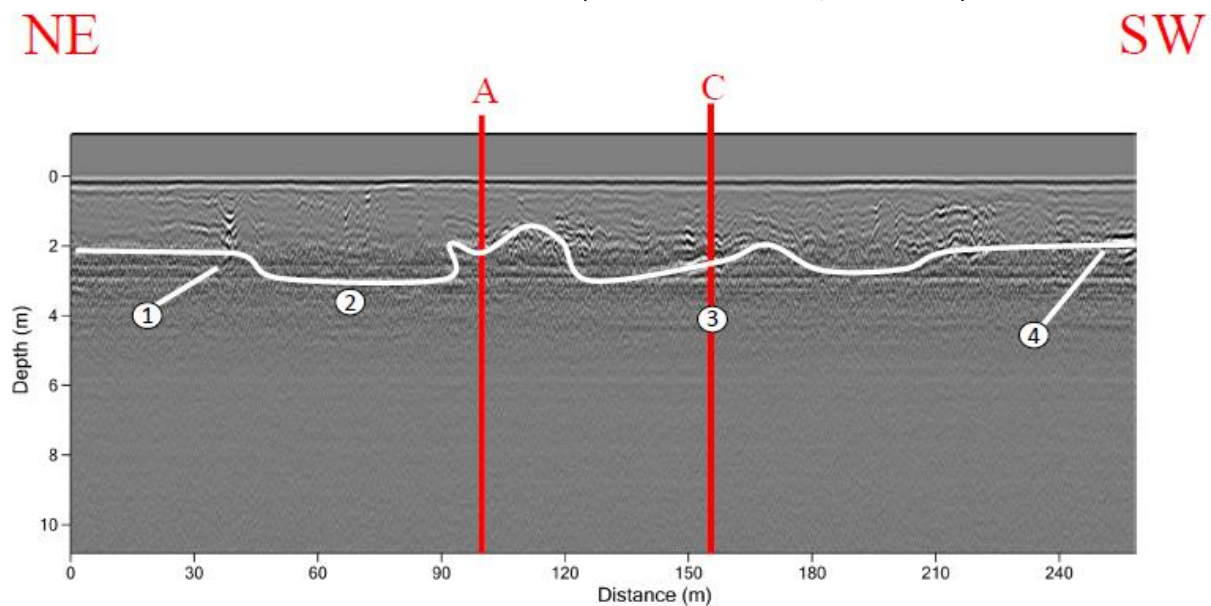
The following images were included in Bradley-Lewis' (2021) thesis for the Department of Earth Sciences at the University of Delaware. The GPR transect lines have been plotted and the GPR data for each transect are included. The captions outline Bradley-Lewis' (Ibid) interpretations of the underlying topography.



Appendix IV; Figure 1: The GRP unit transects across Parsons Island have been plotted on the 2020 satellite image of the island Image taken from Bradley-Lewis (2021: Figure 8).



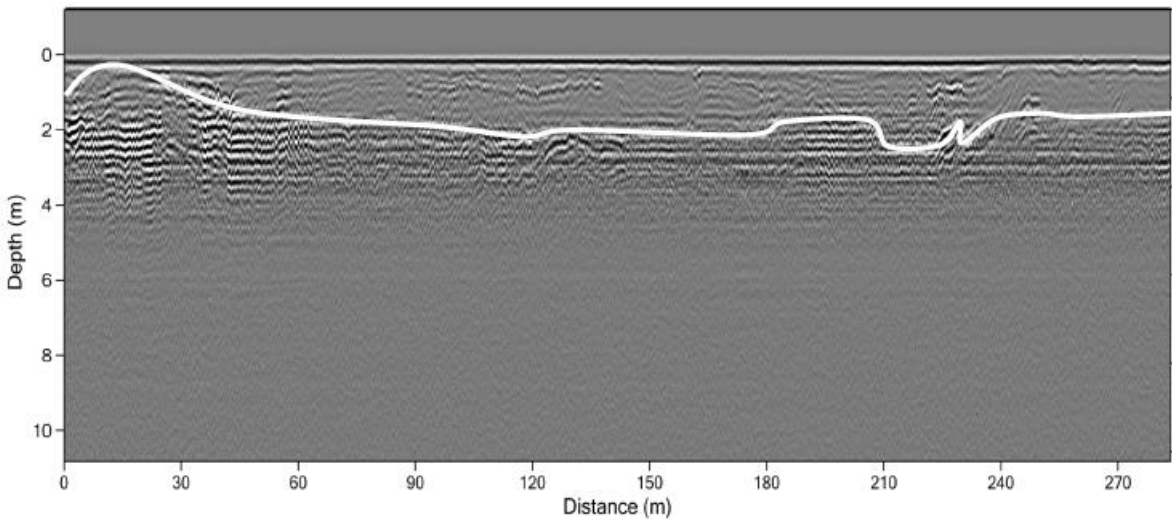
Appendix IV; Figure 2: The image shows the radiogram transect from A to A', as plotted on the 2020 satellite image (see Appendix IV; Figure 1). Anomalies have been numbered and auger core borings, which intersected the transect, have been plotted (red lines). Image taken from Bradley-Lewis (2021: Figure 29). Bradley-Lewis (2021: Figure 29) interpreted the white line as the as underlying paleotopography. However, some of the distortions in the GPR image may be a by-product of tectonic-related isostatic distortions (see van Vliet-Lanoe, et al. 2004).



Appendix IV; Figure 3: The image shows the radiogram transect from B to B', as plotted on the 2020 satellite image (see Appendix IV; Figure 1). Anomalies have been numbered and auger core borings, which intersected the transect, have been plotted (red lines). Image taken from Bradley-Lewis (2021: Figure 30). Bradley-Lewis (2021: Figure 30) interpreted the white line as the as underlying paleotopography. However, some of the distortions in the GPR image may be a by-product of tectonic-related isostatic distortions (see van Vliet-Lanoe, et al. 2004).

N

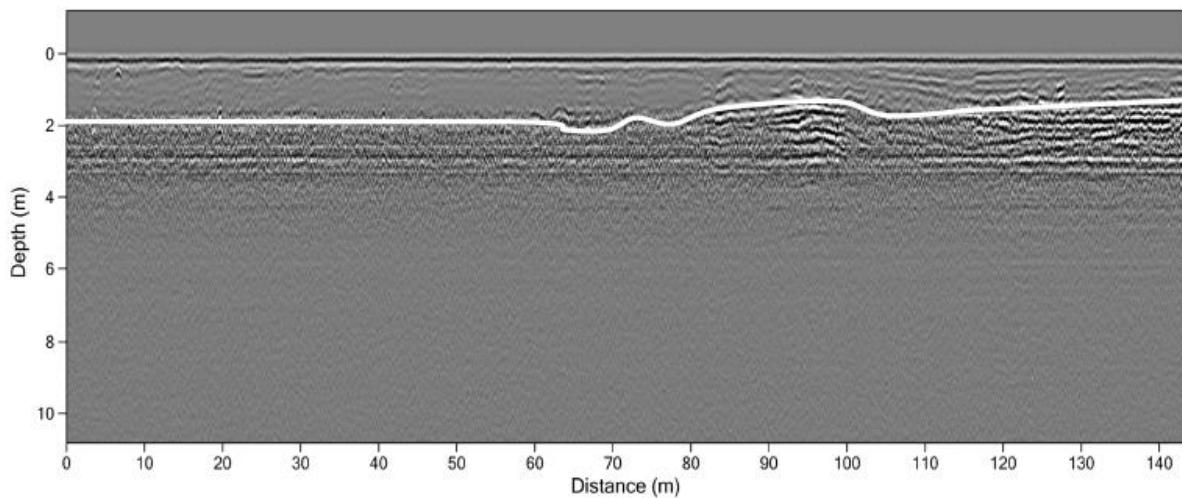
SE



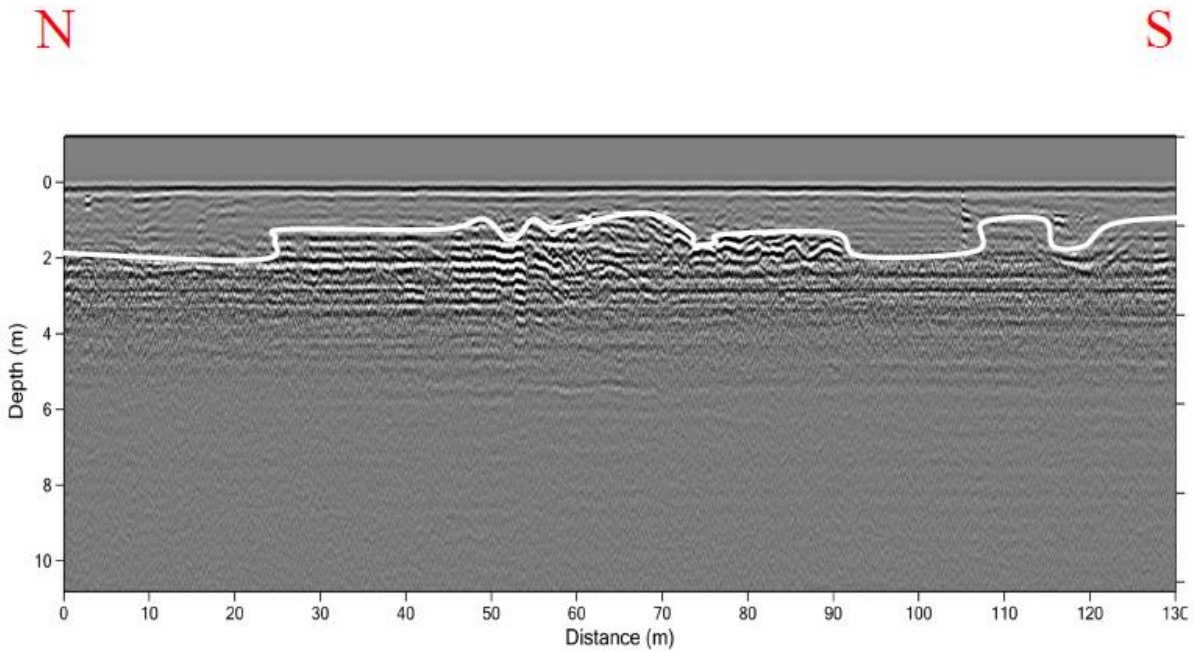
Appendix IV; Figure 4: The image shows the radiogram transect from C to C', as plotted on the 2020 satellite image (see Appendix IV; Figure 1). Bradley-Lewis (2021: Figure 31) interpreted the white line as the as underlying paleo-topography. However, some of the distortions in the GPR image may be a by-product of tectonic-related isostatic distortions (see van Vliet-Lanoe, et al. 2004).

W

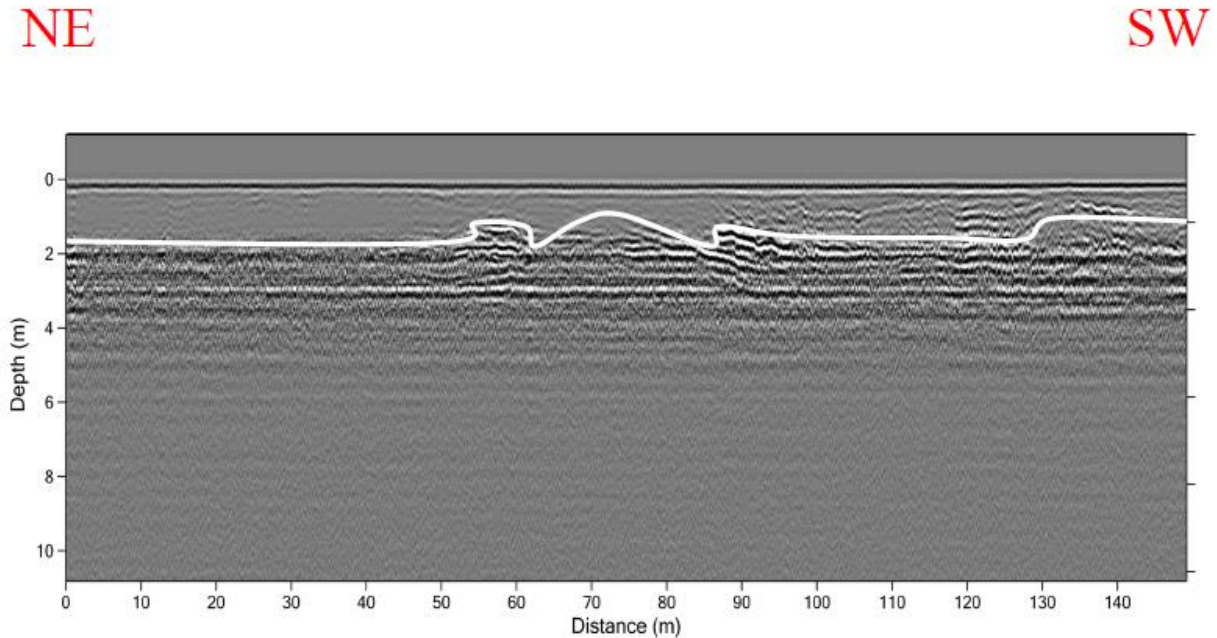
E



Appendix IV; Figure 5: The image shows the radiogram transect from D to D', as plotted on the 2020 satellite image (see Appendix IV; Figure 1). Bradley-Lewis (2021: Figure 32) interpreted the white line as the paleo-topography. However, some of the distortions in the GPR image may be a by-product of tectonic-related isostatic distortions (see van Vliet-Lanoe, et al. 2004).



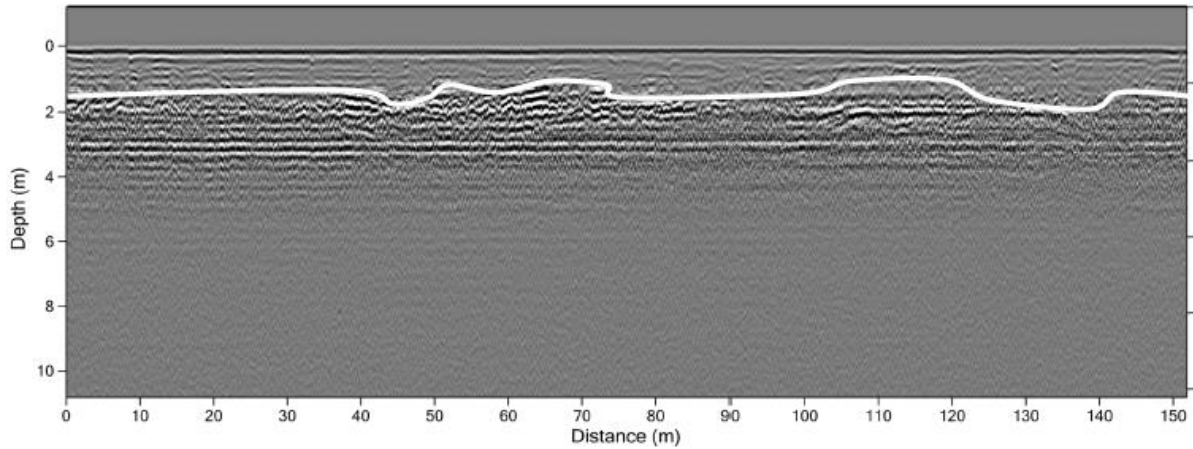
Appendix IV; Figure 6: The image shows the radiogram transect from E to E', as plotted on the 2020 satellite image (see Appendix IV; Figure 1). Bradley-Lewis (2021: Figure 33) interpreted the white line as the paleo-topography. However, some of the distortions in the GPR image may be a by-product of tectonic-related isostatic distortions (see van Vliet-Lanoë, et al. 2004).



Appendix IV; Figure 7: The image shows the radiogram transect from F to F', as plotted on the 2020 satellite image (see Appendix IV; Figure 1). Bradley-Lewis (2021: Figure 34) interpreted the white line as the paleo-topography. However, some of the distortions in the GPR image may be a by-product of tectonic-related isostatic distortions (see van Vliet-Lanoë, et al. 2004).

SE

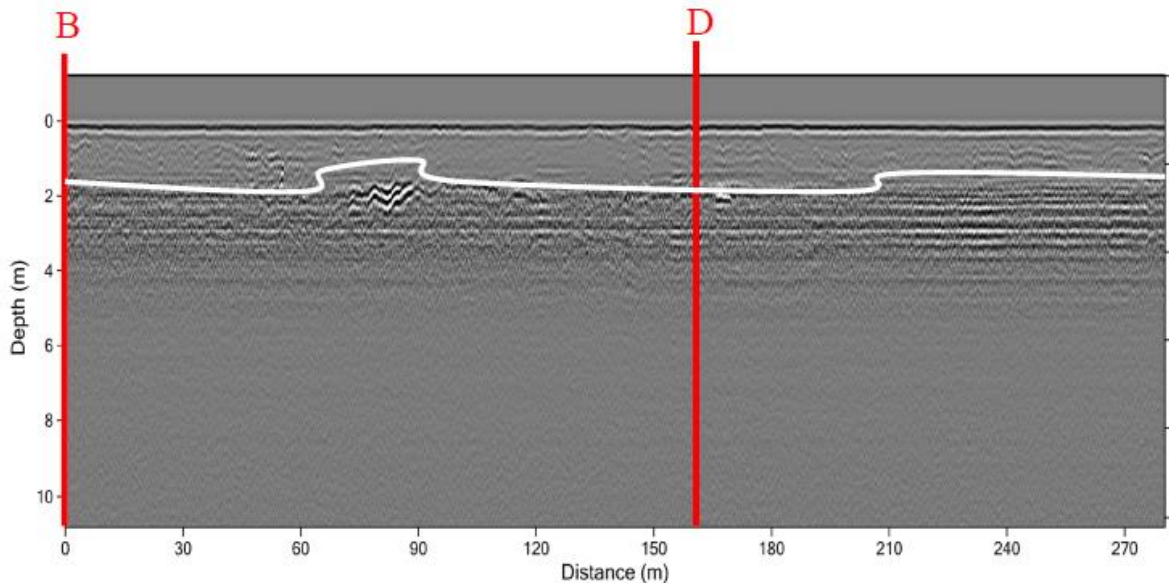
NW



Appendix IV; Figure 8: The image shows the radiogram transect from G to G', as plotted on the 2020 satellite image (see Appendix IV; Figure 1). Bradley-Lewis (2021: Figure 35) interpreted the white line as the paleo-topography. However, some of the distortions in the GPR image may be a by-product of tectonic-related isostatic distortions (see van Vliet-Lanoe, et al. 2004).

NE

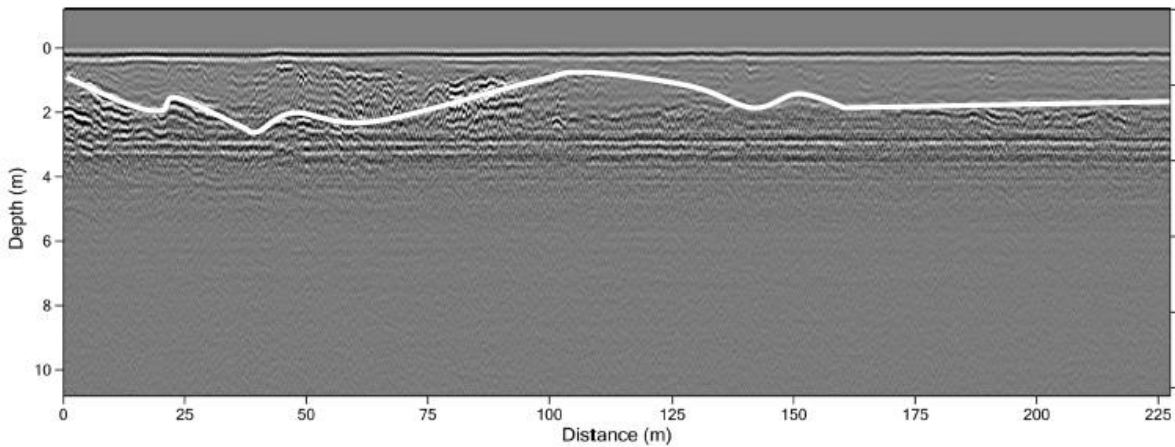
SW



Appendix IV; Figure 9: The image shows the radiogram transect from H to H', as plotted on the 2020 satellite image (see Appendix IV; Figure 1). Auger core borings, which intersected the transect, have been plotted (red lines). Image taken from Bradley-Lewis (2021: Figure 36). Bradley-Lewis (2021: Figure 36) interpreted the white line as the as underlying paleo-topography. However, some of the distortions in the GPR image may be a by-product of tectonic-related isostatic distortions (see van Vliet-Lanoe, et al. 2004).

NE

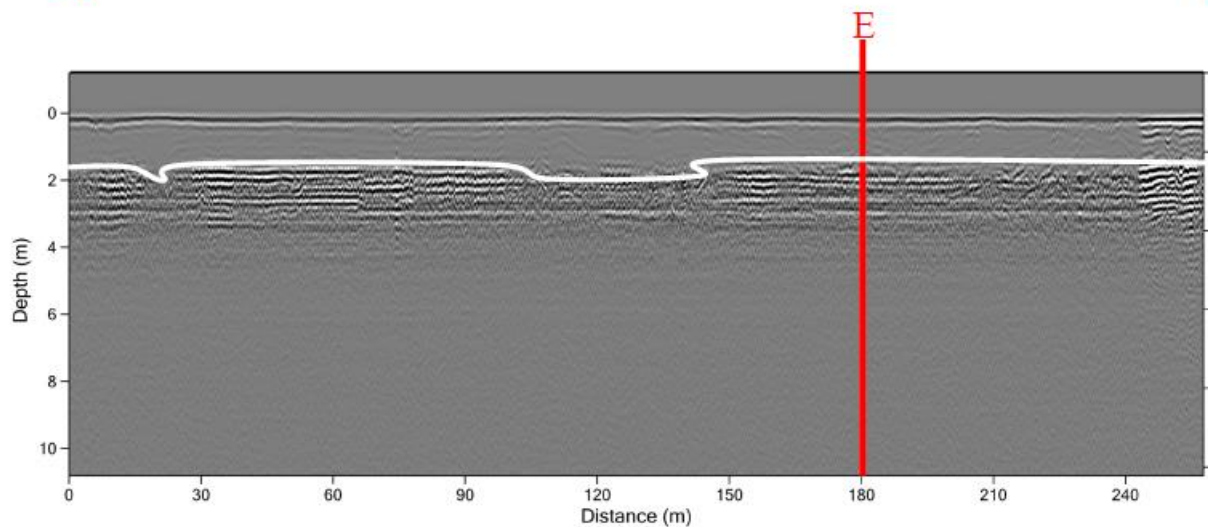
SW



Appendix IV; Figure 10: The image shows the radiogram transect from I to I', as plotted on the 2020 satellite image (see Appendix IV; Figure 1). Bradley-Lewis (2021: Figure 37) interpreted the white line as the paleo-topography. However, some of the distortions in the GPR image may be a by-product of tectonic-related isostatic distortions (see van Vliet-Lanoe, et al. 2004).

N

S



Appendix IV; Figure 11: The image shows the radiogram transect from J to J', as plotted on the 2020 satellite image (see Appendix IV; Figure 1). An auger core boring, which intersected the transect, has been plotted (red line). Image taken from Bradley-Lewis (2021: Figure 38). Bradley-Lewis (2021: Figure 38) interpreted the white line as the as underlying paleo-topography. However, some of the distortions in the GPR image may be a by-product of tectonic-related isostatic distortions (see van Vliet-Lanoe, et al. 2004).

APPENDIX V:

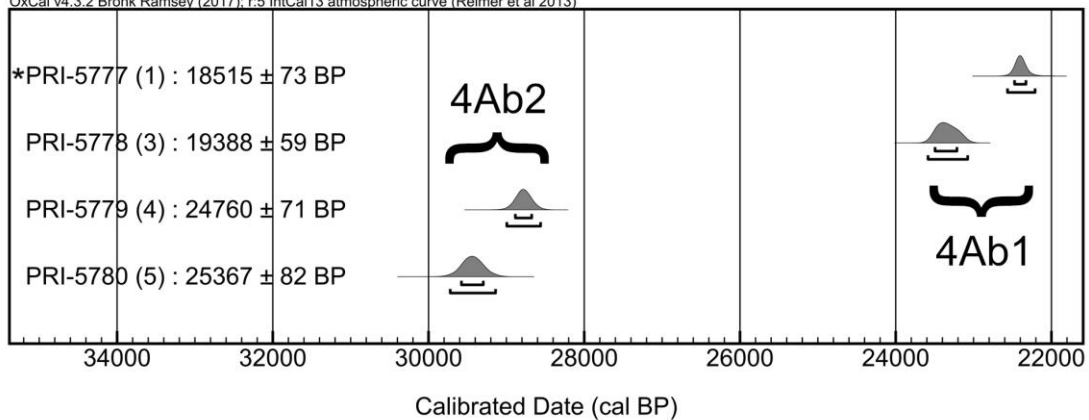
Identified and Dated Charcoal from the 4Ab1 and 4Ab2 Strata at Parsons Island.

PRI AMS No. & Sample No.	Sample Identification	AMS ¹⁴ C Date*	1-sigma Calibrated Date (68.2%)	2-sigma Calibrated Date (95.4%)	δ ¹³ C (‰)
*PRI-5777 1	Unidentifiable charcoal, small	18515 ± 73 RCYBP	22480–22320 CAL yr. BP	22570–22210 CAL yr. BP	-26.4
PRI-5778 3	Charred organics	19388 ± 59 RCYBP	23500–23210 CAL yr. BP	23590–23070 CAL yr. BP	-25.4
PRI-5779 4	Conifer charcoal	24760 ± 71 RCYBP	28890–28670 CAL yr. BP	29000–28560 CAL yr. BP	-26.4
PRI-5780 5	Conifer charcoal	25367 ± 82 RCYBP	29580–29290 CAL yr. BP	29730–29130 CAL yr. BP	-25.0



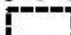


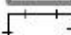
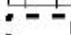



} 4Ab1
 } 4Ab2

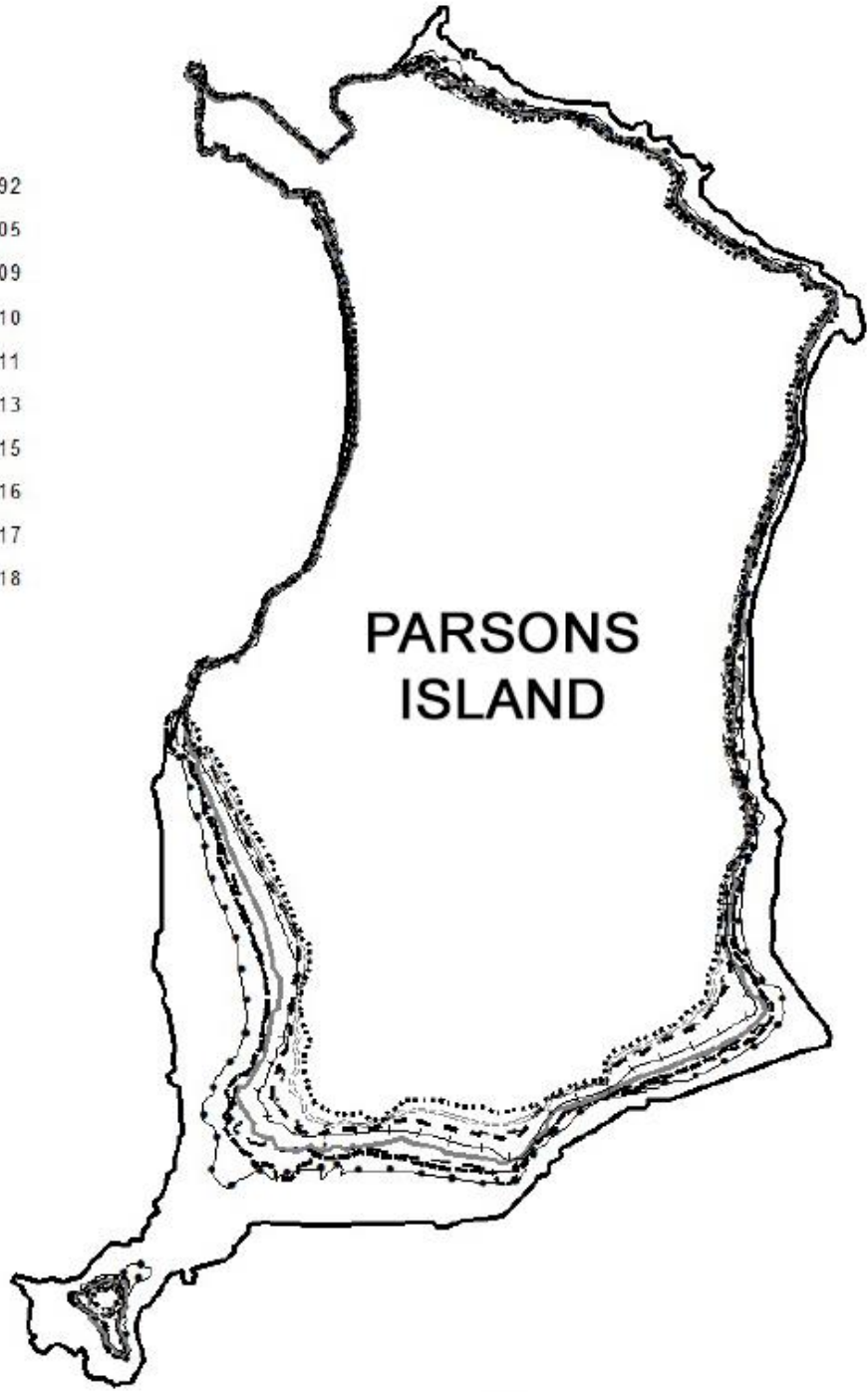
Reported in radiocarbon years at 1 standard deviation measurement precision (68.2%), corrected for δ¹³C.

OxCal v4.3.2 Bronk Ramsey (2017); r5 IntCal13 atmospheric curve (Reimer et al 2013)



Charcoal Identification Analysis and AMS Dating conducted by Dr. Linda Scott Cummings, at the PALEORESEARCH INSTITUTE, Golden, Colorado.

-  Shoreline-1992
-  Shoreline-2005
-  Shoreline-2009
-  Shoreline-2010
-  Shoreline-2011
-  Shoreline-2013
-  Shoreline-2015
-  Shoreline-2016
-  Shoreline-2017
-  Shoreline-2018



PARSONS
ISLAND

